DISCOVERY OF FLUORESCENCE POLARIZATION PROBES AND INHIBITORS FOR TESTIS-SPECIFIC BROMODOMAIN AND EXTRA-TERMINAL (BRDT) PROTEINS

A DISSERTATION

SUBMITTED TO THE FACULTY OF

UNIVERSITY OF MINNESOTA

BY

XIANGHONG GUAN

IN PARTIAL FULFILLMENT OF THE REQUIREMENTS

FOR THE DEGREE OF
DOCTOR OF PHILOSOPHY

ADVISOR: GUNDA I. GEORG

DECEMBER 2020

© Xianghong Guan 2020

Acknowledgements

On the very outset of this thesis, I would like to express my gratitude to my advisor, Dr. Gunda Georg, for providing invaluable guidance throughout this research in her lab.

I have had a really great time and received a lot help from our research group. Thank you to Dr. Jon Hawkinson for your advice on the BRDT project, especially on the development of florescence probes; Drs. Mike Walters and Peter Dosa for their experience and mentorship in organic chemistry and rational drug design; Dr. Henry Wong for teaching animal pharmacology; Dr. Carolyn Paulson for her evaluation of FP probes; Dr. Kwon Hong for his CADD training; Drs. Narsi Cheryala, Soma Maitra and Gurpreet Singh for their synthetic expertise and personal friendship; Drs. Shameem Syeda and Sudhakar Jakkaraj for providing (-)-JQ1 and (+)-JQ1; and Jiewei Jiang for providing compound 2098312-12-8 for the probe development project.

My research would not have progressed without the support from our collaborators at the H. Lee Moffitt Cancer Center, Harvard University and the Department of Chemistry at the University of Minnesota. I am deeply grateful to Dr. Ernst Schönbrunn for his great crystallographic support and cellular assay results; Dr. Alice Chan and Dr. Rezaul Karim for co-crystal structures of monovalent and bivalent compounds with BET proteins; Dr. Jun Qi for compound screening support; Dr. Virangika Wimalasena and Nana Kwaku Offei-Addo for performing the AlphaScreen assays; Dr. William Pomerantz and Alex Ayoub for their BRD4 protein expression.

Thank you to all teachers for providing me with an outstanding education. I would like to extend my acknowledgement to the entire administrative group in the Department of Medicinal Chemistry for their thoughtful service. I also thank Dr. Leigh Allen for her help with thesis editing.

Finally, I am extreme grateful to my family and friends for their support, encouragement, and sacrifices.

This dissertation is dedicated to my parents, Weiming Guan and Sufang Hong.

Abstract

The testis-specific bromodomain (BRDT) protein is a member of the Bromodomain and Extra-Terminal (BET) protein family. BRDT interacts with acetylated lysine (Kac) residues of histones and is important for the process of spermatogenesis. The expression of BRDT in humans is testis-restricted and BRDT-1 knockout mice are infertile. Therefore, the inhibition of BRDT is a promising strategy for male contraception. However, no selective BRDT inhibitors have been discovered yet. High sequence identity between BET proteins has impeded the discovery of selective BRDT inhibitors.

In our research, novel probes were prepared for use in a fluorescence polarization assay. Probes were designed based on the potent pan-BET inhibitor SG3-179. A series of SG3-179 analogs linked to the BODIPY fluorophore was synthesized and photo-physical properties and affinities were measured. Among these probes, **2.18** exhibited the best polarization signal and affinity against BET family proteins (K_d= 4–16 nM). The IC_{50} values that were obtained for published BET inhibitors correlated well with the value obtained using the AlphaScreen assay.

Based on the knowledge that BRDT has a unique Arg54 in the Kac site, compounds were designed based on the SG3-179 scaffold with the goal to engage Arg54 in compound binding. Two binding poses of SG3-179 in the Kac binding site inspired us to generate two series of compounds. Negatively charged side chains were introduced for potential interaction with Arg54. Series I compounds contained a single substituted side chain attached to ring A of the SG3-179 scaffold. They were weak BET inhibitors (8.6 ~ 43 μM) in Alpha Screen and FP assays. Series II compounds with two side chains showed double digital nanomolar activity for BRDT-1 inhibition and up to 13-fold selectivity for BRDT-1 over BRD4-1. As SG3-179 is also a JAK2 and FLT3 inhibitor the new analogs were also tested for inhibition of these two kinases. Compound **3.61** showed more than 400-fold selectivity for BRDT-1 over JAK2 or FLT3. The cocrystal structures of compound **3.61** revealed differences in the binding modes with BRD4-1 and BRDT-1. Series III compounds, which lack the piperidine moiety present in SG3-179, had decreased BRDT/BRD4 activity (0.33 ~ 2.70 μM). In the future, further modification of the most BRDT-1 selective compound **3.61** will be performed to improve BRDT selectivity.

Bivalent SG3-179-derived analogs were designed and synthesized as an alternative strategy. We hypothesized that BRDT selectivity can be achieved through BRDT specific intramolecular or intermolecular binding. Through iterative optimization of chemotypes, attachment, spacer length and spacer position (N38 and C3 site), symmetric and non-symmetric bivalent inhibitors with PEG-linkers were prepared. Compared to the parent compound **2.11**, two series of bivalent compounds showed up to 70-fold improvements in potency for BRDT-1 in the AlphaScreen assay. The best compound **4.17** exhibited 238-fold higher selectivity for BRDT-1 over BRD4-1. The selectivity ratio initially increased and then decreased with the elongation of the PEG linker in these two series of compounds. The ideal linker length varied in different molecule series. To achieve a better understanding of the binding mode, four cocrystal structures were obtained. We observed that bivalent molecules induced the dimerization of BRDT-1 and BRD4-1. However, for tandem BRD constructs, the inhibitory selectivity of these compounds decreased significantly. In cellular assays, these large molecules were able to penetrate the cell membrane and exhibited double digital nanomolar IC_{50} values for inhibition of multiple myeloma (MM1.S) cell proliferation.

Table of contents

List of Figures viii

List of Schemes ix

List of Tables x

List of Compounds xii

List of Abbreviations xviii

Chapter 1: Introduction 1

1.1 General Background 1

1.2 BET proteins 1

1.3 Role of Brdt in gametogenesis 4

1.4 BRDT: target for male contraception 7

1.5 BRDT structure and the Kac site 9

1.6 Strategies for BRDT inhibition 10
1.6.1 BRDT inhibitors 10
1.6.2 Bivalent inhibitors 14

1.7 BRDT selectivity: Arg54 and bivalent strategies 15

1.8 Fluorescence polarization tools for BRDT inhibitor discovery 18

Chapter 2: Design, Synthesis, and Characterization of a Fluorescence Polarization Pan-BET Bromodomain Probe 21

2.1 Induction 21

2.2 Chemistry 22

2.3 UV absorption and fluorescence excitation and emission spectrums 24

2.4 Probe affinity and signal window 25

2.5 Testing of representative BET BRD inhibitors results 28

2.6 Conclusion 33

Chapter 3: Discovery of Selective 2,4-Disubstitued Pyrimidine Derivatives for Extra-Terminal (BET) Family Proteins from a Dual-JAK2 Kinase and Bromodomain Inhibitor 34

3.1 Introduction 34

3.2 Chemistry 38

3.3 Results and discussion 41
3.3.1 Series I compounds are weak BRDT-1/BRD4-1 inhibitors 41

3.3.2 Series II compounds are potent BRDT-1/BRD4-1 inhibitors 44
3.3.3 Series III: deletion of SG3-179 piperidine decreases BRDT-1/BRD4-1 inhibition 46
3.3.4 Crystal structure of compound **3.61** 47
3.3.5 Compound **3.61** has no kinase (JAK2 and FLT3) activity 48
3.4 Conclusions and future directions 50

Chapter 4: Discovery of Selective Bivalent Inhibitors for Testis-Specific Bromodomain (BRDT) 52

4.1 Induction 52
4.2 Chemistry 55
4.3 Results and discussion 58
4.3.1 Bivalent molecules are potent BET protein inhibitors 58
4.3.2 Bivalent molecules can penetrate through the membrane of MM1.S cells 66
4.3.3 Bivalent molecules induced dimerization of BRDT-1 and BRD4-1 67
4.4 Conclusions and future directions 70

Chapter 5: Experimental Data 72

5.1 General chemistry procedures 72
5.2 Chapter 2 synthesis of FP probes 73
5.3 Chapter 3 synthesis of monovalent inhibitors for BRDT 85
5.4 Chapter 4 synthesis of bivalent inhibitors for BRDT 118

Bibliography 140

List of Figures

Figure 1.1 Phylogenetic tree of the human bromodomain proteins 2

Figure 1.2 Acetylation of histone tails induces chromatin remodeling to activate transcription 3

Figure 1.3 Brdt expression level at different stages in mouse 6

Figure 1.4 Role of Brdt in meiosis and post-meiotic differentiation 7

Figure 1.5 (a) BRDT and (b) BRD4 expression levels in human tissues 8

Figure 1.6 Brdt-1 mutant epididymal sperm are abnormal 9

Figure 1.7 Overall structural motifs, domains and binding site architecture of BRDT 10

Figure1.8 Representative potent chemotypes of BRDT inhibitors 11

Figure 1.9 Dual BET bromodomain-kinase inhibitors 14

Figure 1.10 Bivalent compound biBET (PDB: 5AD3) and MT1 (PDB: 5JWM) induced the homodimerization of BRD4-1 15

Figure 1.11 Sequence homology of bromodomains in the BET family 17

Figure 1.12 Domain structures of BRD2, BRD3, BRD4 and BRDT 17

Figure 1.13 Basic principle of fluorescence polarization 18

Figure 1.14 Principle of fluorescence polarization assay 18

Figure 2.1 Molecular docking predicts that compound **2.18** will maintain high affinity for BRDT-1 22

Figure 2.2 UV absorbance and fluorescence spectra of BODIPY, probes **2.18**, **2.19**, and **2.20** 25

Figure 2.3 Pan-BET probe **2.18** showed favorable binding properties compared to related probes **2.19** and **2.20** 26

Figure 2.4 Pan-BET probe **2.18** binds with high affinity to BET BRDs, but only weakly to other BRD proteins 26

Figure 2.5 BRD saturation binding curves with 7.5 nM compound **2.18** 27

Figure 2.6 Competitive displacement of the pan-BET probe **2.18** by 10 reference BET inhibitors at (a) BRDT-BD1 and (b) BRDT-BD2 29

Figure 2.7 Structures of the 10 reference BET inhibitors with various chemical scaffolds selected to validate the FP assay 30

Figure 3.1 TG101209 and SG3-179 34

Figure 3.2 Strategies to approach Arg54 36

Figure 3.3 Molecular simulation of compounds **3.31** and **3.61** using MM/GBSA 38

Figure 3.4 Series I of SG3-179 analogs 41

Figure 3.5 Series II of SG3-179 analogs 44

Figure 3.6 Series III of SG3-179 analogs 46

Figure 3.7 Comparison of **3.61** in BRD4 versus BRDT 48

Figure 3.8 Possible explanation for decreased JAK2 activity of compound **3.61** 50

Figure 4.1 Proposed strategy for the preparation of dimeric inhibitor libraries 52

Figure 4.2 Strategy for spacer connection 54

Figure 4.3 Design of symmetric and non-symmetric bivalent inhibitors 54

Figure 4.4 Effects of bivalent inhibitors on MM1.S cells 66

Figure 4.5 Crystal structures of bivalent inhibitors in complex with BRDT-1 and BRD4-1 68

Figure 4.6 Difference between BRDT-1 and BRD4-1 homodimers 69

List of Schemes

Scheme 2.1 Synthesis of the SG3-179 chemotype 23

Scheme 2.2 Synthesis of the fluorophore moiety and FP probe assemble 24

Scheme 3.1 Series I: t-butyl sulfonamide of SG3-17 replaced with amino acids to approach Arg54 in BRDT-1 39

Scheme 3.2 Series II: various substituents introduced at meta position of t-butyl sulfonamide moiety of SG3-17 to approach Arg54 in BRDT-1 40

Scheme 3.3 Series III: piperidine removal from compound of SG3-179 analogs 41

Scheme 4.1 Series I: synthesis of SG3-179 based bivalent inhibitors using N38-N38, C3-C3 and N38-C3 connection strategy 57

Scheme 4.2 Series II: SG3-179 linked to JQ1 (**4.21**), bivalent symmetrical RVX208 inhibitors **4.23** and **4.24** and SG3-179 linked to RXV208 (**4.27** and **4.28**) 58

List of Tables

Table 1.1 Identity of bromodomain proteins in the BET family 16

Table 2.1 Affinity of pan-BET FP probe **2.18** for BRD proteins 27

Table 2.2 Inhibitory potency (IC_{50}) and affinity (K_i) of representative BRD inhibitors for BET family bromodomains determined using pan-BET FP probe **2.18** 31

Table 3.1 Structure−Activity Relationship of Series I 43

Table 3.2 Structure−Activity Relationship of Series II 45

Table 3.3 Structure−Activity relationship of Series III 47

Table 3.4 Activity of selected compounds against the bromodomain panel 49

Table 4.1 AlphaScreen data of N38–N38 connected series I 61

Table 4.2 AlphaScreen data of three series I spacer strategies 62

Table 4.3 AlphaScreen data of N38–C3 strategy in series I 63

Table 4.4 AlphaScreen data of series II JQ-1/RVX-208 non-symmetric bivalents and bivalent RVX-208 64

Table 4.5 BROMOscan data for BRDT-(1,2) and BRD4-(1,2) 65

Table 4.6 BROMOscan data of compound **4.3** for different bromodomains 66

List of Compounds

tert-Butyl (4-Chloro-3-nitrophenyl)carbamate (**2.2**) 73

tert-Butyl (3-Amino-4-chlorophenyl)carbamate (**2.3**) 73

tert-Butyl (3-((*tert*-Butylsulfinyl)amino)-4-chlorophenyl)carbamate (**2.4**) 74

N-(5-Amino-2-chlorophenyl)-2-methylpropane-2-sulfonamide (**2.5)** 74

N-(5-Amino-2-chlorophenyl)-2-methylpropane-2-sulfonamide (**2.6**) 74

N-(2-Chloro-5-((2-chloro-5-methylpyrimidin-4-yl)amino)phenyl)-2-methylpropane-2-sulfonamide (**2.7**) 75

tert-Butyl 4-(4-Amino-2-fluorobenzamido)piperidine-1-carboxylate (**2.9**) 76

tert-Butyl 4-(4-((4-((4-Chloro-3-((1,1-dimethylethyl)sulfonamido)phenyl)amino)-5-methyl pyrimidin-2-yl)amino)-2-fluorobenzamido)piperidine-1-carboxylate (**2.10**) 76

4-((4-((4-Chloro-3-((1,1-dimethylethyl)sulfonamido)phenyl)amino)-5-methylpyrimidin-2-yl)amino)-2-fluoro-*N*-(piperidin-4-yl)benzamide (**2.11**) 77

5,5-Difluoro-1,3,7,9-tetramethyl-5*H*-4λ^4,5λ^4-dipyrrolo[1,2-*c*:2',1'-*f*][1,3,2] diazaborinine-2-carbaldehyde (**2.12**) 78

5,5-Difluoro-3,7-dimethyl-5*H*-4λ^4,5λ^4-dipyrrolo[1,2-*c*:2',1'-*f*][1,3,2]diazaborinine-2-carboxylic Acid (**2.13**) 79

(*E*)-3-(5,5-Difluoro-1,3,7,9-tetramethyl-5*H*-4λ^4,5λ^4-dipyrrolo [1,2-*c*:2',1'-*f*][1,3,2]diazaborinin-2-yl)acrylic Acid (**2.14**) 79

Methyl (*E*)-3-(5,5-Difluoro-1,3,7,9-tetramethyl-5*H*-4λ^4,5λ^4-dipyrrolo[1,2-*c*:2',1'-*f*][1,3,2] diazaborinin-2-yl)acrylate (**2.15**) 80

3-(5,5-Difluoro-1,3,7,9-tetramethyl-5*H*-4λ^4,5λ^4-dipyrrolo[1,2-*c*:2',1'-*f*][1,3,2]diazaborinin-2-yl)propanoic Acid (**2.16**) 81

3-(5,5-difluoro-1,3,7,9-tetramethyl-5*H*-4λ^4,5λ^4-dipyrrolo[1,2-*c*:2',1'-*f*][1,3,2]diazaborinin-2-yl)propanoic acid (**2.17**) 81

4-((4-((4-Chloro-3-((1,1-dimethylethyl)sulfonamido)phenyl)amino)-5-methylpyrimidin-2-yl)amino)-*N*-(1-(5,5-difluoro-1,3,7,9-tetramethyl-5*H*-4λ^4,5λ^4-dipyrrolo[1,2-*c*:2',1'-*f*][1,3,2]diazaborinine-2-carbonyl)piperidin-4-yl)-2-fluorobenzamide (**2.18**) 82

4-((4-((4-Chloro-3-((1,1-dimethylethyl)sulfonamido)phenyl)amino)-5-methylpyrimidin-2-yl)amino)-*N*-(1-(3-(5,5-difluoro-1,3,7,9-tetramethyl-5*H*-4λ^4,5λ^4-dipyrrolo[1,2-*c*:2',1'-*f*][1,3,2]diazaborinin-2-yl)propanoyl)piperidin-4-yl)-2-fluorobenzamide (**2.19**) 83

(*E*)-4-((4-((4-Chloro-3-((1,1-dimethylethyl)sulfonamido)phenyl)amino)-5-methylpyrimidin-2-yl)amino)-*N*-(1-(3-(5,5-difluoro-1,3,7,9-tetramethyl-5*H*-4λ^4,5λ^4-dipyrrolo[1,2-*c*:2',1'-*f*][1,3,2]diazaborinin-2-yl)acryloyl)piperidin-4-yl)-2-fluorobenzamide (**2.20**) 84

3-((2-Chloro-5-methylpyrimidin-4-yl)amino)benzoic Acid (**3.3**) 85

2-Chloro-5-((2-Chloro-5-methylpyrimidin-4-yl)amino)benzoic Acid (**3.4**) 85

3-((2-((4-((1-(*tert*-Butoxycarbonyl)piperidin-4-yl)carbamoyl)-3-fluorophenyl)amino)-5-methylpyrimidin-4-yl)amino)benzoic Acid (**3.5**) 86

5-((2-((4-((1-(*tert*-Butoxycarbonyl)piperidin-4-yl)carbamoyl)-3-fluorophenyl)amino)-5-methylpyrimidin-4-yl)amino)-2-chlorobenzoic Acid (**3.6**) 86

3-((2-((3-Fluoro-4-(piperidin-4-ylcarbamoyl)phenyl)amino)-5-methylpyrimidin-4-yl)amino)benzoic acid (**3.19**) 87

(3-((2-((3-Fluoro-4-(piperidin-4-ylcarbamoyl)phenyl)amino)-5-methylpyrimidin-4-yl)amino)benzoyl)glycine (**3.20**) 87

(3-((2-((3-Fluoro-4-(piperidin-4-ylcarbamoyl)phenyl)amino)-5-methylpyrimidin-4-yl)amino)benzoyl)-*L*-alanine (**3.21**) 88

(3-((2-((3-Fluoro-4-(piperidin-4-ylcarbamoyl)phenyl)amino)-5-methylpyrimidin-4-yl)amino)benzoyl)-*L*-valine (**3.22**) 89

(3-((2-((3-Fluoro-4-(piperidin-4-ylcarbamoyl)phenyl)amino)-5-methylpyrimidin-4-yl)amino)benzoyl)-*L*-phenylalanine (**3.23**) 90

(3-((2-((3-Fluoro-4-(piperidin-4-ylcarbamoyl)phenyl)amino)-5-methylpyrimidin-4-yl)amino)benzoyl)-*L*-aspartic Acid (**3.24**) 90

(3-((2-((3-Fluoro-4-(piperidin-4-ylcarbamoyl)phenyl)amino)-5-methylpyrimidin-4-yl)amino)benzoyl)-*L*-glutamic Acid (**3.25**) 91

(3-((2-((3-Fluoro-4-(piperidin-4-ylcarbamoyl)phenyl)amino)-5-methylpyrimidin-4-yl)amino)benzoyl)-*L*-allothreonine (**3.26**) 92

(3-((2-((3-Fluoro-4-(piperidin-4-ylcarbamoyl)phenyl)amino)-5-methylpyrimidin-4-yl)amino)benzoyl)-*L*-proline (**3.27**) 92

2-Chloro-5-((2-((3-fluoro-4-(piperidin-4-ylcarbamoyl)phenyl)amino)-5-methylpyrimidin-4-yl)amino)benzoic Acid (**3.28**) 93

(2-Chloro-5-((2-((3-fluoro-4-(piperidin-4-ylcarbamoyl)phenyl)amino)-5-methylpyrimidin-4-yl)amino)benzoyl)glycine (**3.29**) 94

(2-Chloro-5-((2-((3-fluoro-4-(piperidin-4-ylcarbamoyl)phenyl)amino)-5-methylpyrimidin-4-yl)amino)benzoyl)-*L*-alanine (**3.30**) 95

(2-Chloro-5-((2-((3-fluoro-4-(piperidin-4-ylcarbamoyl)phenyl)amino)-5-methylpyrimidin-4-yl)amino)benzoyl)-*L*-glutamic acid (**3.31**) 95

(2-Chloro-5-((2-((3-fluoro-4-(piperidin-4-ylcarbamoyl)phenyl)amino)-5-methylpyrimidin-4-yl)amino)benzoyl)-*L*-allothreonine (**3.32**) 96

Methyl 3,5-diaminobenzoate (**3.34**) 96

Methyl 3-amino-5-((2-chloro-5-methylpyrimidin-4-yl)amino)benzoate (**3.35**) 97

Methyl 3-((*tert*-butylsulfinyl)amino)-5-((2-chloro-5-methylpyrimidin-4-yl)amino)benzoate (**3.36**) 97

Methyl 3-((2-chloro-5-methylpyrimidin-4-yl)amino)-5-((1,1-dimethylethyl)sulfonamido)benzoate (**3.37**) 98

tert-Butyl 4-(4-((4-((3-((1,1-dimethylethyl)sulfonamido)-5-(methoxycarbonyl)phenyl)amino)-5-methylpyrimidin-2-yl)amino)-2-fluorobenzamido)piperidine-1-carboxylate (**3.38**) 99

3-((2-((4-((1-(*tert*-Butoxycarbonyl)piperidin-4-yl)carbamoyl)-3-fluorophenyl)amino)-5-methylpyrimidin-4-yl)amino)-5-((1,1-dimethylethyl)sulfonamido)benzoic acid (**3.39**) 100

Methyl 3-((1,1-dimethylethyl)sulfonamido)-5-((2-((3-fluoro-4-(piperidin-4-ylcarbamoyl)phenyl)amino)-5-methylpyrimidin-4-yl)amino)benzoate (**3.55**) 101

(3-((1,1-dimethylethyl)sulfonamido)-5-((2-((3-fluoro-4-(piperidin-4-ylcarbamoyl)phenyl)amino)-5-methylpyrimidin-4-yl)amino)benzoyl)glycine (**3.56**) 101

(3-((1,1-Dimethylethyl)sulfonamido)-5-((2-((3-fluoro-4-(piperidin-4-ylcarbamoyl)phenyl)amino)-5-methylpyrimidin-4-yl)amino)benzoyl)-*D*-phenylalanine (**3.57**) 102

(3-((1,1-Dimethylethyl)sulfonamido)-5-((2-((3-fluoro-4-(piperidin-4-ylcarbamoyl)phenyl)amino)-5-methylpyrimidin-4-yl)amino)benzoyl)-*D*-phenylalanine hydrochloride (**3.58**) 103

(3-((1,1-Dimethylethyl)sulfonamido)-5-((2-((3-fluoro-4-(piperidin-4-ylcarbamoyl)phenyl)amino)-5-methylpyrimidin-4-yl)amino)benzoyl)-*L*-threonine (**3.59**) 104

(3-((1,1-Dimethylethyl)sulfonamido)-5-((2-((3-fluoro-4-(piperidin-4-ylcarbamoyl)phenyl)amino)-5-methylpyrimidin-4-yl)amino)benzoyl)-*L*-serine (**3.60**) 105

(3-((1,1-Dimethylethyl)sulfonamido)-5-((2-((3-fluoro-4-(piperidin-4-ylcarbamoyl)phenyl)amino)-5-methylpyrimidin-4-yl)amino)benzoyl)-*L*-glutamic acid (**3.61**) 106

(3-((1,1-Dimethylethyl)sulfonamido)-5-((2-((3-fluoro-4-(piperidin-4-ylcarbamoyl)phenyl)amino)-5-methylpyrimidin-4-yl)amino)benzoyl)-*L*-glutamine (**3.62**) 107

4-((4-((3-(*tert*-Butylcarbamoyl)-5-((1,1-dimethylethyl)sulfonamido)phenyl)amino)-5-methylpyrimidin-2-yl)amino)-2-fluoro-*N*-(piperidin-4-yl)benzamide (**3.63**) 107

4-((4-((3-((1,1-Dimethylethyl)sulfonamido)-5-(phenethylcarbamoyl)phenyl)amino)-5-methylpyrimidin-2-yl)amino)-2-fluoro-*N*-(piperidin-4-yl)benzamide (**3.64**) 108

Methyl (3-((1,1-dimethylethyl)sulfonamido)-5-((2-((3-fluoro-4-(piperidin-4-ylcarbamoyl)phenyl)amino)-5-methylpyrimidin-4-yl)amino)benzoyl)glycinate (**3.65**) 109

3-(3-((1,1-Dimethylethyl)sulfonamido)-5-((2-((3-fluoro-4-(piperidin-4-ylcarbamoyl)phenyl)amino)-5-methylpyrimidin-4-yl)amino)benzamido)propanoic acid (**3.66**) 110

4-(3-((1,1-Dimethylethyl)sulfonamido)-5-((2-((3-fluoro-4-(piperidin-4-ylcarbamoyl)phenyl)amino)-5-methylpyrimidin-4-yl)amino)benzamido)butanoic acid hydrochloride (**3.67**) 111

(3-((1,1-Dimethylethyl)sulfonamido)-5-((2-((3-fluoro-4-(piperidin-4-ylcarbamoyl)phenyl)amino)-5-methylpyrimidin-4-yl)amino)benzamido)methanesulfonic acid hydrochloride (**3.68**) 112

4-((4-((3-((1,1-Dimethylethyl)sulfonamido)-5-((2-sulfamoylethyl)carbamoyl)phenyl)amino)-5-methylpyrimidin-2-yl)amino)-2-fluoro-*N*-(piperidin-4-yl)benzamide hydrochloride (**3.69**) 113

4-((4-((3-((2-Amino-2-oxoethyl)carbamoyl)-5-((1,1-dimethylethyl)sulfonamido)phenyl)amino)-5-methylpyrimidin-2-yl)amino)-2-fluoro-*N*-(piperidin-4-yl)benzamide hydrochloride (**3.70**) 114

N-(2-Chloro-5-((5-methyl-2-(phenylamino)pyrimidin-4-yl)amino)phenyl)-2-methylpropane-2-sulfonamide (**3.71**) 115

Methyl 3-((1,1-dimethylethyl)sulfonamido)-5-((5-methyl-2-(phenylamino)pyrimidin-4-yl)amino)benzoate (**3.72**) 115

3-((1,1-Dimethylethyl)sulfonamido)-5-((5-methyl-2-(phenylamino)pyrimidin-4-yl)amino)benzoic acid (**3.73**) 116

(3-((1,1-Dimethylethyl)sulfonamido)-5-((5-methyl-2-(phenylamino)pyrimidin-4-yl)amino)benzoyl)glycine (**3.76**) 116

(3-((1,1-Dimethylethyl)sulfonamido)-5-((5-methyl-2-(phenylamino)pyrimidin-4-yl)amino)benzoyl)-*L*-phenylalanine (**3.77**). 117

N,*N*'-((2,2'-Oxybis(acetyl))bis(piperidine-1,4-diyl))bis(4-((4-((4-chloro-3-((1,1-dimethylethyl)sulfonamido)phenyl)amino)-5-methylpyrimidin-2-yl)amino)-2-fluorobenzamide)(**4.1**) 118

N,*N*'-((2,2'-(Ethane-1,2-diylbis(oxy))bis(acetyl))bis(piperidine-1,4-diyl))bis(4-((4-((4-chloro-3-((1,1-dimethylethyl)sulfonamido)phenyl)amino)-5-methylpyrimidin-2-yl)amino)-2-fluorobenzamide) (**4.2**) 119

N,*N*'-((2,2'-((Oxybis(ethane-2,1-diyl))bis(oxy))bis(acetyl))bis(piperidine-1,4-diyl))bis(4-((4-((4-chloro-3-((1,1-dimethylethyl)sulfonamido)phenyl)amino)-5-methylpyrimidin-2-yl)amino)-2-fluorobenzamide) (**4.3**) 119

N,*N*'-((4,7,10,13-Tetraoxahexadecanedioyl)bis(piperidine-1,4-diyl))bis(4-((4-((4-chloro-3-((1,1-dimethylethyl)sulfonamido)phenyl)amino)-5-methylpyrimidin-2-yl)amino)-2-fluorobenzamide) (**4.4**) 120

N,*N*'-((4,7,10,13,16-Pentaoxanonadecanedioyl)bis(piperidine-1,4-diyl))bis(4-((4-((4-chloro-3-((1,1-dimethylethyl)sulfonamido)phenyl)amino)-5-methylpyrimidin-2-yl)amino)-2-fluorobenzamide) (**4.5**) 121

N,*N*'-((4,7,10,13,16,19,22-Heptaoxapentacosanedioyl)bis(piperidine-1,4-diyl))bis(4-((4-((4-chloro-3-((1,1-dimethylethyl)sulfonamido)phenyl)amino)-5-methylpyrimidin-2-yl)amino)-2-fluorobenzamide) (**4.6**) 122

N,*N*'-((4,7,10,13,16,19,22,25,28-Nonaoxahentriacontanedioyl)bis(piperidine-1,4-diyl))bis(4-((4-((4-chloro-3-((1,1-dimethylethyl)sulfonamido)phenyl)amino)-5-methylpyrimidin-2-yl)amino)-2-fluorobenzamide)(**4.7**) 122

N,*N*'-(((Ethane-1,2-diylbis(oxy))bis(ethane-2,1-diyl))bis(piperidine-1,4-diyl))bis(4-((4-((4-chloro-3-((1,1-dimethylethyl)sulfonamido)phenyl)amino)-5-methylpyrimidin-2-yl)amino)-2-fluorobenzamide) (**4.8**) 123

N,*N*'-((Oxybis(ethane-2,1-diyl))bis(piperidine-1,4-diyl))bis(4-((4-((4-chloro-3-((1,1-dimethylethyl)sulfonamido)phenyl)amino)-5-methylpyrimidin-2-yl)amino)-2-fluorobenzamide) (**4.10**) 124

4,4'-(((((5,8,11-Trioxa-2,14-diazapentadecanedioyl)bis(5-((1,1-dimethylethyl)sulfonamido)-3,1-phenylene))bis(azanediyl))bis(5-methylpyrimidine-4,2-diyl))bis(azanediyl))bis(2-fluoro-*N*-(piperidin-4-yl)benzamide) (**4.11**) 125

(9*H*-Fluoren-9-yl)methyl (2-(2-(3-(4-(4-((4-((4-chloro-3-((1,1-dimethylethyl)sulfonamido)phenyl)amino)-5-methylpyrimidin-2-yl)amino)-2-fluorobenzamido)piperidin-1-yl)-3-oxopropoxy)ethoxy)ethyl)carbamate (**4.12**) 126

(9*H*-Fluoren-9-yl)methyl (2-(2-(2-(3-(4-(4-((4-((4-chloro-3-((1,1-dimethylethyl)sulfonamido)phenyl)amino)-5-methylpyrimidin-2-yl)amino)-2-fluorobenzamido)piperidin-1-yl)-3-oxopropoxy)ethoxy)ethoxy)ethyl)carbamate (**4.13**) 127

(9H-Fluoren-9-yl)methyl (15-(4-(4-((4-((4-chloro-3-((1,1-dimethylethyl)sulfonamido)phenyl)amino)-5-methylpyrimidin-2-yl)amino)-2-fluorobenzamido)piperidin-1-yl)-15-oxo-3,6,9,12-tetraoxapentadecyl)carbamate (**4.14**) 128

(9H-Fluoren-9-yl)methyl (18-(4-(4-((4-((4-chloro-3-((1,1-dimethylethyl)sulfonamido)phenyl)amino)-5-methylpyrimidin-2-yl)amino)-2-fluorobenzamido)piperidin-1-yl)-18-oxo-3,6,9,12,15-pentaoxaoctadecyl)carbamate (**4.15**) 129

4-((4-((4-Chloro-3-((1,1-dimethylethyl)sulfonamido)phenyl)amino)-5-methylpyrimidin-2-yl)amino)-*N*-(1-(3-(2-(2-(3-((1,1-dimethylethyl)sulfonamido)-5-((5-methyl-2-((4-(piperidin-4-ylcarbamoyl)phenyl)amino)pyrimidin-4-yl)amino)benzamido)ethoxy)ethoxy)propanoyl)piperidin-4-yl)-2-fluorobenzamide (**4.16**) 130

4-((4-((4-Chloro-3-((1,1-dimethylethyl)sulfonamido)phenyl)amino)-5-methylpyrimidin-2-yl)amino)-*N*-(1-(1-(3-((1,1-dimethylethyl)sulfonamido)-5-((5-methyl-2-((4-(piperidin-4-ylcarbamoyl)phenyl)amino)pyrimidin-4-yl)amino)phenyl)-1-oxo-5,8,11-trioxa-2-azatridecan-13-oyl)piperidin-4-yl)-2-fluorobenzamide(**4.17**) 131

4-((4-((4-Chloro-3-((1,1-dimethylethyl)sulfonamido)phenyl)amino)-5-methylpyrimidin-2-yl)amino)-*N*-(1-(1-(3-((1,1-dimethylethyl)sulfonamido)-5-((5-methyl-2-((4-(piperidin-4-ylcarbamoyl)phenyl)amino)pyrimidin-4-yl)amino)phenyl)-1-oxo-5,8,11,14-tetraoxa-2-azaheptadecan-17-oyl)piperidin-4-yl)-2-fluorobenzamide (**4.18**) 132

4-((4-((4-Chloro-3-((1,1-dimethylethyl)sulfonamido)phenyl)amino)-5-methylpyrimidin-2-yl)amino)-*N*-(1-(1-(3-((1,1-dimethylethyl)sulfonamido)-5-((5-methyl-2-((4-(piperidin-

133

4-ylcarbamoyl)phenyl)amino)pyrimidin-4-yl)amino)phenyl)-1-oxo-5,8,11,14,17,20-hexaoxa-2-azatricosan-23-oyl)piperidin-4-yl)-2-fluorobenzamide (**4.19**)

(*S*)-2-(4-(4-Chlorophenyl)-2,3,9-trimethyl-6*H*-thieno[3,2-*f*][1,2,4]triazolo[4,3-*a*][1,4]diazepin-6-yl)acetic acid (**4.20**) 133

(*S*)-4-((4-((4-Chloro-3-((1,1-dimethylethyl)sulfonamido)phenyl)amino)-5-methylpyrimidin-2-yl)amino)-*N*-(1-(1-(4-(4-chlorophenyl)-2,3,9-trimethyl-6*H*-thieno[3,2-*f*][1,2,4]triazolo[4,3-*a*][1,4]diazepin-6-yl)-2-oxo-6,9,12-trioxa-3-azatetradecan-14-oyl)piperidin-4-yl)-2-fluorobenzamide (**4.21**) 134

2-(4-(2-Aminoethoxy)-3,5-dimethylphenyl)-5,7-dimethoxyquinazolin-4(1*H*)-one (**4.22**) 135

2,2'-((Oxybis(ethane-2,1-diyl))bis(oxy))bis(*N*-(2-(4-(5,7-dimethoxy-4-oxo-1,4-dihydroquinazolin-2-yl)-2,6-dimethylphenoxy)ethyl)acetamide) (**4.23**) 136

N^1,N^{25}-Bis(2-(4-(5,7-dimethoxy-4-oxo-1,4-dihydroquinazolin-2-yl)-2,6-dimethylphenoxy)ethyl)-4,7,10,13,16,19,22-heptaoxapentacosanediamide (**4.24**) 136

1-(4-(5,7-Dimethoxy-4-oxo-1,4-dihydroquinazolin-2-yl)-2,6-dimethylphenoxy)-4-oxo-6,9,12-trioxa-3-azatetradecan-14-oic acid (**4.25**) 137

1-(4-(5,7-Dimethoxy-4-oxo-1,4-dihydroquinazolin-2-yl)-2,6-dimethylphenoxy)-4-oxo-7,10,13,16,19,22,25-heptaoxa-3-azaoctacosan-28-oic acid (**4.26**) 137

4-((4-((4-Chloro-3-((1,1-dimethylethyl)sulfonamido)phenyl)amino)-5-methylpyrimidin-2-yl)amino)-*N*-(1-(1-(4-(5,7-dimethoxy-4-oxo-1,4-dihydroquinazolin-2-yl)-2,6-dimethylphenoxy)-4-oxo-6,9,12-trioxa-3-azatetradecan-14-oyl)piperidin-4-yl)-2-fluorobenzamide (**4.27**) 138

N^1,N^{25}-Bis(2-(4-(5,7-dimethoxy-4-oxo-1,4-dihydroquinazolin-2-yl)-2,6-dimethylphenoxy)ethyl)-4,7,10,13,16,19,22-heptaoxapentacosanediamide (**4.28**) 139

List of Abbreviations

ACN	acetonitrile
ADME	absorption, distribution, metabolism, and excretion
AlphaScreen	amplified luminescent proximity homogenous assay screen
ATPase	adenosine triphosphatase
BD	bromodomain structural element
BD1	first bromodomain (of tandem bromodomains)
BD2	second bromodomain (of tandem bromodomains)
BET	bromodomain and extra terminal domain
BINAP	2,2′-bis(diphenylphosphino)-1,1′-binaphthyl
Boc	tert-butoxycarbonyl
BRD	bromodomain-containing protein
BODIPY	fluorinated boron-dipyrromethene
BRDT	testes-specific bromodomain-containing protein (human)
Brdt	testes-specific bromodomain-containing protein (mouse)
CatSper	calcium channel of sperm
CDK	cyclin-dependent kinase
CID	chemically induced dimerization
dba	dibenzylideneacetone
DCE	1,2-dichloroethane
DCM	dichloromethane
DIAD	diisopropyl azodicarboxylate
DIEPA	*N,N*-diisopropylethylamine
DMF	*N,N*-dimethylformamide
DMS	dimethyl sulfoxide
DSF	differential scanning fluorimetry
EDC	*N*-(3-dimethylaminopropyl)-*N′*-ethylcarbodiimide hydrochloride
ET Domain	extra-terminal domain
EtOAc	ethyl acetate
Fmoc	fluorenylmethyloxycarbonyl protecting group

FLT3	fms-like tyrosine kinase 3
FP	fluorescence polarization
FRET	fluorescence resonance energy transfer
GAPDHS	glyceraldehyde-3-phosphate dehydrogenase
H-bond	hydrogen bond
HATs	histone acetyltransferases
HATU	1-[bis(dimethylamino)methylene]-1H-1,2,3-triazolo[4,5-b]pyridinium 3-oxid hexafluorophosphate
HCl	hydrochloric acid
HDACs	histone deacetylases
HOBt	1-hydroxybenzotriazole
HOMO	highest occupied molecular orbital
HPLC	high-performance liquid chromatography
HTS	high-through-put screening
H1T	testis-specific histone
H3/H4	histone 3/4
IC_{50}	half maximal inhibitory concentration
ITC	isothermal titration calorimetry
JAK2	Janus kinase 2
Kac	acetylated-lysine
K_d	dissociation constant
K_i	inhibition constant
Kac	lysine acetyltransferase
LUMO	lowest unoccupied molecular orbital
mCPBA	meta-chloroperoxybenzoic acid
MeOH	methanol
MM	multiple myeloma
MM/GBSA	molecular mechanics/Generalized Born surface area
MM/PBSA	molecular mechanics/Poisson Boltzmann surface area
NMR	nuclear magnetic resonance
PEG	polyethylene glycol

PK	pharmacokinetics
PLK1	polo-like kinase 1
PPI	protein-protein interaction
PPII	protein-protein interaction interfaces
PRMT5	arginine-specific histone methyltransferase 5
P-TEFb	positive transcription elongation factor b
RNA Pol II	phosphorylate RNA polymerase II
RAR	retinoic acid receptor
SAR	structure-activity relationship
STAB	sodium triacetoxyborohydrate
SWI/SNF	switch mating type/sucrose nonfermenting
TEA	triethylamine
TFA	trifluoroacetic acid
THF.	tetrahydrofuran
Tndm	tandem
TLC	thin-layer chromatography
TPP	triphenylphosphine
TPs	transition proteins
TRF	time-Resolved Fluorescence
TR-FRET	time-resolved fluorescence energy transfer
TRIM28	tripartite motif-containing 28
TSS	transcriptional start sites
TSSK	testis-specific serine/threonine kinases
UV	ultraviolet
VDW	Van der Waals
WT	wild-type
WPF	tryptophan-proline-phenylalanine

Chapter 1: Introduction

1.1 General Background. Birth control is not a new concept in history. Family planning and economic capacity have always been considered when it comes to family planning. The use of contraceptives is the most common method to avoid unplanned pregnancy today. Despite various contraceptive options for women, male contraceptives are limited to barrier methods and irreversible surgical options like vasectomy. Testosterone, testosterone analogs, and combinations with progestins have been evaluated in multiple clinical trials.[1, 2] Recent research revealed increasing evidence that the use of exogenous testosterone or its analogs can cause mental issues[3] and cardiovascular side effects[4] due to endocrine disruption[5]. Therefore, there is an urgent need for new non-hormonal male conceptive drug discovery and development. The rapid development of reproductive biology and characterization of biological systems facilitated the discovery of new targets for male contraception, including testis-specific serine/threonine kinases (TSSK1-6),[6-9] cation channels of sperm (CatSper),[10] cyclin-dependent kinase 2 (CDK2),[11, 12] retinoic acid receptor α (RAR α),[13, 14] testis-specific bromodomain (BRDT),[15] sodium–potassium adenosine triphosphatase (Na^+/K^+-ATPase),[16, 17] glyceraldehyde-3-phosphate dehydrogenase (GAPDHS)[18] and others.[2, 19] Many of these ongoing projects are moving toward a safe and effective male contraceptive agent. For the purposes of this dissertation, the focus is on testis-specific bromodomain studies to discover and develop a male contraceptive.[20]

1.2 BET proteins. Bromodomains are evolutionarily conserved sequence motifs that identify acetylated lysine residues in many epigenetic controls of gene expression.[21] The bromodomain family is highly diverse. A total of 61 different bromodomains were found in 46 proteins (**Figure 1.1**),[22] where some of these proteins contain more than one bromodomain in the same construct. Each bromodomain has around 110 amino acids with at least 30% sequence identity.[23-25] They share a conserved structural motif composed of a left-handed bundle of four alpha helices (αZ, αA, αB, αC) that are linked by two variable loop regions (ZA and BC loops) and flank a deep central hydrophobic cavity that recognizes sequences containing ε-N-acetylated lysine residues.[2] The bromodomain and

extra terminal domain (BET) family, consisting of BRD2, BRD3, BRD4, and BRDT, contains N- and C-terminal BRDs (designated as BD1 and BD2, respectively) in tandem that have pivotal roles in regulating the transcription of growth-promoting genes and cell cycle regulators.[3]

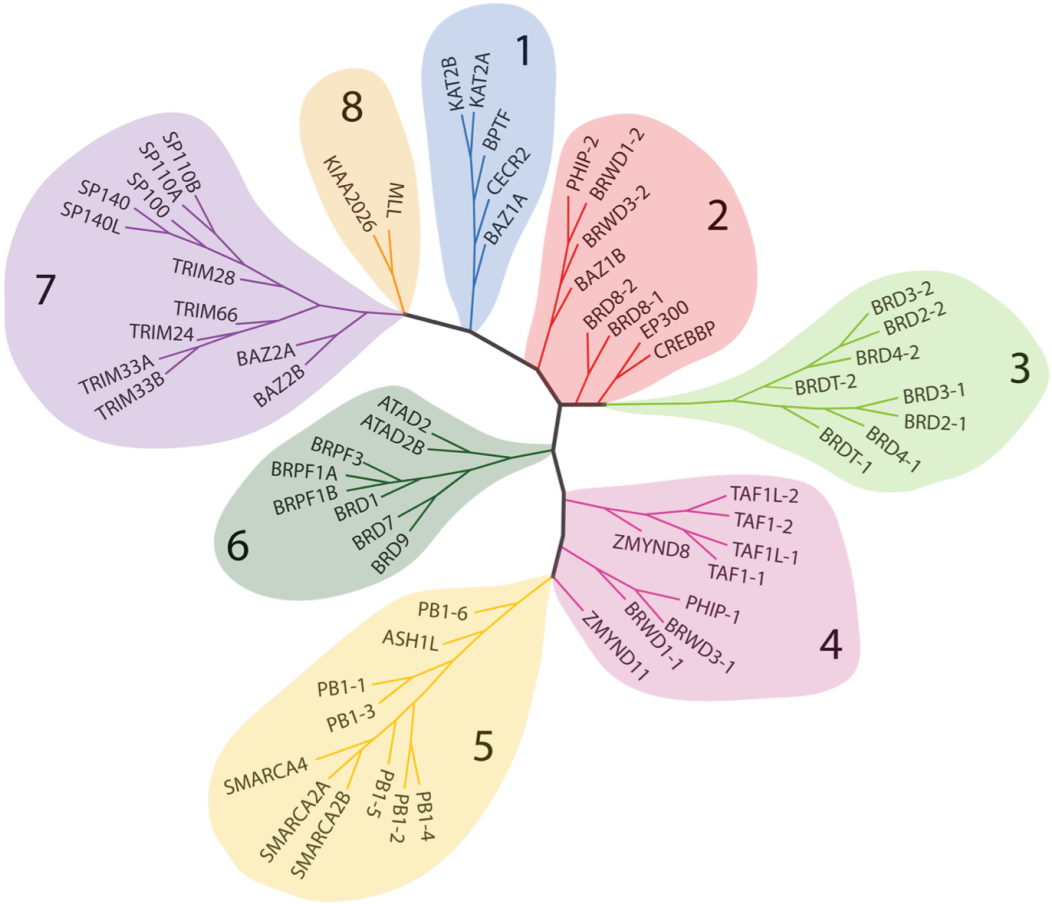


Figure 1.1 Phylogenetic tree of the human bromodomain proteins. Reprinted with permission from reference 22. Copyright (2016) American Chemical Society.

During cell division in humans, most genes are transcriptionally silenced. However, BET family protein genes are still active in mitosis (*BRD2*, *BRD3*, *BRD4* genes) and meiosis (*BRDT* gene) for epigenetic regulation.[26] In a typical transcription procedure (**Figure 1.2**),[27] histone acetyltransferases (HATs) work as epigenetic writers by labeling histone tails with epigenetic marks (acetyl groups) on lysine residues.[28] The acetylation of positively-charged lysine residues disrupts the histone-DNA complex.[22] Chromatin then becomes uncompacted and the corresponding genes are exposed for expression. BET family proteins are considered epigenetic reader proteins like the other bromodomain

family members (**Figure 1.2**).[29] The BET proteins interact with acetylated lysine residues of histones and regulate transcription through a multiprotein complex (discussed below).[28] Finally, epigenetic erasers such as histone deacetylases (HDACs) remove epigenetic marks to terminate the transcription process.[28] The deacylated chromatin becomes compacted and inactive for gene expression.

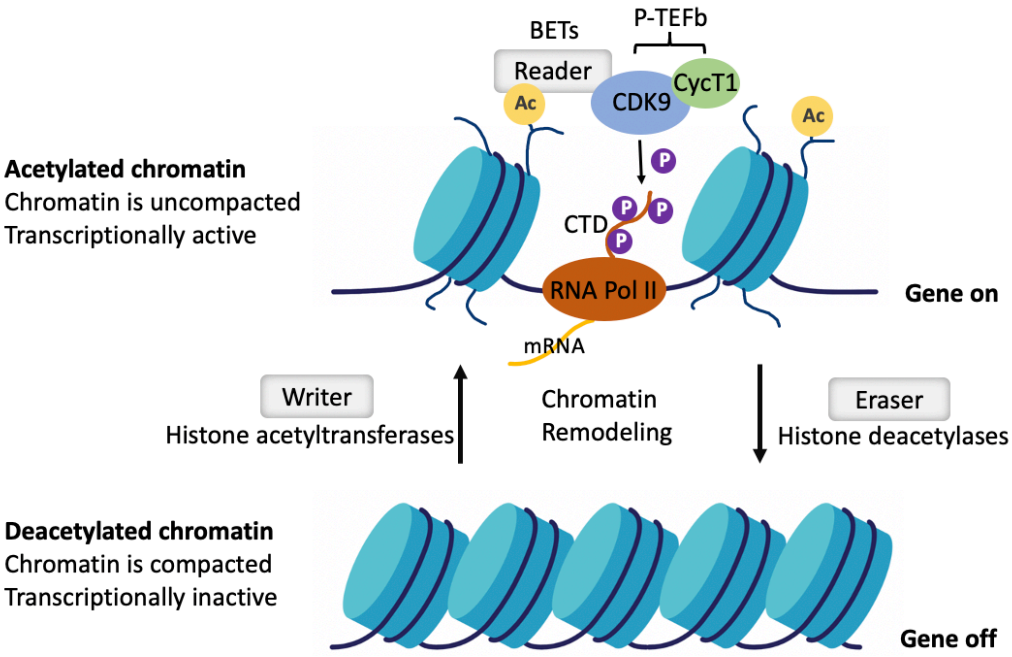


Figure 1.2 Acetylation of histone tails induces chromatin remodeling to activate transcription. Adapted with permission from reference 27 by permission of Springer Nature © 2014.

BETs identify acetylated histones and activate transcription through recruitment of the positive transcription elongation factor (P-TEFb) complex (**Figure 1.2**).[30, 31] Cyclin-dependent kinase-9 (CDK9) together with its regulatory partner cyclin T1 are key members of P-TEFb, which phosphorylates RNA polymerase II (RNA Pol II) at Ser2 and Ser5 during promoter clearance.[26, 30, 32] The phosphorylated RNAPII binds to the upstream promoter of a specific gene to start transcriptional elongation of mRNA.[33] One of the most famous BET-controlled genes is the *c-Myc* gene[34], which is highly overexpressed in the majority of human cancers.[35, 36] The discovery that inhibiting BET proteins downregulated c-Myc levels established the rationale for targeting BET family proteins in anticancer therapy.

P-TEFb is not the only protein that binds to BETs. BRD2 also forms a complex with the E2F transcription factors and the switch mating type/sucrose nonfermenting

(SWI/SNF) complex for diverse gene transcription.[37] BRDT binds to histone deacetylase 1 (HDAC1), arginine-specific histone methyltransferase 5 (PRMT5) and the tripartite motif-containing 28 (TRIM28) protein to form a transcription-regulating complex.[38]

1.3 Role of Brdt in gametogenesis. Mammalian sperms are produced in the testes through gametogenesis. In order to study the role of human BRDT in gametogenesis, mouse Brdt was studied in many animal models. Mouse Brdt shares 72% of identity with human BRDT and both of them are highly expressed in testis[39, 40].

Gametogenesis is a unique and complicated biological process *in vivo*.[41] Spermatogonia (diploid germ cells) are first differentiated to spermatocytes through meiosis I. The generated spermatocytes then become spermatids (haploid cells) through meiosis II, and will be differentiated to spermatozoa in a post-meiotic process that follows. This three-step procedure (**Figure 1.3**) finally gives four spermatozoa or sperms with only one copy of each chromosome from the original spermatogonia. During gametogenesis, the volume of the nucleus will decrease 10-fold[42] and most of the genetic information will be protected or transcriptionally silenced through chromatin compaction.[26] However, Brdt is reported to be active during meiosis.[43] Brdt exhibits a stage-specific function during gametogenesis.[44] After the activation of genes encoding the Brdt protein, spermatogonia move to the early stage of meiosis (**Figure 1.3**).[45] Some somatically active genes are silenced and a set of spermatogenic genes are activated by Brdt, which is highly expressed in spermatocytes. Brdt regulates gene transcription through epigenetic machinery by identifying acetylated histones and regulating testis-specific genes through P-TEFb complex recruitment (**Figure 1.4**).[44] P-TEFb phosphorylates RNA Pol II to initiate testis-specific RNA elongation. In this stage, Brdt also binds to transcriptional start sites of a group of post-meiotic genes (also referred to as bookmarking, see **Figure 1.3**) for their later expression in the spermatid stage.[46] During post-meiosis, Brdt induces chromatin compaction through hyperacetylated H4 binding.[47] In addition to H4K5ac and H4K8ac, further acetylation of four lysines in the histone H4 tail is considered a signature of hyperacetylated H4.[45, 48-51] Removal of hyperacetylated H4 histones is an important sign of chromatin compaction after meiosis.[52] In functional cellular assays, Brdt interacted with hyperacetylated H4 to initiate acetylation-dependent histone removal, which finally

induced chromatin compaction in post-meiotic cells.[47] The Brdt protein level stays high until genome-wide histone removal (**Figure 1.3**).

To better understand the role of Brdt, partial functional or dysfunctional Brdt models were generated in mouse cells. Mouse cells expressing a dominant negative form of Brdt in spermatogonia induced apoptosis and decreased generation of spermatocytes.[44, 45] Spermatogonia with total absence of Brdt (Brdt-KO) could still transfer to spermatocytes but stopped at the third stage (pachytene stage, **Figure 1.3**) in meiosis prophase 1.[44, 45] Mutation of Brdt-1 (*Brdt*$^{\Delta BD1/\Delta BD1}$) did not influence gametogenesis until the post-meiotic phase, and normal elongating spermatids could be generated but failed to replace the histone with transition proteins (TPs) and protamine.[44] TPs and protamine are both involved in sperm chromatin condensation. In normal spermatids, histones in the sperm nuclei are first replaced by TPs, then the TPs are replaced by protamine to pack the genome into a highly condensed nucleus.[53-55] Disruption of the histone-to-protamine transition leads to male infertility.[56]

Further studies disclosed more information about the function of each bromodomain of BRDT. Structural biology studies found that the first bromodomain of BRDT (BRDT-1) bound to acetylated K5 and K8 on the H4 tail.[57] When K5 or K8 have a single acetylation mark, their binding affinity for H4 decreases by more than 50-fold.[58] Subsequent research also indicated that BRDT-1 interacted with DNA to aid histone binding.[59] The function of the second bromodomain of BRDT (BRDT-2) has been characterized as marginalized or minor, because it did not bind to acetylated histone tails like other BRDs.[59] However, some evidence has shown that TPs and protamine are suspected to associate with BRDT-2 and contribute to BRDT-dependent post-meiotic differentiation.[59]

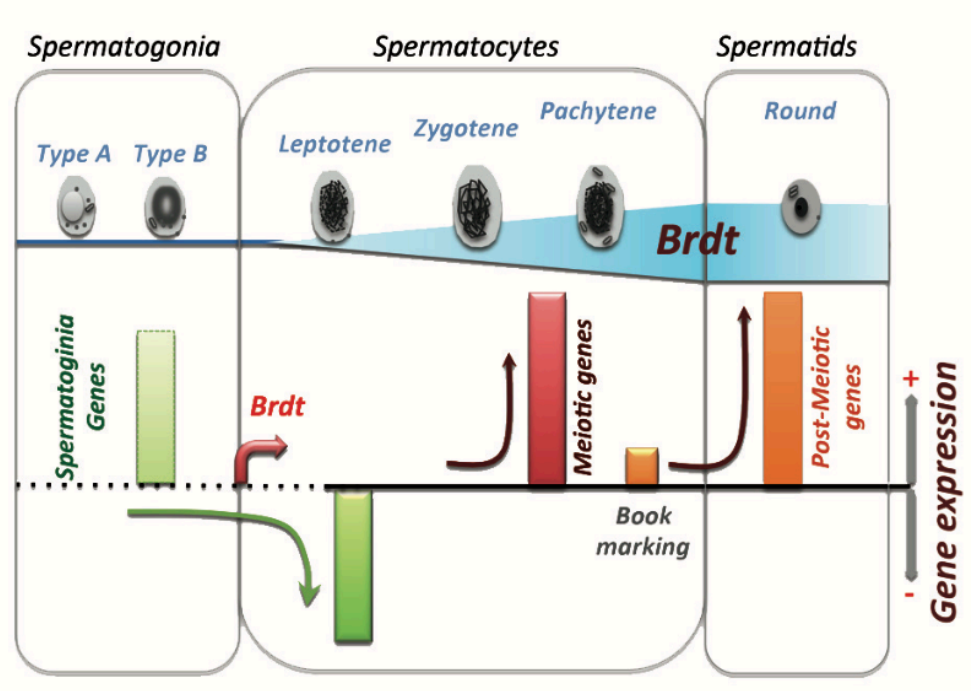


Figure 1.3 Brdt expression level at different stages in mouse gametogenesis. Reprinted from reference 45

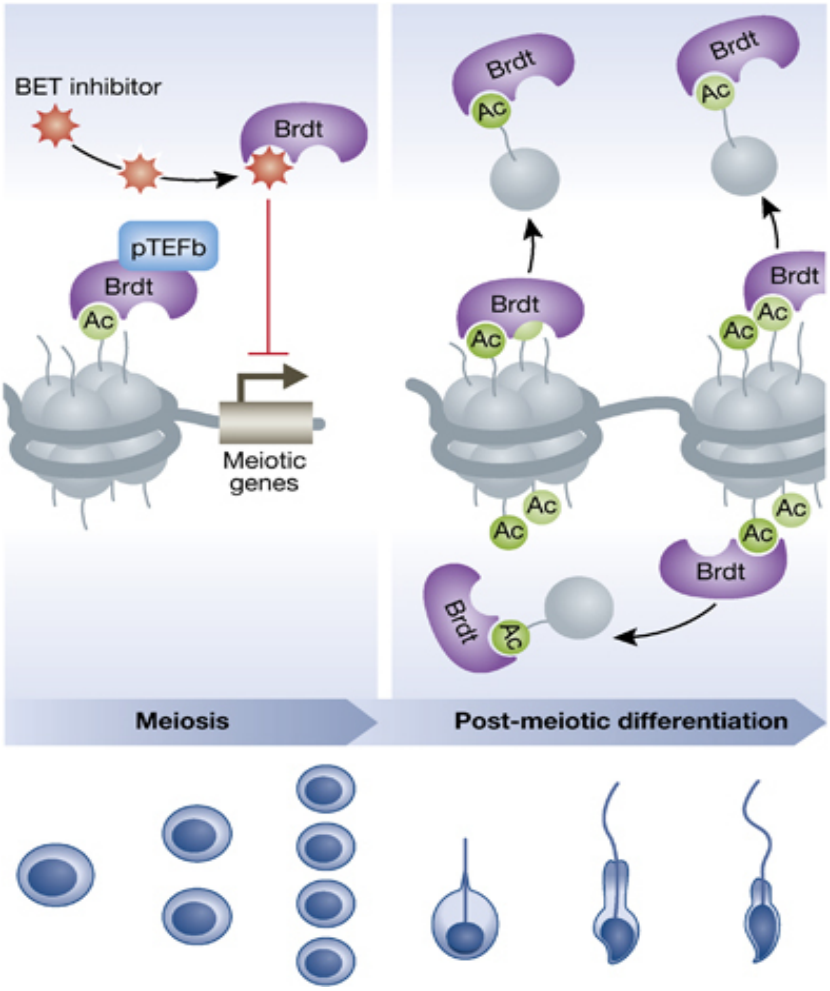


Figure 1.4 Role of Brdt in meiosis and post-meiotic differentiation. Reproduced from reference 48 by permission of John Wiley & Sons, Ltd.

1.4 BRDT: target for male contraception. The experimental evidence above indicated that BRDT plays an important role in meiotic/post-meiotic gene expression, chromatin compaction and histone removal at different stages during gametogenesis. In 2007, Dr. Wolgemuth's group discovered the Brdt truncated mice (*Brdt*$^{\Delta BD1/\Delta BD1}$) were viable and healthy but infertile.[43] Compared to normal mice, *Brdt*$^{\Delta BD1/\Delta BD1}$ homozygous male mice generated a clearly reduced number of sperms with lower motility. Moreover, many of these sperm were also deformed (**Figure 1.6**).[43] In addition, the *BRDT* gene is kept silent in most somatic tissues and is exclusively found in the testis (**Figure 1.5a**).[60, 61] It is also believed that BRDT is a tissue-specific paralogue of BRD4.[44, 61] BRDT levels are also

much higher than those of BRD4 in the testes due to the active meiosis.[61] In contrast, BRD4 is ubiquitously expressed in the somatic cells for mitosis (**Figure 1.5b**). These results imply that BRDT is a good male conceptive target with high specificity and low risk of non-testis organ disruption.

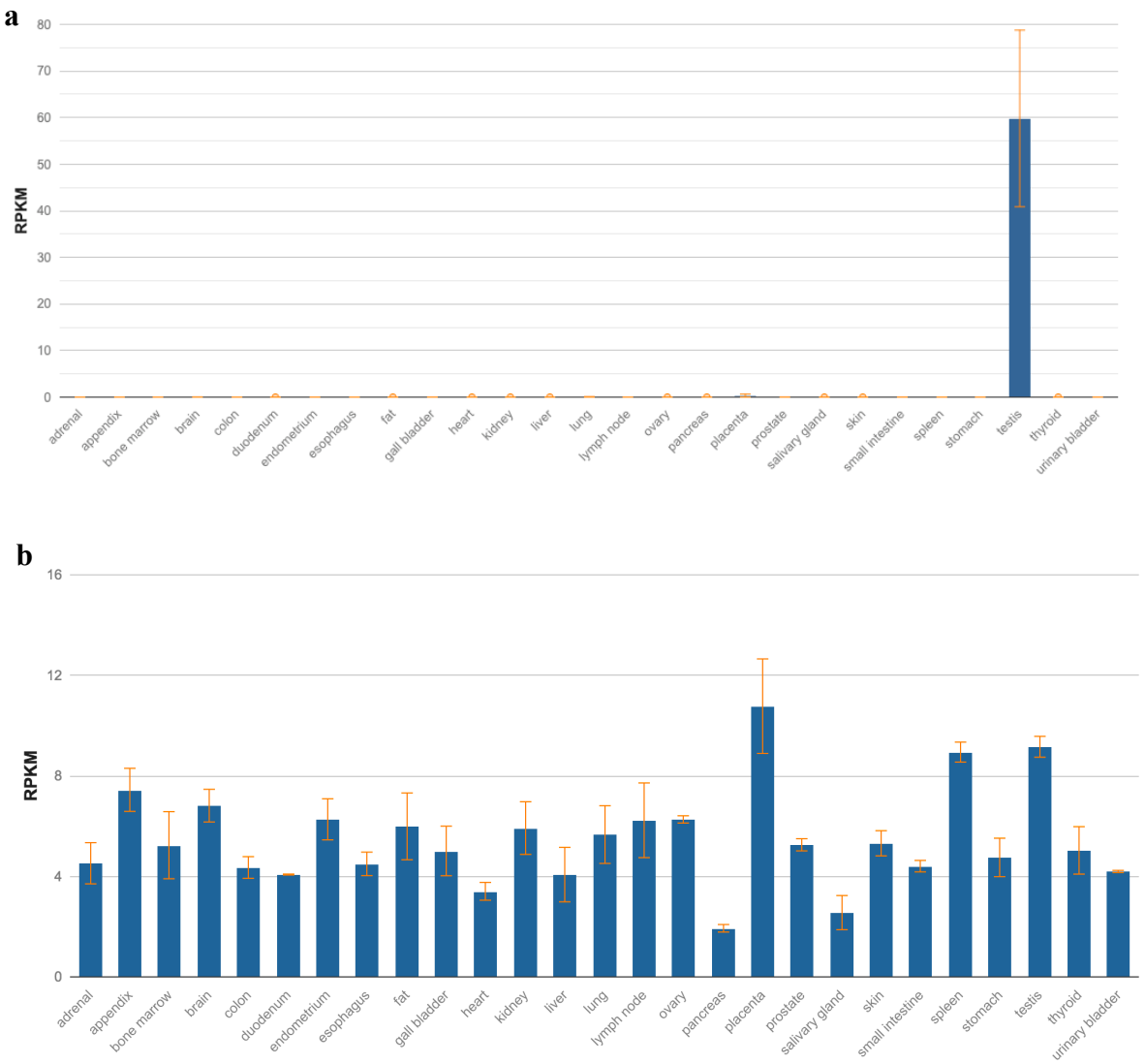


Figure 1.5 (a) BRDT and (**b**) BRD4 expression levels in human tissues. Figure was generated using data from the NCBI protein database.[61, 62] Error bars denote an average of results from multiple (2 to 7 different samples) tissue samples. RPKM: Reads Per Kilobase of transcript per Million mapped reads is a normalized unit of transcript expression.

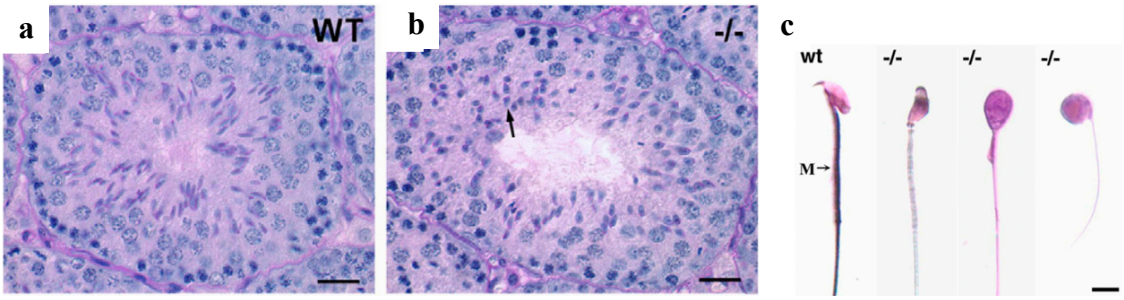


Figure 1.6 Brdt-1 mutant epididymal sperm are abnormal. (**a**, **b**) wild-type (**a**) and Brdt mutant (**b**) mouse histological sections of testes stained by PAS; (**c**) Light microscopy image of sperm from wild-type and *Brdt*$^{\Delta BD1/\Delta BD1}$. Reproduced from reference 43 with the permission of The Company of Biologists Ltd.

1.5 BRDT structure and the Kac site. The human BRDT protein consists of 947 amino acids and features two bromodomains and an ET tail. (**Figure 1.7b**) The bromodomains of BRDT both have conserved structural motifs composed of a left-handed bundle of four alpha helices (αZ, αA, αB, αC) that are linked by two variable loop regions (ZA and BC loops) and flank a deep central hydrophobic cavity that recognizes sequences containing ε-N-acetylated lysine residues (**Figure 1.7a**). In **Figure 1.7c**, the acetylated lysine residue (H4K5ac) forms a H-bond with Asn109, which is the key interaction between BRDT-1 and histone H4 subunit. H4K8ac, the second acetylated lysine of H4, is close to the tryptophan-proline-phenylalanine (WPF) shelf. The hydrophobic interaction between H4K8ac and the WPF shelf confers histone binding affinity.[58] Five conserved waters are spread deep inside the binding site through a H-bond network and form interactions with the backbone of protein residues Tyr66 and Pro51. As seen in Figures **1.7a** and **1.7c**, the water network extends from Asn109 to the ZA channel.

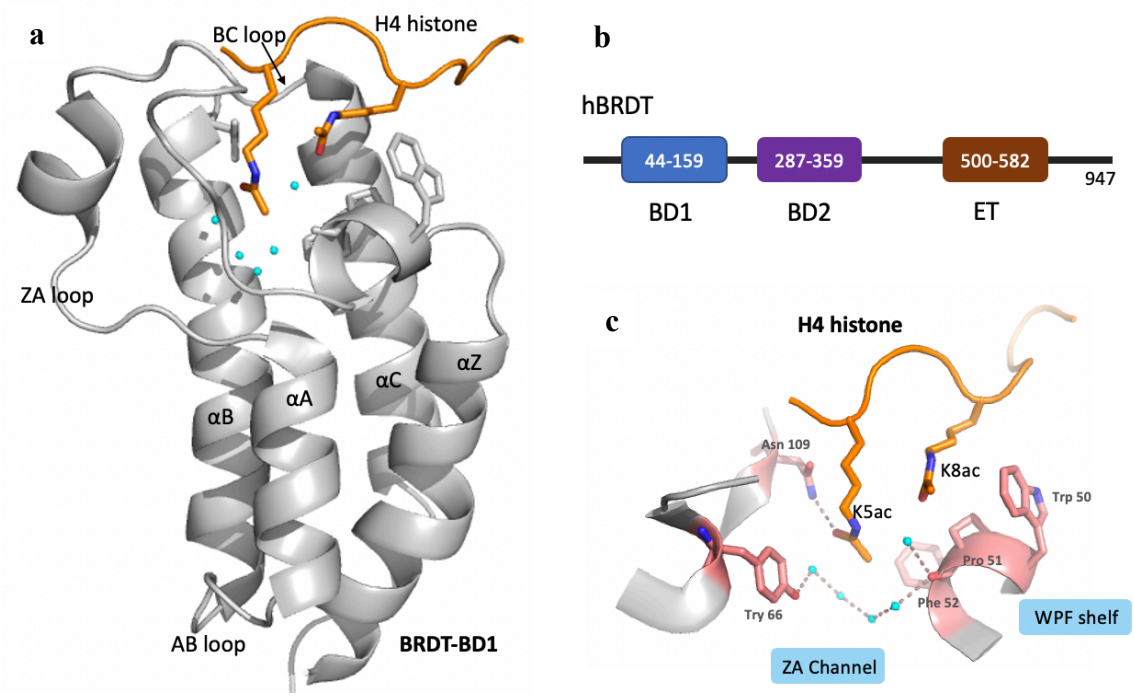


Figure 1.7 Overall structural motifs, domains and binding site architecture of BRDT. (**a)** BRDT-1structure. (**b)** domains of BRDT. **(c)** Kac pocket of BD1 with the orientation of the histone H4 protein. (PDB: 2WP2)

1.6 Strategies for BRDT inhibition. Interfering with protein-protein interactions (PPIs) can be very challenging due to the lack of a clearly defined binding site. However, the Kac site in BRDT is biologically well defined, and a considerable number of small molecule inhibitors have been explored and evaluated. Small molecule inhibitors were designed to mimic acetylated lysine and form interactions with the conserved Asn109 in BRDT-1. Further, based on these inhibitors, bivalent strategies were also introduced to improve BET inhibition activity through dual-bromodomain binding.

1.6.1 BRDT inhibitors. JQ-1 is the first validated BRDT inhibitor developed by the Bradner lab in 2012.[15] It features a benzodiazepine structure, which is a widely used scaffold in medicinal chemistry. Crystallographic studies disclosed that the benzodiazepine core formed a pair of H-bonds with Asn109 of BRDT-1 (PDB: 4FLP).[15] In ITC assays, JQ-1 exhibited a K_d of 190 nM for BRDT-1 and 44 nM for BRDT-2.[15] JQ-1 treated mice were infertile with decreased testis size, spermatozoa number and sperm motility. Infertility induced by JQ-1 was reversible in the first or second generation without hormone

disruption.[15] These promising JQ-1 results validated pharmacologically that BRDT inhibition is a possible target for male contraception.[15] However, JQ-1 is a pan-inhibitor for all BET family members. Several JQ1 analogs are in clinical trials for anticancer therapy.[63] Instead of meiosis, BRD4 regulates mitosis *in vivo* and is widespread throughout multiple important organs in humans. Lymphocyte toxicity, body weight loss and cognitive defects were observed in animal assays after treatment with JQ-1.[64, 65] Modification of JQ-1 led to several other benzodiazepine analogs with good BRDT inhibition activity, but these benzodiazepine analogs still fail to distinguish BRDT from BRD4 effecticely.[66-70]

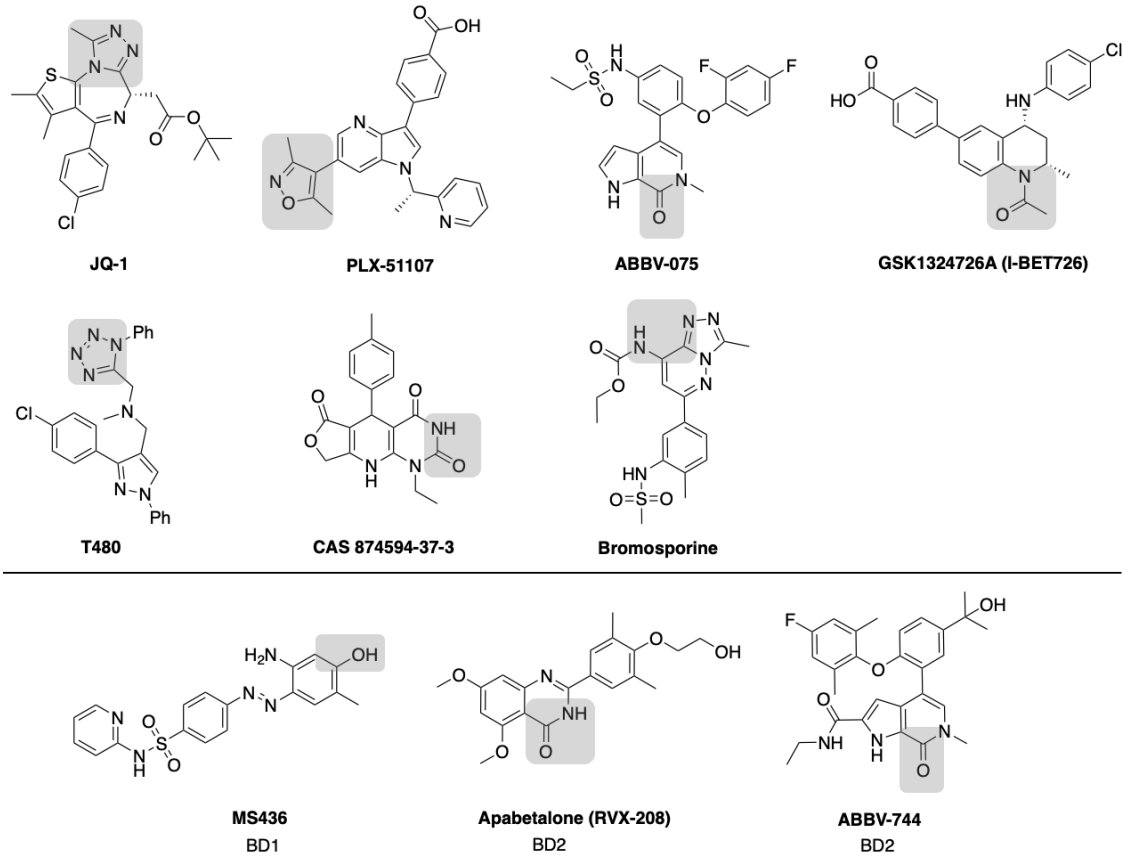


Figure 1.8 Representative potent chemotypes of BRDT inhibitors. Grey box denotes moiety of the small molecule that interacts with conserved Asn residue in the Kac site of BET family proteins.

In addition to the benzodiazepine scaffold, isoxazole, pyridine, tetrazole and even phenol can be recruited as acetylated lysine mimics (**Figure 1.8**). PLX-51107 with an isoxazole chemotype was shown to be a potent pan-BET, showing a K_d of 1.7 nM for BRD4-1 in a time-resolved fluorescence resonance energy transfer (TR-FRET) assay.[71]

ABBV-075 was generated by Abbvie as a potent inhibitor for BET proteins (K_i = 12.2 nM for BRDT-1, TR-FRET assay).[72] The 2-pyridone carbonyl of ABBV-075 inserted into the Kac pocket and formed a H-bond with Asn140 of BRD4-1. GSK1324726A (I-BET726) directly recruited an acetylated nitrogen functionality as a acetylated lysine side chain mimic and exhibited single-digit nanomolar affinity for BRDT-1.[73] Compound T480 came from a virtual screen and was validated as a BET inhibitor with 9.0 μM IC_{50} for BRDT-1.[74] In their computational prediction of binding mode, the substituted tetrazole moiety showed potential ability to form a H-bond with Asn140. The dihydropyridopyrimidine scaffold of CAS 874594-37-3 came from another virtual screen in the Georg group.[75] Part of the uracil-like moiety interacted with Asn140 of BRD4-1 and may be promising for Asn109 binding in BRDT-1. Bromosporine was also found to be a very potent pan-BET inhibitor with a double-digit nanomolar K_d for BRDT-1 by ITC.[76] The triazolopyridazine scaffold and NH in the carbamate side chain form a pair of H-bonds with Asn140 in BRD4-1.

The compounds above are all pan-BET inhibitors for the BET family of bromodomain-containing proteins. Interestingly, despite sequence similarity between BD1 and BD2, some of compounds exhibited domain selectivity. For example, PLX-51107 was 24-fold more potent for BRDT-1 over BRDT-2.[71] For other BET family proteins, the domain selectivity of this compound diminished. MS436 was reported as a BD1-selective inhibitor, where the phenol group of MS436 served as chemotype to approach Asn140 of BRD4.[77] By FP assay, it showed a K_i of 450 nM for BRDT-1 and 3-fold lower activity for BRDT-2.[78] Apabetalone (RVX-208) is BD2-selective with 8- to 20-fold selectivity over BD1 for all BET protein family members.[79] RVX-208 contains a lactam moiety that mimics acetylated lysine of H4K5ac. Micromolar and high nanomolar K_d values were detected for BRDT-1 and BRDT-2, respectively.[79] The reduced potency was presumably due to the lack of direct interaction potential with the WPF shelf in the Kac pocket. ABBV-744 shares the same scaffold with ABBV-075, which exhibited more than 95-fold selectivity for BRDT-1 (K_d = 2.1 nM) over BRDT-2 (K_d = 3300 nM) in a surface plasmon resonance (SPR) assay.[80]

Several kinase inhibitors, like dinaciclib, BI2536 and TG101209, exhibited considerable BRDT activity (**Figure 1.9**).[81, 82] As mentioned above, BRD4 and some

kinases are key factors of mitotic regulation. A dual kinase-bromodomain inhibition strategy was generated to overcome drug resistance induced by kinase inhibition. In early pharmacology studies, kinase inhibitor resistant AML cells were proven to be sensitive to BRD4 inhibition.[83] A successful example is SG3-179, which is an analog of kinase inhibitor TG101209. TG101209 is a 2,4-disubstitued pyrimidine derivative with an IC_{50} of 0.51 nM for Janus kinase 2 (JAK2) and sub-micromolar activity for BET family proteins.[84] The co-crystal structure with TG101209 proved that it bound to BRD4-1 at the Kac site.[85] The pyrimidine nitrogen and the adjacent amine group of TG101209 mimicked H4K5ac and formed a pair of H-bonds with the conserved asparagine found in bromodomains (Asn140 of BRD4-1). A similar binding mode was found in the crystal structure of TG101209 in complex with the JAK2 complex (PDB: 4ji9).[86] The aminopyrimidine moiety of TG101209 also formed a pair of H-bonds with Leu932 of JAK2. Further modification of TG101209 lead to the discovery of more potent BET-JAK2 dual inhibitor SG3-179 with double-digit nanomolar activity for BET family proteins and JAK2.[85]

Kinase inhibitor BI2536 and dinaciclib also exhibited BET family protein activity. BI2536 is a Polo-like kinase 1 (Plk1) inhibitor, which showed a 260 nM IC_{50} for BRDT-1 in the AlphaScreen assay. The dihydropteridine oxygen of BI2536 contributed to H-bond formation with Asn109 (PDB: 5VBQ). Dinaciclib is a very potent ATP site binder for CDK1, CDK2, CDK5 and CDK9.[87-89] Based on a previously obtained crystal structure of the BRDT-dinaciclib complex (PDB: 4KCX), its unique N-oxide moiety binds to Asn109 in the Kac site. Dinaciclib is a weak BET inhibitor with a K_d of 37 μM for BRDT-1,[81] and it is still a new scaffold for BET inhibitors, but effort has been made towards its modification in the Georg group.

The dual kinase-BET inhibitors provide new scaffolds for rapid BRDT inhibitor discovery. However, targeting both kinases and the BET family is not always a beneficial strategy. For example, the most frequent adverse events after JAK2 inhibitor treatment are blood cell differentiation, anemia, thrombocytopenia and other hematologic defects.[90] These inevitable safety concerns of kinase inhibition imply that BET selectivity needs to be achieved for contraceptive purposes, since the treatment group will be healthy individuals.

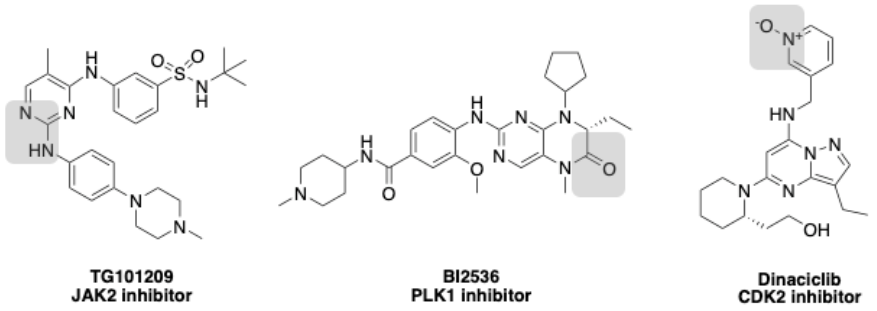


Figure 1.9 Dual BET bromodomain-kinase inhibitors. Grey box denotes moiety of the small molecule that interacts with conserved Asn residue in the Kac site of BET family proteins.

1.6.2 Bivalent inhibitors. In the bromodomain super family, BET family proteins contain two bromodomains. In addition, the structures of BET family proteins show that all family members have a distinct linker length between the two bromodomains (**Figure 1.13**). Based on this difference, a dual-binding strategy was generated for potent and selective BET inhibitor discovery. The hypothesis is that bivalent inhibitors with two Kac site binders or chemotypes may distinguish different BET family members by linker length regulation. Through medicinal chemistry optimization of the linkers, the bivalent inhibitor MT1, a (6S)-JQ1 homodimer with a PEG7 linker (**Figure 1.10d**), with excellent inhibitory potency for several bromodomains, was identified.[91] Biophysical and biochemical efforts indicated that MT1 was an intramolecular bivalent BRD4 inhibitor (**Figures 1.10e** and **1.20f**) that was 100-fold more potent than the corresponding monovalent inhibitor JQ1 in cellular assays, presumably as a result of affinity improvement. Tumors were profoundly reduced with MT1 treatment compared to JQ1 *in vivo* and a significantly increased overall survival ratio was also observed.[91]

Beyond the JQ-1 analogs already discussed, Waring *et al*. described a focused SAR study of biBET, a bivalent triazolopyridazine probe compound (**Figure 1.10a**).[92] The X-ray co-crystal structure of biBET and BRD4-1 showed the ability of biBET to induce protein dimerization (**Figures 1.10b** and **1.10c**). NMR experiments with tandem BRD4 protein demonstrated a bivalent and in *cis* binding mode of biBET bound to BD1 and BD2 of BRD4-tandem. This bivalent probe was more potent than the monovalent ligands in BRD4 inhibition, c-Myc (MM.1S cells) downregulation and cancer cell antiproliferation.

A molecular weight of 531 and a logD7.4 = 2.9 suggested that this probe molecule might be promising as a lead for future drug discovery.

Due to the challenge of tandem BET protein crystallization, limited evidence supported that these bivalent inhibitors interact with the BET proteins intramolecularly. Instead, research showed that BET family proteins could form a homodimer in the presence of a small bivalent molecule, which is also referred to as chemically induced dimerization (CID).[91, 92]

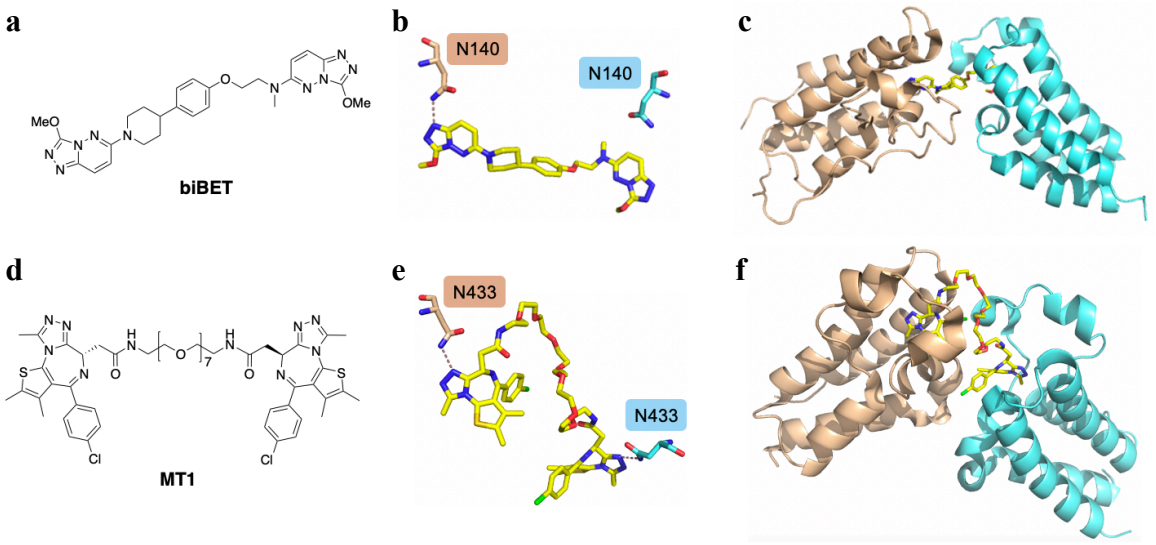


Figure 1.10 Bivalent compound biBET (PDB: 5AD3) and MT1 (PDB: 5JWM) induced the homodimerization of BRD4-1. (**a**) chemical structure of biBET. (**b**) biBET interact with N140 of BRD4-1. (**c**) biBET induced the dimerization of BRD4-1. (**d**) chemical structure of MT1. (**e**) MT1 interact with N433 of BRD4-2. (**f**) MT1 induced the dimerization of BRD4-2.

1.7 BRDT selectivity: Arg54 and bivalent strategies. Mutagenesis studies have shown that loss of the first bromodomain in BRDT results in abnormal spermatids and complete sterility in mice,[5] making BRDT-1 an attractive target for developing non-hormonal male contraceptives.[6] Due to the high identity of Kac binding sites within BRD families (**Table 1.1** and **Figure 1.11**), the greatest challenge for BRD drug discovery efforts is identifying compounds that are selective for individual BRD family proteins.[7] **Table 1.1** shows that BRDT-1 and other first bromodomains of BRD2/3/4 have up to 74.4% identity. The second bromodomain, BRDT-2, has from 83.0% to 97.3% identity with the second bromodomain of BRD2/3/4. In the sequence alignment of the BET family proteins (**Figure 1.11**), BRDT

shares similar secondary structures with other family member(s). All of these bromodomains contained four alpha helices (αZ, αA, αB, αC) that are linked by two variable loop regions (ZA and BC loops).

A possible strategy is targeting Arg54 for BRDT selectivity. Despite high sequence identity, there are still some BRDT-specific features. BRDT-1 contains a unique Arg54 residue (green in **Figure 1.11**) at the terminus of the ZA channel. In other proteins, the same position is glutamine in the first bromodomain or lysine in the second bromodomain. Arg54 contains a positively charged guanidine moiety, which can either form in-plane H-bonds or a salt bridge with small molecule inhibitors. Arginine is more basic (pKa = ~13.8) than lysine (pKa = ~10.5) and glutamine is a neutral amino acid. The electron delocalization of the guanidine ion in the π-bonded system provides a higher aqueous pKa (~13.8) for Arg54.[93] We thus hypothesize that a well-designed molecule with appropriate interaction with Arg54 may bind to BRDT-1 selectively.

Bromodomain identity		**BRD2 (%)**		**BRD3 (%)**		**BRD4 (%)**		**BRDT (%)**	
		D1	D2	D1	D2	D1	D2	D1	D2
BRD2, (%)	D1	100.0	45.9	87.5	41.4	79.6	50.0	74.1	45.9
	D2		100.0	45.0	82.0	48.3	83.0	48.9	97.3
BRD3, (%)	D1			100.0	41.4	81.0	50.0	74.4	45.0
	D2				100.0	43.7	81.1	40.5	85.0
BRD4, (%)	D1					100.0	51.9	74.4	48.3
	D2						100.0	46.1	83.0
BRDT, (%)	D1							100.0	44.1
	D2								100.0

Table 1.1 Identity of bromodomain proteins in the BET family. (Sequence identity was calculated by EMBOSS).[94]

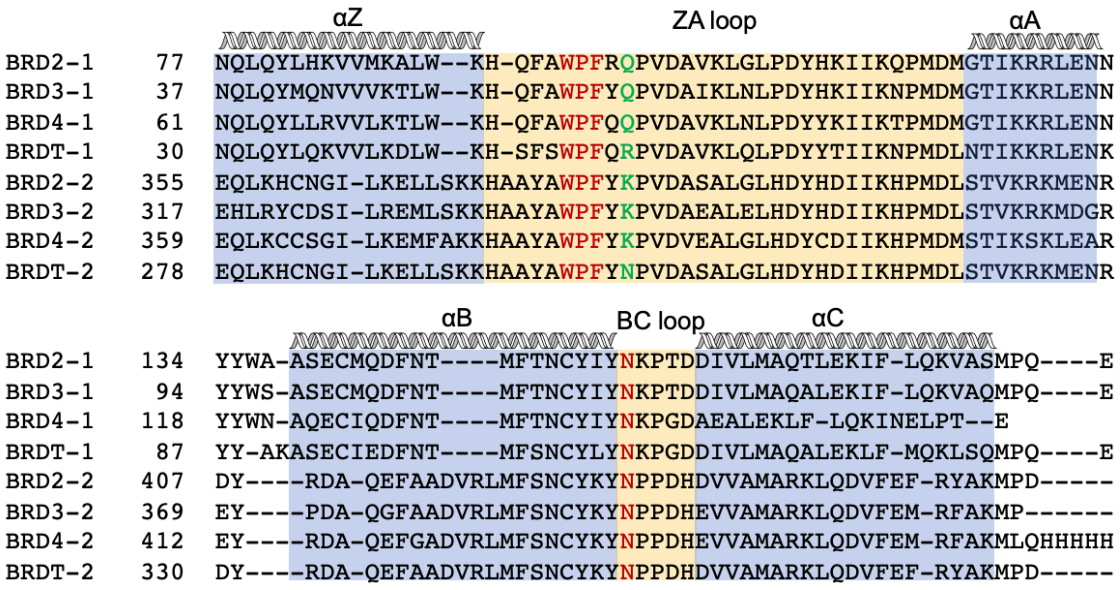


Figure 1.11 Sequence homology of bromodomains in the BET family. Alpha helices are heighted in blue; loop areas are heighted in yellow; residues in red are conserved asparagines in the BC loop and the WPF shelf in the ZA loop; Arg54 of BRDT-1 and the amino acid residues at the same position of other BET family members are noted in green. (CLUSTAL multiple sequence alignment by Kalign 2.0).[95]

The second promising way to achieve BRDT selectivity is a bivalent strategy. Even though the BET Kac binding site is highly conserved, the sequence length between two bromodomains is different (**Figure 1.12**). Unfortunately, no tandem-BET crystal structure was reported, but differing lengths of different BET proteins may imply different distances between the two Kac binding sites. BRDT has 128 amino acids between BRDT-1 and BRDT-2, which is the shortest linker in the BET family. Bivalent small molecules with an optimized linker may selectively occupy Kac pockets of tandem-BRDT. Recent publications found that bivalent inhibitors also induced the dimerization of single bromodomains.[91, 92] Therefore, different dimerization modes could be another strategy for selective BRDT inhibitor discovery.

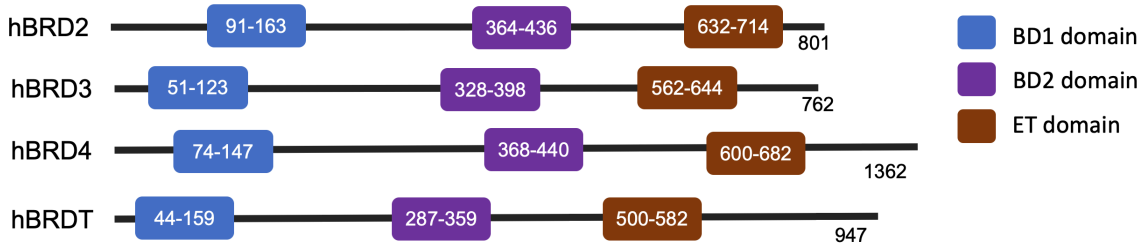
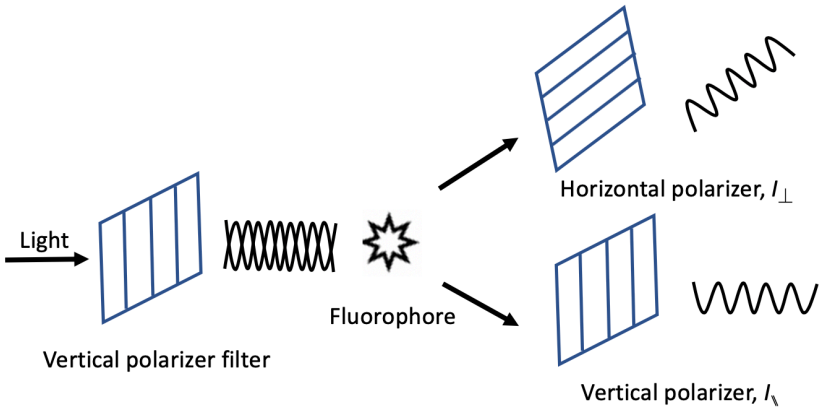


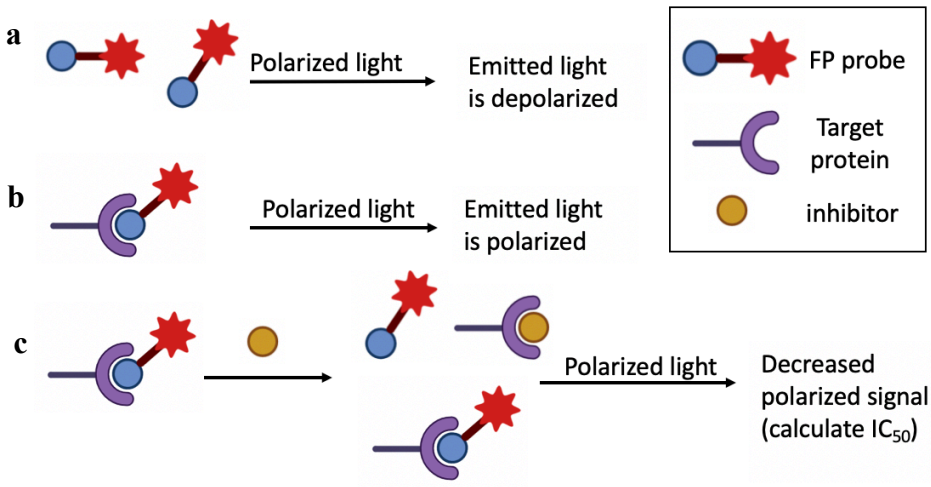
Figure 1.12 Domain structures of BRD2, BRD3, BRD4 and BRDT.

1.8 Fluorescence polarization tools for BRDT inhibitor discovery. Fluorescence polarization (FP) assays are widely used in chemical biology to determine the strength of small molecule interactions. This solution-based assay provides a fast and quantitative technique *in vitro* and even *in vivo*, thus extending its application to preliminary affinity testing and target engagement in cell.



$$FP = \frac{I_{\parallel} - I_{\perp}}{I_{\parallel} + I_{\perp}} \qquad \text{Equation 1}$$

Figure 1.13 Basic principle of fluorescence polarization. Reprinted from reference 97 by permission of Taylor & Francis.



$$\mu = \frac{3\eta V}{RT} \qquad \text{Equation 2}$$

Figure 1.14 Principle of fluorescence polarization assay. (**a**) Free probe emits depolarized light after activation by polarized light. (**b**) Probe-protein complex emits polarized light after activation by polarized light. (**c**) In a competitive binding assay, the mixture of free probe and probe-protein complex emits decreased polarized signal after activation by polarized light, allowing calculation of IC_{50} values. Equation 2: μ is rotational relaxation

time, R is the universal gas constant, V is the molar volume of the rotating molecule, T is the absolute temperature, and η is the solvent viscosity.

The mechanism of the FP assay is derived from the physical law that the polarization ratio is linearly correlated to Brownian motion driven molecular rotation.[96] In a typical FP measuring assay (**Figure 1.13**), the fluorophore is activated by light excitation at a specific wavelength for that compound. After an extremely short period of time (rotation relaxation time, μ) light will be emitted. Light emission can be distinguished as parallel light $I_{\parallel}$ and perpendicular light $I_{\perp}$. The FP value is calculated through equation 1[97] by comparing the difference of $I_{\parallel}$ and $I_{\perp}$ to the total fluorophore intensity. This equation shows that the FP value is independent from the absolute data of emission signal, which excludes the influence of probe or probe-protein complex concentration. $I_{\parallel}$ and $I_{\perp}$ are rarely obtained in a modern FP assay now, because fluorescence plate readers usually calculate the FP values. For molecular biology applications, FP assays are designed based on the principle that fluorescence intensity is enhanced by fluorescence probe aggregation. This principle can be explained by equitation 2,[98] where μ is the rotation relaxation time of the fluorophore, which is highly related to the polarization ratio. R, T and η are constants in this equation. In a regular protein binding event, μ is only dependent on V, which is the size of the rotating molecule. If the FP probe does not bind to the protein, the small molecule probe undergoes rapid rotation driven by Brownian motion in the water/buffer. When a photon is absorbed by the probe, the orientation of the nuclear framework will vary in the moment (rotation relaxation time, μ) between excitation and emission. The fluorophore can then emit the fluorescent light from various directions and the signal is depolarized (**Figure 1.14a**). When the FP probe binds to a protein, the molecular weight of the fluorophore complex increases significantly, which slows down the rotation of the entire complex. During this rotation relaxation time (μ), the orientation of the nuclear framework is limited. In this case, the fluorescence signal will be highly polarized (**Figure 1.14b**).[98] In a completive binding assay, the inhibitor(s) binds to the target protein and kicks out the previously bound fluorescence probe. The dissociated probe becomes free to rapidly rotate. FP signal then decreases with the increase in probe dissociation ratio (**Figure 1.14c**). The IC_{50} can thus be determined from the decreasing curve of the FP signal. The

corresponding K_i can then be calculated from Cheng-Prusoff equation[99, 100] (Equation 3) to describe the binding affinity of the tested compound.

$$K_i = \frac{IC_{50}}{1+\frac{[Ligand]}{K_d}} \qquad \text{Equation 3}$$

Several chemical probes for use in fluorescence polarization (FP) assays have been developed to aid in drug discovery programs for BET proteins. Previously reported probes for BET bromodomains either have low binding affinities or have low polarization signal windows, and most of them are not well characterized. For example, BODIPY-conjugated BI6727 (BI-BODIPY) is reported to have a K_d of 50-110 nM for BRD4-1 and only a 40 mA polarization signal window, while the Alexafluor488-IBET10 and FITC-JQ111-13 probes remain uncharacterized.[75, 101] This prompted us to develop a novel small molecule FP probe with high affinity and a large polarization signal window.

Chapter 2: Design, Synthesis, and Characterization of a Fluorescence Polarization Pan-BET Bromodomain Probe

*As published in: Paulson, C. N.; Guan, X.; Ayoub, A. M.; Chan, A.; Karim, R. M.; Pomerantz, W. C. K.; Schonbrunn, E.; Georg, G. I.; Hawkinson, J. E. *ACS Med. Chem. Lett.* **2018**, *9*, 1223-1229

2.1 Induction. In our study, we developed a novel FP chemical probe utilizing SG3-179, a potent pan-BET inhibitor with high affinity for BRDT-1 (IC_{50} = 23 nM),[102] as scaffold (see structure in **Figure 2.1**). A general challenge for probe development is to avoid a significant loss of binding affinity caused by steric hindrance of the attached fluorescent label. To achieve this endpoint, we docked SG3-179 to a representative BET-family protein BRDT-1 (PDB: 4FLP) to reveal the binding mode of SG3-179 for BRDT-1 (**Figure 2.1**). The predicted binding mode is similar to the later released crystal structure SG3-179 in complex with BRD4-1 (PDB: 5F63). The diaminopyrimidine core of SG3-179 forms a direct hydrogen bond with Asn 109 in the Kac site of BRDT-1 and the water exposed piperidine moiety is far away from this key interaction, which therefore provided a reasonable position to connect to a fluorophore. In the selection of the fluorophore, we chose a BODIPY dye due to its long fluorescence lifetime (5-6 ns)[103] and because tetra-methyl BODIPY is an inexpensive fluorophore among BODIPY dyes and numerous chemistries involving tetra-methyl BODIPY are available for rapid linker incorporation.[104-106] Although a longer linker length may alleviate steric hindrance, local motion of fluorophores attached by flexible linkers can decrease the polarization of the bound probe ('propeller effect').[98] In order to identify the optimal balance between steric hindrance and unrestrained fluorophore motion, linker length and flexibility were explored.

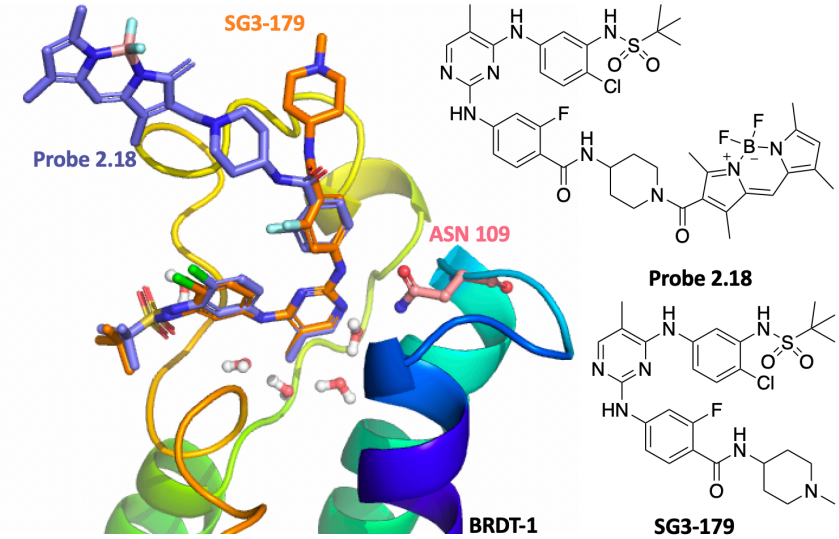
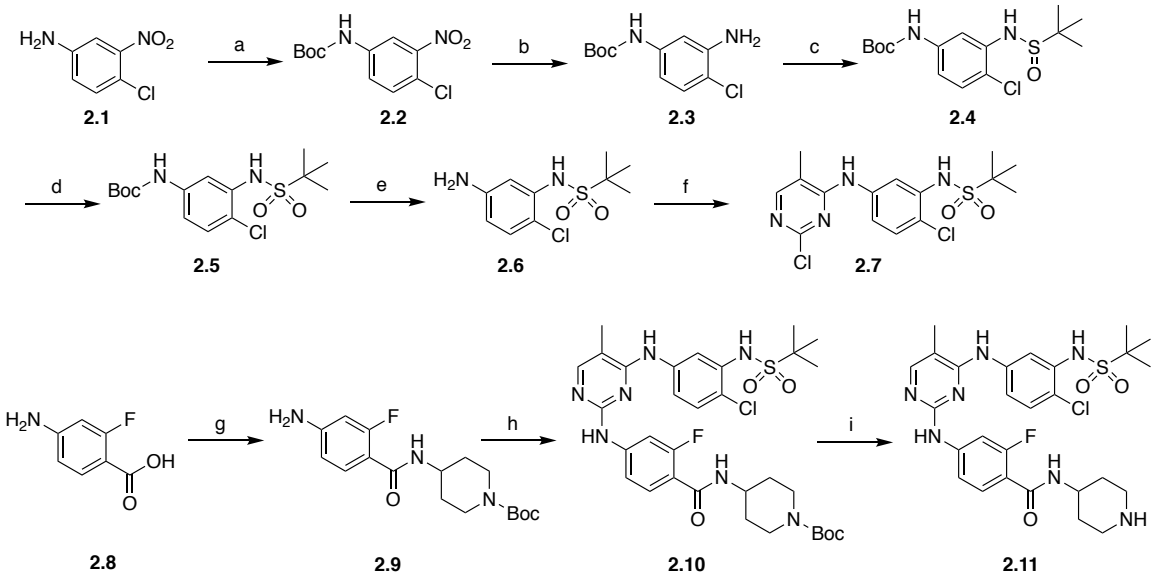


Figure 2.1 Molecular docking predicts that compound **2.18** will maintain high affinity for BRDT-1. Compound **2.18** orients similarly to the parent compound SG3-179 and maintains the key interaction with Asn109 of BRDT-1 (PDB: 4FLP). The fluorophore is solvent exposed without the possibility of any steric hindrance with the protein.

2.2 Chemistry. The synthetic route for SG3-179 based probes **2.18-2.20** is shown in **Schemes 2.1** and **2.2**. The synthesis of the Kac site ligand employed procedures similar to the methods reported for the preparation of SG3-179 (**Scheme 2.1**). Protection of commercially available 4-chloro-3-nitroaniline with Boc anhydride gave **2.1**, followed by reduction of the nitro group with hydrazine to provide aniline **2.2**. Reaction of **2.2** with *tert*-butylsulfinyl chloride furnished *tert*-butylsulfinyl **2.3** that was further oxidized with mCPBA to sulfonamide **2.5**. Deprotection of **2.5** with TFA produced aniline **2.6**, which was reacted with 2,4-dichloro-5-methylpyrimidine to afford chloropyrimidine **2.7**. Intermediate **2.9** was obtained by coupling 4-amino-2-fluorobenzoic acid and *tert*-butyl 4-aminopiperidine-1-carboxylate, using 1-[bis(dimethylamino)methylene]-1H-1,2,3-triazolo[4,5-b]pyridinium 3-oxid hexafluorophosphate (HATU) in the presence of *N,N*-diisopropylethylamine (DIEPA) in dry DMF. Connection of fragment **2.7** and **2.9** by a Buchwald-Hartwig coupling reaction yielded **8** which was then Boc deprotected with TFA to give the Kac site ligand **9**.

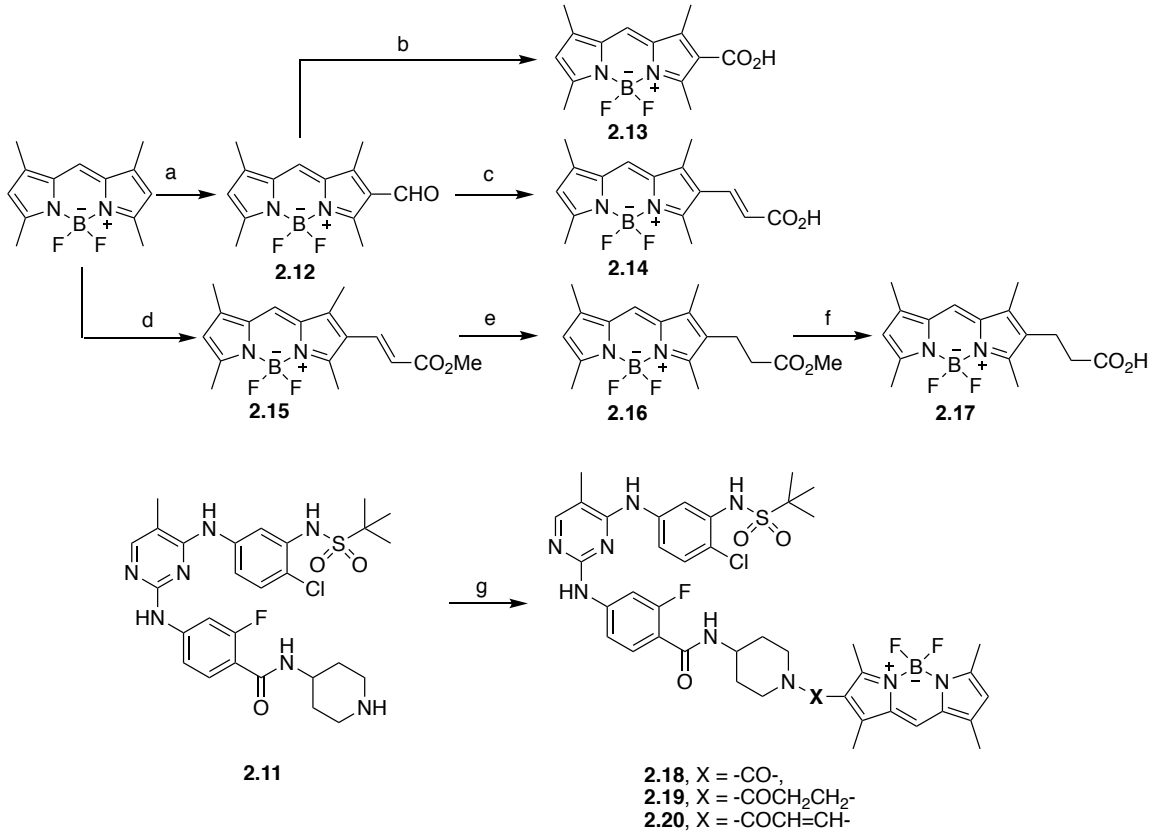
Scheme 2.1 Synthesis of the SG3-179 chemotype



Reagents: (a) $(Boc)_2O$, THF, reflux, 28 h, 58 %; (b) Pd/C, hydrazine monohydrate, MeOH, reflux, 10 h, 64%; (c) 2-methylpropane-2-sulfinic chloride, pyridine, DCM, rt, 20 h, 77%; (d) mCPBA, DCM, rt, overnight, 84%; (e) TFA, DCM, rt, 2 h, 78%; (f) 2,4-dichloro-5-methylpyrimidine, DIPEA, isopropanol, 120 °C, 2 d, 36%; (g) *tert*-butyl 4-aminopiperidine-1-carboxylate, HATU, DIPEA, DMF, rt, 12 h, 95%; (h) Compound **6**, $Pd_2(dba)_3$, BINAP, NaOtBu, 1,4-dioxane, 110 °C, 5 h, 90%; (i) TFA, DCM, 12 h, 91%.

The synthesis of the fluorophore moiety commenced with commercially available tetramethyl-BODIPY (**Scheme 2.2**) by reaction with DMF in the presence of $POCl_3$ to produce aldehyde **2.12**,[17] which was then oxidized to carboxylic acid **2.13**. Acrylic acid **2.14** was synthesized from aldehyde **2.12** by a Knoevenagel condensation.[106] A Heck-type reaction between tetramethyl-BODIPY and methyl acrylate catalyzed by Pd(0) yielded methyl acrylate **2.15**.[105] The double bond in **2.15** was reduced with H_2 to give methyl propionate **2.16**, which was hydrolyzed to yield acid **2.17**. Fluorophores **2.13**, **2.14** and **2.17** were linked to ligand **2.11** (HOBt and EDC) to produce BODIPY based FP probes **2.18**, **2.19** and **2.20**.

Scheme 2.2 Synthesis of the fluorophore moiety and FP probe assemble



Reagents: (a) DMF, $POCl_3$, 0 °C, 2–3 h, then 50 °C, 3 h, 89%; (b) $NaClO_2$, H_2O, NaH_2PO_4, rt, 15 h, 30%; (c) malonic acid, pyridine, DMF, 90 °C, 5 h, 28%; (d) methyl acrylate, 20 mol % of $Pd(OAc)_2$, *tert*-BuOOBz, DMSO, 35 °C, 5 d, 57%; (e) Pd/C, H_2, MeCN, MeOH, rt, 12 h, 80%; (f) NaOH, DCM:MeOH:H_2O, rt, 10 h, then neutralize, 98%; (g) intermediate **2.13**, **2.14** or **2.17**, HOBt, EDC, DIPEA, DCM, rt, 6 h, 72–93%.

2.3 UV absorption and fluorescence excitation and emission spectrums. In comparison to compound **2.18,** which has sharp UV absorption and fluorescence excitation and emission peaks similar to BODIPY, the peaks for compounds **2.19** and particularly **2.20** are broadened and red-shifted. Although it is not clear why compound **2.19** has a red-shifted emission spectrum, the extended π-conjugate system present in compound **2.20** is expected to produce a higher LUMO level and narrowed HOMO-LUMO gap,[84] which likely explains the red-shifted emission spectrum.

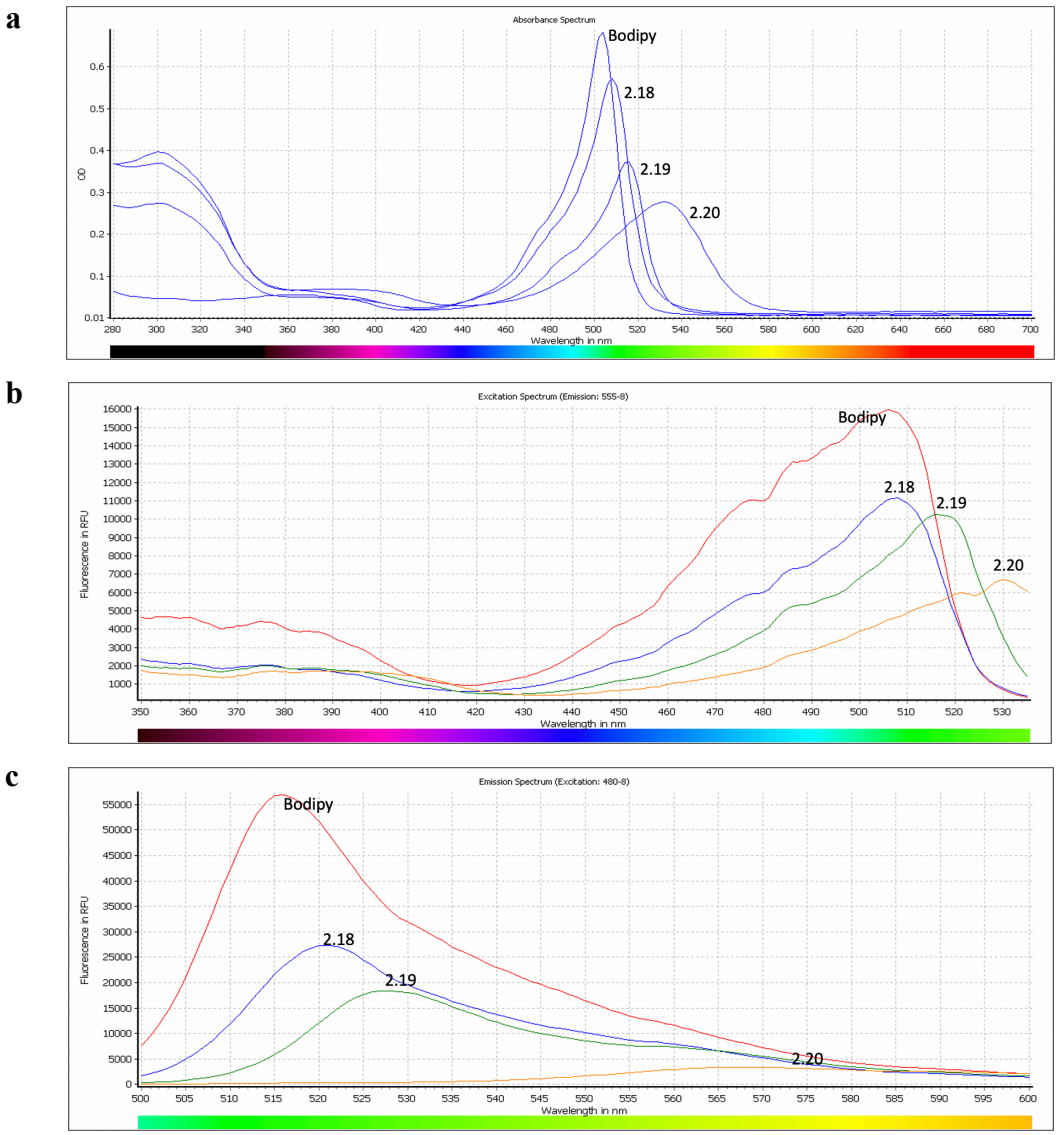
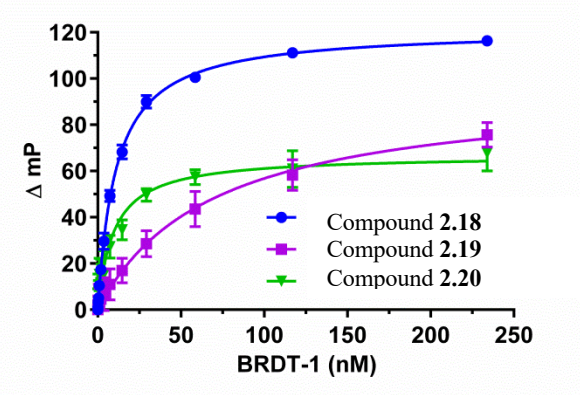


Figure 2.2 UV absorbance and fluorescence spectra of BODIPY, probes **2.18**, **2.19**, and **2.20** (25 μM in DMSO): (**a**) UV absorbance spectrum. (**b**) Excitation spectrum. (**c**) Emission spectrum.

2.4 Probe affinity and signal window. The three probes (**2.18, 2.19** and **2.20**) were then tested against BRDT-1 in a FP assay to assess probe affinity and signal window (**Figure 2.3**). Whereas probes **2.18** and **2.19** have similar affinities, probe **2.18** had the highest FP signal window (B_{max} >100 mP) at the standard BODIPY excitation and emission wavelengths and was therefore selected for further characterization. K_D values for all the BET family proteins (BRDT-1, BRDT-2, BRDT-T, BRD2-1, BRD2-2, BRD3-1, BRD3-2, BRD4-1, BRD4-2, and BRD4-T, where –T designates the BD1 and BD2 tandem domain),

and two representative non-BET family proteins (BRD7 and BRD9) were determined with FP probe **2.18** (**Table 2.1**, **Figure 2.3** and **2.4**).



Compound	K_D (nM)	B_{max} (mP)
2.18	11	120
2.19	69	96
2.20	9.5	67

Figure 2.3 Pan-BET probe **2.18** showed favorable binding properties compared to related probes **2.19** and **2.20**. BRDT-1 protein saturation binding curves with 7.5 nM BODIPY-SG3-179 probes **2.18**, **2.19**, and **2.20** and K_D and B_{max} values.

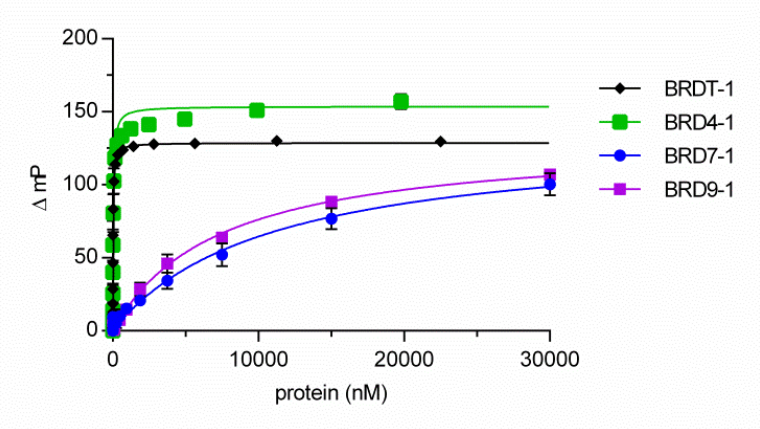


Figure 2.4 Pan-BET probe **2.18** binds with high affinity to BET BRDs, but only weakly to other BRD proteins. Error bars represent ± SEM where n ≥ 3.

Table 2.1 Affinity of pan-BET FP probe **2.18** for BRD proteins

	$K_D \pm SEM$, nM[a]		
	BD1	**BD2**	**Tandem**
BRDT	17 ± 2	10 ± 2	5.5 ± 0.6
BRD4	17 ± 1	9.6 ± 0.4	10 ± 1
BRD3	23 ± 1	7.5 ± 0.5	--
BRD2	56 ± 4	12 ± 1	--
BRD7	12,000 ± 2000	--	--
BRD9	7600 ± 1300	--	--

[a]n ≥ 3 independent experiments.

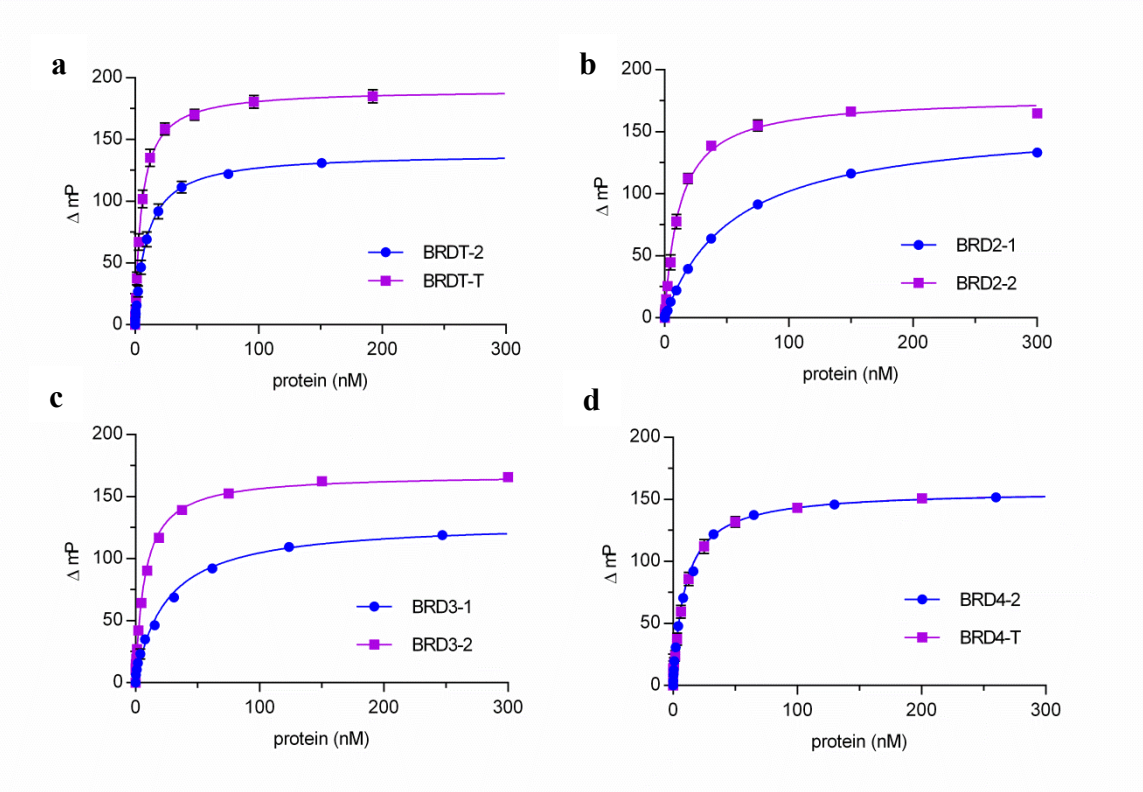


Figure 2.5 BRD saturation binding curves with 7.5 nM compound **2.18**: (**a**) BRDT-2 and BRDT-T, (**b**) BRD2-1 and BRDT-2, (**c**) BRD3-1 and BRD3-2, and (**d**) BRD4-2 and BRD4-T. Error bars represent ± SEM where n ≥ 3.

FP probe **2.18** exhibited low nanomolar affinities for all of the BET family proteins (6-56 nM) but had K_D values in the low micromolar range for the two non-BET family proteins (7-11 μM). The lower affinity of probe **2.18** to BRD7 and BRD9 was expected based upon previously reported SG3-179 BROMOScan data.[85] Therefore, compound **2.18**

is a pan-BET probe. Probe **2.18** has a slight preference for BD2 over BD1 bromodomains, ranging from 1.7- to 4.7-fold higher affinity for BD2 depending on BET family member. In contrast to the BRD4-T protein, the pan-BET probe **2.18** bound BRDT-T with 2- to 3-fold higher affinity than the individual BRDT bromodomains. Although it has been argued that the two bromodomains of BRDT function independently due to the long flexible linker connecting them,[59] the higher affinity of the probe for BRDT-T suggests that there may be cooperativity between the tandem bromodomains or that the 123 aa linker may stabilize one or both bromodomains.

2.5 Testing of representative BET BRD inhibitors results. Ten representative BET BRD inhibitors with varying scaffolds and selectivities were chosen for competition studies to establish that pan-BET probe **2.18** provides the expected affinity and selectivity values for the BET BRDs. The structures of the reference compounds SG3-179, ABBV-075, BI2536, bromosporine, 2098312-12-8, (+)-JQ1, (-)-JQ1, MS436, RVX-208, and TG101209 are illustrated in **Fig 2.7**. IC_{50} values were generated for all ten compounds against the BET-family proteins and K_i values were calculated using the equations of Nikolovska-Coleska *et al*., 2004[72] (**Figure 2.6** and **Table 2**). In some cases, K_i values could not be determined because IC_{50} values were too low relative to the protein concentration (40-75 nM) used in the assay. In these cases, the apparent IC_{50} values likely underestimate the true potency of the inhibitors. As protein concentrations cannot be lowered in order to maintain a sufficient signal window, an alternate method must be employed to obtain accurate affinity estimates for these very potent inhibitors due to this 'floor effect'. Additionally, K_i values are not reported for BRDT-T and BRD4-T as the K_i calculation equation cannot be used for proteins with > 1 ligand binding site.[72]

Parent compound SG3-179 has been reported to have an IC_{50} ~20 nM for both BRDT-1 and BRD4-1 using an AlphaScreen assay.[85] SG3-179 FP K_i values are ~15 nM for these BRDs. SG3-179 FP K_i values for BD1 domains of the four BET BRDs correlate well with the K_D values obtained for the SG3-179-BODIPY probe **2.18**. However, SG3-179 has 3- to 5-fold lower affinity for BD2 domains of the BRDT, BRD2, and BRD4 than predicted by the probe K_D values, perhaps due to a small contribution of the fluorophore to binding.

ABBV-075, also known as mivebresib, is a potent small molecule BET inhibitor presently in a Phase I clinical trial for patients with advanced hematologic malignancies and solid tumors.[72] ABBV-075 has previously been reported to be selective for tandem BRDT, BRD2, and BRD4 proteins (K_i = 1-2 nM) over the tandem BRD3 protein (K_i = 12.2 nM) in TR-FRET assays.[107] When tested in the FP assay reported here, the IC_{50} values ranged from 9-32 nM for all of the BRD proteins. These IC_{50} values likely underestimate the true affinity of ABBV-075 and K_i values could not be calculated due to the 'floor effect' described above, consistent with the high affinity values reported using the TR-FRET assay.[107]

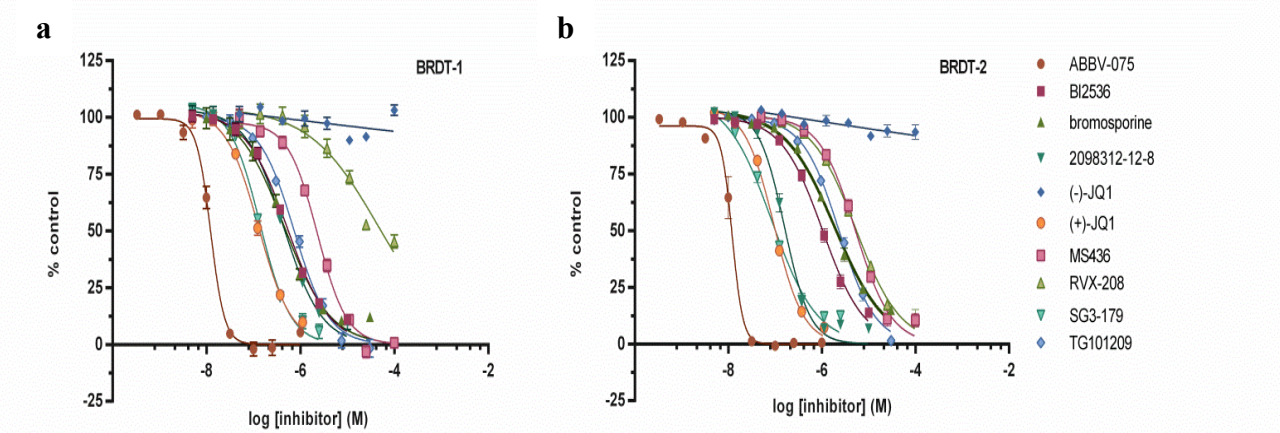


Figure 2.6 Competitive displacement of the pan-BET probe **2.18** by 10 reference BET inhibitors at (a) BRDT-BD1 and (b) BRDT-BD2. Error bars represent ± SEM where n ≥ 3.

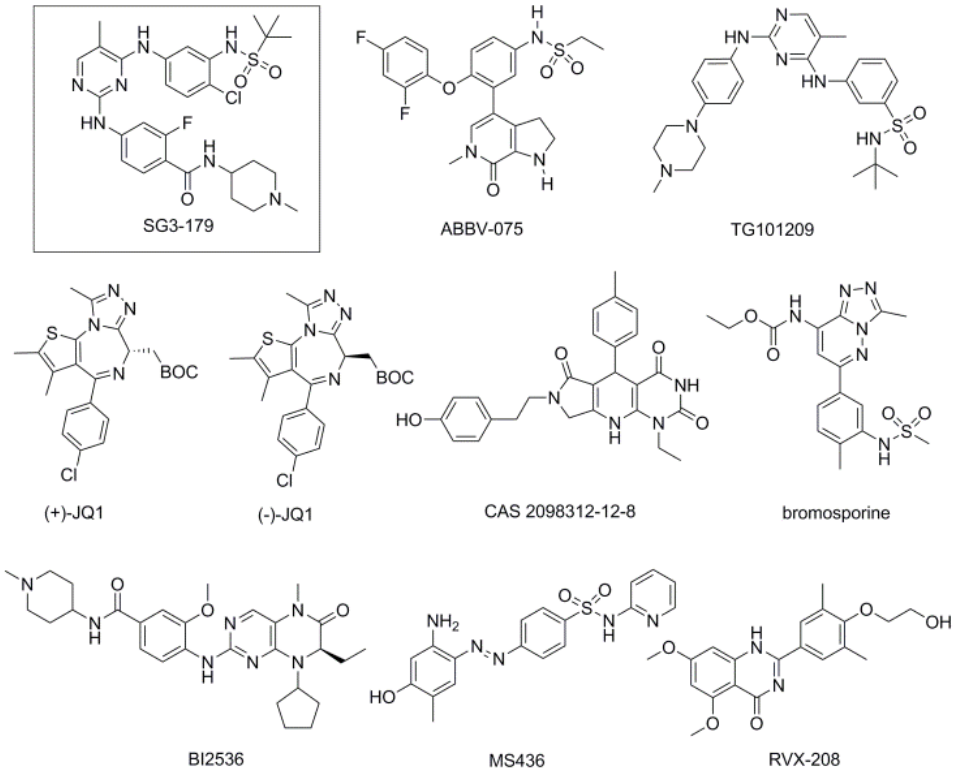


Figure 2.7 Structures of the 10 reference BET inhibitors with various chemical scaffolds selected to validate the FP assay. CAS 2096312-12-8 refers to compound **3s** from Ayoub *et al.*[75]

The prototypic BET inhibitor, (+)-JQ1, is a thieno-triazolo-1,4-diazepine with reported AlphaScreen and TR-FRET IC_{50} values ranging from 18-91 nM for BRD4-1,[82, 85, 108-110] 14-33 nM for BRD4-2 and BRD3-1,[108-110] and 100-150 nM for BRDT-1 and BRD2-1.[82, 85] In general, the reported IC_{50} values indicate that (+)-JQ1 has ~5-fold higher affinity for BRD4-1 over BRDT-1.[82, 85] A similar behavior was observed in the FP assay in which (+)-JQ1 has a K_i value of 13 and 2.6 nM for BRDT-1 and BRD4-1, respectively.

Table 2.2 Inhibitory potency (IC_{50}) and affinity (K_i) of representative BRD inhibitors for BET family bromodomains determined using pan-BET FP probe **2.18**. Values are mean ± SEM in nM, where n ≥ 3. K_i values are included for BRDs containing a single binding domain (BD1 or BD2) if potency values are greater than the lower sensitivity limit of the assay (IC_{50} ≥ 1.5X BRD concentration)

Compound		BRDT-1	BRD2-1	BRD3-1	BRD4-1	BRDT-2	BRD2-2	BRD3-2	BRD4-2	BRDT-T	BRD4-T
SG3-179	IC_{50}	140 ± 10	114 ± 1	200 ± 20	250 ± 16	237 ± 8	250 ± 25	90 ± 10	220 ± 20	307 ± 7	137 ± 7
	K_i	15 ± 2	42 ± 1	20 ± 3	17 ± 1	50 ± 2	41 ± 6	6 ± 2	27 ± 341	--	--
ABBV-075	IC_{50}	12 ± 1	9.0 ± 0.5	17 ± 2	19 ± 2	11 ± 1	14.3 ± 0.6	7.7 ± 0.7	13 ± 1	32 ± 3	11.5 ± 0.3
(+)-JQ1	IC_{50}	130 ± 10	60 ± 7	110 ± 10	120 ± 10	85 ± 7	110 ± 10	60 ± 7	97 ± 4	170 ± 12	70 ± 5
	K_i	13 ± 2	--	--	--	15 ± 1	14 ± 2	--	8.6 ± 0.6	--	--
CAS 2098312-12-8	IC_{50}	380 ± 10	7.4 ± 0.2	21 ± 2	260 ± 10	130 ± 10	12.5 ± 0.9	8.3 ± 0.7	180 ± 16	120 ± 16	15 ± 1
	K_i	60 ± 2	--	--	18 ± 2	27 ± 3	--	--	21 ± 3	--	--
bromosporine	IC_{50}	390 ± 9	18 ± 2	43 ± 5	410 ± 40	1300 ± 300	52 ± 7	27 ± 2	700 ± 100	39 ± 1	8.5 ± 0.2
	K_i	62 ± 2	--	--	35 ± 5	310 ± 40	--	--	90 ± 20	--	--
BI2536	IC_{50}	441 ± 7	9.0 ± 0.9	34 ± 2	240 ± 20	1050 ± 80	86 ± 7	25 ± 1	360 ± 10	68 ± 3	12.4 ± 0.7
	K_i	71 ± 1	--	--	15 ± 2	250 ± 20	9.3 ± 1	--	49 ± 2	--	--
TG101209	IC_{50}	830 ± 60	1390 ± 40	1800 ± 100	1100 ± 90	2400 ± 100	3900 ± 200	1120 ± 10	2000 ± 80	2300 ± 100	740 ± 10
	K_i	140 ± 10	700 ± 20	320 ± 20	120 ± 10	560 ± 30	760 ± 40	146 ± 1	300 ± 10	--	--
MS436	IC_{50}	2400 ± 100	620 ± 20	1300 ± 80	1200 ± 100	4700 ± 500	2700 ± 400	1550 ± 70	3400 ± 100	5700 ± 300	1200 ± 100
	K_i	450 ± 20	300 ± 10	220 ± 20	130 ± 10	1200 ± 100	540 ± 80	205 ± 9	536 ± 5	--	--
RVX-208	IC_{50}	43000 ± 1600	13000 ± 600	43000 ± 3000	11000 ± 200	4800 ± 500	4000 ± 200	3300 ± 100	3000 ± 400	26000 ± 3000	9000 ± 1000
	K_i	8200 ± 300	6700 ± 300	7800 ± 500	1300 ± 30	1200 ± 100	800 ± 50	450 ± 10	450 ± 60	--	--
(-)-JQ1	IC_{50}	>10000	>10000	>10000	>10000	>10000	>10000	>10000	>10000	>10000	>10000

The dihydropyridopyrimidine compound (CAS registry number: 2098312-12-8) is a potent BET inhibitor that has been shown to have submicromolar affinity (BRDT-1, K_i = 200 nM; BRD4-1, K_i = 110 nM) in a FP assay using BI-BODIPY.[75] Three- to six-fold higher affinity values were obtained using the SG3-179-BODIPY probe for BRDT-1 and BRD4-1, respectively. The prior report by Ayoub et al.[75] carried out the experiment at a 5-fold higher DMSO concentration (0.5% vs. 0.1%), which is known to affect bromodomain binding interactions.[111] Additionally, 2098312-12-8 has higher affinity for BRD2 and BRD3 BD1 and BD2 that exceeded the sensitivity of the assay.

Bromosporine is a promiscuous BRD inhibitor that was developed to target the conserved BRD fold of BRD-containing proteins. While IC_{50} and K_i information could not be found in the literature, K_D values for bromosporine against all of the BET proteins using ITC have been reported to be in the 40- 100 nM range for BRD2, BRD3, BRD4, and BRDT BD1 and BD2, excluding BRDT-2 which had a significantly higher K_D value (K_D = 172 nM).[76] Similarly, K_i values obtained in the FP assay for BRD4-1, BRD4-2, and BRDT-1 ranged from 35 – 90 nM, and bromosporine had lower affinity for BRDT-2 (K_i = 310 nM). In contrast, bromosporine had higher affinities for BRD2 and BRD3 BD1 and BD2 in the FP assay that exceeded the sensitivity of the assay.

BI2536 is a potent and selective inhibitor of PLKI (IC_{50} = 0.83 nM) and has antitumor activity against relapsed or refractory acute myeloid lymphoma (AML) and non-small cell lung cancer in phase I/II clinical trials. It binds to the Kac site of BRD4 through an elaborate network of hydrogen bonding and Van der Waals interactions.[82] B12536 was shown to be selective for BRD4-1 over BRDT-1 with IC_{50} values of 25 and 260 nM, respectively, in an AlphaScreen assay.[82] Similarly, in the FP assay, BI2536 has a higher affinity for BRD4-1 (K_i = 15 nM) over BRDT-1 (K_i = 71 nM). We also found that BI2536 has high affinity for BRDT-T (K_i = 4.3 nM) and BRD2-1 (K_i = 9.3 nM).

TG101209, a dual BET bromodomain and JAK2 kinase inhibitor, has been reported in the literature to have lower affinity for BRD2-1 (IC_{50} = 680 nM) relative to BRD3-1, BRD4-1, and BRDT-1 (IC_{50} = 130-290 nM).[82] The K_i values determined in the FP assay for these BRDs revealed a similar profile in which TG101209 was 2-5 times less active against BRD2-1 (K_i = 700 nM) than the other BRD BD1s (K_i = 140-320 nM).

The BD1-selective diazobenzene-based inhibitor MS436 has been reported to have a K_i < 85 nM for BRD4-1 and had >4-fold lower affinity for BD2.[77] In our assay, MS436 showed similar activity with a BRD4-1 K_i of 130 nM and 4-fold lower affinity for BRD4-2. MS436 had 2- to 4-fold lower affinity for the other BET BRDs and showed lower selectivity for their BD2 domains.

RVX-208 has been evaluated in several clinical trials for the treatment of atherosclerosis and associated cardiovascular disease. RVX-208 has been reported to be a BD2-selective inhibitor of BET proteins with K_D values measured by ITC for BD1 that are 8 times higher than those determined for BD2.[79, 109] In the FP assay, a similar trend was observed where RVX-208 is 3-17 times selective for BD2 over BD1 depending on the BRD protein, with highest BD2 selectivity in BRD3.

(-)-JQ1, the inactive enantiomer of (+)-JQ1, is considerably less potent with reported IC_{50} values of 8354 and >10000 nM for BRD4-1 and 52120 nM for BRD4-2.[108, 110] We report similar findings in our FP assay in which (-)-JQ1 had IC_{50} values >10000 nM for all BET bromodomains.

Several compounds, including (+)-JQ1, MS436, RVX-208, SG3-179, and TG101209 inhibited the binding of the pan-BET probe **2.18** to the BRDT-T and BRD4-T proteins with IC_{50} values close to, and generally intermediate between, the individual BD1 and BD2 domains, as expected assuming no effect of the 123 aa linker. In contrast, BI2536, bromosporine, and 2098312-12-8 had considerably lower IC_{50} values for the tandem BRDT and BRD4 bromodomains compared to the individual BD1 and BD2 domains, presumably these inhibitors bind to bromodomains in the tandem protein in a cooperative manner or the amino acid linker in the tandem proteins induces conformational changes in the BD1 and/or BD2 domains that increase the affinity of certain inhibitors.

2.6 Conclusion. The novel pan-BET probe **2.18** has high affinity for the BD1, BD2 and tandem BRDs of BET family members, provides a high FP signal window, and assay robustness suitable for HTS (Z' value = 0.78 ± 0.04). It can be used to establish the SAR for inhibitor series, determine compound selectivity within intra-BET sub-family or inter-domains of a BET protein, and for HTS of BET BRDs to identify novel inhibitor scaffolds.

Chapter 3: Discovery of Selective 2,4-Disubstitued Pyrimidine Derivatives for Extra-Terminal (BET) Family Proteins from a Dual-JAK2 Kinase and Bromodomain Inhibitor

3.1 Introduction. As mentioned in previous chapters, BRDT binds to dual kinase-bromodomain inhibitors with good potency, but kinase activity may increase health risk due to their anti-proliferation potential. For our studies, we want to decrease kinase activity and gain BRDT selectivity.

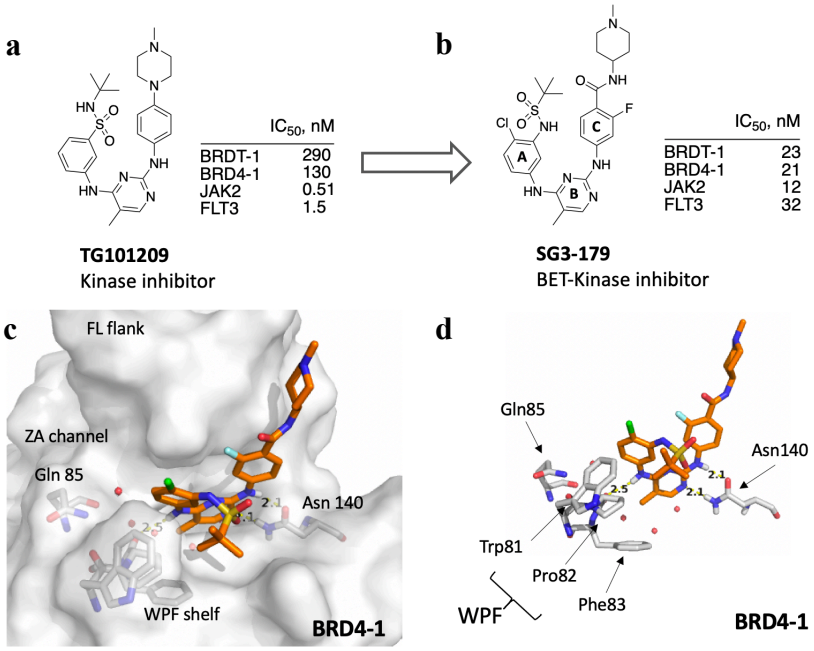


Figure 3.1 TG101209 and SG3-179. (**a**) Structure of TG101209 and its AlphaScreen IC_{50} values; (**b**) Structure of SG-179 and its AlphaScreen IC_{50} values; **(c)** SG3-179 binds to BRD4-1 in the Kac site of BRD4-1(PDB: 5F63); **(d)** in Kac site of BRD4-1, SG3-179 formed H-bonds (in yellow) with Asn140 and Pro82.

Our lead compound is the 2,4-disubstitued pyrimidine derivative SG3-179[85] (**Figure 3.1b**), which is a dual BET-kinase inhibitor derived from JAK2 inhibitor TG101209 (**Figure 3.1a**).[112] In the cocrystal structure of BRD4-1 with SG3-179 (**Figures 3.1c** and **3.1d**), the pyrimidine core (ring B) and the NH between rings B and C of SG3-179 form a pair of H-bonds with conserved Asn140. The NH between rings A and B forms a hydrogen bond with Pro82 of the WPF shelf, the *t*-butyl group is located in the hydrophobic cavity in the WPF shelf and the piperidine moiety is exposed to the solvent.

Our BRDT inhibitors were designed based on the Arg54 hypothesis. The Kac site of BRDT-1 features a unique arginine residue, Arg54. The other BET family members contain alternative residues (Gln/Lys/Asn) at this same position of the Kac site. We thus hypothesized that BRDT selective inhibition could arise from interaction between Arg54 and our designed analogs. In our compound design, we determined two possible strategies to approach Arg54 in BRDT-1: replace the *t*-butylsulfonamide group of SG30179 with a new side chain or introduce a new side chain at the meta position of the *t*-butyl group. These strategies were inspired by the crystal structure of BRD4-1 in complex with SG3-179-based bivalent inhibitor **4.5** (**Figure 3.2d)** from the Schönbrunn group (unpublished data). These SG3-179-derived symmetric bivalent inhibitors contained two SG3-179 chemotypes (**Figure 3.2d)** and these two chemotypes had a different binding pose in the Kac site of each chain in the BRD4-1 homodimer (**Figures 3.2e** and **3.2f)**. In the crystal structure of **4.5** in complex with BRD4-1, the *t*-butyl group of the SG3-179 chemotype occupied either the ZA channel or the WPF shelf, depending on the protein chain. Binding pose 1 (**Figure 3.2e**) from chain B of the structure showed that the *t*-butyl sulfonamide of the SG3-179 chemotype stretched toward Gln85 of BRD4-1, which is where Arg54 is located in BRDT-1 (**Figures 3.2b** and **3.2c**). For the design of series I, we hypothesized that the *t*-butyl sulfonamide moiety of SG3-179 would also stretch toward Arg54 in BRDT-1. We modified SG3-179 at the *t*-butyl sulfonamide site using different L-amino acids in place of this *t*-butyl sulfonamide to promote Arg54 interaction (**Figure 3.2h**). L-Amino acids provided a carboxylic acid, which could form a salt bridge/H-bond with Arg54 of BRDT-1. Since L-amino acids are a source of a variety of side chain sizes and shapes, they provided a way to regulate the geometry of the carboxylic group toward Arg54. In binding pose 2 (**Figure 3.2f**) from chain A of the BRD4-1 homodimer, the *t*-butyl sulfonamide of SG3-179 bound to the WPF shelf instead of the ZA channel. Superimposing the SG3-179 molecules from the two chains of the BRD4-1 dimeric cocrystal structure (**Figure 3.2g**) revealed that the SG3-179 chemotypes had very similar binding modes, except for the position of the *t*-butyl sulfonamide. Aromatic rings A of these two compounds overlap very well. The rotation of the *t*-butyl sulfonamide moiety indicated a second strategy to approach Arg54. When the *t*-butyl sulfonamide moiety shifted to WPF shelf, its meta position was very close to the *t*-butyl sulfonamide position of binding pose 1 from chain B.

We hypothesized that if we introduced a new side chain meta to the *t*-butyl sulfonamide, the introduced side chain could also stretch toward Arg54. Series II was designed based on this hypothesis (**Figure 3.2i**). L-Amino acids, β/γ amino acids and hydrophobic moieties were introduced to explore the SAR in this series. To explore the SAR of the piperidine moiety of SG3-179, this moiety was removed in the series III compounds.

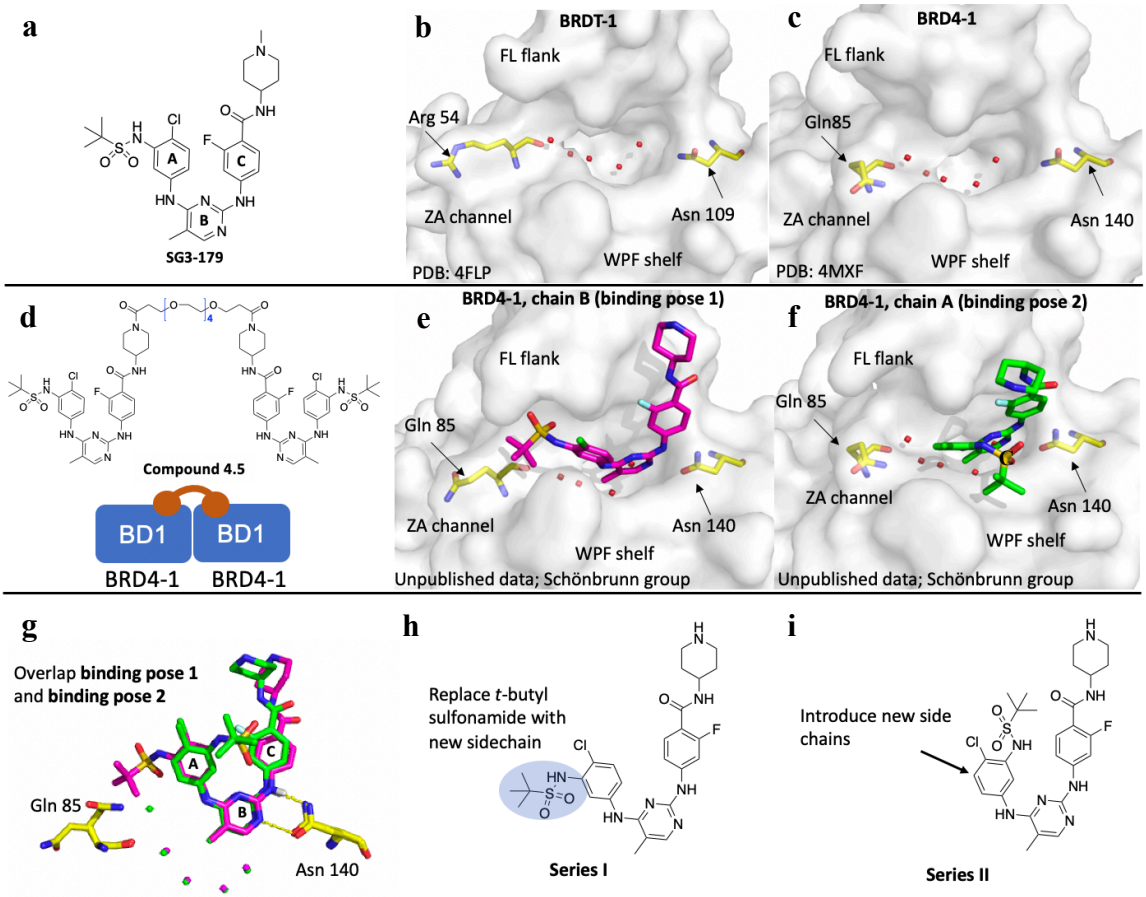


Figure 3.2 Strategies to approach Arg54. (**a**) Structure of SG3-179; (**b**) Kac pocket of BRDT-1; (**c**) Kac pocket of BRD4-1; (**d**) compound **4.5** and cartoon of how this bivalent inhibitor induced the dimerization of BRD4-1; (**e**) binding pose 1 of SG3-179 chemotype (magenta) with BRD4-1 chain B; (**f**) binding pose 2 of SG3-179 chemotype (green) with BRD4-1 chain A; (**g**) overlay of two binding poses; (**h**) strategy for series I compound design; (**i**) strategy for series II compound design.

These two series of compounds with Arg54 targeting side chains (α/β/γ amino acids, hydrophobic moieties, sulfonamides, amides, etc.) were screened virtually with BRDT-1 (PDB: 4FLP).[113-115] The Molecular Mechanics/Generalized Born Surface Area (MM/GBSA) method (Schrödinger) was used to evaluate the tested ligands. Molecular Mechanics (MM) are widely used in dynamics simulations and allowed us to predict

dynamics of the BRDT protein.[116] Generalized Born's model (GB) was used to calculate the free energy and rank binding affinity of tested compounds.[117] MM/GBSA is more time consuming, but has better ligand pose accuracy than Glide docking.[118] Compared with another MM based method Molecular Mechanics/Poisson Boltzmann Surface Area (MM/PBSA), MM/GBSA also had better performance in ranking the binding affinity of studied binders.[119] The MM/GBSA approach revealed binding free energy (ΔG_{bind}) values for the SG3-179 analogs ranging from -74.667 to -116.645, where the SG3-179 ΔG_{bind} is -91.094. In the docking experiments, some of the compounds in series I and II formed interactions with Arg54. Representative results, **3.31** (ΔG_{bind}: -106.985) in series I and **3.61** in series II (ΔG_{bind}: -110.668), using MM/GBSA are shown in **Figure 3.3**. The glutamic acid side chain of these two compounds is close to the ZA channel (**Figures 3.3b** and **3.3e**). In **Figures 3.3c** and **3.3f**, both compounds formed interactions with Arg54 and Lys60 through their Glu side chain. The distance between Arg54 and the carboxylic acids of compounds **3.31** and **3.61** was approximately 2 Å, which was close enough to form ionic interaction(s). Additionally, both compounds did not disrupt Asn109 and Pro51 binding. Encouraged by promising results from the docking simulations, compound series I and II were synthesized.

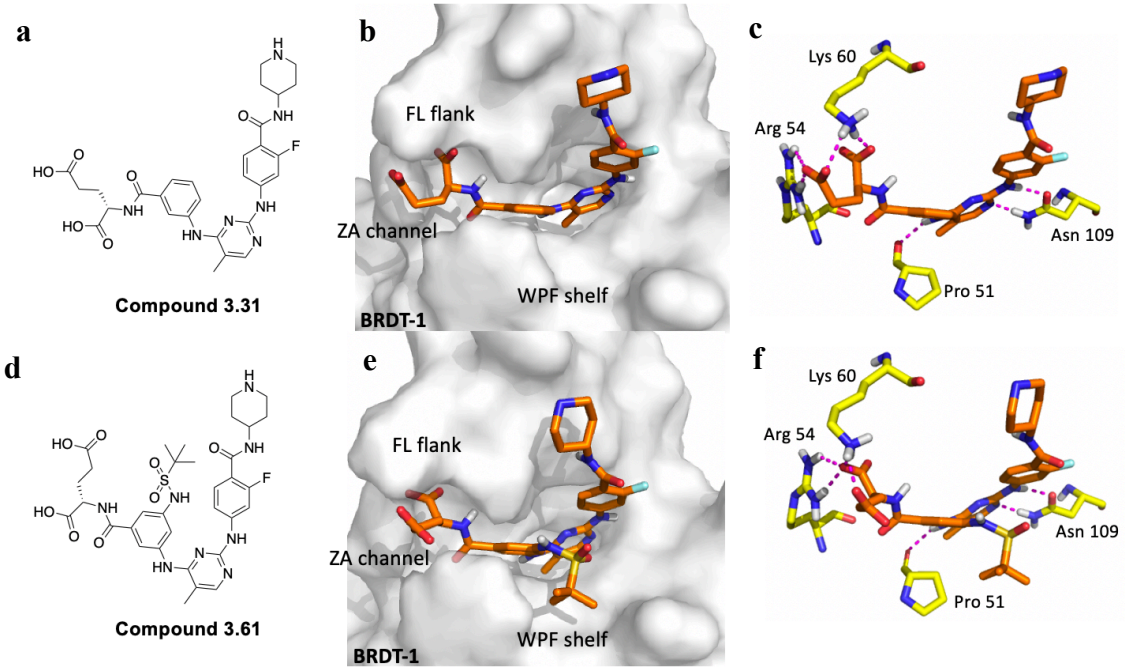


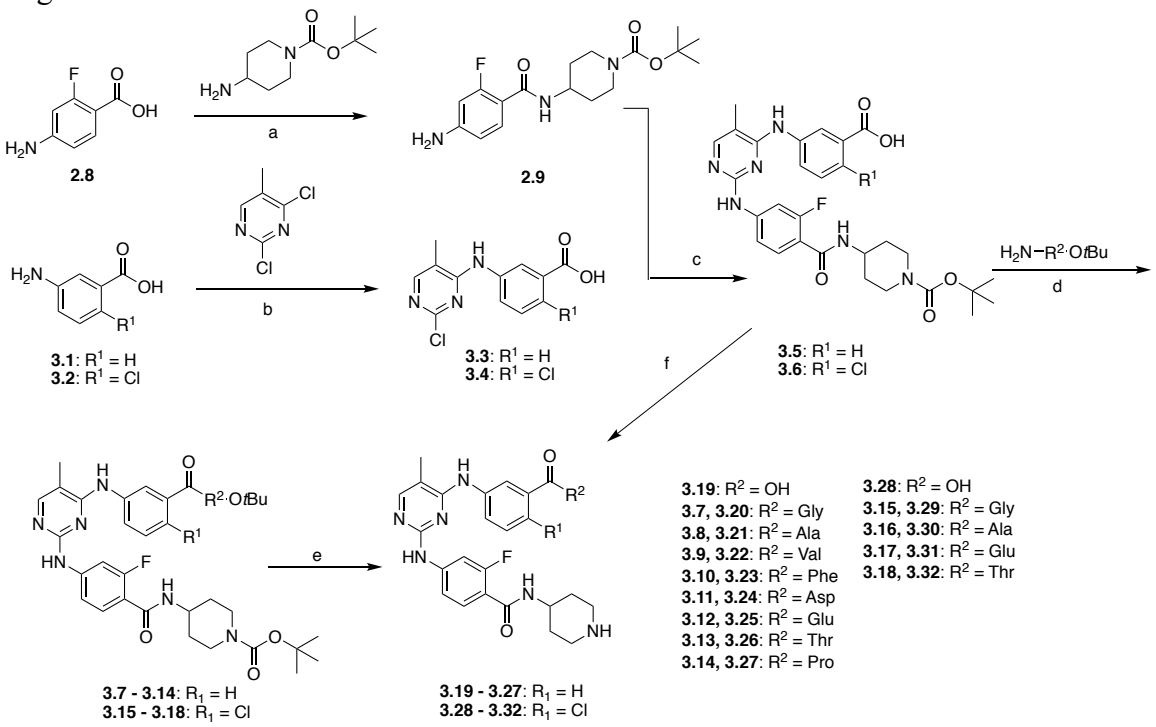
Figure 3.3 Molecular simulation of compounds **3.31** and **3.61** using MM/GBSA. (**a**) Structure of **3.31**; (**b**) compound **3.31** docked into the Kac site of BRDT-1 (PDB: 4FLP); (**c**) hydrogen bonding network surrounding compound **3.31**; (**d**) structure of **3.61**; (**e**) compound **3.61** docked into the Kac site of BRDT-1 (PDB: 4FLP); (**f**) hydrogen bonding network surrounding compound **3.61**.

3.2 Chemistry. A six-step synthetic route was designed for the series I compounds (**Scheme 3.1**). Condensation of commercially available 4-amino-2-fluorobenzoic acid (**2.8**) with *t*-butyl 4-aminopiperidine-1-carboxylate gave first fragment **2.9**. Aminobenzoic acids **3.1** and **3.2** were substituted with 2,4-dichloro-5-methylpyrimidine to provide second fragments **3.3** and **3.4**. Connection of the first and second fragments through a Buchwald-Hartwig coupling reaction yielded **3.5** and **3.6**, which could both be deprotected by TFA to generate target molecules **3.19** and **3.28**, respectively.[78] Different side chains were introduced onto intermediates **3.5** and **3.6** by coupling them with *t*-butyl protected amino acids under EDC, HOBT and DIPEA in DMF and yielded **3.7–3.14** and **3.15–3.18**, which were then globally deprotected by TFA to give desired molecules **3.20–3.27** and **3.29–3.32**. Because fragment **2.9** was prepared in the first series of compounds, the synthetic route for series II was reduced to 8 steps (**Scheme 3.2**). Commercially available **3.33** was methylated with MeOH to give **3.34**,[120] followed by single substitution of 2,4-dichloro-5-methylpyrimidine to afford chloropyrimidine **3.35**. Reaction of **3.35** with *t*-butylsulfinyl chloride furnished *t*-butylsulfinyl **3.36** that was further oxidized with mCPBA to

sulfonamide **3.37**. Connection of fragment **3.37** and **2.9** by a Buchwald-Hartwig coupling reaction yielded **3.38**, which was then hydrolyzed with LiOH to give key intermediate **3.39**. Different side chains were introduced by coupling with *t*-butyl protected amino acids to yield **3.40**–**3.54**, which were then globally deprotected by TFA to give desired molecules **3.56**–**3.71**. Target molecule **3.55** can be obtained directly from **3.38** through a Boc deprotection procedure.

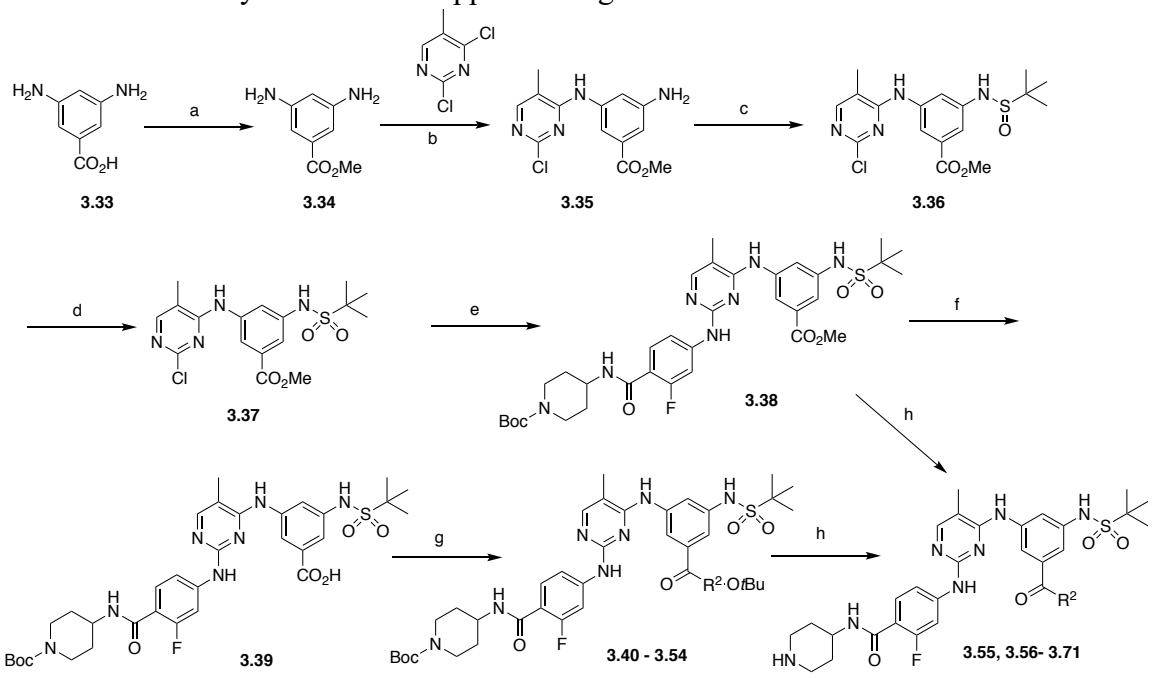
Series III was synthesized based on previous fragments **2.7** and **3.37** (**Scheme 3.3**). Compounds **3.71** and **3.72** were obtained from a Buchwald-Hartwig coupling reaction using **2.7** and **3.37** as the starting material, respectively. Compound **3.37** was hydrolyzed with LiOH to give key intermediate **3.73**. *t*-Butyl-protected Gly and Phe were introduced through a coupling reaction with HATU in DMF to yield **3.74** and **3.75**, which were finally deprotected by TFA to give **3.76** and **3.77**.

Scheme 3.1 Series I: *t*-butyl sulfonamide of SG3-17 replaced with amino acids to approach Arg54 in BRDT-1



Reagents and conditions: (a) *t*-butyl 4-aminopiperidine-1-carboxylate, HATU, DIPEA, DMF, rt, 12 h; (b) 2,4-dichloro-5-methylpyrimidine, DIPEA, isopropanol, 120 °C, 2 d; (c) compound **2.9**, $Pd_2(dba)_3$, BINAP, NaO*t*-Bu, 1,4-dioxane, 110 °C, 5 h; (d) EDC, HOBT, DIPEA, DMF, rt, 12 h.

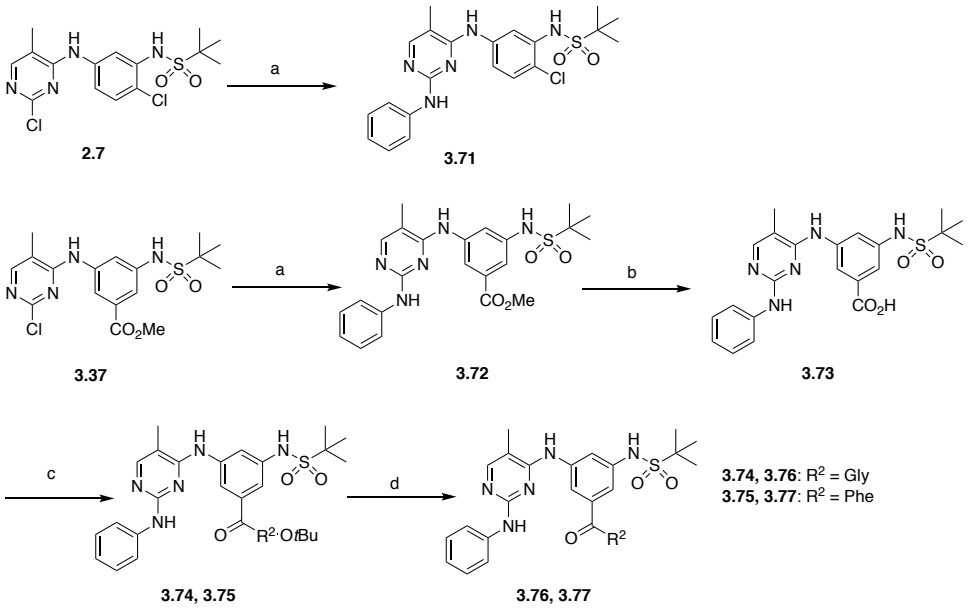
Scheme 3.2 Series II: various substituents introduced at meta position of *t*-butyl sulfonamide moiety of SG3-17 to approach Arg54 in BRDT-1



3.55: R^2 = OMe
3.40, 3.56: R^2 = Gly
3.41, 3.57: R^2 = Phe
3.42, 3.58: R^2 = D-Phe
3.43, 3.59: R^2 = The
3.44, 3.60: R^2 = Ser
3.45, 3.61: R^2 = Glu
3.46, 3.62: R^2 = Gln
3.47, 3.63: R^2 = *t*-butyl
3.48, 3.64: R^2 = phenethylamine
3.49, 3.65: R^2 = $NHCH_2CO_2Me$
3.50, 3.66: R^2 = $NH(CH_2)_2CO_2H$
3.51, 3.67: R^2 = $NH(CH_2)_2CO_2H$
3.52, 3.68: R^2 = $NHCH_2SO_3H$
3.53, 3.69: R^2 = $NHCH_2SO_3NH_2$
3.54, 3.70: R^2 = $NHCH_2CONH_2$

Reagents and conditions: (a) MeOH, H_2SO_4, reflux, 4 h; (b) 2,4-dichloro-5-methylpyrimidine, DIPEA, isopropanol, 120 °C, 2 d; (c) 2-methylpropane-2-sulfinic chloride, pyridine, DCM, rt, 20 h; (d) mCPBA, DCM, rt, overnight; (e) compound **2.9**, $Pd_2(dba)_3$, BINAP, NaO*t*-Bu, 1,4-dioxane, 110 °C, 12 h; (f) LiOH, THF/MeOH/H_2O, 60 °C, 3 h; (g) EDC, HOBt, RNH_2, rt, 12 h; (h) TFA, DCM, 2 h.

Scheme 3.3 Series III: piperidine removal from compound of SG3-179 analogs



Reagents and conditions: (a) aniline, $Pd_2(dba)_3$, BINAP, NaO*t*-Bu, 1,4-dioxane, 110 °C, 12 h; (b) LiOH, THF/MeOH/H_2O, 60 °C, 3 h; (c) EDC, HOBt, protected R^2NH_2, rt, 12 h; (d) TFA, DCM, 2 h.

3.3 Results and discussion

3.3.1 Series I compounds are weak BRDT-1/BRD4-1 inhibitors

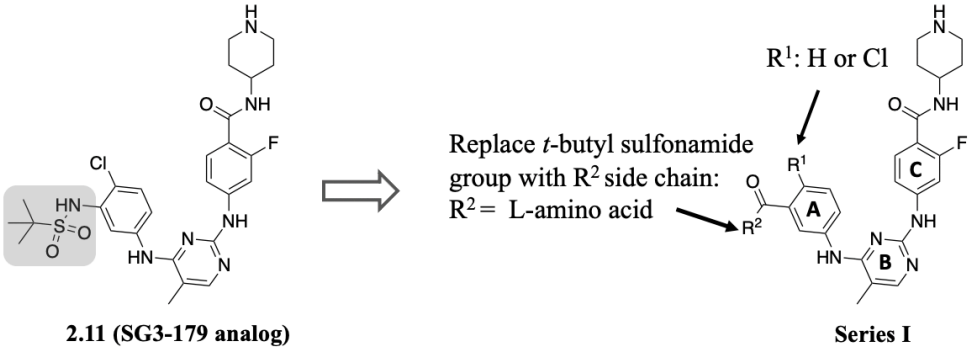
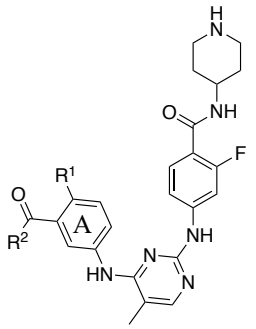


Figure 3.4 Series I of SG3-179 analogs.

The first compound series, series I, was designed based on the binding pose 1 of SG3-179 chemotype in **Figure 3.2e**. Compound **2.11** was an SG3-179 analog from our FP probe project that showed IC_{50} values of 49.0 nM for BRDT-1 and 80.1 nM for BRD4-1. Compared with SG3-179, it lacked a methyl group at the piperidine ring and maintained potency for BRDT-1 and BRD4-1. Based on expertise gained from the FP project, the

series I compounds were generated based on compound **2.11** (**Figure 3.4**). In this series, R^1 was either H or Cl and R^2 represents different side chains. L-Amino acid side chains were introduced to target Arg54 in the ZA channel. K_i and IC_{50} values were then determined by FP assay and AlphaScreen. Compound **3.19** contained the smallest acidic side chain and exhibited no activity in both assays. We then extended side chain length by appending a Gly moiety and obtained compound **3.20**. This compound was still a very weak BRDT-1 (IC_{50} = 43.4 μM) and BRD4-1 inhibitor (IC_{50} = 17.1 μM). Hydrophobic (Ala, Val, Phe), negatively charged (Asp, Glu) and uncharged (Thr, Pro) amino acids were also explored, but all led to significant activity loss for BRDT-1 and BRD4-1. Because the chlorine of SG3-179 was deleted in our first compound set, a second set of compounds **3.28** – **3.32** were obtained to determine the influence of the deleted chlorine in ring A. Disappointingly, these of compounds were also very weak inhibitors of BRDT-1/BRD4-1 (10–30 μM). While re-analyzing these two sets of compounds, we noticed that compounds with hydrophobic side chains (compounds **3.22**, **3.23** and **3.30**) always had relatively better activity compared to those with polar side chains (compounds **3.25**, **3.26** and **3.31**). Hydrophobic groups at ring A, like *t*-butyl sulfonamide, might be important to maintain the potency of SG3-179, so we kept the *t*-butyl sulfonamide in series II.

Table 3.1 Structure−Activity Relationship of Series I



Compound	R^1	R^2 Side chain	AlphaScreen,[1] IC_{50} (μM)		SI	FP assay,[2] K_i (μM)		SI
			BRDT-1	BRD4-1		BRDT-1	BRD4-1	
3.19	H	OH	> 50	> 50	NA	> 3.4	> 4.2	NA
3.20	H	Gly	43.4	17.1	0.39	> 3.4	> 4.2	NA
3.21	H	Ala	> 50	> 50	NA	> 3.4	> 4.2	NA
3.22	H	Val	12.7	9.8	0.77	2.6	2.0	0.77
3.23	H	Phe	15.3	13.0	0.85	2.5	3.9	1.6
3.24	H	Asp	> 50	> 50	NA	> 3.4	> 4.2	NA
3.25	H	Glu	> 50	> 50	NA	> 3.4	> 4.2	NA
3.26	H	Thr	29.6	28.2	0.95	> 3.4	> 4.2	NA
3.27	H	Pro	15.2	20.3	1.3	> 3.4	> 4.2	NA
3.28	Cl	OH	> 50	> 50	NA	> 3.4	> 4.2	NA
3.29	Cl	Gly	> 50	40.5	NA	> 3.4	> 4.2	NA
3.30	Cl	Ala	12.9	8.6	0.67	2.6	2.5	NA
3.31	Cl	Glu	> 50	73.1	NA	> 3.4	> 4.2	NA
3.32	Cl	Thr	30.6	20.1	0.66	> 3.4	3.8	NA
2.11	Cl	NA	0.0490	0.0801	1.6	NA	NA	NA
JQ-1	NA	NA	0.133	0.0650	0.49	NA	NA	NA

[1]AlphaScreen performed by the Jun Qi group, single experiment performed in quadruplicate.
[2]FP assay performed by Jonathan Solberg, single experiment performed in duplicate.
[3]NA means data is not available.

3.3.2 Series II compounds are potent BRDT-1/BRD4-1 inhibitors

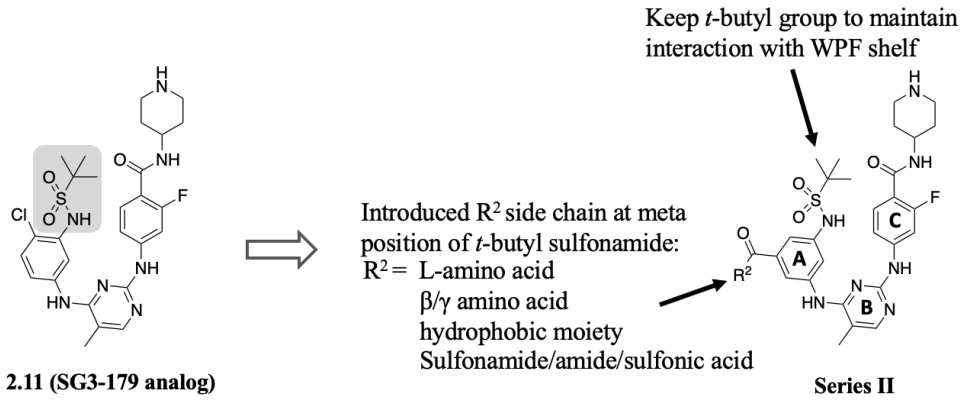
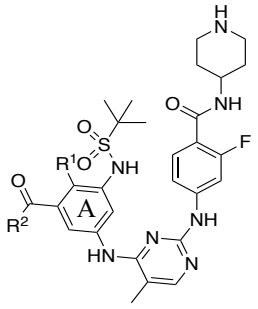


Figure 3.5 Series II of SG3-179 analogs.

Series II compounds were designed based on the SG3-179 binding pose in **Figure 3.2f**. To maintain hydrophobic interactions with the WPF shelf, the *t*-butyl group was kept in this series but is devoid of the ortho-chlorine substituent. A side chain at the R^2 position was introduced to target Arg54 in the ZA channel (**Figure 3.5**). L-Amino acids, β/γ amino acids or sulfonic acid was introduced as R^2 to form ionic interactions with the guanidine of Arg54. In addition to the ionic interactions, the sulfonamide or amide side chains at R^2 were designed to form H-bond(s) with Arg54. Additionally, we investigated hydrophobic moieties to attempt to form hydrophobic interactions with the backbone of Arg54.

Compound **3.55** (**Table 3.2**) was synthesized first and compared with compound **2.11**. It maintained potency for BRDT-1 and BRD4-1. The introduction of different amino acid side chains further increased activity up to five-fold. Compared with series I, the potency of this series of compounds increased around 1000-fold. Gly, Phe, and D-Phe were explored in compounds **3.56**, **3.67** and **3.58**, but all led to pan-inhibition for BRDT-1 and BRD4-1. Compounds **3.59**, **3.60** and **3.61** showed 3.3-fold, 13-fold and 5.9-fold selectivity, respectively, for BRDT-1 over BRD4-1 via decreased BRD4-1 activity. To determine which carboxylic acid of Glu (in **3.61**) had the potential to interact with Arg54, compounds **3.65**, **3.67**, and **3.62** were synthesized.

Table 3.2 Structure−Activity Relationship of Series II



Compound	R^1	R^2 Side chain	AlphaScreen,[1] IC_{50} (nM)		SI	FP,[2] K_i (nM)		SI
			BRDT-1	BRD4-1		BRDT-1	BRD4-1	
3.55	H	OMe	29.5	51.3	1.7	NA	NA	NA
3.56	H	Gly	13.7	16.7	1.2	28	16	0.58
3.57	H	Phe	17.3	28.4	1.6	18	14	0.77
3.58	H	D-Phe	12.7	14.3	1.1	20	20	1.0
3.59	H	Thr	15.9	52.8	3.3	31	59	1.9
3.60	H	Ser	19.3	255.9	13	TBD	TBD	TBD
3.61	H	Glu	21.3	124.3	5.9	21	71	3.4
3.62	H	Gln	22.0	119.4	5.4	TBD	TBD	TBD
3.63	H	*t*-butyl	24.5	43.7	1.3	50	30	0.74
3.64	H	phenethylamine	39.3	92.0	2.3	30	30	1.0
3.65	H	$NHCH_2CO_2Me$	20.4	32.2	1.7	40	20	0.62
3.66	H	$NH(CH_2)_2CO_2H$	12.7	53.0	4.2	20	30	1.6
3.67	H	$NH(CH_2)_3CO_2H$	11.1	29.2	2.6	30	30	1.3
3.68	H	$NHCH_2SO_3H$	11.5	22.2	2.0	NA	NA	NA
3.69	H	$NHCH_2CH_2SO_2NH_2$	9.2	16.9	1.8	NA	NA	NA
3.70	H	$NHCH_2CONH_2$	12.2	12.2	1.0	NA	NA	NA
2.11	Cl	NA	49.0	80.1	1.6	NA	NA	NA
JQ-1	NA	NA	133.3	65.0	0.49	NA	NA	NA

[1]AlphaScreen performed by Jun Qi group, single experiment performed in quadruplicate.
[2]FP assay performed by Jonathan Solberg, single experiment performed in duplicate.
[3]NA means data is not available, TBD means data is to be determined.

Compound **3.56**, which had the same α-carboxylic acid as **3.61**, did not exhibit selectivity for BRDT-1. Compound **3.65**, containing a methylated Gly at the terminus, showed similar activity to compound **3.56**, which indicated that the α-carboxylic acid of compound **3.56** failed to interact with Arg54 of BRDT-1. Compound **3.67** had the same γ-

carboxylic acid as **3.61**, but **3.67** only exhibited 2.6-fold selectivity for BRDT-1. Compound **3.62** contained a Gln side chain, which blocks the γ-carboxylic chemotype, and it showed 5.4-fold selectivity for BRDT-1, so selectivity may not be directly related to the carboxylic acid of the Glu side chain in compound **3.61**. Compounds **3.56**, **3.66** and **3.67** were synthesized to explore side chain length, and we determined that extending the aliphatic acid chain did not improve selectivity for BRDT-1. In addition to the carboxylic acid, a sulfonic acid (compound **3.68**), sulfonamide (compound **3.69**), and amide (compound **3.70**) were utilized to form a salt bridge or hydrogen bond(s) with Arg54. Compounds **3.68**–**3.70** all exhibited pan inhibition for BRDT-1 and BRD4-1.

In summary, this series of compounds was up to 5-fold more potent than the parent compound **2.11**. Some compounds (**3.60**, **3.61** and **3.62**) showed >5 fold selectivity for BRDT-1 over BRD4-1, which is promising for further selective analog development. In fact, recent AlphaScreen results revealed that compound **3.60** showed 13-fold selectivity for BRDT-1 over BRD4-1, which makes it the most selective compound in all series synthesized in this work.

3.3.3 Series III: deletion of SG3-179 piperidine decreases BRDT-1/BRD4-1 inhibition

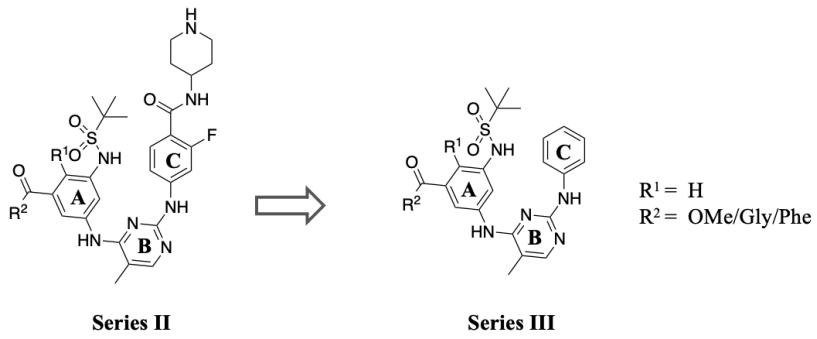
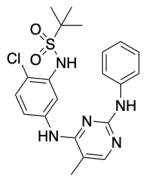


Figure 3.6 Series III of SG3-179 analogs.

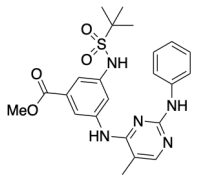
After two rounds of modifications, the molecular weight of these compounds began to exceed 500. The cocrystal structure of SG3-179 and BRDT-1 (PDB: 4FLT)[85] shows that the polar piperidine moiety is solvent exposed. When modifying our FP probes, modification of the piperidine did not influence the binding affinity of FP probes, so this moiety was targeted for modification at the piperidine in series III (**Figure 3.6**). We removed the piperidine moiety of compounds **2.11**, **3.55**, **3.56** and **3.57** in series II to

decrease molecular size. Series III (**3.71**, **3.72**, **3.76** and **3.77**) was then generated. Disappointingly, these compounds demonstrated very weak BRDT-1 and BRD4-1 activity (**Table 3.3**). We concluded that the deleted piperidine moiety may not only improve solubility but also may play an important role in maintaining the correct binding pose of the entire molecule.

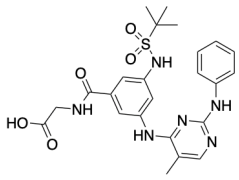
Table 3.3 Structure−Activity relationship of Series III



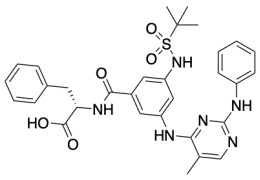
3.71



3.72



3.76



3.77

Compound	AlphaScreen,[1] IC_{50} (nM)		SI
	BRDT-1	BRD4-1	
3.71	1478	2699	2.7
3.72	336	648	1.9
3.76	378	649	1.7
3.77	849	1490	1.8

[1]AlphaScreen performed by Jun Qi group, single experiment performed in quadruplicate.

3.3.4 Crystal structure of compound 3.61. The crystal structure of compound **3.61** in complex with BRD4-1 and BRDT-1 is shown in **Figure 3.7**. Compound **3.61** is bound to BRD4-1 and BRDT-1 in a similar mode: the *t*-butyl group of **3.61** is located in the hydrophobic cavity of the WPF shelf, the Glu side chain is located in the ZA channel, and the piperidine moiety is solvent exposed (**Figures 3.7a** and **3.7c**). **Figures 3.7d** and **3.7e** show interactions between compound **3.61** and the amino acid residues of BRD4-1 and BRDT-1. The pyrimidine core (ring B) and adjacent NH of compound **3.61** formed a pair of H-bonds with conserved Asn140 in BRD4-1 and Asn109 in BRDT-1. The NH between rings A and B of **3.61** formed a hydrogen bond with Pro82 in BRD4-1 and Pro51 in BRDT-1. In **Figure 3.7d**, the α-carboxylic acid of the glutamic acid side chain stretched toward Gln85, which is the BRD4 residue in the same position as Arg54 in BRDT-1. However, the Glu side chain of compound **3.61** did not exhibit adequate engagement with Arg54 in **Figure 3.7e**.

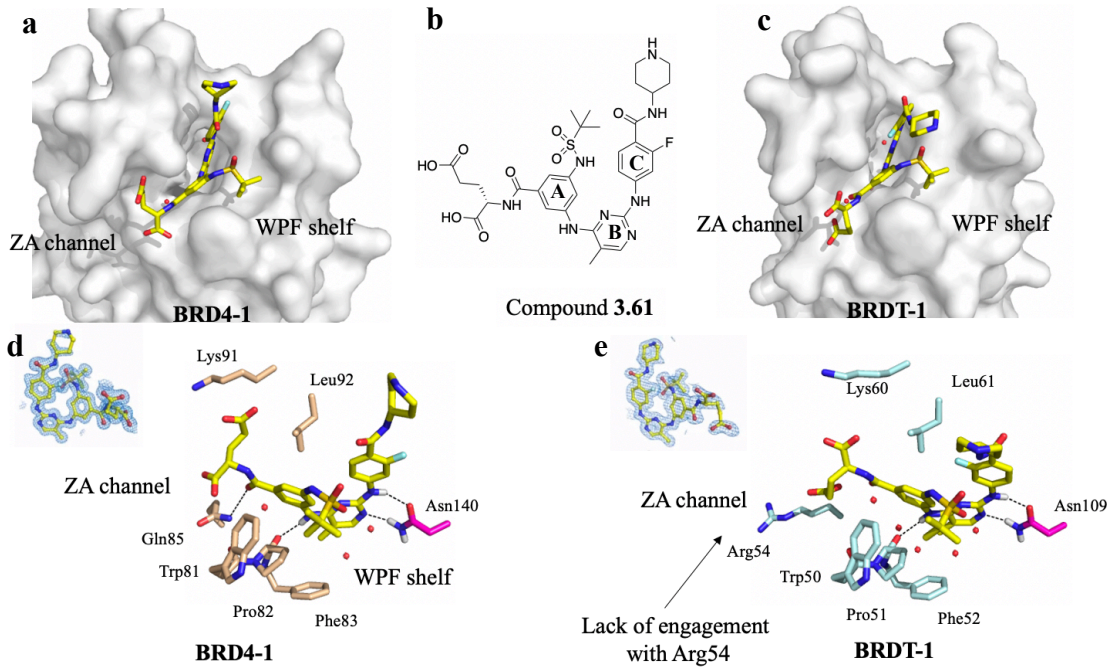


Figure 3.7 Comparison of **3.61** in BRD4 versus BRDT. **(a)** Compound **3.61** in complex with BRD4-1; **(b)** structure of compound **3.61**; **(c)** compound **3.61** in complex with BRDT-1; **(d)** hydrogen bond network around compound **3.61** in the active site of BRD4-1 involved Asn140, Pro82 and Gln85; **(e)** hydrogen bond network around compound **3.61** in the active site of BRDT-1 involved Asn109, Pro51. Crystal structures of **3.61** in complex with BRD4-1 and BRDT-1 were provided by the Ernst Schönbrunn group at the Moffitt Cancer Center.

The conserved network of water molecules in the ZA channel was disrupted by compound **3.61** in the Kac site of BRD4-1 in **Figure 3.7d**. Compared with the cocrystal structures containing SG-179 (**Figure 3.1**), two conserved water molecules close to the ZA channel were absent. BRDT-1 in complex with **3.61** maintained all five conserved water in the Kac site in **Figure 3.7e.** Disrupting the conserved water network may influence the stability of the loop area as well as binding affinity. The AlphaScreen assay showed decreased BRD4 activity (IC_{50} = 124.3 nM) for compound **3.61** but BRDT-1 activity was maintained. Water network disruption in the BRD4-1 Kac site might explain why compound **3.61** showed 5.9-fold selectivity for BRDT-1 over BRD4-1.

3.3.5 Compound 3.61 has no kinase (JAK2 and FLT3) activity. Parent compound SG3-179 is a dual JAK2 kinase-BET inhibitor. Since the structure of JAK2 has not been solved in complex with SG3-179, we used a cocrystal structure with its analog TG101209 for analysis (PDB: 4JI9). The pyrimidine core and adjacent NH of TG101209 forms a pair of

key H-bonds with conserved Leu932 (**Figure 3.8**) in JAK 2 (PDB: 4JI9) and Asp140 in BRD4-1 (PDB: 4O76).[85, 86, 112] In the JAK2 ATP binding site, the meta position of the *t*-butyl group was blocked by the backbone containing Gly856 and Leu855 (**Figure 3.8**). Since compound **3.61** contained a Glu side chain at the position meta to the *t*-butyl moiety, we hypothesized that the JAK2 ATP pocket could not provide enough space for compound **3.61** to bind. To test this idea, we docked series II compounds (docking scores ranged from -6.1165 to -10.680), SG3-179 (docking score: -10.680), and TG101209 (docking score: -10.011) to JAK2 in Maestro (**Figures 3.8d, 3.8e** and **3.8f**) and representative compounds **3.61** (magenta), TG101209 (green) and SG3-179 (orange) are shown. In the docking simulation, TG101209 and SG 3-179 maintained the key H-bonds with Leu932 of JAK2 (**Figure 3.8e**), but compound **3.61** (docking score: -6.120) failed to have enough engagement with Leu932 in **Figure 3.8f**. None of the series II compounds maintained H-bonds with Leu932. Virtual simulation of compound **3.61** implied that compound **3.61** could be a weak binder of JAK2. In the results from the AlphaScreen assay (**Table 3.4**), compound **3.61** exhibited no activity for JAK2 (IC_{50} > 10,000 nM). Losing key H-bonds with Leu932 might explain the significant decrease in activity. In addition to JAK2, receptor-type tyrosine-protein kinase FLT3 activity was also evaluated. SG3-179 was a potent FLT3 inhibitor with an IC_{50} of 32 nM, but our compound **3.61** was a weak FLT3 binder with more than 400-fold selectivity for BRDT-1 (**Table 3.4**).

Table 3.4 Activity of selected compounds against the bromodomain panel

Compound	BET,[1] IC_{50} (nM)		Kinase[2], IC_{50} (nM)	
	BRDT-1	**BRD4-1**	**JAK2**	**FLT3**
TG101209	290	130	0.51	1.5
SG-179	23	21	12	32
3.61	21	124	>10,000	>10,000

[1]BET AlphaScreen assay performed by Jun Qi group, single experiment performed in quadruplicate.
[2]Kinase AlphaScreen assay performed by Reaction Biology, single experiment performed in duplicate.

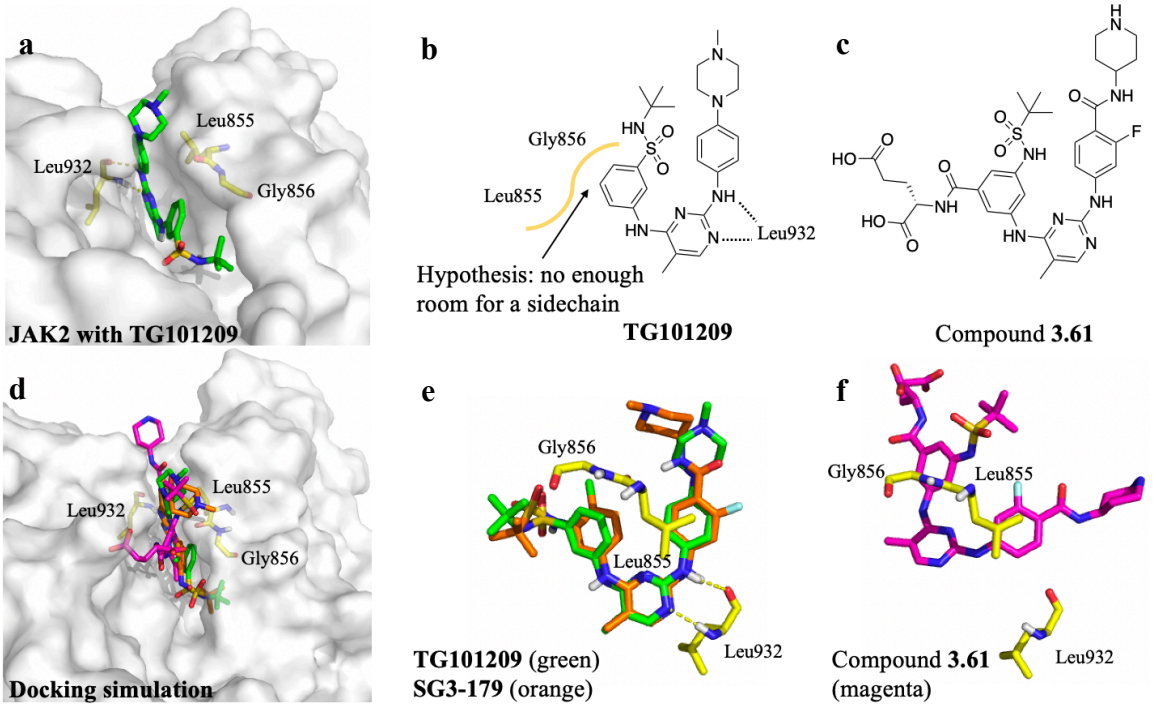


Figure 3.8 Possible explanation for decreased JAK2 activity of compound **3.61.** (**a**) TG101209 in complex with JAK2 (PDB: 4JI9); (**b**) structure of TG101209; (**c**) structure of compound **3.61**; (**d**) TG101209 (green) and compound **3.61** (magenta) docked into JAK2 (PDB: 4JI9); (**e**) in docking simulation, TG101209 maintained the key interaction with Leu932; (**f**) in docking simulation, compound **3.61** failed to formed H-bonds with Leu932.

3.4 Conclusions and future directions. 2,4-Disubstitued pyrimidine derivative TG101209 was generated by TargeGen Incas a JAK2 kinase inhibitor for anticancer therapy.[112] Discovery of its BET inhibition activity initiated its modification toward BET inhibitors. SG3-179 was then developed by the Moffit group with dual inhibition for kinases (JAK2 and FLT3) and BET family proteins. As both BRD4 and JAK2 are validated cancer targets, the inhibition profile of SG3-179 containing multiple targets should lead to improved potency for anti-cancer therapy. However, the low selectivity of SG3-179 limits its application in male contraception. Moreover, the cytotoxicity induced by JAK2 and FLT3 inhibition calls for new 2,4-disubstitued pyrimidine derivatives for male contraception. In our studies, we used the two binding poses of the SG3-179 chemotype observed in a dimeric BRD4-1 crystal structure to design two strategies to target interaction with Arg54 of BRDT (series I and series II compounds). In series I, the *t*-butylsuloamide group was replaced amides of with various amino acid side chains. Two sets of compounds

were generated that yielded weak BET inhibitors. A total of 16 compounds were synthesized and evaluated based on the second strategy (series II) with a new side chain meta to the *t*-butyl group. The structure-activity relationship was explored. Compared with series I, the potency of series II increased from double digital micromolar to double digital nano molecular activity for BRDT-1 inhibition. Compound **3.60** exhibited 13-fold selectivity for BRDT-1 over BRD4-1. The cocrystal structure of compound **3.61** with BRD4-1 and BRDT-1 disclosed its binding mode. Results from the kinase activity assay showed that compound **3.61** exhibited >400-fold selectivity for BRDT-1 over JAK2 and FLT3. In addition, we attempted to decrease the molecular weight by deleting the piperidine moiety in series III, but this polar solvent-exposed side chain was deemed important for potency.

In the future, further modification of compound **3.60** will be performed to improve BRDT selectivity and its physicochemical properties. In conjunction with the Qi and Schönbrunn groups, cellular assays and determination of c-Myc levels will be performed to monitor cellular activity of the synthesized compounds.

Chapter 4: Discovery of Selective Bivalent Inhibitors for Testis-Specific Bromodomain (BRDT)

4.1 Induction. BET family proteins regulate gene transcription and chromatin remodeling through a multivalent interaction with acetylated histone and transcription proteins.[30, 37, 38, 59, 121] However, a monovalent strategy seemed challenging for the discovery of BRDT-1 selective compounds, because BET proteins share high homology in the Kac site and a common Kac recognition motif with conserved Asn.[122] BET family proteins contain two Kac recognition motifs, the first bromodomain (BD1) and the second bromodomain (BD2).[123] Thomas' work on the Kac recognition mechanism indicated that the BET family interact with histones in a bivalent manner.[59] Subsequent research found that bivalent BRD4 inhibitors were up to 100-fold more potent than the corresponding monovalent compound in protein binding assay and cell assays.[91, 92] The chemotypes of these bivalent compounds (JQ-1, i-BET762 and AZD3514) are potent Kac site binders. Multiple experiments (crystal structures, SAXS, NMR, SEC) have been performed to elucidate the ligand binding mode, but it is still unclear whether bivalent molecules bind to BRD4 intermolecularly or intramolecularly.

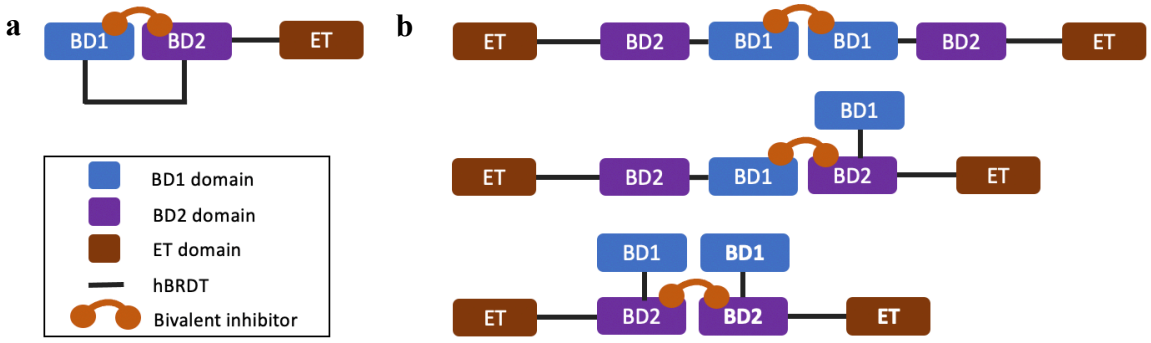


Figure 4.1 Proposed strategy for the preparation of dimeric inhibitor libraries.
(a) intramolecular binding; **(b)** intermolecular binding.

In our research, we focused on BRDT inhibitor development. As a member of the BET family of bromodomain proteins, BRDT also contained the characteristic first and second bromodomains. Therefore, bivalent inhibitors can either interact with BRDT intramolecularly or intermolecularly (BD1 and BD2; **Figure 4.1a**). Due to BRDT containing the shortest sequence length between the two bromodomains (**Figure 1.23**),

BRDT selectivity may be achieved through spacer length modification of a bivalent molecule targeting the intramolecular interaction of the two bromodomains.

In contrast to intramolecular binding, intermolecular binding is a second strategy for bivalent molecule design. For full length BET proteins, there are three possible intermolecular binding modes between two bromodomains: BD1-BD1, BD1-BD2 and BD2-BD2.

Because Dr. Wolgemuth's group discovered that Brdt-1 knock-out mice (*Brdt*$^{\Delta BD1/\Delta BD1}$) were healthy but infertile,[43] we decided to harness the benefits of intermolecular interactions and aim at inhibiting the BRDT BD1-BD1 interaction (**Figure 4.1b**). Two recent literature reports showed that single bromodomains (BRD4-1 or BRD4-2) could form a homodimer induced by small bivalent molecules.[91, 92] In addition to the stability derived from the interaction between ligand and protein, protein-protein interactions (PPIs) in the interface further decrease the free energy of the dimer ($\Delta G_{interface}$ in PDB 5AD2 = -8.512 kcal/mol for BRD4-1 dimer induced by AZD3514 based bivalent inhibitor, $\Delta G_{interface}$ in PDB 5JWM = -8.585 kcal/mol for BRD4-2 dimer induced by JQ-1 based bivalent inhibitor; interface binding energy was calculated by jsPISA2.0.5).[124, 125] The reported BRD4-1 and BRD4-2 homodimers were induced by different molecules but both of these bivalent molecules were still pan-inhibitors for all BRD proteins. If we could increase the interfacial binding energy of a specific BET family protein using a bivalent molecule,[126] selectivity for that specific BET family member may be feasible.

Previously reported bivalent BET inhibitors were designed based on AZD3514 and JQ-1, but we chose to explore SG3-179 as a chemotype. SG3-179 is potent but non-selective binder for BET family proteins (IC_{50} = 23 nM for BRDT-1, IC_{50} = 21 nM for BRD4-1).[85] Crystallographic characterization and the synthetic experience obtained in our monovalent SG3-179 analog project facilitated our synthetic route design as well as the development of a spacer connection strategy (**Figure 4.2**).

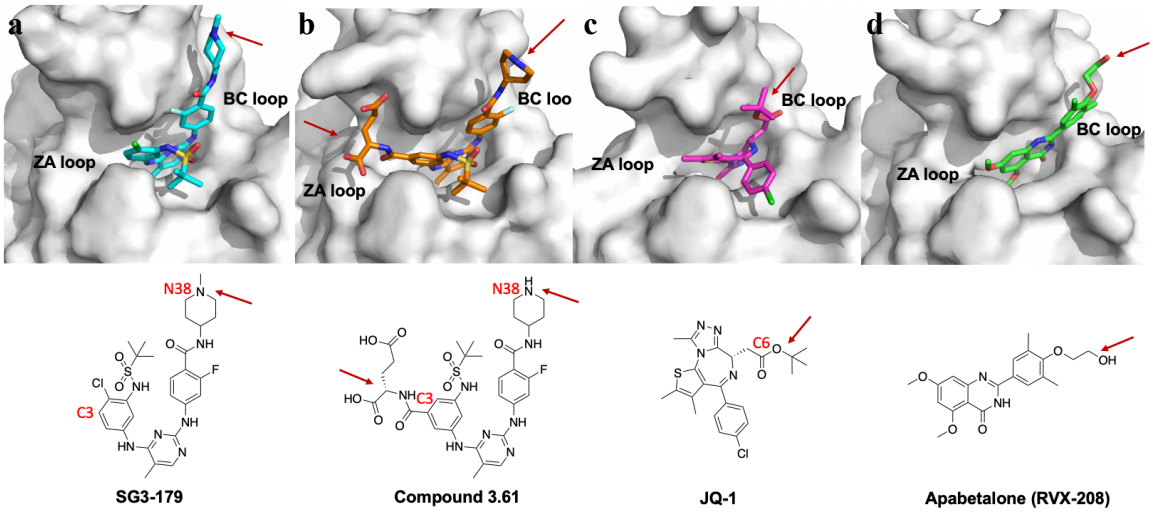


Figure 4.2 Strategy for spacer connection. (**a**) SG3-179 in complex with BRD4-1 (PDB: 5F63); (**b**) compound **3.61** in complex with BRD4-1 (unpublished data from the Schönbrunn group); (**c**) JQ-1 in complex with BRDT-1 (PDB: 4FLP); and (**d**) RVX-208 in complex with BRD4-1 (PDB: 4MR4). Red text denotes the atom numbering of the small molecule and the red arrows in the structural rendering correspond with the arrows and area of the small molecule that can be used for spacer attachment.

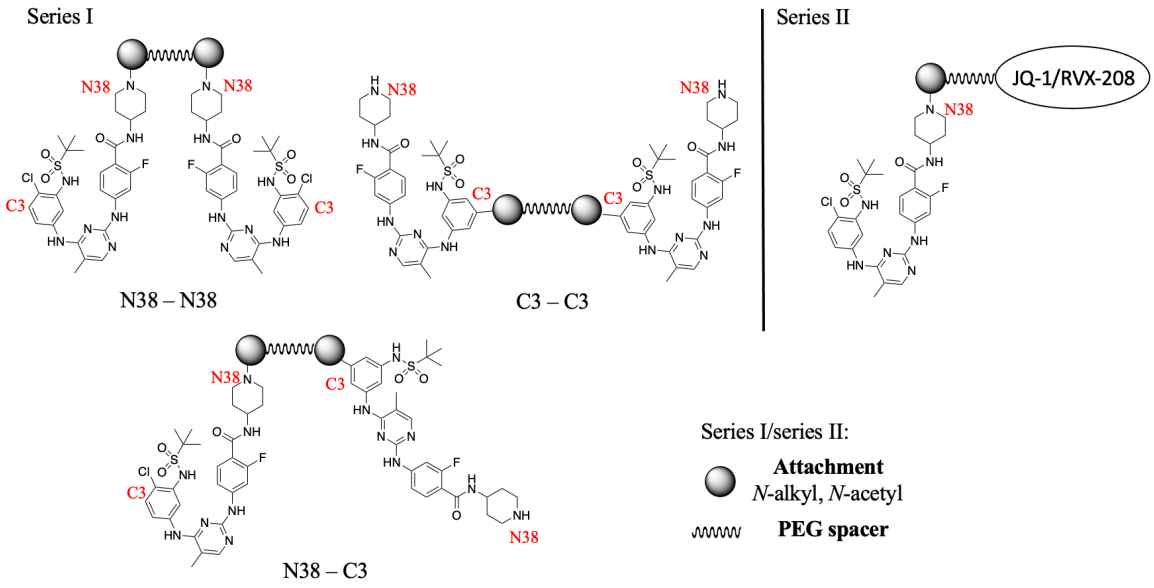


Figure 4.3 Design of symmetric and non-symmetric bivalent inhibitors. Red text denotes the atom numbering of the small molecule.

For compound design of series I (Figure **4.3**), we initially pursued N38–N38, C3–C3 and N38–C3 connecting strategies to link two SG3-179 chemotypes, where N38 and C3 denote the atom numbering of SG3-179. Because a JQ-1 symmetric bivalent inhibitor successfully induced the dimerization of BRD4-2, we first explored symmetric bivalent

SG3-179 inhibitors. The crystal structure of SG3-179 in complex with BRD4-1 indicated that the N38 of SG3-179 is solvent exposed (**Figure 4.2a**).[85] Therefore, we used the N38 of SG3-179 as a handle for spacer attachment. In further support of this approach, our previous FP probe studies also demonstrated that modification of N38 did not influence its BET protein affinity.[78] For the first set (N38 – N38) of compounds in series I, we connected N38 of two SG3-179 chemotypes to form symmetric bivalent inhibitors. Both *N*-alkyl and *N*-acetyl attachments were explored in this set. For these symmetric bivalent compounds, the spacer was introduced at N38 nearby the BC loop (**Figure 4.2a**). To modulate protein dimerization, we were interested in introducing spacers at alternative positions. Through analysis of the crystal structure of compound **3.61** with BRD4-1 (**Figure 4.2b**), the C3 of SG3-179 analog **3.61** in the ZA channel was also a reasonable option as a spacer attachment point. For the second set of series I compounds (C3 – C3), we connected C3 of two SG3-179 chemotypes to form a second type of symmetric bivalent inhibitors. Finally, connecting the C3 of one SG3-179 chemotype to the N38 of another SG3-179 chemotype formed the third compound set in series I (N38–C3).

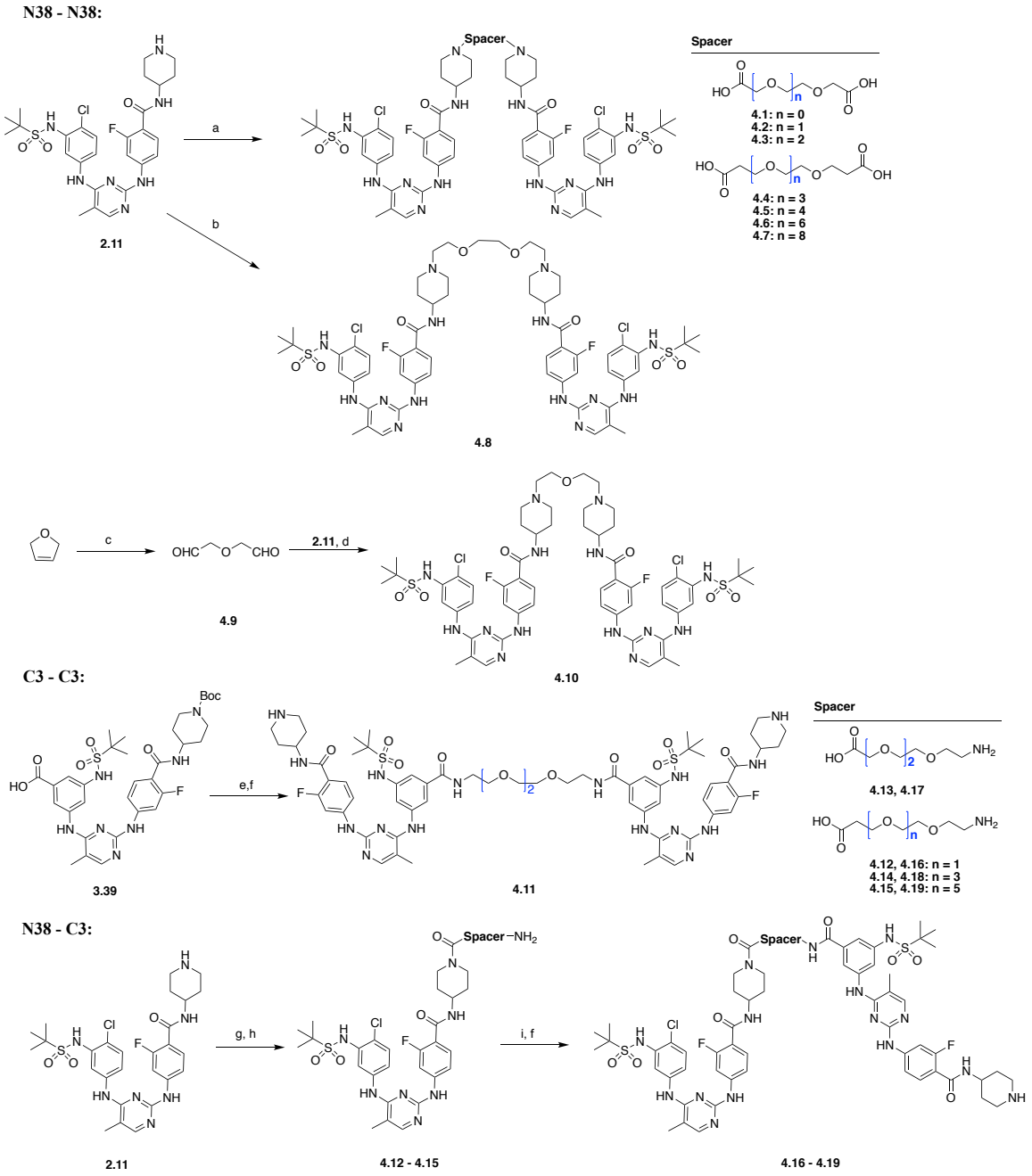
Since JQ-1 and RVX208 are known BET inhibitors,[79, 91] we connected these two compounds to the SG3-179 chemotype at its N38 atom for series II (Figure **4.3**). The ester moiety of JQ-1 has previously been established to be suitable for the attachment of a spacer connection (**Figure 4.2c**).[91] RVX-208 contains a glycol tail for solubility regulation,[79] which was selected for the attachment of the second chemotype (**Figure 4.2d**). In these two series of compounds, we chose PEG spacers to avoid non-specific binding.[127] Moreover, the commercial availability of bifunctional PEG spacers provided a convenient linker library for spacer length exploration.

4.2 Chemistry. In series I (**Scheme 4.1**), the symmetric SG3-179 molecules were generated using previously synthesized compounds **2.11** and **3.39** (discussed in chapters 2 and 3, respectively). Symmetric SG3-179 bivalent molecules **4.1**–**4.7** were generated by base-catalyzed coupling of compound **2.11** with dicarboxylic acid PEG spacers using HATU. A PEG dibromide spacer was introduced under basic conditions through nucleophilic substitution with compound **2.11** to yield N-alkyl modified analog **4.8**. Due to cyclization of bis(2-bromoethyl) ether with **2.11** in regular nucleophilic substitution

conditions, a new strategy was adopted. 2,5-Dihydrofuran was oxidized to yield dialdehyde spacer **4.9**,[128] which was further reacted with **2.11** through reductive amination to give **4.10**. Two equivalents of compound **3.39** were coupled with the dicarboxylic PEG spacer and then the Boc group was deprotected in the presence of piperidine to yield target molecule **4.11**. Fmoc-protected PEG spacers were connected to **2.11** using HATU in the presence of DIPEA. Fmoc deprotection with piperidine provided PEG linkers **4.12**–**4.15**. The connection of fragment **3.39** to PEG linkers **4.12**–**4.15** was performed by a HATU-mediated coupling reaction, followed by Boc deprotection with TFA to furnish non-symmetric SG3-179 molecules **4.16**–**4.19**.

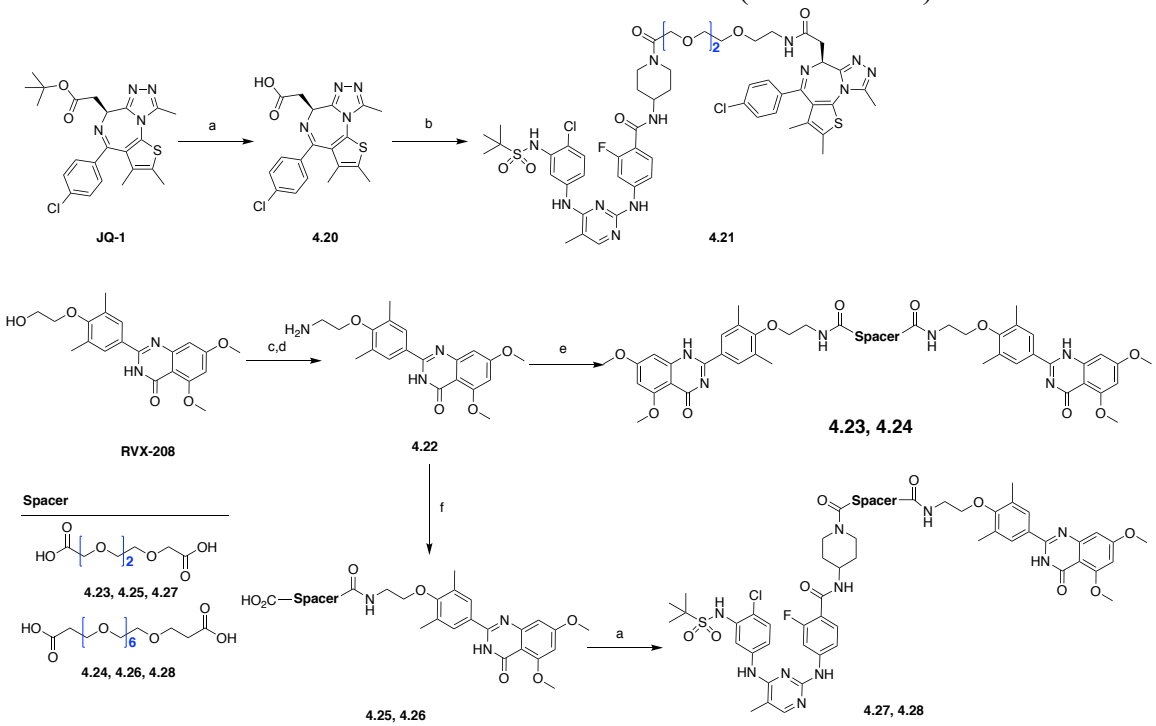
In series II (**Scheme 4.2**), SG3-179 was linked to JQ-1 and RVX-208. In addition, two RVX-208 molecules were connected. After removing the *t*-butyl group of JQ1 with TFA, the corresponding acid **4.20** was connected to intermediate **4.12** to provide non-symmetrical bivalent analog **4.21**. The aliphatic hydroxyl moiety of RVX-208 was transformed to an amine via Gabriel synthesis.[129] Dicarboxylic PEG spacers were then introduced to give disubstituted symmetric RVX-208 analogs **4.23** and **4.24** as well as single substituted intermediates **4.25** and **4.26**. These single substituted intermediates were connected to **2.11** to yield non-symmetric SG3-179-RVX-208 analogs **4.27** and **4.28**.

Scheme 4.1 Series I: synthesis of SG3-179 based bivalent inhibitors using N38-N38, C3-C3 and N38-C3 connection strategy



Reagents and conditions: (a) dicarboxylic PEG spacers, HATU, DIPEA, DMF, rt, 12 h; (b) 1,2-bis(2-bromoethoxy)ethane, KI, DIPEA, DMF, 60 °C, 12 d; (c) ozone, DCM, -78°C, 20 min; PPh_3, 0 °C, 3 h; (d) **2.11**, $NaBH(OAc)_3$, AcOH, $MgSO_4$, rt, 17 h. (e) diamine PEG spacer, HATU, DIPEA, DMF, rt, 12 h; (f) TFA, DCM, rt, 5 h; (g) Fmoc protected spacer, TBTU, DIPEA, DMF, rt, 12 h; (h) piperidine, DMF, rt, 2 h; (i) **3.39**, HATU, DIPEA, DMF, rt, 12 h.

Scheme 4.2 Series II: SG3-179 linked to JQ1 (**4.21**), bivalent symmetrical RVX208 inhibitors **4.23** and **4.24** and SG3-179 linked to RXV208 (**4.27** and **4.28**)



Reagents and conditions: (a) TFA, DCM, rt, 5 h; (b) **4.12**, HATU, DIPEA, DMF, rt, 12 h; (c) isoindoline-1,3-dione, PPh_3, DIAD, anhydrous THF, rt, 16 h; (d) $N_2H_2 \cdot H_2O$, EtOH, reflux, overnight;[130] (e) 0.5 eq of dicarboxylic PEG spacer, HATU, DIPEA, DMF, rt, 12 h; (f) 1.2 eq of dicarboxylic PEG spacer, HATU, DIPEA, DMF, rt, 12 h.

4.3 Results and discussion. A well-established AlphaScreen assay (performed by our collaborators) and the commercially available BROMOscan technology were adopted as our primary screening methods. Our collaborators obtained crystal structures of BET family proteins in complex with bivalent inhibitors and monitored cell anti-proliferation activity and c-Myc levels to reveal the cellular consequences of BET protein inhibition.

4.3.1 Bivalent molecules are potent BET protein inhibitors. For series I, we used three ways (N38–N38, C3–C3 and N38–C3) to connect two SG3-179 chemotypes. Since the JQ-1 based symmetric bivalent inhibitor induced the dimerization of BRD4-2, we first explored another symmetric strategy (N38–N38) to determine whether symmetric SG3-179 analogs would also induce dimerization. The N38–N38 compounds were prepared by conjugating varying lengths of PEG spacers with the piperidine tail of SG3-179 at N38 through an amide attachment. Bivalent molecule **4.1** contained the shortest spacer, and in

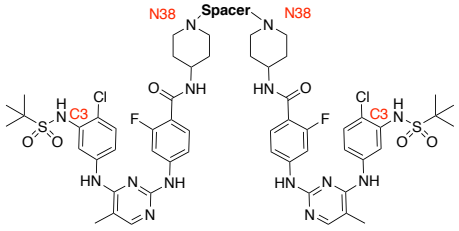
the AlphaScreen assay, it exhibited similar activity against both BRDT-1 and BRD4-1 (**Table 4.1**). With the extension of spacer length from 1 to 6 PEGs, BRDT-1 inhibitory activity increased between 5- and 10-fold in a non-linear manner, while the IC_{50} decreased between 2- and 8-fold for BRD4-1. Among these compounds, **4.2** and **4.3** showed more than 40-fold selectivity for BRDT-1 over BRD4-1. Selectivity was further improved to 70-fold as spacer length increased in compounds **4.4**, **4.5** and **4.6**. This trend was terminated when the spacer length grew up to 7 PEGs. Compound **4.7** with an 8-PEG spacer only showed 18-fold selectivity for BRDT-1 over BRD4-1. To investigate the influence of amide attachment, we transformed this rigid amide attachment into a more flexible *N*-alkyl moiety to obtain compounds **4.10** and **4.8**. Bivalent molecule **4.10** contained the shortest spacer and exhibited no selectivity for BRDT-1 or BRD4-1. Compound **4.8**, which contained the same spacer length as **4.2**, exhibited decreased selectivity for BRDT-1. Amide attachment, it seemed, was beneficial to maintain selectivity for BRDT-1 over BRD4-1 in the bivalent SG3-179 series.

All compounds above introduced functional moieties at N38 close to the BC loop (**Figure 4.2a**). Therefore, we proposed an alternative spacer introduction strategy to influence selectivity and potency. The crystal structure of **3.61** in complex with BRD4-1 showed that the glutamic acid moiety at the C3 position was close to the ZA channel (**Figure 4.2b**). From our previous monovalent SG3-179 analog development, compound **3.55** (BRDT-1: IC_{50} = 29.5 nM, BRD4-1: IC_{50} = 51.3 nM) (**Table 3.2**), which has a carboxylic group at C3 of SG3-179, was introduced as a SG3-179 chemotype. For this C3–C3 set, compound **4.11** was prepared by connecting C3 of compound **3.55** with a PEG spacer. This compound exhibited an IC_{50} of 22.5 nM for BRDT-1 and was 6-fold less potency for BRD4-1 in the AlphaScreen assay (**Table 4.2**). In the N38–C3 set of compounds, compound **4.16** was assembled using the N38 position of compound **2.11** and was joined to **3.55** at C3. Similar to the symmetric N38–N38 set, this compound also exhibited selectivity for BRDT-1 over BRD4-1 (26-fold) in the AlphaScreen assay (**Table 4.3**). With increasing PEG spacer length, the selectivity ratio increased initially but then decreased after a maximal length. Compared with the parent compounds **2.11** and **3.55**, the best compound (**4.17**) was at least 40-fold more potent against BRDT-1 than BRD4-1. The selectivity of **4.17** was also enhanced to 238-fold for BRDT-1 in this series. In **Table 4.2**,

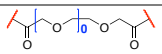
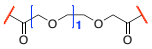
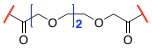
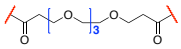
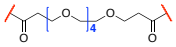
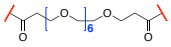
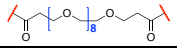
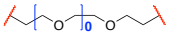
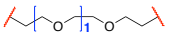
the three series I strategies (N38–N38, C3–C3 and N38–C3) were compared using the same spacer length. Compounds **4.3**, **4.11** and **4.17** shared similar IC_{50} values for BRD4-1, whereas their potency varied from double-digit nanomolar to sub-nanomolar for BRDT-1. The N38–C3 strategy provided the most selective compound for BRDT-1 over BRD4-1. Based on their exquisite selectivity, these bivalent inhibitors most likely form special bivalent interactions with BRDT-1 that do not exist for BRD4-1.

We also wanted to explore whether the improved BRDT-1 selectivity was ligand/chemotype dependent. Therefore, in series II a hybrid strategy was used to form non-symmetric bivalent inhibitors (**Table 4.4**). BET inhibitor JQ-1- and RVX-208-linked SG3-179 hybrids **4.21**, **4.27** and **4.28** were connected with moderate-length PEG spacers. Again, none of these compounds exhibited selectivity for BRDT-1 over BRD4-1 in the AlphaScreen assay. Spacer extension of the RVX-208/SG3-179 hybrid compounds showed sub-micromolar activity and up to 5-fold selectivity for BRDT-1. Symmetric bivalent RVX-208 molecules (compounds **4.23** and **4.24**) were very weak BET inhibitors. (**Table 4.4**).

Table 4.1 AlphaScreen data of N38–N38 connected series I

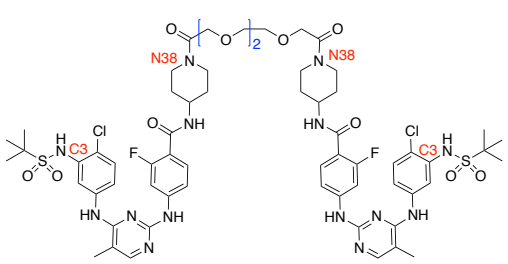


4.1 - 4.8
4.10

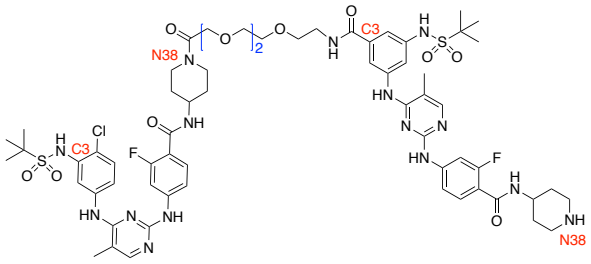
Compound	Spacer	Number of atoms in spacer	AlphaScreen,[1] IC_{50} (nM)		SI
			BRDT-1	BRD4-1	
4.1		5	57.9	101.9	1.8
4.2		8	6.7	266.5	40
4.3		11	3.7	158.7	43
4.4		16	11.3	816.2	72
4.5		19	4.5	338.0	76
4.6		25	4.1	308.3	75
4.7		31	13.9	254.8	18
4.10		5	25.5	46.7	1.8
4.8		8	11.4	117.8	10
2.11	--	--	49.0	80.1	1.6
JQ-1	--	--	133.3	65.0	0.49

[1]AlphaScreen performed by Jun Qi group, single experiment performed in quadruplicate.

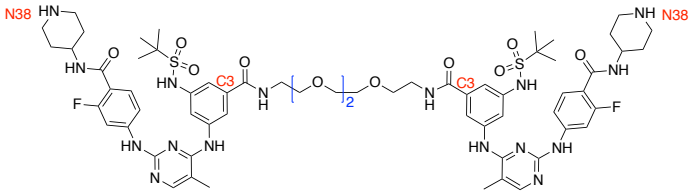
Table 4.2 AlphaScreen data of three series I spacer strategies



4.3



4.17

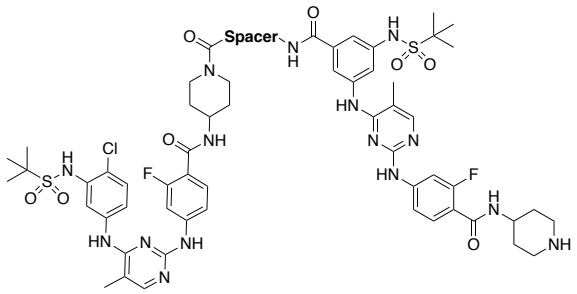


4.11

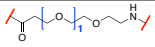
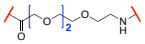
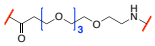
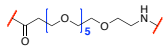
Compound	Spacer position	AlphaScreen,[1] IC_{50} (nM)		SI
		BRDT-1	BRD4-1	
4.3	N38 – N38	3.7	158.7	43
4.11	C3 – C3	22.5	138.6	6.2
4.17	C3 – N38	0.7	170.1	238

[1]AlphaScreen performed by Jun Qi group, single experiment performed in quadruplicate.

Table 4.3 AlphaScreen data of N38–C3 strategy in series I

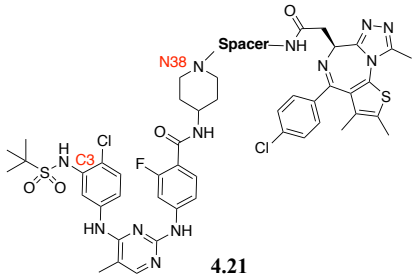


4.16 - 4.19

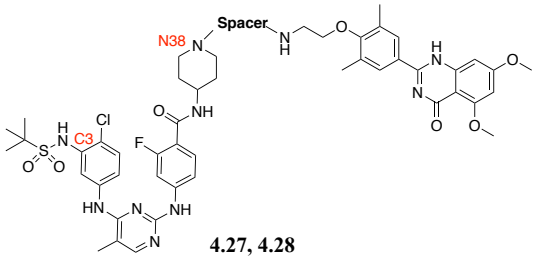
Compound	Spacer	Number of atoms in spacer	AlphaScreen,[1] IC_{50} (nM)		SI
			BRDT-1	BRD4-1	
4.16		10	2.4	61.2	26
4.17		12	0.7	170.1	238
4.18		16	0.9	69.5	77
4.19		22	0.8	74.9	90
2.11	--	--	49.0	80.1	1.6
3.55	--	--	29.5	51.3	0.21
JQ-1	--	--	133.3	65.0	0.49

[1]AlphaScreen performed by Jun Qi group, single experiment performed in quadruplicate.

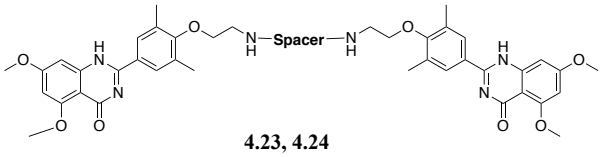
Table 4.4 AlphaScreen data of series II JQ-1/RVX-208 non-symmetric bivalents and bivalent RVX-208



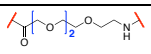
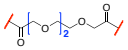
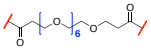
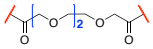
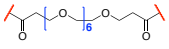
4.21



4.27, 4.28



4.23, 4.24

Compound	Spacer	Number of atoms in spacer	AlphaScreen,[1] IC_{50} (nM)		SI
			BRDT-1	BRD4-1	
4.21		11	11.1	23.5	2.1
4.27		11	369.6	811.0	2.2
4.28		25	136.9	684.4	5.0
4.23		11	>50,0000	>50,0000	NA
4.24		25	>50,0000	>50,0000	NA
2.11	--	--	49.0	80.1	1.6
RVX-208	--	--	5,405	1,142	0.21
JQ-1	--	--	133.3	65.0	0.49

[1]AlphaScreen performed by Jun Qi group, single experiment performed in quadruplicate.

Table 4.5 BROMOscan data for BRDT-(1,2) and BRD4-(1,2)

Compound	Bromoscan,[1] K_d (nM)	
	BRDT-(1,2)	**BRD4-(1,2)**
4.2	0.59	3.6
4.3	2.6	4.8
4.4	1.5	2.8
4.5	0.8	1.6

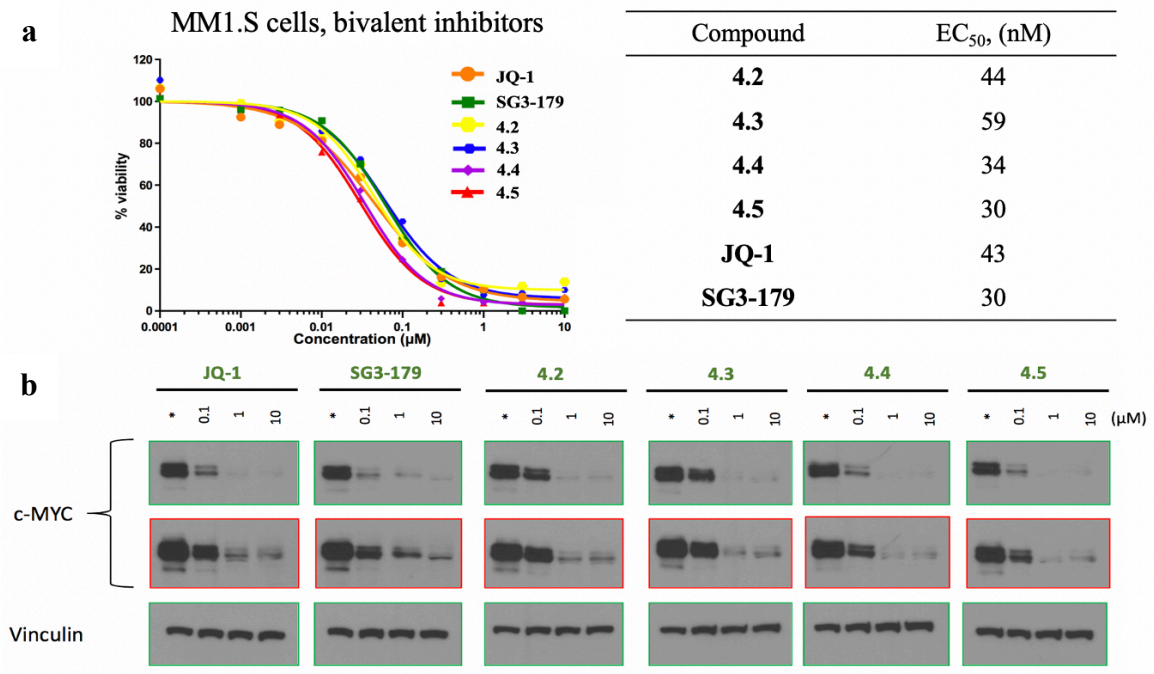
[1]Bromoscan performed by DiscoverX as a single experiment performed in duplicate.

The next question was whether these bivalent compounds had the potential for biased affinity for either of the tandem bromodomains (BRDT-(1,2) or BRD4-(1,2). The BROMOscan by DiscoverX was adopted to measure this in a tandem bromodomain assay. As full length of BRDT is not available, a construct containing BRDT/4-1 and BRDT/4-2 was utilized in the BROMOscan assay. Surprisingly, the selectivity of compounds **4.2**, **4.3**, **4.4** and **4.5** decreased significantly for tandem BRDT (**Table 4.5**). To investigate this selectivity loss, we obtained the affinity of compound **4.3** for different bromodomains in the BET family (**Table 4.6**). In the BROMOscan assay, 40-fold selectivity for BRDT-1 over BRD4-1 was observed, which validated previous AlphaScreen data. However, compound **4.3** showed almost equivalent affinity for BRDT-2 and BRD4-2. In the BRDT-(1,2) and BRD4-(1,2) assays, compound **4.3** might either bind BRD4-2 with high affinity or induce dimerization between two BRD4-2 domains in BRD4-(1,2). In addition to the homodimer, heterodimers between the first and second bromodomains in different tandem constructs or intramolecular interactions between the first and second bromodomain in the same tandem constructs might be induced in the BRDT-(1,2) and BRD4-(1,2) assays. We do not have any evidence about which binding mode was preferred in the tandem BET assay, but the possibility of multiple binding modes may be the reason for selectivity loss of bivalent compound **4.3** in this assay.

Table 4.6 BROMOscan data of compound **4.3** for different bromodomains

Bromodomain	Compound 4.3, K_d (nM)
BRDT-1	0.6
BRDT-2	8.2
BRD4-1	28
BRD4-2	8.9

[1]Bromoscan performed by DiscoverX, single experiment performed in duplicate.



Compound	EC_{50}, (nM)
4.2	44
4.3	59
4.4	34
4.5	30
JQ-1	43
SG3-179	30

Figure 4.4 Effects of bivalent inhibitors on MM1.S cells. (**a**) EC_{50} values from the cellular assay; (**b**) Western blot analysis of c-Myc.

4.3.2 Bivalent molecules can penetrate through the membrane of MM1.S cells. To measure cellular penetration, we next assessed the cellular effects of the bivalent inhibitors in MM1.S cells, which was previously used in the JQ-1 bivalent molecule study.[91] After treatment with our bivalent inhibitors **4.2**, **4.3**, **4.4** and **4.5**, cell viability was inhibited in a concentration-dependent manner. All bivalent inhibitors tested exhibited double-digit nanomolar activity for MM1.S cells (**Figure 4.4a**). As c-Myc-induced proliferation inhibition is regulated through BET-mediated epigenetic machinery,[34] c-Myc transcription levels were also monitored by western blot (**Figure 4.4b**). As expected, these compounds

downregulated c-Myc levels in a concentration-dependent manner. Compared with compounds **4.2** and **4.3**, compounds **4.4** and **4.5** with a longer PEG spacer showed improved c-Myc inhibition. Taken together, these data support that high molecular weight bivalent molecules can penetrate the cell membrane and exhibit on-target BRD4 activity. Additionally, spacer length appeared to influence c-Myc activity. However, due to the lack of a biological marker of BRDT inhibition, a cell-based functional assay for BRDT is not yet available.

4.3.3 Bivalent molecules induced dimerization of BRDT-1 and BRD4-1. To better understand the binding mode of these bivalent BET inhibitors, several cocrystal structures were obtained. In **Figures 4.5a** and **4.5b**, bivalent compounds **4.3** and **4.4**, varying only by one unit in spacer lengths, promoted the association of BRDT-1 into a similar dimer (as shown in **Figure 4.6a** as well). The chemotypes of these compounds retained the same binding site architecture as their monovalent counterparts, including the key interaction with Asn109 and the WPF shelf occupancy. Hydrophobic residues Phe48, Met118 and Leu117 at the interface of BRDT-1 monomer A (orange) formed an interaction with Trp50 from BRDT-1 monomer B (cyan) (**Figure 4.6b**). Bivalent compounds **4.3** and **4.5** also induced the dimerization of BRD4-1 (**Figures 4.5c** and **4.5d**). The SG3-179 chemotype maintained a similar binding site architecture as its monovalent counterpart, including the interaction with conserved Asn140. Interactions between two BRD4-1 monomers are also observed in **Figure 4.6e**.

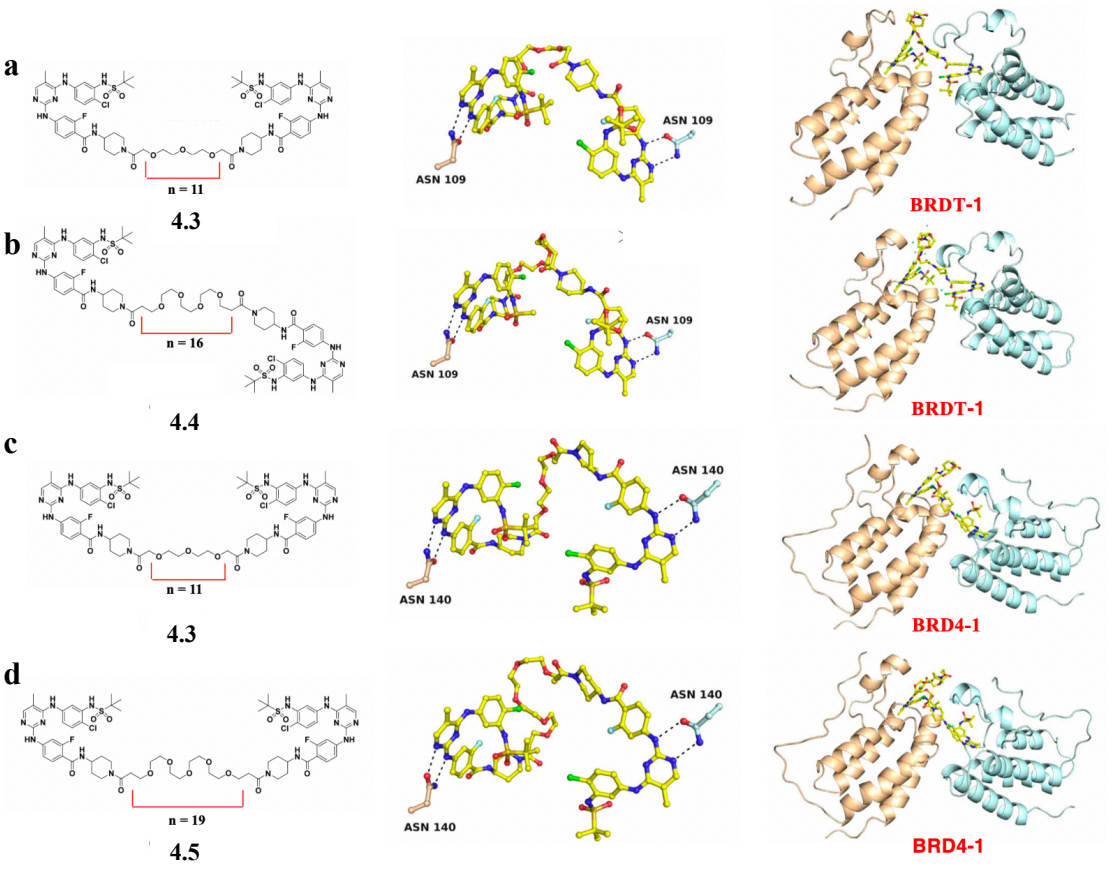


Figure 4.5 Crystal structures of bivalent inhibitors in complex with BRDT-1 and BRD4-1: (**a**) **4.3** with BRDT-1; (**b**) **4.4** with BRDT-1; (**c**) **4.3** with BRD4-1; (**d**) **4.5** with BRD4-1.

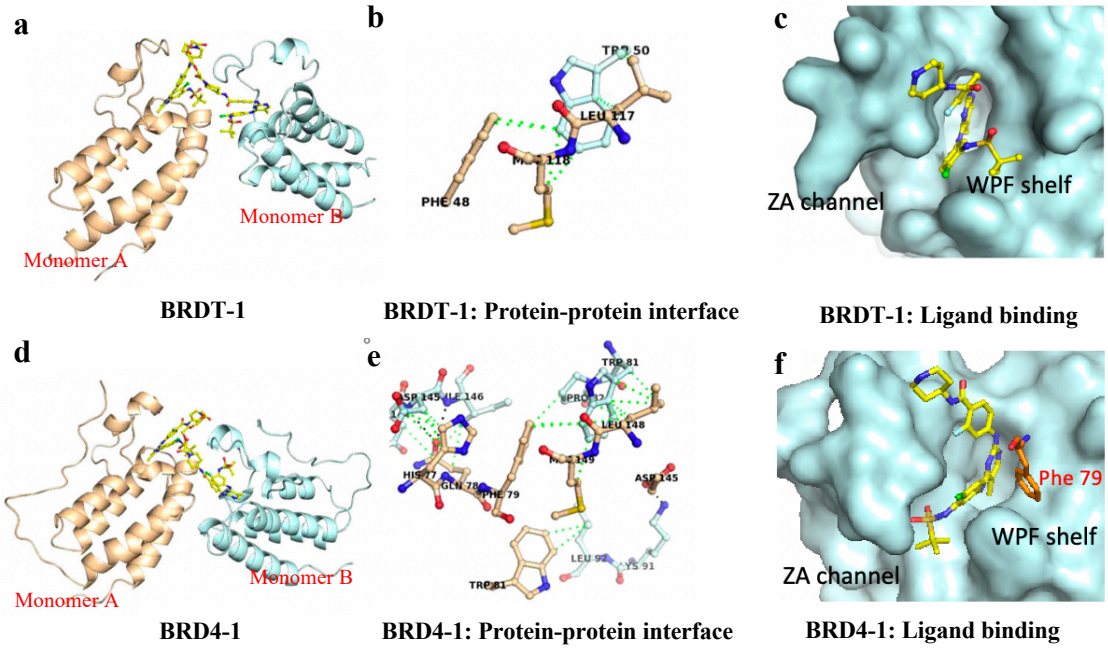


Figure 4.6 Difference between BRDT-1 and BRD4-1 homodimers. (**a**) Compound-induced dimerization of BRDT-1; (**b**) residues involved in the protein-protein interface of the BRDT-1 homodimer; (**c**) binding mode of compound **4.3** in the BRDT-1 homodimer; (**d**) compound induced dimerization of BRD4-1; (**e**) residues involved in the protein-protein interaction of the BRD4-1 homodimer; (**f**) binding mode of compound **4.5** in the BRD4-1 homodimer.

Even though the binding modes of these compounds were similar to the BRDT dimers, but there were some differences in protein-protein interactions and chemotype binding pose. Compared with the BRDT-1 dimer, monomer A (orange) of BRD4-1 approached monomer B (cyan) in a different orientation (**Figures 4.6a** and **4.6d**). Many more amino acid residues at the protein-protein interface participated in the interaction to form the BRD4-1 dimer than the BRDT-1 dimer (**Figures 4.6b** and **4.6e**). In protein-protein interactions, hydrophobic residues are typically the driving force for protein association. Hydrophilic residues could form specific ionic interactions or H-bonds intermolecularly in the interface, but these interactions are not favored due to the energy penalty of desolvation.[126] In our free energy calculation, the hydrophobic amino acid residues preferred to interact with other hydrophobic areas to minimize contact with the solvent, which contributed to the free energy of solvation for BRDT-1 with compound **4.3** ($\Delta G_{interface}$ = -2.94 kcal/mol) and BRD4-1 with compound **4.5** ($\Delta G_{interface}$ = -6.29 kcal/mol) homodimers (interface binding energy was calculated by jsPISA2.0.5[124, 125]). Published

BRD4-1 homodimers (PDB: 5KHM, 5DA2 and 5AD3) showed a $\Delta G_{interface}$ ranging from -9.44 to -5.99 kcal/mol (interface binding energy was calculated by jsPISA2.0.5[124, 125]). Unfortunately, there were no BRDT-1 homodimer published for comparison. It seemed that compound **4.5** was a moderate promoter of BRD4-1 homodimerization and compound **4.3** is a weak promoter of BRDT-1 homodimerization. Moreover, interactions between amino acid residues on each monomer of BRD4-1 disrupted typical SG3-179 chemotype binding in monomer B of the BRD4-1 dimer. Phe79 of BRD4-1 monomer A (orange) interacts with Trp81 and Pro82 of the WPF shelf in monomer B (cyan) (**Figure 4.6e**), and as a result, the *t*-butyl group of SG3-179 was excluded from the WPF shelf in monomer B and relocated to the ZA channel (**Figure 4.6f**). Our experience with the monovalent inhibitor series emphasized how crucial WPF shelf occupancy was to maintaining ligand affinity. Partial loss of WPF interaction with compounds **4.3** and **4.5** most likely explained the reduced BRD4-1 affinity in the AlphaScreen. However, more interactions between the two BRD4-1 monomers might enhance the binding affinity of compounds **4.3** and **4.5** for BRD4-1, but we do not know how strong the protein-protein interactions influence the total binding affinity of these two compounds.

4.4 Conclusions and future directions. In conclusion, we generated two series of bivalent inhibitors with different spacer strategies (N38–N38, C3–C3 and C3–N38). Spacer length, attachment types and ligands were explored for SAR discussion. In the AlphaScreen assay, series I of SG-179 based bivalent inhibitors exhibited up to 238-fold selectivity for BRDT-1 over BRD4-1. For the N38–N38 strategy in series I, selectivity first increased with elongation of the spacer, then decreased when the spacer was longer than 7 PEG units. For the C3–N38 strategy in series I, the turning point was 5 PEGs. Compared with the strategies above, the C3–C3 strategy exhibited decreased selectivity. Series II compounds contained known BET ligands JQ-1 and RVX208 in addition to SG3-179, but none of them exhibited selectivity for BRDT-1. Several cocrystal structures disclosed that BRDT-1 and BRD4-1 molecules were induced to form homodimers by our bivalent small molecules. Notably, this was the first crystallographic evidence showing that BRDT-1 can be induced to form a homodimer by small bivalent molecules. Differences in protein interfaces and chemotype binding modes were observed between the two isoforms. These structural differences

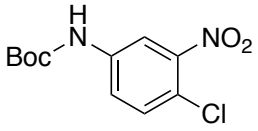
might contribute to BRDT-1 selectivity in the AlphaScreen and BROMOscan. Disappointingly, the selectivity decreased significantly in the BRDT-(1,2) and BRD4-(1,2) assays. Pan affinity for second bromodomain of BRD4 and BRDT as well as multiple binding modes in the tandem assay of these bivalent compounds might explain their low selectivity for BRDT in a tandem assay. In the cellular assays, several bivalent compounds successfully penetrated through the cell membrane and downregulated c-Myc levels. Evaluation of the physicochemical properties, PK and safety of bivalent compounds for further *in vivo* testing is ongoing.

In the future we may need to develop selective inhibitors for tandem BRDT. A potential idea for compound improvement is to modify spacer flexibility. All of our previous compounds contained a flexible PEG spacer, but specific ligand binding poses might be preferred for BRDT dimerization events. A rigid spacer may help to lock in a certain ligand conformation for selective binding to BRDT or other BET family members.

Chapter 5: Experimental Data

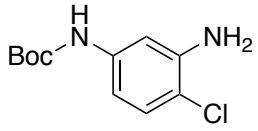
5.1 General chemistry procedures. All chemicals and reagents used for chemistry were purchased and used directly as supplied. Solvents were dried over aluminum using a PURESOLV Solvent Purification System. All non-aqueous reactions were performed in oven-dried glassware. All oxygen sensitive reactions were performed in a glove box. Reaction progress was monitored by thin-layer chromatography using silica gel plates (silica gel 60 F_{254}) and visualized with UV light (254 nm/365 nm). Compounds were purified by flash column chromatography. NMR experiments were performed on a Bruker 400/100 MHz instrument. NMR spectra were processed with the MestReNova program. Chemical shifts are reported in ppm relative to methanol-d_4 (3.31 ppm for ^{1}H, 49.00 ppm for ^{13}C), $CDCl_3$ (7.26 ppm for ^{1}H, 77.16 ppm for ^{13}C), or DMSO-d_6 (2.50 ppm for ^{1}H, 39.5 ppm for ^{13}C). ^{1}H NMR coupling constants (J) are expressed in Hertz (Hz), and multiplicity is described as follows: s = singlet; d = doublet; t = triplet; q = quartet; p = pentet; br = broad; m = multiplet. MS analysis of compounds was performed on a Bruker BioTOF II ESI/TOF-MS instrument in positive and negative ion mode. Melting points were determined on a melting point apparatus and are uncorrected. All tested compounds (synthesized and purchased) were characterized and their purity was >95%, except for 2098321-12-8 where purity was >92% as determined by analytical LCMS. For LCMS purity testing, compounds were dissolved in DMSO to make 10 mM stock solutions. The stock solutions were then diluted 1000-fold using methanol and filtered (0.2 μm, PTFE) prior to purity analysis using an Acquity UPLC (Waters Corporation) equipped with an Acquity BEH UPLC C18, 1.7 μm (2.1 × 50 mm) column for separation. Light was detected at 214 nm using a photo diode array detector. Mass data was acquired using a Micromass ZQ mass spectrometer. LC was completed using a gradient method with each of the following mobile phase systems: Mobile Phase A2: 95% Water, 5% Acetonitrile, 0.1% Formic Acid; Mobile Phase B2: 95% Acetonitrile, 5% Water, 0.1% Formic Acid; Mobile Phase A1: 95% Water, 5% Methanol, 0.1% Formic Acid; Mobile Phase B1: 95% Methanol, 5% Water, 0.1% Formic Acid.

5.2 Chapter 2 synthesis of FP probes



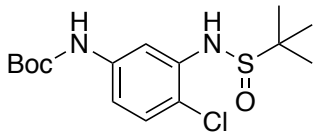
2.2

***tert*-Butyl (4-Chloro-3-nitrophenyl)carbamate (2.2).** 4-Chloro-3-nitroaniline (5.18 g, 30.0 mmol) and di-*tert*-butyl carbonate (7.2 g, 33.0 mmol) were dissolved in dry THF (20 mL). The mixture was stirred and refluxed for 28 h. The solvent was removed under reduced pressure and the resulting yellow oil was triturated using EtOAc:hexanes to provide the title compound as a yellow solid (4.75 g, 58%). Mp: 104.2-104.8 °C. ^{1}H NMR (400 MHz, $CDCl_3$) δ 8.07 (d, J = 2.4 Hz, 1H), 7.44 (m, 2H), 6.80 (s, 1H), 1.52 (s, 9H). ^{13}C NMR (100 MHz, $CDCl_3$) δ 152.1, 148.0, 138.2, 132.0, 122.4, 120.0, 114.9, 82.0, 28.2. MS: calcd for $C_{11}H_{12}ClN_2O_2$ $[M-H]^-$, 271.1; found 271.1.



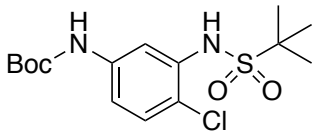
2.3

***tert*-Butyl (3-Amino-4-chlorophenyl)carbamate (2.3).** To a solution of *tert*-butyl (4-chloro-3-nitrophenyl)carbamate (**2.2**, 5.45 g, 20.0 mmol) in MeOH (deoxygenated with bubbled nitrogen) was added 10% Pd/C (0.21 g, 2.0 mmol) and hydrazine monohydrate (64%, 3.5 g, 70.0 mmol) under nitrogen. The solution was stirred and heated at reflux for 10 h, cooled to rt and then filtered over Celite. The solvent was removed under reduced pressure and the resulting yellow oil was triturated using EtOAc:hexanes to give the title compound as a brown solid (3.12 g, 64%). Mp: 139.8-140.1 °C. ^{1}H NMR (400 MHz, $CDCl_3$) δ 7.1 (m, 2H), 6.5 (dd, J = 2.4 Hz, J = 8.6 Hz, 1H), 6.4 (s, 1H), 4.04 (s, 2H), 1.51 (s, 9H). ^{13}C NMR (100 MHz, $CDCl_3$) δ 152.6, 143.4, 137.9, 129.4, 113.3, 109.12, 105.5, 80.7, 28.3. 265.1. MS: calcd for $C_{11}H_{15}ClN_2NaO_2$ $[M+Na]^+$, 265.1; found 265.1.



2.4

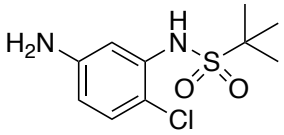
***tert*-Butyl (3-((*tert*-Butylsulfinyl)amino)-4-chlorophenyl)carbamate (2.4)**[85, 131] To a solution of *tert*-butyl (3-amino-4-chlorophenyl)carbamate (**2.3**, 500 mg, 2.06 mmol) and pyridine (0.50 mL, 6.2 mmol) in DCM (1 mL) was added a solution of *tert*-butylsulfinyl chloride (0.25 mL, 2.0 mmol) in DCM (1 mL) dropwise at 0 °C under nitrogen. The mixture was stirred at 0 °C for 2 h, then warmed to rt and further stirred for 20 h. The reaction mixture was diluted with EtOAc (20 mL) and washed with HCl (1 M, 1 × 50 mL) and water (1 × 50 mL). The organic layer was dried (Na_2SO_4) and concentrated under reduced pressure. The brown oil was purified by silica gel column chromatography (EtOAc:hexanes, 1:5) to give the title compound as a pale-yellow foam (550 mg, 77%). Mp: 123.1-123.6 °C. ^{1}H NMR (400 MHz, $CDCl_3$) δ 7.42 (d, J = 2.4 Hz, 1H), 7.19 (d, J = 8.6 Hz, 1H), 6.96 (dd, J = 2.4 Hz, J = 8.6 Hz, 1H), 6.75 (s, 1H), 6.06 (s, 1H), 1.51 (s, 9H), 1.35 (s, 9H). ^{13}C NMR (100 MHz, $CDCl_3$) δ 152.4, 138.9, 138.5, 129.70, 116.1, 113.1, 107.2, 80.8, 57.1, 28.3, 22.4. MS: calcd for $C_{15}H_{22}ClN_2O_3S$ $[M-H]^-$, 345.1; found 345.1.



2.5

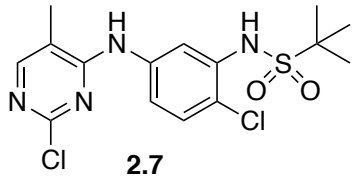
***N*-(5-Amino-2-chlorophenyl)-2-methylpropane-2-sulfonamide (2.5).** To a solution of *tert*-butyl (4-chloro-3-((1,1-dimethylethyl)sulfonamido)phenyl)carbamate (**2.4**, 2.81 g, 8.10 mmol) in DCM (30 mL) was added and mCPBA (1.40 g, 8.10 mmol) under nitrogen at 0 °C for 1 h, then warmed to rt and further stirred overnight. The reaction mixture was diluted with DCM (20 mL) and washed with saturated $NaHCO_3$ solution (2 × 200 mL) and brine (1 × 200 mL). The organic layer was dried (Na_2SO_4) and concentrated under reduced pressure. The yellow oil was purified by silica gel column chromatography (EtOAc/hexanes, 1:5) to give the title compound as a light-yellow solid (2.47 g, 84%) Mp: 193.4 – 194.2 °C. ^{1}H NMR (400 MHz, DMSO-d_6) δ 9.54 (s, 1H), 9.22 (s, 1H), 7.80 (d, J = 1.9 Hz, 1H), 7.39 – 7.24 (m, 2H), 1.48 (s, 9H), 1.32 (s, 9H). ^{13}C NMR (100 MHz, DMSO-

d_6) δ 152.5, 138.9, 135.6, 129.4, 120.2, 116.8, 116.4, 79.3, 60.5, 28.0, 23.8. MS: calcd for $C_{15}H_{23}ClN_2NaO_4S$ $[M+Na]^+$, 385.1; found 385.1.



2.6

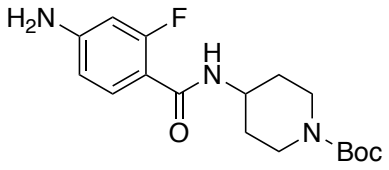
***N*-(5-Amino-2-chlorophenyl)-2-methylpropane-2-sulfonamide (2.6).**[85, 131] To a solution of *N*-(5-amino-2-chlorophenyl)-2-methylpropane-2-sulfonamide (**2.5**, 450 mg, 1.24 mmol) in DCM (1.5 mL) was added TFA (1.5 mL) at rt and stirred for 2 h. The solvent was removed under reduced pressure and then the pH was adjusted to pH = 12 by adding NaOH (1 N). The aqueous phase was extracted with EtOAc (2 × 20 mL). The combined organic phases were washed with a saturated $NaHCO_3$ aqueous solution (20 mL) and brine (20 mL), and dried over Na_2SO_4), and concentrated under reduced pressure. The residues were purified by silica gel column chromatography (EtOAc/hexanes) to give the title compound as a yellow solid (254 mg, 78%). Mp: 122.7 -123.2 °C. ^{1}H NMR ($CDCl_3$, 400 MHz) δ 7.19 (d, *J* = 2.7 Hz, 1H), 7.09 (d, *J* = 8.6 Hz, 1H), 6.51 (s, 1H), 6.37 (dd, *J* = 8.6, 2.7 Hz, 1H), 3.76 (s, 2H), 1.41 (s, 9H). ^{13}C NMR (100 MHz, $CDCl_3$) δ146.4, 135.9, 129.70, 111.9 (2C), 107.2, 62.4, 24.7. MS: calcd for $C_{10}H_{15}ClN_2NaO_2S$ $[M+Na]^+$, 285.1; found 285.1.



2.7

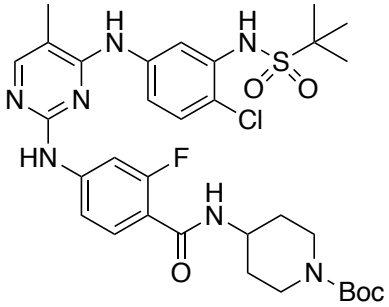
***N*-(2-Chloro-5-((2-chloro-5-methylpyrimidin-4-yl)amino)phenyl)-2-methylpropane-2-sulfonamide (2.7).**[131] To a solution of *N*-(5-amino-2-chlorophenyl)-2-methylpropane-2-sulfonamide (**2.6**, 254 mg, 0.967 mmol) and 2,4-dichloro-5-methylpyrimidine (158 mg, 0.967 mmol) in isopropanol (2 mL) was added DIPEA (1 mL, 5.80 mmol). The mixture was stirred at 120 °C for 2 days, then cooled to rt. The solvent was removed under reduced pressure and the residue was purified by silica gel column chromatography (MeOH:DCM, 1.5:100) to give the title compound as a grey solid (135 mg, 36%). Mp: 273.6-274.2 °C. ^{1}H NMR (400 MHz, DMSO-d_6) δ 9.31 (s, 1H), 8.99 (s, 1H), 8.08 (s, 1H), 7.96 (d, *J* = 2.5

Hz, 1H), 7.59 (dd, J = 2.5, 8.9 Hz, 1H), 7.46 (d, J = 8.7 Hz, 1H), 2.18 (s, 3H), 1.35 (s, 9H). ^{13}C NMR (100 MHz, DMSO-d_6) δ 160.0, 156.6, 156.6, 138.0, 135.4, 129.2, 122.0, 120.5, 120.3, 114.8, 60.5, 23.9, 13.5. MS: calcd for $C_{15}H_{18}Cl_2N_4NaO_2S$ $[M+Na]^+$, 411.1; found 411.1.



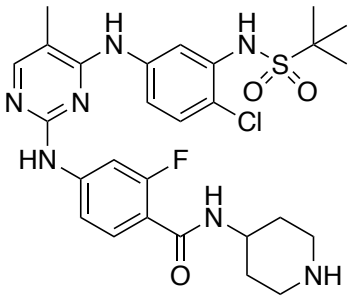
2.9

***tert*-Butyl 4-(4-Amino-2-fluorobenzamido)piperidine-1-carboxylate (2.9).** To a solution of 4-amino-2-fluorobenzoic acid (200 mg, 1.46 mmol) in DMF (5 mL) were added HATU (610 mg, 1.60 mmol), DIPEA (0.51 mL, 2.92 mmol). The solution was stirred at rt for 30 min followed by the addition of *tert*-butyl 4-aminopiperidine-1-carboxylate (350 mg, 1.75 mmol). The reaction mixture was further stirred at rt for 12 h. The DMF was removed under reduced pressure and the residue was diluted with EtOAc (50 mL). The organic layer was washed with brine (3 × 20 mL) and dried over Na_2SO_4. The solvent was removed and the residues was purified by silica gel column chromatography (EtOAc:hexanes) to give the title compound as a pale-yellow solid (440 mg, 95%). Mp: 137.6 – 138.1 °C. ^{1}H NMR (400 MHz, $CDCl_3$) δ 7.89 (t, J = 8.9 Hz, 1H), 6.56 – 6.43 (m, 2H), 6.32 (dd, J = 2.2, 14.4 Hz, 1H), 4.06 - 4.28 (m, 3H), 4.03 (s, 2H), 2.95 (t, J = 12.1 Hz, 2H), 2.06 – 1.94 (m, 2H), 1.46 (s, 9H), 1.45 – 1.32 (m, 2H). ^{13}C NMR (100 MHz, $CDCl_3$) δ 162.8 (d, J = 3.6 Hz), 162.2 (d, J = 244.4 Hz), 154.7, 151.5 (d, J = 12.7 Hz), 133.4 (d, J = 4.3 Hz), 110.9 (d, J = 1.9 Hz), 110.3 (d, J = 11.5 Hz), 100.8 (d, J = 28.9 Hz), 79.6, 46.8, 32.1, 29.3, 28.4. MS: calcd for $C_{17}H_{24}FN_3NaO_3$ $[M+Na]^+$, 360.2; found 360.2.



2.10

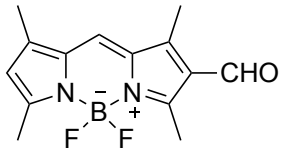
***tert*-Butyl 4-(4-((4-((4-Chloro-3-((1,1-dimethylethyl)sulfonamido)phenyl)amino)-5-methyl pyrimidin-2-yl)amino)-2-fluorobenzamido)piperidine-1-carboxylate (2.10).** To a solution of *tert*-butyl 4-(4-amino-2-fluorobenzamido)piperidine-1-carboxylate (**2.9**, 260 mg, 0.771 mmol) and sodium *tert*-butoxide (148 mg, 1.54 mmol) in 1,4-dioxane (3 mL), a solution of *N*-(2-chloro-5-((2-chloro-5-methylpyrimidin-4-yl)amino)phenyl)-2-methylpropane-2-sulfonamide (**2.7**, 300 mg, 0.771 mmol), $Pd_2(dba)_3$ (35.3 mg, 0.0385 mmol) and BINAP (48.0 mg, 0.0771 mmol) in 1,4-dioxane (3 mL) was added. The mixture was degassed and heated at 110 °C for 5 h under nitrogen. The mixture was cooled to rt, diluted with EtOAc, and the organic layer was washed with brine (3 × 20 mL) and dried over Na_2SO_4. The solvent was removed and the residues was purified by silica gel column chromatography (MeOH:DCM, 3:100) to give the title compound as a pale-yellow solid (477 mg, 90%). Mp: 177.2 -177.8 °C. ^{1}H NMR (400 MHz, DMSO-d_6) δ 9.44 (s, 1H), 9.32 (s, 1H), 8.65 (s, 1H), 8.00 (s, 1H), 7.82 (dd, J = 3.2, 7.7 Hz, 1H), 7.78 (dt, J = 2.8, 8.6 Hz, 3H), 7.53 – 7.36 (m, 3H), 4.00 – 3.80 (m, 3H), 2.88 (s, 2H), 2.14 (s, 3H), 1.84 -1.72 (m, 2H), 1.41 (s, 9H), 1.40 – 1.34 (m, 2H), 1.33 (s, 9H). ^{13}C NMR (100 MHz, DMSO-d_6) δ 162.9 (d, J = 3.0 Hz), 159.8(d, J = 244 Hz), 158.6, 157.3, 155.8, 153.8, 144.8 (d, J = 12 Hz), 139.0, 135.4, 130.2 (d, J = 5 Hz), 129.1, 121.2, 121.0, 120.6, 114.8 (d, J = 13 Hz), 113.2, 107.4, 104.2 (d, J = 29 Hz), 78.6, 60.6, 55.8, 46.2, 29.6, 28.1, 23.8, 13.5. MS: calcd $C_{32}H_{40}ClFN_7O_5S$ $[M-H]^-$, 688.3; found 688.4.



2.11

4-((4-((4-Chloro-3-((1,1-dimethylethyl)sulfonamido)phenyl)amino)-5-methylpyrimidin-2-yl)amino)-2-fluoro-*N*-(piperidin-4-yl)benzamide (2.11). To a solution of *tert*-butyl 4-(4-((4-((4-chloro-3-((1,1-dimethylethyl)sulfonamido)phenyl)amino)-5-methylpyrimidin-2-yl)amino)-2-

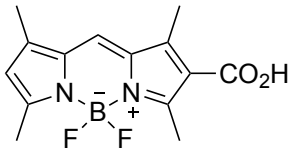
fluorobenzamido)piperidine-1-carboxylate (**2.10**, 200 mg, 0.290 mmol) in DCM (1.6 mL) was added TFA (0.4 mL) and the mixture was stirred at rt for 12 h. The solvent was removed under reduced pressure and then the pH was adjusted to pH = 13 by adding NaOH (1 N). The grey precipitate was filtered, washed with water (2 × 10 mL) and then with acetone (5 mL). The residue was dried under high vacuum to give the title compound as a colorless solid (156 mg, 91%). Mp: 233.0 -233.4 °C. ^{1}H NMR (400 MHz, DMSO-d_6) δ 9.30 (s, 1H), 8.42 (s, 1H), 7.86 (s, 1H), 7.76 (dd, J = 3.1, 7.6 Hz, 1H), 7.72 – 7.66 (m, 1H), 7.64 (d, J = 2.4 Hz, 1H), 7.47 – 7.27 (m, 3H), 7.21 (d, J = 8.7 Hz, 1H), 3.67 – 3.87 (m, 1H), 2.97 (d, J = 12.1 Hz, 2H), 2.59 (t, J = 11.8 Hz, 2H), 2.03 (s, 3H), 1.80 – 1.62 (m, 2H), 1.48 – 1.30 (m, 2H), 1.21 (s, 9H). ^{13}C NMR (100 MHz, DMSO-d_6) δ 162.9 (d, J = 3 Hz), 160.2 (d, J = 170 Hz), 158.6, 157.4, 155.5, 144.9 (d, J = 13 Hz), 139.9, 138.5, 130.1 (d, J = 5 Hz), 128.6, 120.8, 119.3, 118.0, 114.8 (d, J = 14 Hz), 113.1, 107.1, 104.1 (d, J = 28 Hz), 59.2, 46.1, 44.0, 31.1, 24.3, 13.6. MS: calcd $C_{27}H_{34}ClFN_7O_3S$ $[M+H]^+$, 590.2; found 590.3.



2.12

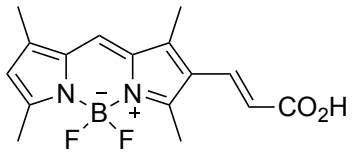
5,5-Difluoro-1,3,7,9-tetramethyl-5*H*-4λ^4,5λ^4-dipyrrolo[1,2-*c*:2',1'-*f*][1,3,2] diazaborinine-2-carbaldehyde (2.12).[104] When DMF (0.57 mL, 7.8 mmol) was added to $POCl_3$ (0.54 mL, 5.8 mmol) dropwise under nitrogen at 0-5 °C a colorless solid formed. To this mixture, a solution of 5,5-difluoro-1,3,7,9-tetramethyl-5*H*-4λ^4,5λ^4-dipyrrolo[1,2-*c*:2',1'-*f*][1,3,2]diazaborinine (360 mg, 1.45 mmol) in 1,2-dichloroethane (60 mL) was added. The mixture was heated at 50 °C for 3 h and then the mixture was poured into ice water and the pH was adjusted to pH = 7-8 with a $NaHCO_3$ saturated aqueous solution, extracted with DCM, and dried over Na_2SO_4. The solvent was removed under reduced pressure and the residue was purified by silica gel column chromatography (EtOAc/hexanes) to give the title compound as an orange solid (0.36 g, 89%). Mp: 251.3 °C, decomposition. ^{1}H NMR (400 MHz, $CDCl_3$) δ 10.04 (s, 1H), 7.23 (s, 1H), 6.22 (s, 1H), 2.78 (s, 3H), 2.60 (s, 3H), 2.51 (s, 3H), 2.31 (s, 3H). ^{13}C NMR (100 MHz, $CDCl_3$) δ 185.6,

163.5, 157.2, 145.5, 140.5, 136.5, 131.1, 125.7, 122.0, 121.5, 15.3, 12.9, 11.5, 10.5. MS: calcd $C_{14}H_{15}BF_2N_2NaO$ $[M+Na]^+$, 299.1; found 299.1.



2.13

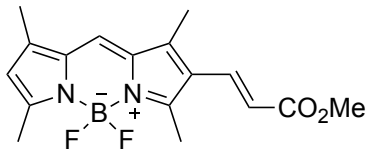
5,5-Difluoro-3,7-dimethyl-5*H*-4λ^4,5λ^4-dipyrrolo[1,2-*c*:2',1'-*f*][1,3,2]diazaborinine-2-carboxylic Acid (2.13).[106] To a solution of 5,5-difluoro-1,3,7,9-tetramethyl-5*H*-4λ^4,5λ^4-dipyrrolo[1,2-*c*:2',1'-*f*][1,3,2]diazaborinine-2-carbaldehyde (**2.12**, 50.0 mg, 0.18 mmol) in THF (1 mL) was added H_2O (0.4 mL) and NaH_2PO_4 (130 mg, 0.110 mmol). The mixture was stirred at rt for 10 min and then $NaClO_2$ (54 mg, 0.6 mmol) and H_2O_2 (30%, 0.04 mL, 0.4 mmol) in H_2O (0.4 mL) were then added into the mixture. The mixture was then stirred at room temperature for 3 h. The solvent was removed under reduced pressure and then diluted with water and adjusted the pH to ~13 with NaOH (1 N), and washed with DCM (2 × 20 mL). The aqueous phase was acidified with HCl (1 N). An orange precipitate was collected, washed with water (5 mL) and purified by preparative HPLC (MeCN:H_2O) to give the title compound as an orange solid (16 mg, 30%). Mp: 293.4 °C, decomposition. ^{1}H NMR (400 MHz, DMSO-d_6) δ 12.48 (s, 1H), 7.90 (s, 1H), 6.39 (s, 1H), 2.66 (s, 3H), 2.50 (s, 3H), 2.48 (s, 3H), 2.33 (s, 3H). ^{13}C NMR (100 MHz, DMSO-d_6) δ 165.3, 160.8, 155.6, 145.4, 142.1, 135.1, 130.7, 123.6, 121.2, 119.0, 14.6, 14.1, 11.6, 11.1. MS: calcd $C_{14}H_{14}BF_2N_2O_2$ $[M-H]^-$, 291.1; found 291.2.



2.14

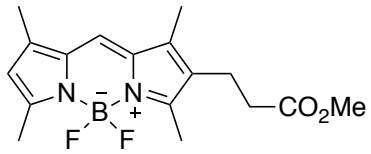
(*E*)-3-(5,5-Difluoro-1,3,7,9-tetramethyl-5*H*-4λ^4,5λ^4-dipyrrolo [1,2-*c*:2',1'-*f*][1,3,2]diazaborinin-2-yl)acrylic Acid (2.14).[105] To a solution of 5,5-difluoro-1,3,7,9-tetramethyl-5*H*-4λ^4,5λ^4-dipyrrolo[1,2-*c*:2',1'-*f*][1,3,2]diazaborinine-2-carbaldehyde (**2.12**, 72 mg, 0.26 mmol) and malonic acid (271 mg, 2.61 mmol) in DMF (1.0 mL) was added

pyridine (0.11 mL, 1.3 mmol). The mixture was stirred at 90 °C for 5 h and then diluted with water (60 mL) and acidified to pH = 1 with HCl (2 N). The aqueous layer was extracted with EtOAc (5 × 60 mL). The combined organic layer was washed with brine (20 mL) and dried over $MgSO_4$. The solvent was removed, and the residues was purified by preparative HPLC (MeCN/H_2O) to give the title compound as a purple solid (23.6 mg, 28%). Mp: 255.7 °C, decomposition. ^{1}H NMR (DMSO-d_6, 400 MHz) δ 12.22 (s, 1H), 7.88 (s, 1H,), 7.53 (d, J = 16.2 Hz, 1H), 6.35 (s, 1H), 6.13 (d, J = 16.2 Hz, 1H), 2.56 (s, 3H), 2.49 (s, 3H), 2.42 (s, 3H), 2.33 (s, 3H). ^{13}C NMR (100 MHz, DMSO-d_6) δ 167.9, 159.5, 154.4, 144.5, 138.6, 134.8, 134.6, 131.7, 122.9, 120.6(2C), 117.7, 14.5, 13.1, 11.1, 11.0. MS: calcd $C_{16}H_{16}BF_2N_2O_2$ $[M-H]^-$, 317.1; found 317.2.



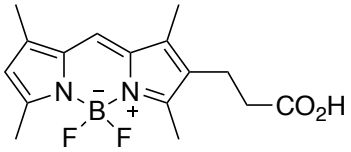
2.15

Methyl (*E*)-3-(5,5-Difluoro-1,3,7,9-tetramethyl-5*H*-4λ^4,5λ^4-dipyrrolo[1,2-*c*:2',1'-*f*][1,3,2] diazaborinin-2-yl)acrylate (2.15).[105] To a solution of 5,5-difluoro-1,3,7,9-tetramethyl-5*H*-4λ^4,5λ^4-dipyrrolo[1,2-*c*:2',1'-*f*][1,3,2]diazaborinine (50 mg, 0.20 mmol), *tert*-butyl perbenzoate (78 mg, 0.40 mmol) and methyl acrylate (87 mg, 1.00 mmol) in AcOH:dioxane:DMSO (3:9:1, 1.5 mL), $Pd(OAc)_2$ (9.0 mg, 0.040 mmol) was added. The mixture was stirred at 35 °C for 5 days. The mixture was diluted with water (15 mL), extracted with diethyl ether (3 × 15 mL) and dried over $MgSO_4$. The solvent was removed and the residues was purified by silica gel column chromatography (DCM/MeOH) to give the title compound as an orange solid (38 mg, 57%). Mp: 247.1 °C, decomposition. ^{1}H NMR (400 MHz, $CDCl_3$) δ 7.66 (d, J = 16.2 Hz, 1H), 7.12 (s, 1H), 6.23 – 6.05 (m, 2H), 3.80 (s, 3H), 2.65 (s, 3H), 2.56 (s, 3H), 2.35 (s, 3H), 2.27 (s, 3H). ^{13}C NMR (100 MHz, $CDCl_3$) δ 168.0, 160.3, 155.6, 143.6, 138.0, 136.0, 135.1, 132.1, 123.5, 120.6 (2C), 116.2, 51.6, 15.0 (2C), 13.5, 11.4. MS: calcd $C_{17}H_{19}BF_2N_2NaO_2$ $[M+Na]^+$, 355.2; found 355.2.



2.16

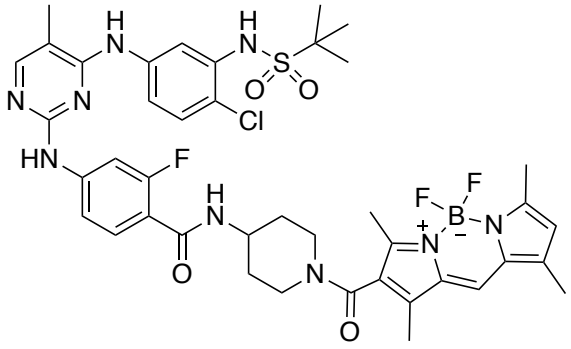
3-(5,5-Difluoro-1,3,7,9-tetramethyl-5*H*-4λ^4,5λ^4-dipyrrolo[1,2-*c*:2',1'-*f*][1,3,2]diazaborinin-2-yl)propanoic Acid (2.16). To a solution of methyl (*E*)-3-(5,5-difluoro-1,3,7,9-tetramethyl-5*H*-4λ^4,5λ^4-dipyrrolo[1,2-*c*:2',1'-*f*][1,3,2] diazaborinin-2-yl)acrylate (**2.15**, 60 mg, 0.18 mmol) in MeCN:EtOH (1:1, 10 mL), 5 drops of water and Pd/C (10%) (1.9 mg, 0.018 mmol) were added. The reaction was stirred at room temperature under H_2 overnight. The mixture was filtered through Celite. The solvent was removed under reduced pressure to give the title compound as an orange solid (48 mg, 80%). The product was used directly for the next step.



2.17

3-(5,5-difluoro-1,3,7,9-tetramethyl-5*H*-4λ^4,5λ^4-dipyrrolo[1,2-*c*:2',1'-*f*][1,3,2]diazaborinin-2-yl)propanoic acid (2.17). To a solution of methyl 3-(5,5-difluoro-1,3,7,9-tetramethyl-5*H*-4λ^4,5λ^4-dipyrrolo[1,2-*c*:2',1'-*f*][1,3,2]diazaborinin-2-yl)propanoate (10 mg, 0.030 mmol) in DCM (0.4 mL), a solution of NaOH (72 mg, 1.8 mmol) in MeOH:H_2O (1:4, 9.6 mL) was added dropwise at 0 °C. The reaction was stirred at room temperature for 10 h and then water (30 mL) was added and the aqueous phase was washed with DCM (3 × 10 mL). The aqueous phase was acidified with HCl (2N) to pH = 1. The mixture then emitted green fluorescence under UV at 365 nm. The mixture was extracted with DCM (3 × 30 mL) and dried over $MgSO_4$. The solvent was removed, and the residue was purified by silica gel column chromatography (DCM/MeOH) to give the title compound as an orange solid (9.4 mg, 98%). Mp: 269.2 °C, decomposition. ^{1}H NMR (methanol-d_4, 400 MHz) δ 7.23 (s, 1H), 5.98 (s, 1H), 2.63 (t, J = 7.6 Hz, 2H), 2.30 – 2.43 (m, 8H), 2.16 (s, 3H), 2.14 (s, 3H). ^{13}C NMR (100 MHz, methanol-d_4) δ 176.6, 156.9,

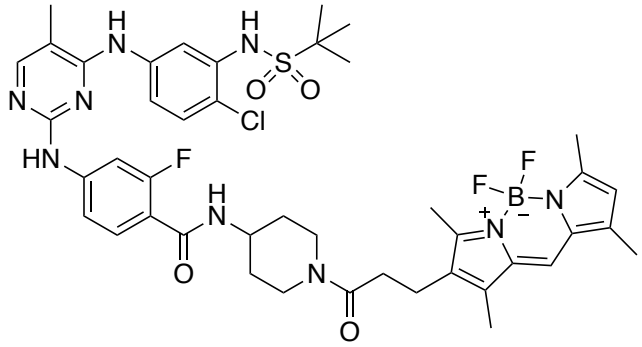
156.8, 142.6, 140.2, 134.5, 134.21, 129.9, 121.6, 119.5, 35.1, 20.5, 14.5, 12.8, 11.1, 9.5. MS: calcd $C_{16}H_{18}BF_2N_2O_2$ $[M-H]^-$ 319.2, found 319.2.



2.18

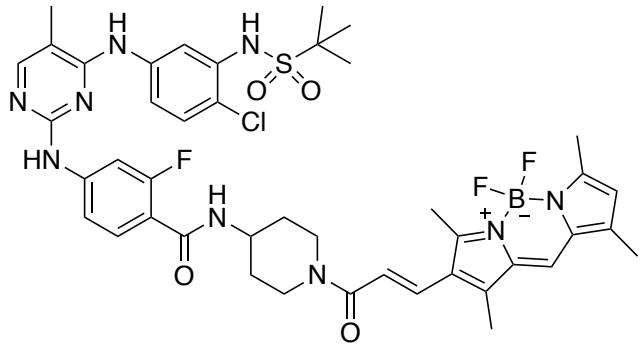
4-((4-((4-Chloro-3-((1,1-dimethylethyl)sulfonamido)phenyl)amino)-5-methylpyrimidin-2-yl)amino)-*N*-(1-(5,5-difluoro-1,3,7,9-tetramethyl-5*H*-4λ^4,5λ^4-dipyrrolo[1,2-*c*:2',1'-*f*][1,3,2]diazaborinine-2-carbonyl)piperidin-4-yl)-2-fluorobenzamide (2.18). To a solution of 5,5-difluoro-3,7-dimethyl-5*H*-4λ^4,5λ^4-dipyrrolo[1,2-*c*:2',1'-*f*][1,3,2]diazaborinine-2-carboxylic acid (**2.13**, 5.0 mg 17 μmol) in anhydrous DCM (1 mL) were added 1-(3-dimethylaminopropyl)-3-ethylcarbodiimide hydrochloride (EDC, 3.9 mg, 21 μmol), HOBt × H_2O (3.2 mg, 21 μmol). The reaction was stirred at room temperature for 20 min, and then 4-((4-((4-chloro-3-((1,1-dimethylethyl)sulfonamido)phenyl)amino)-5-methylpyrimidin-2-yl)amino)-2-fluoro-*N*-(piperidin-4-yl)benzamide (**2.11**, 13 mg, 22 μmol) and DIPEA (12 μL, 69 μmol) were added. The reaction solution was stirred at room temperature for 6 h. The mixture was diluted with EtOAc, and the organic layer was washed with brine (3 × 20 mL) and dried over Na_2SO_4. The solvent was removed under reduced pressure and the residue was purified by preparative HPLC to give the title compound as an orange solid (11 mg, 74%). Mp: >250 °C, decomposition. Purity: >99% (HPLC). ^{1}H NMR (400 MHz, DMSO-d_6) δ 9.47 (s, 1H), 9.35 (s, 1H), 8.67 (s, 1H), 8.00 (s, 1H), 7.95 – 7.85 (m, 1H), 7.85 – 7.73 (m, 4H), 7.49 (t, J = 8.5 Hz, 1H), 7.42 (1H, d, J = 8.6), 7.38 (1H, d, J = 8.8), 6.31 (s, 1H), 4.56 – 4.24 (m, 1H), 4.13 – 3.98 (m, 1H), 3.75 – 3.45 (m, 1H), 3.28 – 3.12 (m, 1H), 3.08 (m, 1H), 2.47 (s, 3H), 2.38 (d, J = 19.8 Hz, 3H), 2.31 (s, 3H), 2.25 (d, J = 20.6 Hz, 3H), 2.13 (s, 3H), 1.96 – 1.81 (m, 2H), 1.56 – 1.43 (m, 2H), 1.32 (s, 9H). ^{13}C NMR (100 MHz,

DMSO-d_6) δ 164.0, 162.9, 160.0 (d, J = 210 Hz), 159.1, 158.6, 157.3, 155.7, (151.4, 150.9, rotamer) 144.9 (d, J = 12 Hz), 144.0, 139.0, (137.1, 136.6, rotamer) 135.4, 134.3, 131.2 (d, J = 7 Hz), 130.2, 129.1, 125.7, 123.2, 121.2, 121.0, 120.7, 120.2, 114.8 (d, J = 14 Hz), 113.2, 107.4, 104.2 (d, J = 28 Hz), 60.6, 59.7, 46.2, 29.7, 23.8, 14.5, 13.5, 12.8, 11.1, 9.9. MS: calcd $C_{41}H_{47}BClF_3N_9O_4S$ $[M+H]^+$ 864.3, found 864.6.



2.19

4-((4-((4-Chloro-3-((1,1-dimethylethyl)sulfonamido)phenyl)amino)-5-methylpyrimidin-2-yl)amino)-*N*-(1-(3-(5,5-difluoro-1,3,7,9-tetramethyl-5*H*-4λ^4,5λ^4-dipyrrolo[1,2-*c*:2',1'-*f*][1,3,2]diazaborinin-2-yl)propanoyl)piperidin-4-yl)-2-fluorobenzamide (2.19). Compound **2.19** was obtained as an orange solid (8.4 mg, 72%) from acid **2.17** (4.2 mg, 13 μmol) and amine **2.11** (9.3 mg, 16 μmol), according to the procedure described for amide **2.18**. Mp: >250 °C, decomposition. Purity: >99% (UPLC). ^{1}H NMR (400 MHz, DMSO-d_6) δ 9.45 (s, 1H), 9.35 (s, 1H), 8.65 (s, 1H), 8.01 (s, 1H), 7.79 (s, 2H), 7.77 (d, J = 4.0, 1H) 7.69 (dd, J = 4.0, 7.7 Hz, 1H), 7.61 (s, 1H), 7.49 – 7.37 (m, 3H), 6.14 (s, 1H), 4.30 (d, J = 12.7 Hz, 1H), 4.06 – 3.89 (m, 1H), 3.81 (d, J = 12.7 Hz, 1H), 3.09 (t, J = 12.4 Hz, 1H), 2.76 (t, J = 12.4 Hz, 1H), 2.62 (t, J = 5.6 Hz, 2H), 2.49 (t, J = 5.6 Hz, 2H), 2.44 (s, 3H), 2.40 (s, 3H), 2.25 (s, 3H), 2.24 (s, 3H), 2.15 (s, 3H), 1.84 – 1.76 (m, 2H), 1.38 -1.28 (m, 11H). ^{13}C NMR (100 MHz, DMSO-d_6) δ 169.7, 162.9 (d, J = 2 Hz), 159.8 (d, J = 196 Hz), 159.1, 158.6, 157.3, 155.7, 154.4, 144.9 (d, J = 12 Hz), 140.8, 139.1, 139.0, 135.5, 132.5, 132.4, 130.2 (d, J = 4 Hz), 129.4, 129.0, 121.3, 121.2, 120.9, 120.6, 118.4, 114.7 (d, J = 14 Hz), 113.2, 107.4, 104.2 (d, J = 28 Hz), 60.5, 55.80, 46.30, 32.0, 29.6, 23.9, 19.50, 14.2, 13.5, 12.5, 10.9, 9.2. MS: calcd $C_{43}H_{51}BClF_3N_9O_4S$ $[M+H]^+$ 892.3, found 892.6.

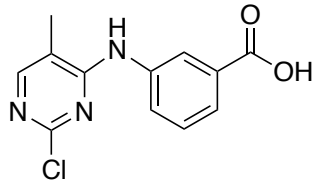


2.20

(***E***)**-4-((4-((4-Chloro-3-((1,1-dimethylethyl)sulfonamido)phenyl)amino)-5-methylpyrimidin-2-yl)amino)-*N*-(1-(3-(5,5-difluoro-1,3,7,9-tetramethyl-5*H*-4λ^4,5λ^4-dipyrrolo[1,2-*c*:2',1'-*f*][1,3,2]diazaborinin-2-yl)acryloyl)piperidin-4-yl)-2-fluorobenzamide (2.20).** Compound **2.20** was obtained as a purple solid (21 mg, 93%) from acid **2.14** (8.1 mg, 25 μmol) and amine **2.11** (18 mg, 31 μmol), according to the procedure described for amide **2.18**. Mp: >250 °C, decomposition. Purity: >96% (HPLC). ^{1}H NMR (400 MHz, DMSO-d_6) δ 9.45 (s, 1H), 9.35 (s, 1H), 8.65 (s, 1H), 8.00 (s, 1H), 7.93 – 7.86 (m, 1H), 7.85 – 7.74 (m, 4H), 7.54 – 7.38 (m, 4H), 6.79 (d, J = 15.5 Hz, 1H), 6.30 (s, 1H), 4.53 – 4.33 (m, 1H), 4.16 (s, 1H), 4.10 – 3.99 (m, 1H), 3.27 (s, 1H), 2.91 (s, 1H), 2.58 (s, 3H), 2.48 (s, 3H), 2.43 (s, 3H), 2.32 (s, 3H), 2.14 (s, 3H), 1.96 – 1.84 (m, 2H), 1.58 -1.43 (m, 2H), 1.34 (s, 9H). ^{13}C NMR (100 MHz, DMSO-d_6) δ 164.7, 163.0 (d, J = 2 Hz), 159.8 (d, J = 244 Hz), 159.1, 158.5, 157.3, 155.8, 154.6, 144.9 (d, J = 12 Hz), 143.8, 139.0, 138.4, 135.4, 134.2, 132.3, 131.9, 130.2 (d, J = 5 Hz), 129.1, 124.2, 122.7, 121.2, 121.0, 120.6, 120.2, 117.4, 114.8 (d, J = 14 Hz), 113.2, 107.4, 104.2 (d, J = 28 Hz), 60.6, 54.9, 46.4, 32.3, 23.8, 14.5, 13.5, 13.2, 11.1, 10.9. MS: calcd $C_{43}H_{49}BClF_3N_9O_4S$ $[M+H]^+$ 890.3, found 890.6.

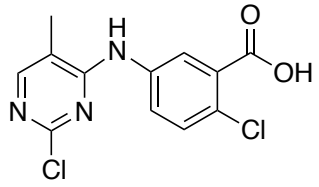
Absorption and fluorescence spectra. BODIPY and probes **2.18**, **2.19**, and **2.20** were dissolved in DMSO at 25 μM. UV absorption (280 -700 nm), fluorescence excitation (excitation: 350 -535 nm, emission: 555-8 nm) and emission spectra (excitation: 480-8 nm, 500 nm-600 nm) were obtained on a CLARIOstar (BMG Labtech) plate reader. Curves were smoothed by moving average (width: 3, spectrum range: 1) based on raw data.

5.3 Chapter 3 synthesis of monovalent inhibitors for BRDT



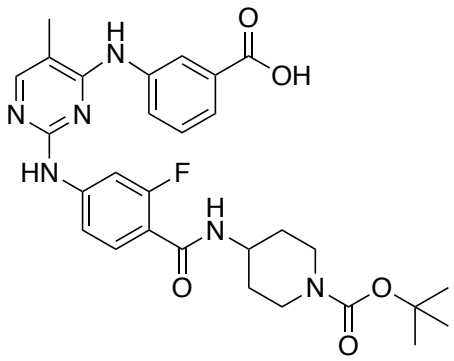
3.3

3-((2-Chloro-5-methylpyrimidin-4-yl)amino)benzoic Acid (3.3).[131] Compound **3.3** was obtained as a white solid (0.89 g, 55%) from 3-aminobenzoic acid (0.84 g, 6.1 mmol) and 2,4-dichloro-5-methylpyrimidine (1.0 g, 6.1 mmol), according to the procedure described for **2.7**. Mp: 234.1 -234.4 °C. ^{1}H NMR (400 MHz, DMSO-d_6) δ 12.99 (s, 1H), 9.03 (s, 1H), 8.24 (t, J = 1.9 Hz, 1H), 8.10 (d, J = 1.1 Hz, 1H), 7.99 (ddd, J = 8.2, 2.4, 1.1 Hz, 1H), 7.69 (dt, J = 7.7, 1.3 Hz, 1H), 7.50 (t, J = 7.9 Hz, 1H), 2.20 (s, 3H).



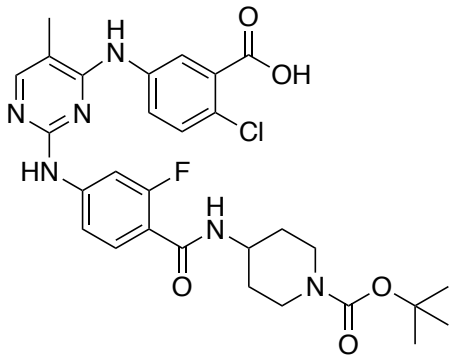
3.4

2-Chloro-5-((2-chloro-5-methylpyrimidin-4-yl)amino)benzoic Acid (3.4). Compound **3.4** was obtained as a white solid (563 mg, 23%) from 5-amino-2-chlorobenzoic acid (1.4 g, 8.2 mmol) and 2,4-dichloro-5-methylpyrimidine (1.6 g, 9.8 mmol), according to the procedure described for **2.7**. Mp: >250 °C. ^{1}H NMR (400 MHz, DMSO-d_6) δ 13.21 (s, 1H), 9.05 (s, 1H), 8.13 (d, J = 4 Hz, 1H), 8.11 (s, 1H), 7.97 – 7.90 (dd, J = 4.0, 12.0 Hz, 1H), 7.54 (d, J = 12.0 Hz, 1H), 2.19 (s, 3H).



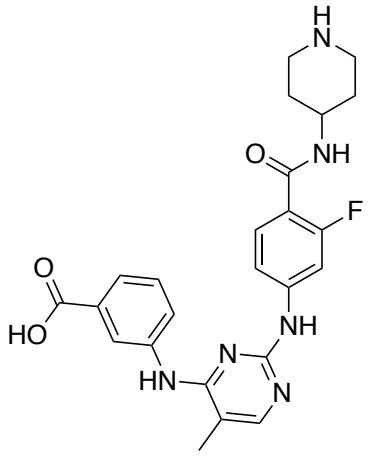
3.5

3-((2-((4-((1-(*tert*-Butoxycarbonyl)piperidin-4-yl)carbamoyl)-3-fluorophenyl)amino)-5-methylpyrimidin-4-yl)amino)benzoic Acid (3.5). Compound **3.5** was obtained as a pale yellow solid (97 mg, 49%) from **3.3** (92 mg, 0.35 mmol) and amine **2.9** (0.12 g, 0.35 mmol), according to the procedure described for **2.10**. Mp: decomposition at 186.2 – 189.0 °C. ^{1}H NMR (400 MHz, Methanol-d_4) δ 8.20 (s, 1H), 7.80 (s, 1H), 7.72 (t, J = 7.2 Hz, 2H), 7.64 (d, J = 15.1 Hz, 1H), 7.48 – 7.35 (m, 2H), 7.14 (d, J = 8.7 Hz, 1H), 4.07 – 3.82 (m, 3H), 2.85 (s, 2H), 2.09 (s, 3H), 1.88 – 1.78 (m, 2H), 1.37 (s, 11H).



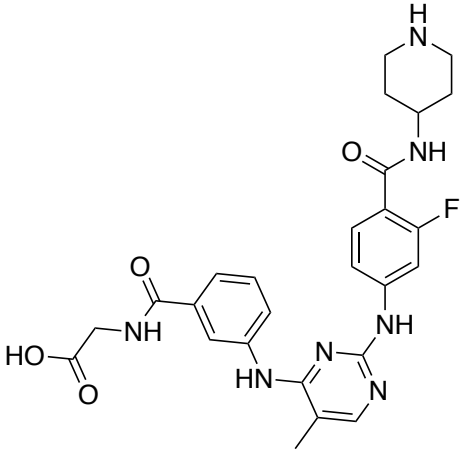
3.6

5-((2-((4-((1-(*tert*-Butoxycarbonyl)piperidin-4-yl)carbamoyl)-3-fluorophenyl)amino)-5-methylpyrimidin-4-yl)amino)-2-chlorobenzoic Acid (3.6). Compound **3.6** was obtained as a white solid (112 mg, 63%) from **3.4** (100 mg, 296 μmol) and amine **2.9** (88 mg, 0.30 mmol), according to the procedure described for **2.10**. Mp: decomposition at 202.9 – 203.7 °C. ^{1}H NMR (400 MHz, Acetone-d_6) δ 9.10 (s, 1H), 8.22 (s, 1H), 8.17 (s, 1H), 8.09 – 7.97 (m, 2H), 7.89 (d, J = 15.0 Hz, 1H), 7.76 (t, J = 8.7 Hz, 1H), 7.50 (d, J = 8.6 Hz, 1H), 7.42 (d, J = 8.9 Hz, 1H), 7.11 (t, J = 7.9 Hz, 1H), 4.16 – 4.01 (m, 3H), 2.96 (s, 2H), 2.25 (s, 3H), 1.98 – 1.89 (m, 2H), 1.61 – 1.50 (m, 2H), 1.46 (s, 9H).



3.19

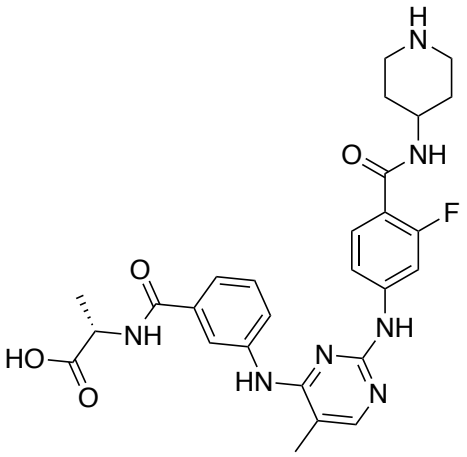
3-((2-((3-Fluoro-4-(piperidin-4-ylcarbamoyl)phenyl)amino)-5-methylpyrimidin-4-yl)amino)benzoic acid (3.19). Compound **3.19** was obtained as a white solid (74 mg, 93%) from **3.5** (97 mg, 0.17 mmol), according to the procedure described for **2.11**. Mp: 236.1 - 236.4 °C. Purity: 98% (HPLC). ^{1}H NMR (400 MHz, Methanol-d_4) δ 8.10 (s, 1H), 7.89 (d, J = 7.7 Hz, 1H), 7.86 (s, 1H), 7.70 (d, J = 8.2 Hz, 1H), 7.62 (t, J = 7.8 Hz, 1H), 7.56 (t, J = 8.3 Hz, 1H), 7.43 (d, J = 13.1, 1.9 Hz, 1H), 7.25 (d, J = 8.5, 2.0 Hz, 1H), 4.28 – 4.17 (m, 1H), 3.49 (dt, J = 13.3, 4.1 Hz, 2H), 3.19 (td, J = 12.5, 3.1 Hz, 2H), 2.29 (s, 3H), 2.24 (dd, J = 14.2, 3.9 Hz, 2H), 1.98 – 1.82 (m, 2H).



3.20

(3-((2-((3-Fluoro-4-(piperidin-4-ylcarbamoyl)phenyl)amino)-5-methylpyrimidin-4-yl)amino)benzoyl)glycine (3.20). To a mixture of compound **3.5** (34 mg, 60 μmol), HATU

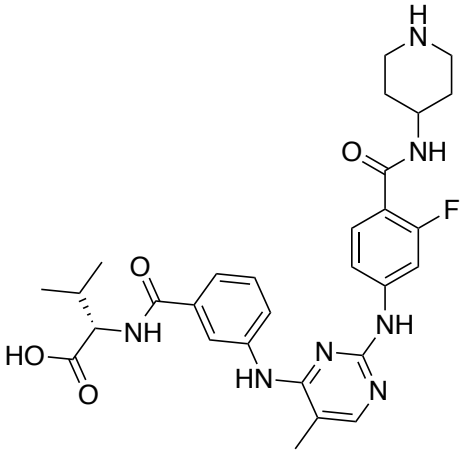
(25 mg, 67 μmol) in anhydrous DMF (1 mL), DIPEA (21 μL, 121 μmol) was added. The solution was stirred at room temperature for 30 min followed by the addition of amine (12 mg, 73 μmol). The reaction solution was stirred at room temperature for 6 h. The mixture was diluted with EtOAc, and the organic layer was washed with brine (3 × 20 mL) and dried over Na_2SO_4. The solvent was removed under reduced pressure. The residues were added to a mixture of DCM (0.8 mL) and TFA (0.2 mL) and stirred at room temperature for 2 h. Solvent was removed in vacuo and the residues was purified by preparative HPLC to give the title compound as a white solid (33 mg, 81%). Mp: 168.2 – 169.0 °C. Purity: >99% (UPLC). ^{1}H NMR (400 MHz, Methanol-d_4) δ 8.10 (s, 1H), 7.89 (d, J = 7.7 Hz, 1H), 7.86 (s, 1H), 7.70 (d, J = 8.2 Hz, 1H), 7.62 (t, J = 7.8 Hz, 1H), 7.56 (t, J = 8.3 Hz, 1H), 7.43 (d, J = 13.1Hz, 1H), 7.25 (d, J = 8.5 1H), 4.20 (td, J = 10.4, 5.1 Hz, 1H), 4.08 (s, 2H), 3.49 (dt, J = 13.3, 4.1 Hz, 2H), 3.19 (td, J = 12.5, 3.1 Hz, 2H), 2.29 (s, 3H), 2.24 (dd, J = 14.2, 3.9 Hz, 2H), 1.98 – 1.82 (m, 2H). ^{13}C NMR (101 MHz, DMSO) δ 171.22, 166.16, 163.16 (d, J = 1Hz), 160.73, 159.11 (d, J = 191Hz), 158.47, 158.28, 143.58 (d, J = 12Hz), 138.82, 134.40, 130.13 (d, J = 4Hz), 128.52, 126.51, 122.85, 122.61, 116.10 (d, J = 17Hz), 113.99, 107.47, 105.19 (d, J = 28Hz), 44.06, 42.14, 41.21, 28.08, 13.41. MS: calcd for $C_{26}H_{29}FN_7O_4$ $[M+H]^+$ 522.2, found 522.3.



3.21

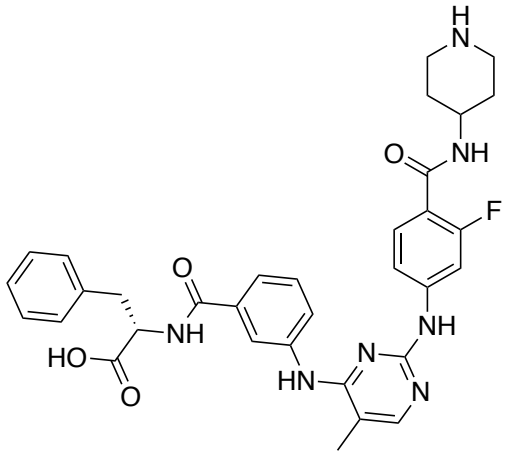
(3-((2-((3-Fluoro-4-(piperidin-4-ylcarbamoyl)phenyl)amino)-5-methylpyrimidin-4-yl)amino)benzoyl)-*L*-alanine (3.21). Compound **3.21** was prepared in the same manner as compound **3.20** from compound **3.5** using *tert*-butyl *L*-alaninate. Yield (14 mg, 90%) as a

white solid. Mp: 136.1 -136.4 °C. Purity >99% (UPLC). ^{1}H NMR (400 MHz, Methanol-d_4) δ 8.10 (s, 1H), 7.90 (d, J = 7.6 Hz, 1H), 7.86 (s, 1H), 7.68 (d, J = 8.1 Hz, 1H), 7.62 (t, J = 7.9 Hz, 1H), 7.56 (t, J = 8.3 Hz, 1H), 7.42 (d, J = 13.1 Hz, 1H), 7.25 (d, J = 8.5 Hz, 1H), 4.56 (q, J = 7.4 Hz, 1H), 4.19 (tt, J = 10.4, 3.9 Hz, 1H), 3.58 – 3.43 (m, 2H), 3.25 – 3.13 (m, 2H), 2.29 (s, 3H), 2.27 – 2.20 (m, 2H), 2.01 – 1.82 (m, 2H), 1.47 (d, J = 7.4 Hz, 3H); MS: calcd for $C_{27}H_{31}FN_7O_4$ $[M+H]^+$ 536.2, found 536.5.



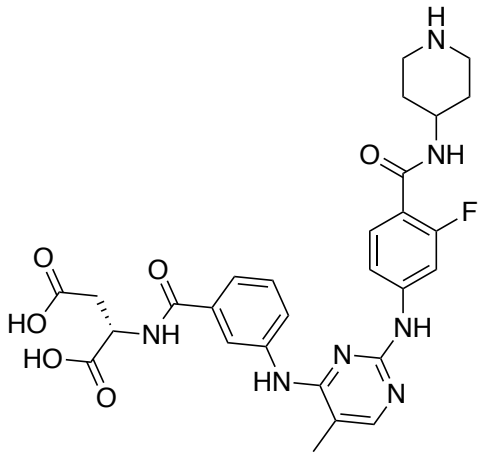
3.22

(3-((2-((3-Fluoro-4-(piperidin-4-ylcarbamoyl)phenyl)amino)-5-methylpyrimidin-4-yl)amino)benzoyl)-*L*-valine (3.22). Compound **3.22** was prepared in the same manner as compound **3.20** from compound **3.5** using *tert*-butyl *L*-valinate. Yield (35 mg, 88%) as a white solid. Mp: 140.0 – 140.5 °C. Purity >99% (UPLC). ^{1}H NMR (400 MHz, Methanol-d_4) δ 8.07 (s, 1H), 7.92 – 7.83 (m, 2H), 7.70 (d, J = 8.1 Hz, 1H), 7.63 (t, J = 7.8 Hz, 1H), 7.55 (t, J = 8.3 Hz, 1H), 7.43 (d, J = 13.2 Hz, 1H), 7.24 (d, J = 8.5 Hz, 1H), 4.43 (d, J = 6.3 Hz, 1H), 4.20 (tt, J = 10.2, 4.0 Hz, 1H), 3.56 – 3.43 (m, 2H), 3.27 – 3.12 (m, 2H), 2.29 (s, 3H), 2.26 – 2.19 (m, 2H), 2.01 – 1.83 (m, 2H), 0.99 (t, J = 4.0, 6H) (two duplicate peaks overlapping). MS: calcd for $C_{29}H_{35}FN_7O_4$ $[M+H]^+$ 564.3, found 564.2.



3.23

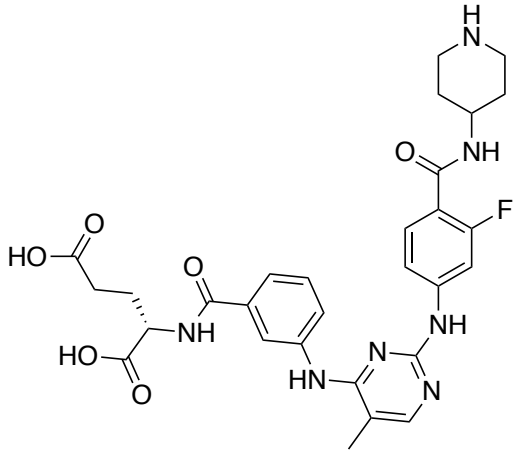
(3-((2-((3-Fluoro-4-(piperidin-4-ylcarbamoyl)phenyl)amino)-5-methylpyrimidin-4-yl)amino)benzoyl)-*L*-phenylalanine (3.23). Compound **3.23** was prepared in the same manner as compound **3.20** from compound **3.5** using *tert*-butyl *L*-phenylalaninate. Yield (13 mg, 73%) as a white solid. Mp: 201.3 – 202.1 °C. Purity >99% (UPLC). ^{1}H NMR (400 MHz, Methanol-d_4) δ 7.94 (s, 1H), 7.86 (s, 1H), 7.75 (d, J = 7.7 Hz, 1H), 7.70 – 7.63 (m, 1H), 7.62 – 7.50 (m, 2H), 7.39 (d, J = 12.0 Hz, 1H), 7.32 – 7.11 (m, 6H), 4.82 – 4.76 (m, 1H), 4.18 (tt, J = 10.1, 4.0 Hz, 1H), 3.54 – 3.43 (m, 2H), 3.31 – 3.25 (m, 1H), 3.24 – 3.13 (t, J = 12.0 Hz, 2H), 3.08 (dd, J = 13.9, 9.0 Hz, 1H), 2.28 (s, 3H), 2.22 (dd, J = 14.4, 4.0 Hz, 2H), 1.97 – 1.83 (m, 2H). MS: calcd for $C_{33}H_{35}FN_7O_4$ $[M+H]^+$, 612.3; found 612.0.



3.24

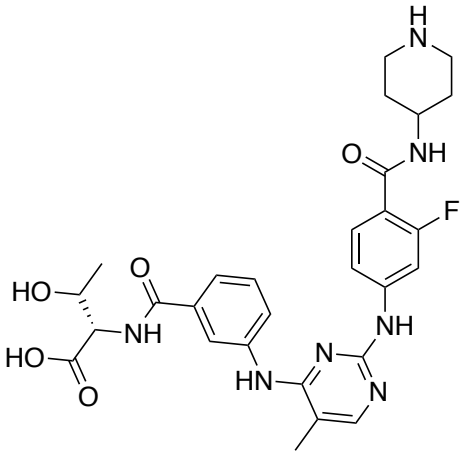
(3-((2-((3-Fluoro-4-(piperidin-4-ylcarbamoyl)phenyl)amino)-5-methylpyrimidin-4-yl)amino)benzoyl)-*L*-aspartic Acid (3.24). Compound **3.24** was prepared in the same

manner as compound **3.20** from compound **3.5** using di-*tert*-butyl *L*-aspartate. Yield (19 mg, 56%) as a white solid. Mp: 157.7 – 158.7°C. Purity >99% (UPLC). ^{1}H NMR (400 MHz, Methanol-d_4) δ 8.08 (s, 1H), 7.91 – 7.82 (m, 2H), 7.68 (d, J = 8.1 Hz, 1H), 7.62 (t, J = 7.8 Hz, 1H), 7.55 (t, J = 8.4 Hz, 1H), 7.43 (dd, J = 13.3, 1.9 Hz, 1H), 7.23 (dd, J = 8.6, 1.9 Hz, 1H), 4.97 (t, J = 8.0 Hz, 1H), 4.25 – 4.16 (m, 1H), 3.50 (dt, J = 13.3, 4.1 Hz, 2H), 3.19 (td, J = 12.5, 3.1 Hz, 2H), 2.98 (dd, J = 16.7, 5.6 Hz, 1H), 2.85 (dd, J = 16.8, 6.9 Hz, 1H), 2.36 – 2.20 (m, 5H), 2.00 – 1.84 (m, 2H). MS: calcd for $C_{28}H_{31}FN_7O_6$ $[M+H]^+$, 580.2; found 580.2.



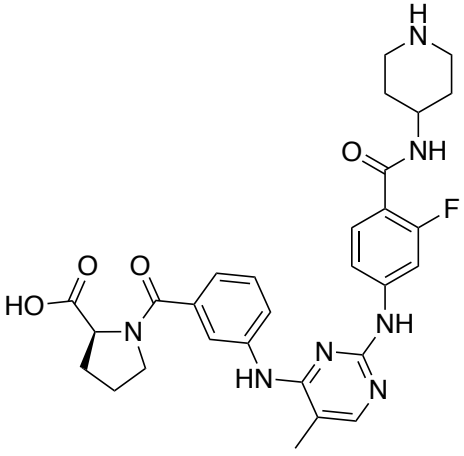
3.25

(3-((2-((3-Fluoro-4-(piperidin-4-ylcarbamoyl)phenyl)amino)-5-methylpyrimidin-4-yl)amino)benzoyl)-*L*-glutamic Acid (3.25). Compound **3.25** was prepared in the same manner as compound **3.20** from compound **3.5** using di-*tert*-butyl *L*-glutamate. Yield (13 mg, 78%) as a white solid. Mp: 150.1 – 150.4 °C. Purity >99% (UPLC). ^{1}H NMR (400 MHz, Methanol-d_4) δ 8.09 (s, 1H), 7.90 (d, J = 7.6, 1H), 7.85 (s, 1H), 7.72 – 7.59 (m, 2H), 7.55 (t, J = 8.4 Hz, 1H), 7.42 (dd, J = 13.2, 3.0 Hz, 1H), 7.24 (dd, J = 8.5, 2.0 Hz, 1H), 4.59 (dd, J = 9.2, 5.1 Hz, 1H), 4.20 (tt, J = 10.0, 4.0 Hz, 1H), 3.51 (d, J = 13.0 Hz, 2H), 3.19 (td, J = 13.0, 12.5, 3.2 Hz, 2H), 2.49 – 2.37 (m, 2H), 2.35 – 2.21 (m, 6H), 2.13 -2.10 (m, 1H), 1.99 – 1.84 (m, 2H). MS: calcd for $C_{29}H_{33}FN_7O_6$ $[M+H]^+$, 594.2; found 594.3.



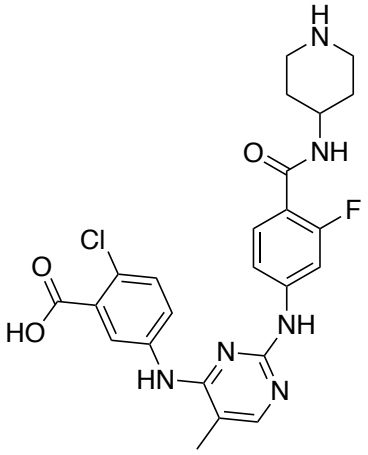
3.26

(3-((2-((3-Fluoro-4-(piperidin-4-ylcarbamoyl)phenyl)amino)-5-methylpyrimidin-4-yl)amino)benzoyl)-*L*-allothreonine (3.26). Compound **3.26** was prepared in the same manner as compound **3.20** from compound **3.5** using *tert*-butyl *L*-allothreoninate. Yield (19 mg, 92%) as a white solid. Mp: 105.3 – 105.6 °C. Purity >99% (UPLC). ^{1}H NMR (400 MHz, Methanol-d_4) δ 8.07 (s, 1H), 7.93 (d, J = 7.7 Hz, 1H), 7.85 (s, 1H), 7.72 (d, J = 8.3, 1H), 7.65 (t, J = 7.8 Hz, 1H), 7.55 (t, J = 8.4 Hz, 1H), 7.43 (d, J = 13.3, 1H), 7.23 (d, J = 8.5, 1H), 4.63 (d, J = 3.1 Hz, 1H), 4.41 (dq, J = 6.6, 3.5 Hz, 1H), 4.23 – 4.12 (m, 1H), 3.56 – 3.44 (m, 2H), 3.18 (td, J = 12.5, 3.1 Hz, 2H), 2.29 (s, 3H), 2.23 (dd, J = 14.3, 3.8 Hz, 2H), 1.90 (q, J = 10.5 Hz, 2H), 1.19 (d, J = 6.4 Hz, 3H). MS: calcd for $C_{28}H_{33}FN_7O_5$ $[M+H]^+$, 566.2; found 566.5.



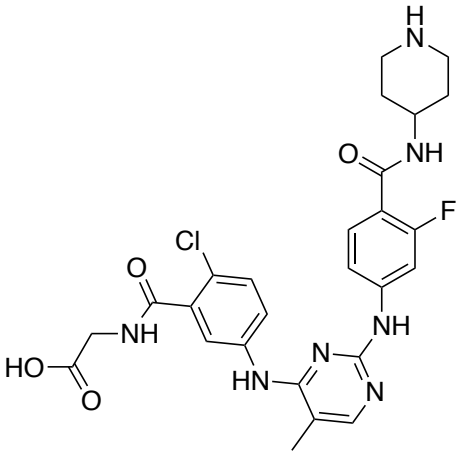
3.27

(3-((2-((3-Fluoro-4-(piperidin-4-ylcarbamoyl)phenyl)amino)-5-methylpyrimidin-4-yl)amino)benzoyl)-*L*-proline (3.27). Compound **3.26** was prepared in the same manner as compound **3.20** from compound **3.5** using *tert*-butyl *L*-prolinate. Yield (17 mg, 89%) as a white solid. Mp: 182.2 – 183.0 °C. Purity >99% (UPLC). Mp: >250 °C. purity 90%. ^{1}H NMR (400 MHz, Methanol-d_4) δ 7.82 (s, 1H), 7.75 (s, 1H), 7.69 – 7.53 (m, 4H), 7.37 (d, J = 13.0 Hz, 1H), 7.25 (d, J = 8.0, 1H), 4.57 (dd, J = 8.4, 5.3 Hz, 1H), 4.18 (tt, J = 10.5, 4.5 Hz, 1H), 3.78 – 3.47 (m, 4H), 3.19 (td, J = 12.6, 3.2 Hz, 2H), 2.46 – 2.31 (m, 1H), 2.27 (s, 3H), 2.25 – 2.19 (m, 2H), 2.05 – 1.78 (m, 5H). MS: calcd for $C_{29}H_{33}FN_7O_4$ $[M+H]^+$, 562.3; found 562.3.



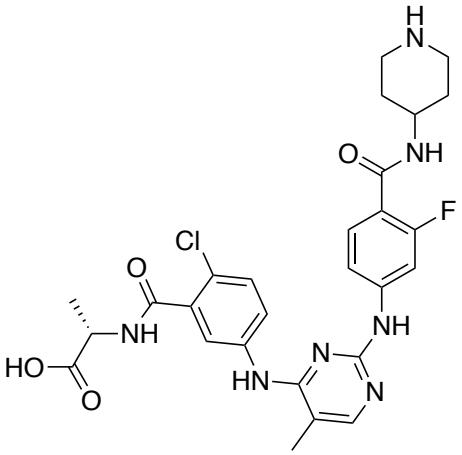
3.28

2-Chloro-5-((2-((3-fluoro-4-(piperidin-4-ylcarbamoyl)phenyl)amino)-5-methylpyrimidin-4-yl)amino)benzoic Acid (3.28). Compound **3.28** was prepared in the same manner as compound **3.19** from compound **3.6**. Yield (12 mg, 99%) as a white solid. Purity >99% (UPLC). ^{1}H NMR (400 MHz, Methanol-d_4) δ 8.08 (d, J = 2.4 Hz, 1H), 7.87 (s, 1H), 7.71 – 7.55 (m, 3H), 7.45 (dd, J = 13.3, 1.9 Hz, 1H), 7.25 (dd, J = 8.5, 1.9 Hz, 1H), 4.21 (tt, J = 9.7, 4.0 Hz, 1H), 3.50 (dt, J = 13.2, 4.2 Hz, 2H), 3.20 (td, J = 12.4, 3.1 Hz, 2H), 2.36 – 2.19 (m, 5H), 1.99 – 1.83 (m, 2H). MS: calcd for $C_{24}H_{25}ClFN_6O_3$ $[M+H]^+$, 499.2; found 499.2.



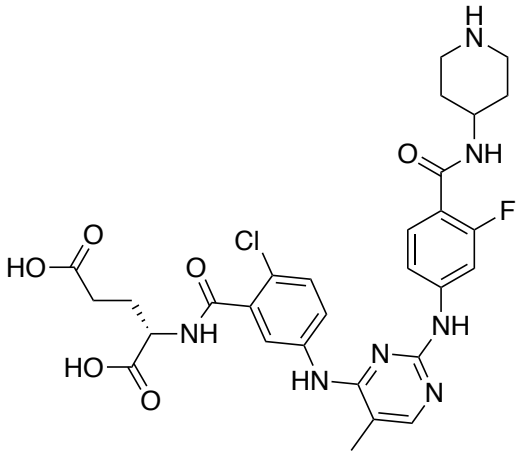
3.29

(2-Chloro-5-((2-((3-fluoro-4-(piperidin-4-ylcarbamoyl)phenyl)amino)-5-methylpyrimidin-4-yl)amino)benzoyl)glycine (3.29). Compound **3.29** was prepared in the same manner as compound **3.20** from compound **3.6** using *tert*-butyl glycinate hydrochloride. Yield (16 mg, 80%) as a white solid. Mp: 147.6 – 148.2 °C. Purity >99%. ^{1}H NMR (400 MHz, Methanol-d_4) δ 7.87 (s, 1H), 7.83 (s, 1H), 7.68 – 7.53 (m, 3H), 7.41 (d, J = 13.1 Hz, 1H), 7.26 (d, J = 8.5 Hz, 1H), 4.22 (tt, J = 8.9, 3.7 Hz, 1H), 4.05 (s, 2H), 3.51 (dt, J = 13.6, 4.2 Hz, 2H), 3.28 – 3.13 (m, 2H), 2.35 – 2.20 (m, 5H), 2.02 – 1.84 (m, 2H). ^{13}C NMR (101 MHz, DMSO) δ 170.81, 166.37, 163.25 (d, J = 2 Hz), 159.30 (d, J = 173 Hz), 159.15, 156.54, 154.24 144.35 (d, J = 11 Hz), 138.29, 136.02, 130.20 (d, J = 5 Hz), 129.58, 124.44, 123.63, 122.37, 115.41 (d, J = 13 Hz), 113.60, 107.55, 104.73 (d, J = 28 Hz), 44.03, 42.11, 40.91, 28.09, 13.44. MS: calcd for $C_{26}H_{28}ClFN_7O_4$ $[M+H]^+$, 556.2; found 556.3.



3.30

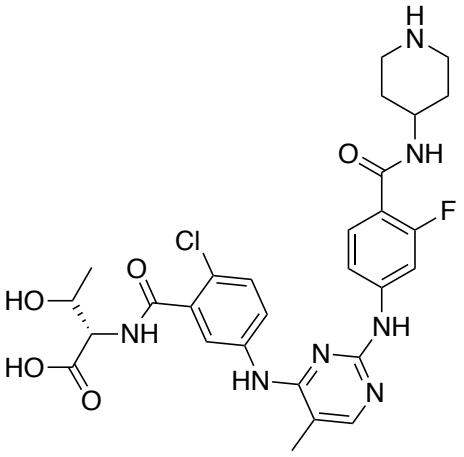
(2-Chloro-5-((2-((3-fluoro-4-(piperidin-4-ylcarbamoyl)phenyl)amino)-5-methylpyrimidin-4-yl)amino)benzoyl)-*L*-alanine (3.30). Compound **3.30** was prepared in the same manner as compound **3.20** from compound **3.6** using *tert*-butyl *L*-alaninate. Yield (16 mg, 91%) as a white solid. Mp: 138.1 – 138.4 °C. Purity >99% (UPLC). ^{1}H NMR (400 MHz, Methanol-d_4) δ 7.88 (s, 1H), 7.80 (s, 1H), 7.70 – 7.52 (m, 3H), 7.42 (dd, J = 13.1, 2.0 Hz, 1H), 7.26 (dd, J = 8.5, 2.0 Hz, 1H), 4.51 (q, J = 7.3 Hz, 1H), 4.22 (tt, J = 9.6, 3.9 Hz, 1H), 3.51 (dt, J = 13.5, 4.3 Hz, 2H), 3.28 – 3.12 (m, 2H), 2.31 – 2.19 (m, 5H), 2.02 – 1.87 (m, 2H), 1.44 (d, J = 7.3 Hz, 3H). MS: calcd for $C_{27}H_{30}ClFN_7O_4$ $[M+H]^+$, 570.2; found 570.0.



3.31

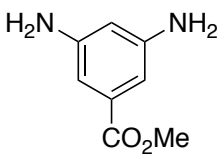
(2-Chloro-5-((2-((3-fluoro-4-(piperidin-4-ylcarbamoyl)phenyl)amino)-5-methylpyrimidin-4-yl)amino)benzoyl)-*L*-glutamic acid (3.31). Compound **3.31** was prepared in the same manner as compound **3.20** from compound **3.6** using di-*tert*-butyl *L*-

glutamate. Yield (19 mg, 67%) as a white solid. Mp: 172.1 – 173.1 °C. Purity >99% (UPLC). ^{1}H NMR (400 MHz, Methanol-d_4) δ 7.75 (s, 1H), 7.64 (s, 1H), 7.57 – 7.42 (m, 3H), 7.24 (d, J = 12.0 Hz, 1H), 7.12 (d, J = 8.0 Hz, 1H), 4.47 (q, J = 5.3, Hz, 1H), 4.10 (tt, J = 9.3, 4.0 Hz, 1H), 3.41 (dt, J = 13.1, 4.3 Hz, 2H), 3.10 (t, J = 11.1 Hz, 2H), 2.33 (t, J = 7.3 Hz, 2H), 2.21 – 2.09 (d, J = 11.4 Hz, 6H), 1.90 – 1.79 (s, 3H). MS: calcd for $C_{29}H_{32}ClFN_7O_6$ $[M+H]^+$, 628.2; found 627.9.



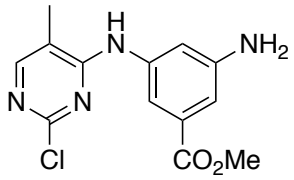
3.32

(2-Chloro-5-((2-((3-fluoro-4-(piperidin-4-ylcarbamoyl)phenyl)amino)-5-methylpyrimidin-4-yl)amino)benzoyl)-*L*-allothreonine (3.32). Compound **3.31** was prepared in the same manner as compound **3.20** from compound **3.6** using *tert*-butyl *L*-allothreoninate. Yield (13.5 mg, 94%) as a white solid. Mp: 187.4-189.1 °C. Purity >99% (UPLC). ^{1}H NMR (400 MHz, Methanol-d_4) δ 7.87 (s, 1H), 7.83 (s, 1H), 7.74 – 7.54 (m, 3H), 7.42 (d, J = 12.0 Hz, 1H), 7.24 (d, J = 8.0 Hz,1H), 4.57 (d, J = 2.8 Hz, 1H), 4.38 (dt, J = 8.8, 5.9 Hz, 1H), 4.21 (tt, J = 10.1, 4.0 Hz, 1H), 3.51 (dt, J = 13.5, 4.3 Hz, 2H), 3.27 – 3.13 (m, 2H), 2.33 -3.20 (m, 5H), 2.02 – 1.84 (m, 2H), 1.22 (d, J = 6.4 Hz, 3H). MS: calcd for $C_{28}H_{32}ClFN_7O_5$ $[M+H]^+$, 600.2; found 600.0.



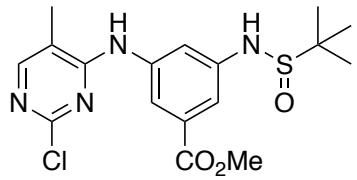
3.34

Methyl 3,5-Diaminobenzoate (3.34).[120] To a mixture of 4-aminobenzoic acid (4.0 g, 26 mmol) and MeOH (75 mL), concentrated sulfuric acid (3.5 mL, 66 mmol) was added slowly at 0 °C dropwise. The mixture was stirred at rt for 5 h. The mixture was washed with a saturated solution of $NaHCO_3$ and extracted with EtoAc. The organic layer was dried over $MgSO_4$ and concentrated under vacuum to provide the title compound as a white solid (4.0 g, 91%). Mp: 129.6 – 130.1 °C. ^{1}H NMR (400 MHz, Acetone-d_6) δ 6.64 (d, J = 2.1 Hz, 2H), 6.23 (d, J = 2.0 Hz, 1H), 4.56 (brs, 3H), 3.78 (s, 3H).



3.35

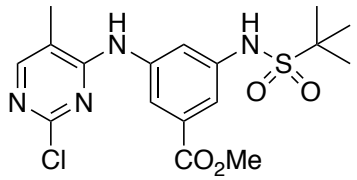
Methyl 3-Amino-5-((2-chloro-5-methylpyrimidin-4-yl)amino)benzoate (3.35). To a solution of methyl 3,5-diaminobenzoate (80 mg, 0.33 mmol) and 2,4-dichloro-5-methylpyrimidine (**3.34**, 54 mg, 0.33 mmol) in n-BuOH (1 mL) was added DIPEA (0.23 mL, 1.3 mmol). The mixture was stirred at 120 °C for 24 h, then cooled to rt. The solvent was removed under reduced pressure and the residue was purified by silica gel column chromatography (MeOH:DCM) to give the title compound as a brown solid (84 mg, 69%). Mp: 130.1 – 130.7 °C. ^{1}H NMR (400 MHz, DMSO-d_6) δ 8.76 (s, 1H), 8.04 (s, 1H), 7.38 (s, 1H), 7.15 (s, 1H), 6.99 (s, 1H), 5.46 (s, 2H), 3.82 (s, 3H), 2.16 (s, 3H).



3.36

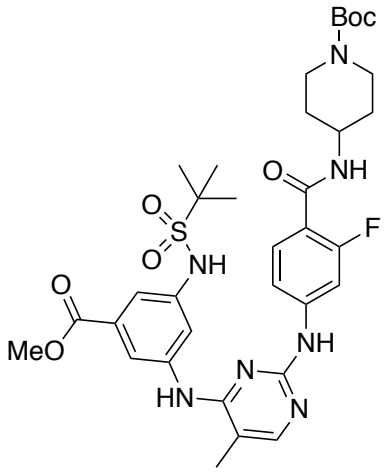
Methyl 3-((*tert*-Butylsulfinyl)amino)-5-((2-chloro-5-methylpyrimidin-4-yl)amino)benzoate (3.36).[131] To a solution of methyl 3-amino-5-((2-chloro-5-methylpyrimidin-4-yl)amino)benzoate (**3.35**, 1.3 g, 4.4 mmol) in pyridine (10 mL) was added a solution of *tert*-butylsulfinyl chloride (0.55 mL, 4.4 mmol) in DCM (10mL) dropwise at 0 °C under nitrogen. The mixture was stirred at 0 °C for 2 h, then warmed to

rt and further stirred for 20 h. Solvent was removed under vacuum. The residue was diluted with EtOAc (20 mL) and washed with HCl (1 M, 1 × 50 mL) and water (1 × 50 mL). The organic layer was dried (Na_2SO_4) and concentrated under reduced pressure. The yellow oil was purified by silica gel column chromatography (EtOAc:hexanes, gradient) to give the title compound as a pale-yellow foam (1.6 g, 89%). ^{1}H NMR (400 MHz, Acetone-d_6) δ 8.34 (s, 1H), 8.11 (s, 1H), 8.05 (s, 1H), 7.94 (s, 1H), 7.50 (s, 1H), 7.31 (s, 1H), 3.89 (s, 3H), 2.31 (s, 3H), 1.35 (d, J = 1.2 Hz, 9H).



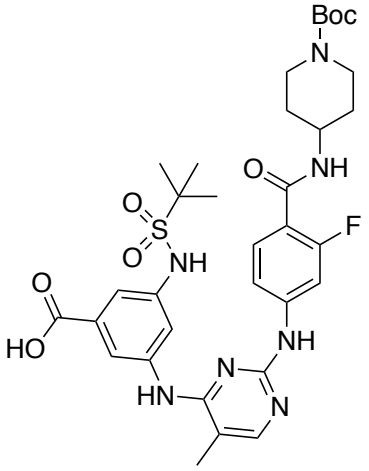
3.37

Methyl 3-((2-Chloro-5-methylpyrimidin-4-yl)amino)-5-((1,1-dimethylethyl)sulfonamido)benzoate (3.37).[131] To a solution of methyl 3-((*tert*-butylsulfinyl)amino)-5-((2-chloro-5-methylpyrimidin-4-yl)amino)benzoate (**3.36**, 10 mg, 25 μmol) in DCM (1 mL) was added mCPBA (4.4 mg, 25 μmol) under nitrogen at 0 °C for 1 h, then warmed to rt and further stirred overnight. The reaction mixture was diluted with DCM (20 mL) and washed with saturated $NaHCO_3$ solution (2 × 20 mL) and brine (1 × 20 mL). The organic layer was dried (Na_2SO_4) and concentrated under reduced pressure. The yellow oil was purified by silica gel column chromatography (EtOAc/hexanes, gradient) to give the title compound as a light-yellow solid (8.4 mg, 81%). Mp: 251.3 - 251.9 °C. ^{1}H NMR (400 MHz, Chloroform-*d*) δ 8.08 (s, 1H), 7.97 (s, 1H), 7.81 (s, 1H), 7.54 (s, 1H), 7.00 (s, 1H), 6.72 (s, 1H), 3.86 (s, 3H), 2.16 (s, 3H), 1.41 (s, 9H).



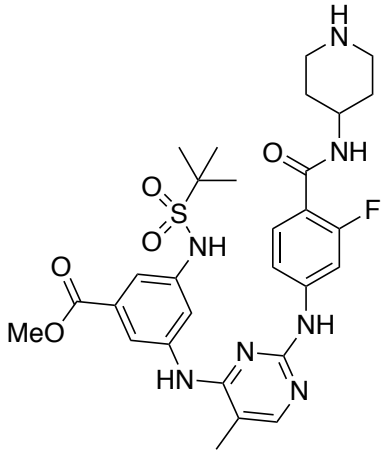
3.38

***tert*-Butyl 4-(4-((4-((3-((1,1-Dimethylethyl)sulfonamido)-5-(methoxycarbonyl)phenyl)amino)-5-methylpyrimidin-2-yl)amino)-2-fluorobenzamido)piperidine-1-carboxylate (3.38).** To a solution of *tert*-butyl 4-(4-amino-2-fluorobenzamido)piperidine-1-carboxylate (**2.9**, 16 mg, 48 μmol) and sodium *tert*-butoxide (9.3 mg, 97 μmol) in 1,4-dioxane (0.5 mL), a solution of methyl 3-((2-chloro-5-methylpyrimidin-4-yl)amino)-5-((1,1-dimethylethyl)sulfonamido)benzoate (**3.37**, 20 mg, 48 μmol), $Pd_2(dba)_3$ (2.2 mg, 2.4 μmol) and BINAP (3.0 mg, 4.8 μmol) in 1,4-dioxane (0.5 mL) was added. The mixture was degassed and heated at 110 °C for 7 h. The mixture was cooled to rt, diluted with EtOAc, and the organic layer was washed with brine (3 × 20 mL) and dried over Na_2SO_4. The solvent was removed and the residues was purified by silica gel column chromatography (MeOH:DCM, gradient) to give the title compound as an off-white solid (22 mg, 64%). Mp: 192.9. – 193.4 °C. ^{1}H NMR (400 MHz, Methanol-d_4) δ 7.79 (d, J = 1.7 Hz, 1H), 7.77 – 7.67 (m, 3H), 7.56 – 7.36 (m, 2H), 7.07 (d, J = 8.5 Hz, 1H), 4.06 – 3.90 (m, 3H), 3.76 (s, 3H), 2.88 (s, 2H), 2.14 (s, 3H), 1.84 (dd, J = 13.3, 3.8 Hz, 2H), 1.49 – 1.39 (m, 2H), 1.38 (s, 9H), 1.26 (s, 9H).



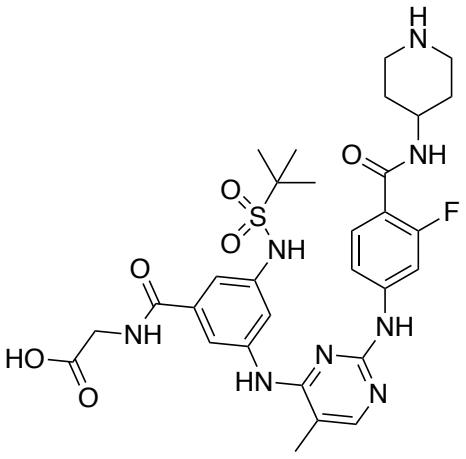
3.39

3-((2-((4-((1-(*tert*-Butoxycarbonyl)piperidin-4-yl)carbamoyl)-3-fluorophenyl)amino)-5-methylpyrimidin-4-yl)amino)-5-((1,1-dimethylethyl)sulfonamido)benzoic acid (3.39). To a solution of *tert*-butyl 4-(4-((4-((3-((1,1-dimethylethyl)sulfonamido)-5-(methoxycarbonyl)phenyl)amino)-5-methylpyrimidin-2-yl)amino)-2-fluorobenzamido)piperidine-1-carboxylate (**3.38**, 10 mg, 14 μmol) in MeOH (0.125 mL) and THF (0.125 mL), a solution of LiOH (1.0 mg, 42 μmol) in H_2O (0.25 mL) was added. The reaction was allowed to stir at 60 °C for 3 h. The mixture was cooled to rt, diluted with EtOAc (10 mL), washed with 2 N HCl, and the organic layer was washed with brine (3 × 20 mL) and dried over Mg_2SO_4. The solvent was removed and the residue was purified by silica gel column chromatography (MeOH:DCM:AcOH, gradient) to give the title compound as a grey solid (5.6 mg, 57%). Mp: 166.2 – 167.1 °C. Purity: 98% (HPLC). ^{1}H NMR (400 MHz, DMSO-d_6) δ 12.81(brs, 1H), 9.89 (d, J = 2.8 Hz, 1H), 9.76 (s, 1H), 9.14 (s, 1H), 8.01 (s, 1H), 7.83 (s, 1H), 7.77 (d, J = 8.0 Hz 1H), 7.73 (s, 2H), 7.64 (d, J = 14.0 Hz, 1H), 7.42 (t, J = 8.5 Hz, 1H), 7.31 (d, J = 8.9 Hz, 1H), 3.96 – 3.84 (m, 3H), 2.87 (s, 2H), 2.16 (s, 3H), 1.78 (dd, J = 13.2, 3.9 Hz, 2H), 1.41 (s, 9H), 1.40 – 1.34 (m, 2H), 1.30 (s, 9H). ^{13}C NMR (101 MHz, DMSO) δ 172.0, 166.6, 162.6 (d, J = 2 Hz), 159.5 (d, J = 170 Hz), 158.2, 153.8, 152.9, 142.2 (d, J = 12 Hz), 140.8, 138.8, 131.9, 130.2 (d, J = 4 Hz), 120.4, 118.8, 117.1 (d, J = 13 Hz), 116.4, 114.3, 107.9, 105.7 (d, J = 29 Hz), 78.6, 61.1, 55.8, 46.3, 29.6, 28.1, 24.2, 13.4.



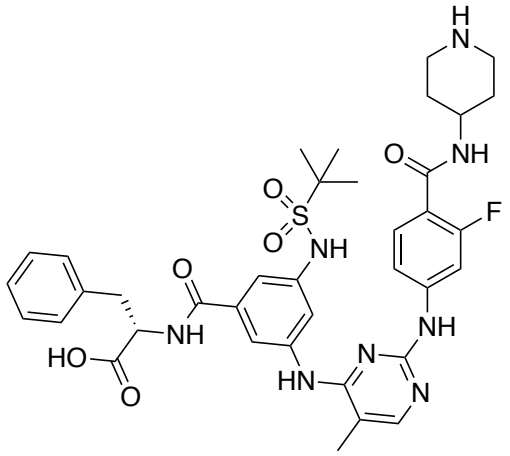
3.55

Methyl 3-((1,1-Dimethylethyl)sulfonamido)-5-((2-((3-fluoro-4-(piperidin-4-ylcarbamoyl)phenyl)amino)-5-methylpyrimidin-4-yl)amino)benzoate (3.55). Compound **3.55** was prepared in the same manner as compound **3.19** from compound **3.38**. Yield (11 mg, 94%) as a white solid. Mp: 142.2. – 143.1 °C. Purity 97%. ^{1}H NMR (400 MHz, Methanol-d_4) δ 7.86 (dd, J = 2.2, 1.4 Hz, 1H), 7.78 (t, J = 1.7 Hz, 1H), 7.76 (d, J = 1.2 Hz, 1H), 7.59 (t, J = 2.1 Hz, 1H), 7.49 (t, J = 8.4 Hz, 1H), 7.35 (dd, J = 13.2, 2.1 Hz, 1H), 7.10 (dd, J = 8.5, 2.1 Hz, 1H), 4.14 – 4.01 (m, 1H), 3.76 (s, 3H), 3.38 (dt, J = 13.6, 4.1 Hz, 2H), 3.14 – 3.01 (m, 2H), 2.17 (d, J = 1.1 Hz, 3H), 2.11 (dd, J = 12.7, 5.1, 2H), 1.86 – 1.72 (m, 2H), 1.26 (s, 9H). MS: calcd for $C_{29}H_{37}FN_7O_5S$ $[M+H]^+$, 614.3; found 614.2.



3.56

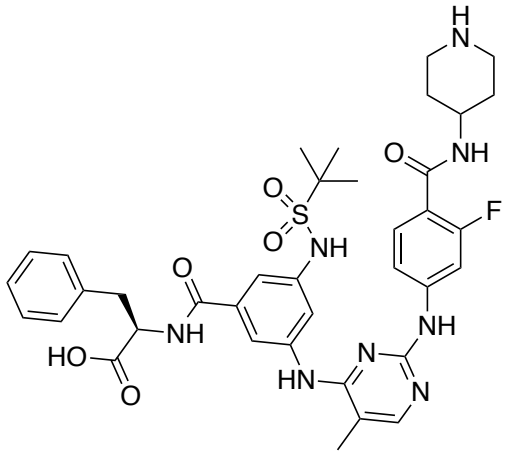
(3-((1,1-Dimethylethyl)sulfonamido)-5-((2-((3-fluoro-4-(piperidin-4-ylcarbamoyl)phenyl)amino)-5-methylpyrimidin-4-yl)amino)benzoyl)glycine (3.56). Compound **3.56** was prepared in the same manner as compound **3.20** from compound **3.39** using *tert*-butyl glycinate hydrochloride. Yield (25 mg, 73%) as a white solid. Mp: 216.7 – 217.4 °C. Purity >99%. ^{1}H NMR (400 MHz, DMSO-d_6) δ 10.44 (s, 1H), 9.91 (s, 1H), 9.58 (s, 1H), 8.72 (d, J = 10.3 Hz, 1H), 8.59 (d, J = 7.5 Hz, 1H), 8.46 (d, J = 10.7 Hz, 1H), 8.06 (s, 1H), 8.02 (dd, J = 7.5, 2.4 Hz, 1H), 7.87 – 7.77 (m, J = 1.7 Hz, 1H), 7.66 (t, J = 1.7 Hz, 1H), 7.61 (t, J = 2.0 Hz, 1H), 7.50 (dd, J = 13.5, 2.0 Hz, 1H), 7.40 (t, J = 8.4 Hz, 1H), 7.30 (dd, J = 8.6, 2.0 Hz, 1H), 4.35 (ddd, J = 9.6, 7.4, 5.0 Hz, 1H), 4.09 – 3.95 (m, 1H), 3.31 (d, J = 12.6 Hz, 2H), 3.11 – 2.94 (m, 2H), 2.26 (t, J = 7.7 Hz, 1H), 2.18 (s, 3H), 2.02 – 1.95 (m, 2H), 1.78 – 1.64 (m, 2H), 1.28 (s, 9H). MS: calcd for $C_{30}H_{38}FN_8O_6S$ $[M+H]^+$, 657.3; found 657.3.



3.57

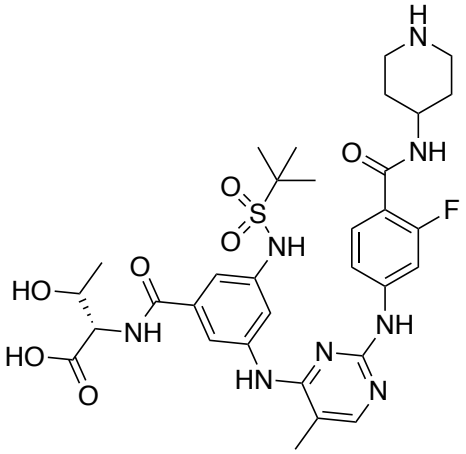
(3-((1,1-Dimethylethyl)sulfonamido)-5-((2-((3-fluoro-4-(piperidin-4-ylcarbamoyl)phenyl)amino)-5-methylpyrimidin-4-yl)amino)benzoyl)-*D*-phenylalanine (3.57). Compound **3.57** was prepared in the same manner as compound **3.20** from compound **3.39** using *tert*-butyl *L*-phenylalaninate. Yield (31 mg, 77%) as a white solid. Mp: 184.5 – 185.5 °C. Purity >99%. ^{1}H NMR (400 MHz, Methanol-d_4) δ 7.89 – 7.68 (m, 2H), 7.55 (s, 1H), 7.52 – 7.38 (m, 3H), 7.28 (d, J = 13.4, 1H), 7.12 – 7.00 (m, 5H), 4.65 (dd, J = 8.9, 5.1 Hz, 1H), 4.07 (tt, J = 10.2, 3.9 Hz, 1H), 3.37 (d, J = 13.5, 2H), 3.16 (dd, J = 13.8, 5.1 Hz, 1H), 3.07 (t, J = 12.8, Hz, 2H), 2.94 (dd, J = 13.9, 8.8 Hz, 1H),

2.15 (s, 3H), 2.13 – 2.07 (m, 2H), 1.84 – 1.74 (m, 2H), 1.26 (s, 9H). MS: calcd for $C_{37}H_{44}FN_8O_6S$ $[M+H]^+$, 747.3; found 747.2.



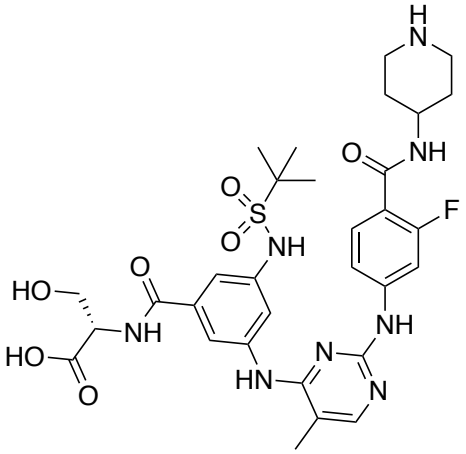
3.58

(3-((1,1-Dimethylethyl)sulfonamido)-5-((2-((3-fluoro-4-(piperidin-4-ylcarbamoyl)phenyl)amino)-5-methylpyrimidin-4-yl)amino)benzoyl)-*D*-phenylalanine hydrochloride (3.58). Compound **3.58** was prepared in the same manner as compound **3.20** from compound **3.39** using *tert*-butyl *D*-phenylalaninate. Yield (17 mg, 77%) as a white solid; Mp: 189.7 – 190.2 °C. Purity >99%. ^{1}H NMR (400 MHz, DMSO-d_6) δ 10.00 (s, 1H), 9.84 (s, 1H), 9.16 (s, 1H), 8.66 (s, 1H), 8.59 (d, J = 7.9 Hz, 1H), 8.41 (d, J = 10.4 Hz, 1H), 8.07 – 7.99 (m, 2H), 7.71 (s, 1H), 7.65 (s, 1H), 7.58 (d, J = 1.9 Hz, 1H), 7.50 (s, 1H), 7.44 – 7.30 (m, 2H), 7.24 (d, J = 7.2 Hz, 2H), 7.19 – 7.06 (m, 3H), 4.59 – 4.53 (m, 1H), 4.01 (d, J = 8.2 Hz, 1H), 3.30 (d, J = 12.4 Hz, 2H), 3.14 (dd, J = 13.8, 4.6 Hz, 1H), 3.01 (dd, J = 13.3, 9.7 Hz, 3H), 2.16 (s, 3H), 2.00 – 1.94 (m, 2H), 1.73 – 1.64 (m, J = 10.4 Hz, 2H), 1.28 (s, 9H). ^{13}C NMR (101 MHz, DMSO) δ 172.94, 166.13, 163.12 (d, J = 2 Hz), 160.80, 160.06, 159.55 (d, J = 247 Hz), 158.34, 143.62 (d, J = 10 Hz), 140.43, 139.30, 137.92, 135.32, 130.23 (d, J = 4 Hz), 128.95, 128.02, 126.28, 117.61, 117.27, 115.97 (d, J = 15 Hz), 114.69, 113.70, 107.62, 104.94 (d, J = 28 Hz), 61.00, 54.28, 44.04, 42.13, 36.19, 28.08, 24.21, 13.40. MS: calcd for $C_{37}H_{44}FN_8O_6S$ $[M+H]^+$, 747.3; found 747.3.



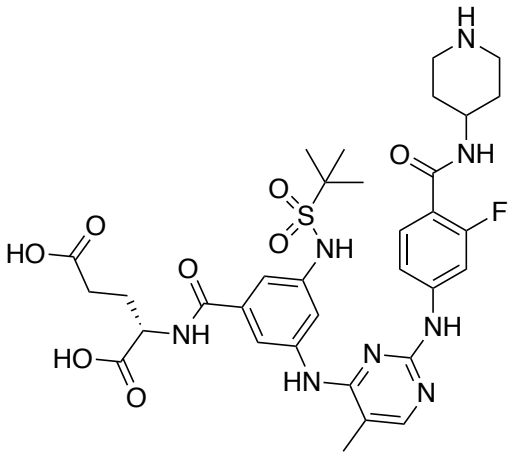
3.59

(3-((1,1-Dimethylethyl)sulfonamido)-5-((2-((3-fluoro-4-(piperidin-4-ylcarbamoyl)phenyl)amino)-5-methylpyrimidin-4-yl)amino)benzoyl)-*L*-threonine (3.59). Compound **3.59** was prepared in the same manner as compound **3.20** from compound **3.39** using *tert*-butyl *L*-allothreoninate. Yield (10 mg, 78%) as a white solid. Mp: 178.9. – 179.4 °C. purity >99% (HPLC). ^{1}H NMR (400 MHz, Methanol-d_4) δ 7.75 (s, 1H), 7.73 (s, 1H), 7.64 (s, 1H), 7.57 (s, 1H), 7.48 (t, J = 8.3 Hz, 1H), 7.33 (dd, J = 13.3, 2.1 Hz, 1H), 7.11 (dd, J = 8.4, 2.0 Hz, 1H), 4.50 (d, J = 3.0 Hz, 1H), 4.30 (tt, J = 9.5, 4.5 Hz, 1H), 4.09 (tt, J = 9.9, 4.1 Hz, 1H), 3.90 (s, 1H), 3.40 (dt, J = 13.4, 4.3 Hz, 2H), 3.09 (td, J = 11.8, 11.0, 3.6 Hz, 2H), 2.17 (s, 3H), 2.16 – 2.09 (m, 2H), 1.88 – 1.77 (m, 2H), 1.28 (s, 9H), 1.07 (d, J = 6.4 Hz, 3H). ^{13}C NMR (101 MHz, DMSO) δ 171.90, 165.97, 163.01 (d, J = 2 Hz), 159.44 (d, J = 261 Hz),158.90, 158.56, 158.23, 142.62 (d, J = 12 Hz), 140.68, 138.82, 135.18, 130.22 (d, J = 3 Hz), 118.20, 117.89, 116.77 (d, J = 14 Hz), 115.16, 114.22, 107.74, 105.64 (d, J = 2 Hz), 66.42, 61.01, 58.58, 44.07, 42.12, 28.07, 24.16, 20.33, 13.31. MS: calcd for $C_{32}H_{42}FN_8O_7S$ $[M+H]^+$, 701.3; found 701.6.



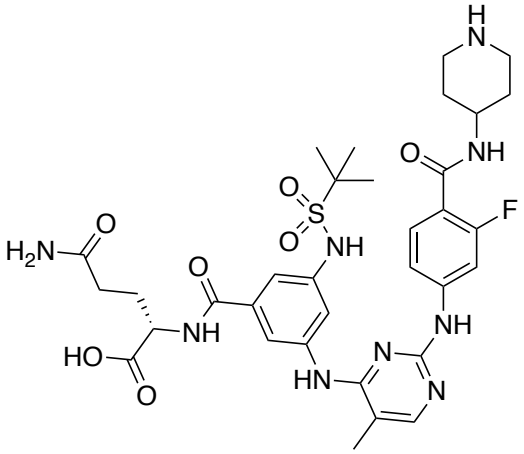
3.60

(3-((1,1-Dimethylethyl)sulfonamido)-5-((2-((3-fluoro-4-(piperidin-4-ylcarbamoyl)phenyl)amino)-5-methylpyrimidin-4-yl)amino)benzoyl)-*L*-serine (3.60). Compound **3.60** was prepared in the same manner as compound **3.20** from compound **3.39** using *tert*-butyl *L*-serinate. Yield (12mg, 72%) as a white solid. Mp: 144.4 – 145.3 °C. Purity 95% (HPLC). ^{1}H NMR (400 MHz, DMSO-d_6) δ 10.71 (s, 1H), 9.94 (s, 1H), 9.76 (s, 1H), 8.81 (d, J = 11.0 Hz, 1H), 8.55 (d, J = 10.3 Hz, 1H), 8.32 (d, J = 7.6 Hz, 1H), 8.14 – 8.05 (m, 2H), 7.81 (s, 1H), 7.71 (t, J = 1.8 Hz, 1H), 7.63 (d, J = 2.0 Hz, 1H), 7.51 – 7.38 (m, 2H), 7.30 (d, J = 8.5, 1H), 4.53 – 4.40 (m, 1H), 4.02 (brs, 1H), 3.76 (m, 2H), 3.35 (d, J = 15.5 Hz, 1H), 3.14 – 2.99 (m, 4H), 2.19 (s, 3H), 1.98 (dd, J = 14.1, 4.1 Hz, 2H), 1.70 (q, J = 12.2, 10.7 Hz, 2H), 1.28 (s, 9H). ^{13}C NMR (101 MHz, DMSO) δ 171.7, 165.5, 163.0 (d, J = 2 Hz), 161.1, 159.5 (d, J = 211 Hz) 159.4, 152.6, 142.1 (d, J = 12 Hz), 140.7, 138.4, 135.2, 130.2 (d, J = 4 Hz), 118.7, 117.9, 117.3 (d, J = 15 Hz), 115.7, 114.5, 107.8, 106.0 (d, J = 27 Hz) , 61.1, 61.0, 55.6, 44.1, 42.1, 28.0, 24.1, 13.3. MS: calcd for $C_{31}H_{40}FN_8O_7S$ $[M+H]^+$, 687.3; found 687.6.



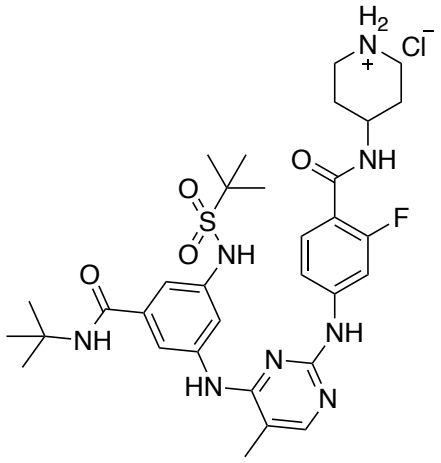
3.61

(3-((1,1-Dimethylethyl)sulfonamido)-5-((2-((3-fluoro-4-(piperidin-4-ylcarbamoyl)phenyl)amino)-5-methylpyrimidin-4-yl)amino)benzoyl)-*L*-glutamic acid (3.61). Compound **3.61** was prepared in the same manner as compound **3.20** from compound **3.39** using di-*tert*-butyl *L*-glutamate. Yield (7.6 mg, 89%) as a white solid; Mp: 189.2 – 189.9 °C. Purity 98% (HPLC).^{1}H NMR (400 MHz, Methanol-d_4) δ 7.93 (s, 2H), 7.74 (d, J = 15.0 Hz, 1H), 7.66 (s, 1H), 7.63 – 7.50 (m, 2H), 7.17 (d, J = 8.5 Hz, 1H), 4.45 (q, J = 4.5 Hz, 1H), 4.18 (s, 1H), 3.99 – 3.81 (m, 2H), 3.47 (d, J = 13.7 Hz, 2H), 3.14 (t, J = 11.7 Hz, 2H), 2.70 – 2.59 (m, 2H), 2.22 – 2.19 (m, 5H), 1.98 (d, J = 12.6 Hz, 2H), 1.39 (s, 9H). ^{13}C NMR (101 MHz, DMSO) δ 172.3, 171.3, 165.0, 163.2 (d, J = 2 Hz), 161.0, 158.4 (d, J = 202 Hz), 158.6, 155.8, 145.0 (d, J = 11 Hz), 140.4, 140.3, 135.8, 130.0 (d, J = 4 Hz), 116.6, 116.2, 114.6 (d, J = 13 Hz), 113.3, 113.2, 107.2, 104.2 (d, J = 28Hz), 60.9, 55.8, 44.4, 42.2, 32.1, 29.6, 28.7, 24.3, 13.6. MS: calcd for $C_{33}H_{42}FN_8O_8S$ $[M+H]^+$, 729.3; found 729.2.



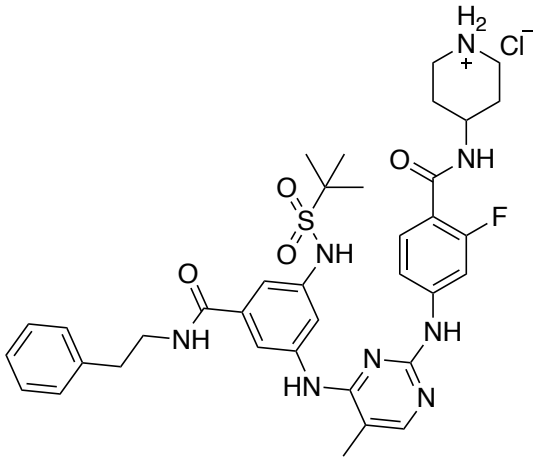
3.62

(3-((1,1-Dimethylethyl)sulfonamido)-5-((2-((3-fluoro-4-(piperidin-4-ylcarbamoyl)phenyl)amino)-5-methylpyrimidin-4-yl)amino)benzoyl)-*L*-glutamine (3.62). Compound **3.62** was prepared in the same manner as compound **3.20** from compound **3.39** using *tert*-butyl *L*-glutaminate. Yield (7.6 mg, 82%) as a white solid. Mp: 183.6. – 183.9 °C. Purity >99% (HPLC). ^{1}H NMR (400 MHz, Methanol-d_4) δ 7.74 (s, 1H), 7.67 (dt, J = 9.4, 1.7 Hz, 2H), 7.52 (t, J = 2.0 Hz, 1H), 7.45 (t, J = 8.4 Hz, 1H), 7.29 (dd, J = 13.3, 2.1 Hz, 1H), 7.10 (dd, J = 8.5, 2.1 Hz, 1H), 4.40 (dd, J = 8.8, 4.9 Hz, 1H), 4.13 – 4.01 (m, 1H), 3.46 – 3.32 (m, 2H), 3.08 (t, J = 13.0, 2H), 2.29 – 2.05 (m, 8H), 1.94 (dt, J = 14.3, 9.0, 1H), 1.89 – 1.77 (m, 2H), 1.26 (s, 9H). MS: calcd for $C_{33}H_{43}FN_8O_8S$ $[M+H]^+$, 728.3; found 728.5.



3.63

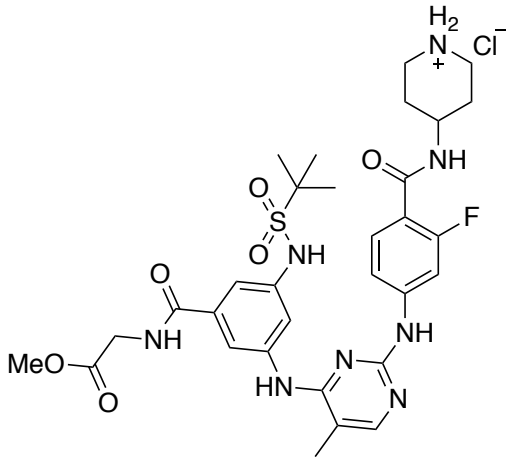
4-((4-((3-(*tert*-Butylcarbamoyl)-5-((1,1-dimethylethyl)sulfonamido)phenyl)amino)-5-methylpyrimidin-2-yl)amino)-2-fluoro-*N*-(piperidin-4-yl)benzamide (3.63). Compound **3.63** was prepared in the same manner as compound **3.20** from compound **3.39** using 2-methylpropan-2-amine hydrochloride. Yield (29 mg, 91%) as a grey solid. Mp: 186.7 – 187.5 °C. Purity 96%. ^{1}H NMR (400 MHz, DMSO-d_6) δ 10.72 (s, 1H), 9.88 (s, 1H), 9.73 (s, 1H), 8.77 (d, J = 11.0 Hz, 1H), 8.55 (t, J = 10.6 Hz, 1H), 8.18 – 8.00 (m, 2H), 7.76 (s, 1H), 7.66 – 7.49 (m, 3H), 7.49 – 7.38 (m, 2H), 7.33 (dd, J = 8.6, 1.9 Hz, 1H), 4.09 – 3.95 (m, 1H), 3.31 (d, J = 12.3 Hz, 2H), 3.03 (q, J = 11.3 Hz, 2H), 2.18 (s, 3H), 2.04 – 1.92 (m, 2H), 1.78 – 1.61 (m, 2H), 1.29 (s, 18H). ^{13}C NMR (101 MHz, DMSO) δ 165.3, 162.9 (d, J = 2 Hz), 162.0 (d, J = 204 Hz), 160.5, 158.1, 152.6, 142.2 (d, J = 12 Hz), 140.4, 138.1, 136.9, 130.3 (d, J = 4 Hz), 124.1, 118.7, 117.2 (d, J = 13 Hz), 115.8, 114.3, 107.8, 105.7 (d, J = 14 Hz), 61.0, 50.8, 44.1, 42.1, 28.4, 28.1, 24.2, 13.3. MS: calcd for $C_{32}H_{44}FN_8O_4S$ $[M+H]^+$, 655.3; found 655.3.



3.64

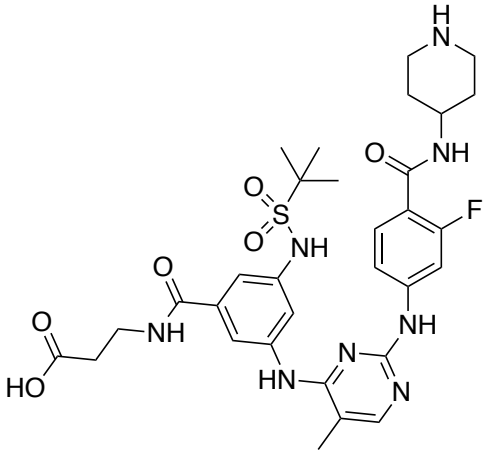
4-((4-((3-((1,1-Dimethylethyl)sulfonamido)-5-(phenethylcarbamoyl)phenyl)amino)-5-methylpyrimidin-2-yl)amino)-2-fluoro-*N*-(piperidin-4-yl)benzamide (3.64). Compound **3.64** was prepared in the same manner as compound **3.20** from compound **3.39** using 2-phenylethan-1-amine. Yield (19 mg, 67%) as a white solid. Mp: 124.2. – 124.4 °C. Purity 98%. ^{1}H NMR (400 MHz, DMSO-d_6) δ 10.86 (s, 1H), 9.94 (s, 1H), 9.87 (s, 1H), 8.75 (d, J = 11.2 Hz, 1H), 8.62 – 8.42 (m, 2H), 8.11(d, J = 4 Hz, 1H), 8.07 (s, 1H), 7.76 (s, 1H), 7.71 (d, J = 2.1 Hz, 1H), 7.50 (s, 1H), 7.45 – 7.34 (m, 2H), 7.32 – 7.22 (m, 3H), 7.20 – 7.14 (m, 3H), 4.04 – 3.95 (m, 1H), 3.44 – 3.36 (m, 2H), 3.29 (d, J = 12.6 Hz, 2H), 3.01

(d, J = 11.2 Hz, 2H), 2.72 (t, J = 7.6 Hz, 2H), 2.19 (s, 3H), 1.98 – 1.90 (m, 2H), 1.74 – 1.62 (m, 2H), 1.28 (s, 9H). ^{13}C NMR (101 MHz, DMSO) δ 165.3, 162.9 (d, J = 2 Hz), 161.2, 159.2 (d, J = 247 Hz), 153.8, 152.0, 141.8 (d, J = 12 Hz), 140.6, 139.4, 138.1, 135.8, 130.2 (d, J = 4 Hz), 128.5, 128.2, 126.0, 124.1, 119.0, 117.6 (d, J = 15 Hz), 116.1, 114.7, , 107.9, 106.3 (d, J = 28 Hz), 61.1, 44.1, 42.1, 40.9, 35.0, 28.0, 24.2, 13.3. MS: calcd for $C_{36}H_{44}FN_8O_4S$ $[M+H]^+$, 703.3; found 703.2.



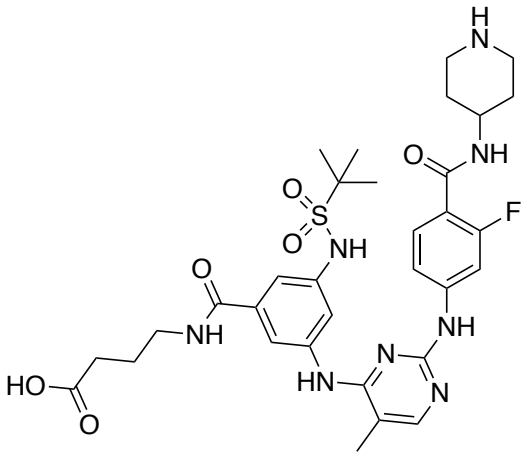
3.65

Methyl (3-((1,1-Dimethylethyl)sulfonamido)-5-((2-((3-fluoro-4-(piperidin-4-ylcarbamoyl)phenyl)amino)-5-methylpyrimidin-4-yl)amino)benzoyl)glycinate (3.65). Compound **3.65** was prepared in the same manner as compound **3.20** from compound **3.39** using methyl glycinate. Yield (37 mg, 84%) as a white solid; Mp: 152.1 – 152.7 °C. Purity 94% (HPLC).^{1}H NMR (400 MHz, DMSO-d_6) δ 10.09 (s, 1H), 9.89 (s, 1H), 9.31 (s, 1H), 8.86 (t, J = 5.8 Hz, 1H), 8.71 – 8.58 (m, 1H), 8.40 (d, J = 10.6 Hz, 1H), 8.04 (s, 2H), 7.81 (s, 1H), 7.62 (d, J = 12.4, 2H), 7.53 (d, J = 13.5 Hz, 1H), 7.45 – 7.30 (m, 2H), 4.06 – 3.99 (m, 1H), 3.94 (d, J = 8.0, 2H), 3.63 (s, 3H), 3.31 (d, J = 12.5 Hz, 2H), 3.03 (q, J = 11.4 Hz, 2H), 2.17 (s, 3H), 1.98 (dd, J = 13.8, 3.9 Hz, 2H), 1.74 – 1.65 (m, 2H), 1.29 (s, 9H). ^{13}C NMR (101 MHz, DMSO) δ 170.22, 166.07, 163.08 (d, J = 2 Hz), 161.47, 160.65, 159.26 (d, J = 215 Hz), 154.62, 143.90 (d, J = 13 Hz), 140.54, 139.19, 134.86, 130.18 (d, J = 4 Hz), 118.13, 117.81, 116.24 (d, J = 11 Hz), 114.96, 114.01, 107.57, 105.34 (d, J = 29 Hz), 61.03, 51.68, 44.04, 42.15, 41.26, 28.10, 24.20, 13.39. MS: calcd for $C_{31}H_{40}FN_8O_6S$ $[M+H]^+$, 671.3; found 671.2.



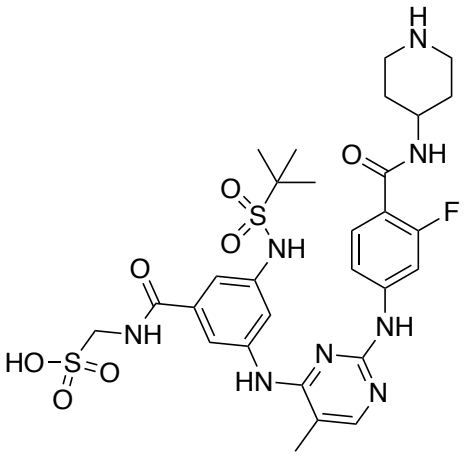
3.66

3-(3-((1,1-Dimethylethyl)sulfonamido)-5-((2-((3-fluoro-4-(piperidin-4-ylcarbamoyl)phenyl)amino)-5-methylpyrimidin-4-yl)amino)benzamido)propanoic acid (3.66). Compound **3.66** was prepared in the same manner as compound **3.20** from compound **3.39** using *tert*-butyl 3-aminopropanoate hydrochloride. Yield (32 mg, 90%) as a white solid; Mp: 195.1 – 195.8°C. Purity >99%. ^{1}H NMR (400 MHz, DMSO-d_6) δ 10.52 (s, 1H), 9.77 (s, 1H), 9.58 (s, 1H), 8.62 (d, J = 11.0 Hz, 1H), 8.47 – 8.27 (m, 2H), 8.04 – 7.89 (m, 2H), 7.64 (t, J = 1.6 Hz, 1H), 7.54 (t, J = 1.8 Hz, 1H), 7.39 (t, J = 1.9 Hz, 1H), 7.35 – 7.21 (m, 2H), 7.16 (dd, J = 8.6, 2.0 Hz, 1H), 3.95 – 3.81 (m, 1H), 3.26 (q, J = 7.0 Hz, 2H), 3.18 (d, J = 12.4 Hz, 2H), 2.90 (q, J = 11.3 Hz, 2H), 2.30 (t, J = 7.2 Hz, 2H), 2.04 (s, 3H), 1.90 – 1.80 (m, 2H), 1.65 –1.48 (m, 2H), 1.14 (s, 9H). ^{13}C NMR (101 MHz, DMSO) δ 172.77, 165.40, 162.97 (d, J = 2 Hz), 159.88 (d, J = 218 Hz), 158.46, 158.01, 153.82, 142.18 (d, J = 12 Hz) , 140.55, 138.34, 135.52, 130.13 (d, J = 4 Hz) 124.12, 118.70, 117.24 (d, J = 17 Hz), 115.76, 114.53, 107.76, 106.08 (d, J = 29 Hz), 61.02, 44.06, 42.09, 35.6, 33.6, 28.05, 24.17, 13.30. MS: calcd for $C_{31}H_{40}FN_8O_6S$ $[M+H]^+$, 671.3; found 671.4.



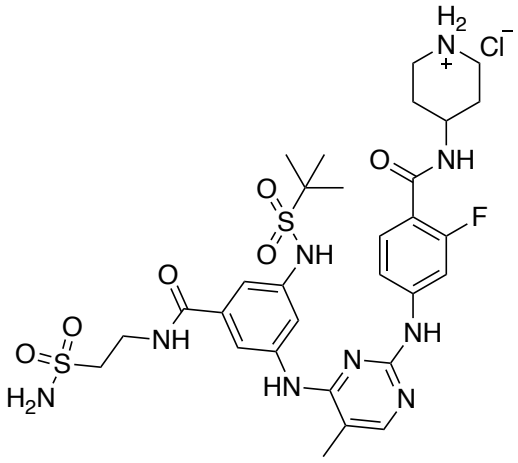
3.67

4-(3-((1,1-Dimethylethyl)sulfonamido)-5-((2-((3-fluoro-4-(piperidin-4-ylcarbamoyl)phenyl)amino)-5-methylpyrimidin-4-yl)amino)benzamido)butanoic acid hydrochloride (3.67). Compound **3.67** was prepared in the same manner as compound **3.20** from compound **3.39** using *tert*-butyl 4-aminobutanoate hydrochloride. Yield (17 mg, 71%) as a white solid; Mp: 179.4 – 180.1 °C. Purity 96%. ^{1}H NMR (400 MHz, DMSO-d_6) δ 10.51 (s, 1H), 9.88 (s, 1H), 9.61 (s, 1H), 8.71 (d, J = 11.0 Hz, 1H), 8.53 – 8.36 (m, 2H), 8.14 – 8.00 (m, 2H), 7.79 (s, 1H), 7.66 (s, 1H), 7.53 (s, 1H), 7.44 (d, J = 12.0 Hz, 1H), 7.38 (t, J = 8.3 Hz, 1H), 7.30 (dd, J = 8.6, 1.9 Hz, 1H), 4.06 – 3.98 (m, 1H), 3.32 (d, J = 12.6 Hz, 2H), 3.20 (q, J = 6.6 Hz, 2H), 3.03 (q, J = 11.3 Hz, 2H), 2.22 – 2.10 (m, 5H), 2.04 – 1.93 (m, 2H), 1.80 – 1.59 (m, 4H), 1.28 (s, 9H). ^{13}C NMR (101 MHz, DMSO) δ 174.2, 165.5, 163.0 (d, J = 2 Hz) 159.8 (d, J = 202 Hz), 158.8, 158.4, 158.0, 142.4 (d, J = 12 Hz), 140.5, 138.5, 135.7, 130.1 (d, J = 4 Hz), 124.1, 118.6, 117.0 (d, J = 14 Hz), 115.6, 114.4, 107.7, 105.9 (d, J = 27 Hz), 61.0, 44.1, 42.1, 38.7, 31.0, 28.1, 24.3, 24.2, 13.3. MS: calcd for $C_{32}H_{42}FN_8O_6S$ $[M+H]^+$, 685.3; found 685.3.



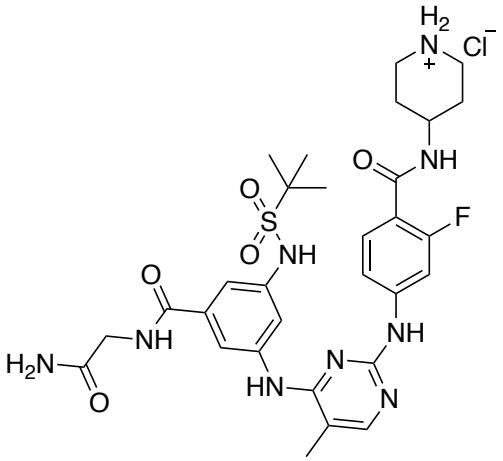
3.68

(3-((1,1-Dimethylethyl)sulfonamido)-5-((2-((3-fluoro-4-(piperidin-4-ylcarbamoyl)phenyl)amino)-5-methylpyrimidin-4-yl)amino)benzamido)methanesulfonic acid hydrochloride (3.68). Compound **3.68** was prepared in the same manner as compound **3.20** from compound **3.39** using aminomethanesulfonic acid. Yield (15 mg, 68%) as a white solid. Mp: 284.3 – 285.0 °C. Purity 97% (HPLC). ^{1}H NMR (400 MHz, DMSO-d_6) δ 10.41 (s, 1H), 9.98 (s, 1H), 9.50 (s, 1H), 8.81 (s, 1H), 8.57 (s, 1H), 8.31 – 8.01 (m, 2H), 7.92 (s, 1H), 7.78 (s, 1H), 7.68 (s, 1H), 7.58 (d, J = 13.3 Hz, 1H), 7.39 (t, J = 8.0 Hz, 1H), 7.24 (d, J = 9.1 Hz, 1H), 4.01 (s, 1H), 3.77 (s, 2H), 3.30 (d, J = 11.5 Hz, 2H), 3.01 (d, J = 11.8 Hz, 2H), 2.16 (s, 3H), 1.96 (d, J = 12.3 Hz, 2H), 1.68 (d, J = 11.6 Hz, 2H), 1.28 (s, 9H). ^{13}C NMR (101 MHz, DMSO) δ 165.0, 163.1 (d, J = 2 Hz), 160.7, 160.6, 159.4 (d, J = 251 Hz), 153.6, 142.6 (d, J = 10 Hz), 140.4, 138.7, 135.7, 130.2 (d, J = 4 Hz), 118.6, 117.7, 116.8 (d, J = 11 Hz), 115.6, 114.4, 107.7, 105.8 (d, J = 27 Hz), 61.0, 55.9, 43.9, 42.0, 27.9, 24.2, 13.4. MS: calcd for $C_{29}H_{36}FN_8O_7S_2$ $[M-H]^-$, 691.2; found 691.5.



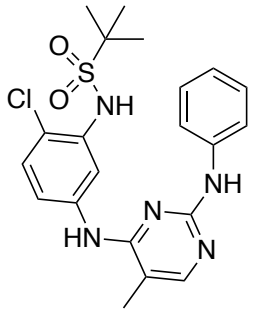
3.69

4-((4-((3-((1,1-Dimethylethyl)sulfonamido)-5-((2-sulfamoylethyl)carbamoyl)phenyl)amino)-5-methylpyrimidin-2-yl)amino)-2-fluoro-*N*-(piperidin-4-yl)benzamide hydrochloride (3.69). Compound **3.69** was prepared in the same manner as compound **3.20** from compound **3.39** using aminomethanesulfonamide. Yield (21 mg, 91%) as a white solid. Mp: 187.0 – 187.6 °C. Purity >99%. ^{1}H NMR (400 MHz, DMSO-d_6) δ 10.27 (s, 1H), 9.89 (s, 1H), 9.43 (s, 1H), 8.70 (d, J = 11.0 Hz, 1H), 8.55 (t, J = 5.5 Hz, 1H), 8.44 (d, J = 9.7 Hz, 1H), 8.15 – 8.01 (m, 2H), 7.80 (s, 1H), 7.64 (s, 1H), 7.60 – 7.49 (m, 2H), 7.44 – 7.28 (m, 2H), 6.92 (s, 2H), 4.10 – 3.96 (m, 1H), 3.66 – 3.51 (m, 2H), 3.31 (d, J = 12.6 Hz, 2H), 3.15 (t, J = 6.0 Hz, 2H), 3.03 (q, J = 11.3 Hz, 2H), 2.17 (s, 3H), 2.03 – 1.95 (m, 2H), 1.69 (q, J = 10.9 Hz, 2H), 1.29 (s, 9H). ^{13}C NMR (101 MHz, DMSO) δ 165.6, 163.1 (d, J = 3 Hz), 160.6, 160.6, 159.3 (d, J = 235 Hz), 154.1, 143.0 (d, J = 11 Hz), 140.5, 138.9, 135.1, 130.1 (d, J = 3 Hz), 118.2, 117.7, 116.5 (d, J = 12 Hz), 115.1, 114.1, 107.6, 105.6 (d, J = 27 Hz), 61.03, 53.4, 44.1, 42.1, 34.7, 28.1, 24.2, 13.4. MS: calcd for $C_{30}H_{41}FN_9O_6S_2$ $[M+H]^+$, 706.3; found 706.2.



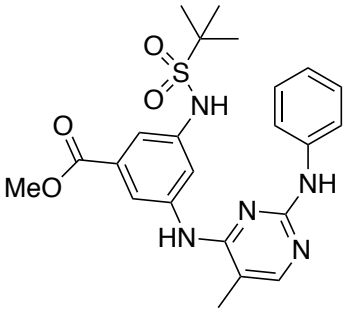
3.70

4-((4-((3-((2-Amino-2-oxoethyl)carbamoyl)-5-((1,1-dimethylethyl)sulfonamido)phenyl)amino)-5-methylpyrimidin-2-yl)amino)-2-fluoro-*N*-(piperidin-4-yl)benzamide hydrochloride (3.70). Compound **3.70** was prepared in the same manner as compound **3.20** from compound **3.39** using 2-aminoacetamide. Yield (12 mg, 73%) as a pale yellow solid. Mp: 286.6 – 287.6 °C. Purity >99%. ^{1}H NMR (400 MHz, DMSO-d_6) δ 10.66 (s, 1H), 9.93 (s, 1H), 9.76 (s, 1H), 8.74 (s, 1H), 8.59 – 8.40 (m, 2H), 8.16 – 8.04 (m, 2H), 7.80 (s, 1H), 7.71 (s, 1H), 7.56 (s, 1H), 7.52 – 7.34 (m, 3H), 7.27 (dd, J = 8.6, 1.9 Hz, 1H), 7.04 (s, 1H), 4.10 – 3.97 (m, 1H), 3.78 (d, J = 5.7 Hz, 2H), 3.31 (d, J = 12.3 Hz, 2H), 3.03 (q, J = 11.5 Hz, 2H), 2.18 (s, 3H), 2.08 – 1.94 (m, 2H), 1.81 – 1.57 (m, 2H), 1.28 (s, 9H). ^{13}C NMR (101 MHz, DMSO) δ 170.74, 165.52, 163.0 (d, J = 2 Hz), 161.10, 159.50 (d, J = 195 Hz, 2H), 158.88, 158.03, 142.1 (d, J = 11 Hz), 140.61, 138.37, 135.36, 130.2 (d, J = 4 Hz), 118.90, 118.23, 117.3 (d, J = 14 Hz), 115.82, 114.85, 107.82, 106.05 (d, J = 28 Hz), 61.04, 44.07, 42.36, 42.11, 28.05, 24.17, 13.30. MS: calcd for $C_{30}H_{39}FN_9O_5S$ $[M+H]^+$, 656.3; found 656.3.



3.71

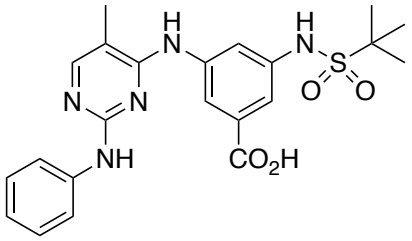
***N*-(2-Chloro-5-((5-methyl-2-(phenylamino)pyrimidin-4-yl)amino)phenyl)-2-methylpropane-2-sulfonamide (3.71).** Compound **3.71** was prepared in the same manner as compound **3.38** from compound **2.7** using aniline. Yield (32 mg, 70%) as a white solid; Mp: 154.1 – 155.0 °C. Purity >99%. ^{1}H NMR (400 MHz, DMSO-d_6) δ 9.35 (s, 1H), 8.91 (s, 1H), 8.51 (s, 1H), 7.96 – 7.87 (m, 2H), 7.76 (dd, J = 8.9, 2.5 Hz, 1H), 7.65 (d, J = 8.1 Hz, 2H), 7.38 (d, J = 8.7 Hz, 1H), 7.21 (t, J = 7.8 Hz, 2H), 6.86 (t, J = 7.3 Hz, 1H), 2.12 (s, 3H), 1.33 (s, 9H). ^{13}C NMR (101 MHz, DMSO) δ 158.92, 157.98, 155.98, 140.97, 139.23, 135.33, 128.83, 128.29, 120.78, 120.72, 120.47, 120.43, 118.34, 106.05, 60.54, 23.85, 13.50. MS: calcd for $C_{21}H_{23}ClN_5O_2S$ [M-H]$^-$, 444.1; found 444.0.



3.72

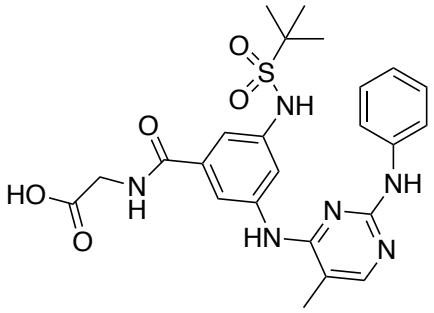
Methyl 3-((1,1-Dimethylethyl)sulfonamido)-5-((5-methyl-2-(phenylamino)pyrimidin-4-yl)amino)benzoate (3.72). Compound **3.72** was prepared in the same manner as compound **3.38** from compound **3.37** using aniline. Yield (17 mg, 76%) as a white solid; Mp: 124.2 – 124.6 °C. Purity >99%. ^{1}H NMR (400 MHz, DMSO-d_6) δ 8.83 (s, 1H), 8.64 (s, 1H), 7.95 (d, J = 2.8 Hz, 2H), 7.90 (t, J = 1.7 Hz, 1H), 7.65 (t, J = 1.8 Hz, 1H), 7.64 – 7.57 (m, 2H), 7.10 (t, J = 8.0 Hz, 2H), 6.82 (t, J = 7.2 Hz, 1H), 3.80 (s, 3H), 2.12 (s, 3H), 1.30 (s, 9H). ^{13}C NMR (101 MHz, DMSO) δ 165.95, 159.07, 157.90, 156.21, 140.86,

140.81, 140.51, 130.16, 128.15, 120.33, 118.47, 118.16, 117.75, 114.05, 106.06, 61.08, 52.17, 24.24, 13.43. MS: calcd for $C_{23}H_{26}N_5O_4S$ $[M-H]^-$, 468.2; found 468.1.



3.73

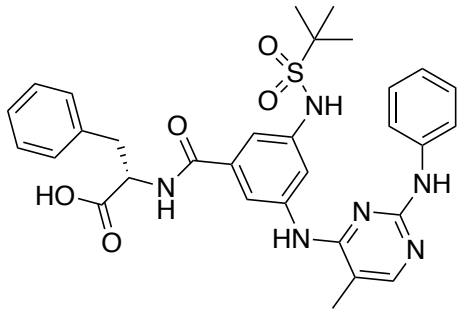
3-((1,1-Dimethylethyl)sulfonamido)-5-((5-methyl-2-(phenylamino)pyrimidin-4-yl)amino)benzoic acid (3.73). Compound **3.73** was prepared in the same manner as compound **3.39** from compound **3.72**. Mp: 259.7 – 260.1 °C. The product was used directly for the next step.



3.76

(3-((1,1-Dimethylethyl)sulfonamido)-5-((5-methyl-2-(phenylamino)pyrimidin-4-yl)amino)benzoyl)glycine (3.76). Compound **3.76** was prepared in the same manner as compound **3.20** from compound **3.73** using *tert*-butyl glycinate. Yield (21 mg, 82%) as a white solid. Mp: 199.5 – 200.2 °C. Purity >99%. ^{1}H NMR (400 MHz, DMSO-d_6) δ 12.35 (s, 1H), 9.78 (s, 1H), 8.86 (s, 1H), 8.70 (t, J = 5.9 Hz, 1H), 8.62 (s, 1H), 7.93 (s, 1H), 7.84 (s, 1H), 7.74 (s, 1H), 7.60 (d, J = 8.0 Hz, 2H), 7.49 (s, 1H), 7.12 (t, J = 7.7 Hz, 2H), 6.81 (t, J = 7.3 Hz, 1H), 3.88 (d, J = 5.7 Hz, 2H), 2.12 (s, 3H), 1.30 (s, 9H). ^{13}C NMR (101 MHz, DMSO) δ 172.0, 171.2, 166.4, 159.4, 157.8, 140.8, 140.3, 140.1, 135.0, 128.2, 120.3, 118.2,

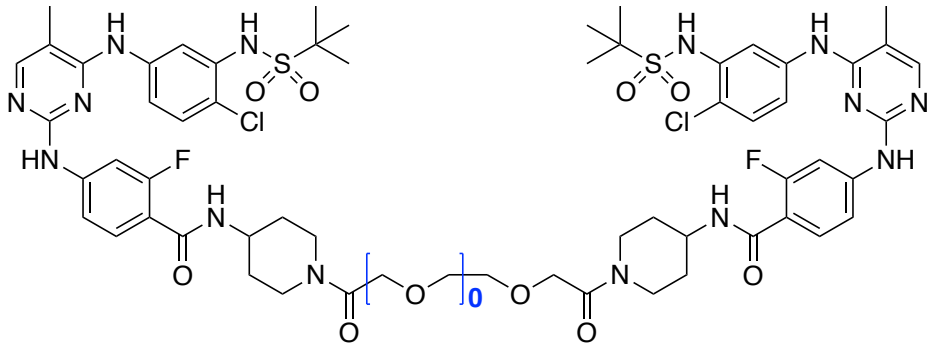
117.2, 117.0, 113.7, 105.9, 61.0, 45.6, 24.3, 13.5. MS: calcd for $C_{24}H_{27}N_6O_5S$ $[M-H]^-$, 511.2; found 511.3.



3.77

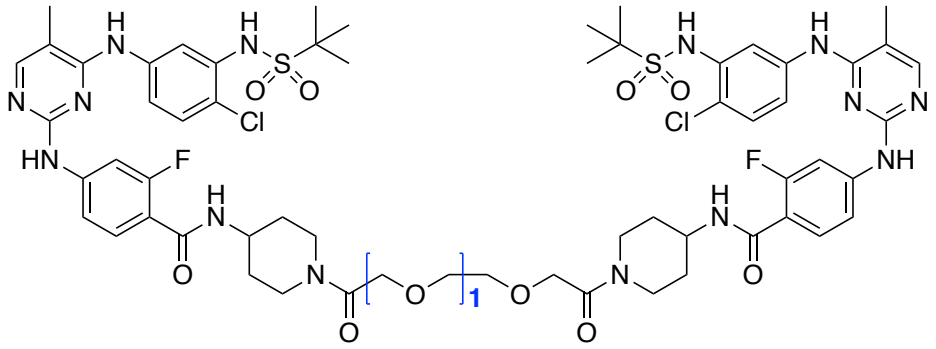
(3-((1,1-Dimethylethyl)sulfonamido)-5-((5-methyl-2-(phenylamino)pyrimidin-4-yl)amino)benzoyl)-*L*-phenylalanine (3.77). Compound **3.77** was prepared in the same manner as compound **3.20** from compound **3.73** using *tert*-butyl glycinate. Yield (24 mg, 83%) as a white solid. Mp: 165.2 – 165.7 °C. Purity >99%. ^{1}H NMR (400 MHz, Methanol-d_4) δ 7.58 (s, 1H), 7.53 (s, 1H), 7.50 (s, 1H), 7.46 (s, 1H), 7.20 (d, J = 7.9 Hz, 2H), 7.15 – 7.02 (m, 7H), 6.95 (t, J = 7.4 Hz, 1H), 4.75 – 4.65 (m, 1H), 3.21 (dd, J = 15.6, 7.8 Hz, 1H), 2.98 (dd, J = 13.8, 8.8 Hz, 1H), 2.09 (s, 3H), 1.22 (s, 9H). ^{13}C NMR (101 MHz, MeOD) δ175.3, 168.8, 163.7, 153.0, 142.2, 142.1, 139.6, 138.7, 138.0, 137.1, 130.3, 130.2, 129.5, 127.8, 126.1, 122.8, 121.1, 120.8, 117.6, 109.1, 62.9, 56.0, 38.3, 25.0, 13.5. MS: calcd for $C_{31}H_{33}N_6O_5S$ $[M-H]^-$, 601.2; found 601.1.

5.4 Chapter 4 synthesis of bivalent inhibitors for BRDT



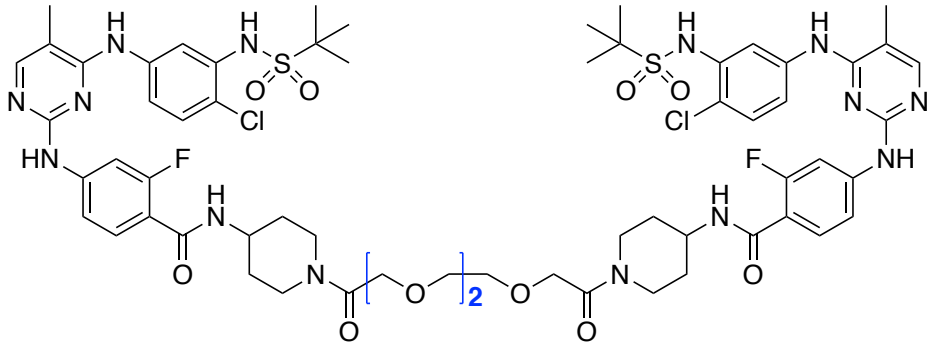
4.1

***N*,*N*'-((2,2'-Oxybis(acetyl))bis(piperidine-1,4-diyl))bis(4-((4-((4-chloro-3-((1,1-dimethylethyl)sulfonamido)phenyl)amino)-5-methylpyrimidin-2-yl)amino)-2-fluorobenzamide) (4.1).** To a mixture of 2,2'-oxydiacetic acid (1.1 mg, 8.2 µmol) and HATU (25 mg, 67 µmol) in anhydrous DMF (1 mL), DIPEA (21 µL, 121 µmol) was added. The solution was stirred at room temperature for 30 min followed by the addition of compound **2.11** (9.7 mg, 16 µmol) were added. The reaction solution was stirred at room temperature for 15 h. The mixture was diluted with EtOAc, and the organic layer was washed with brine (3 × 20 mL) and dried over Na_2SO_4. The solvents were removed under reduced pressure. The residue was portioned between ethyl acetate and 1M sodium bicarbonate solution. The organic phase was washed with 1M sodium bicarbonate solution and brine, dried over magnesium sulfate, filtered and concentrated. The residues were purified by silica gel column chromatography (MeOH/DCM) to give the title compound as a white solid (5.7 mg, 56%). Mp: 222.1 – 222.6 °C. Purity: >99% (HPLC). ^{1}H NMR (400 MHz, DMSO-d_6) δ 10.29 (s, 2H), 9.60 – 9.37 (m, 4H), 8.08 – 7.94 (m, 4H), 7.72 (d, J = 2.4 Hz, 2H), 7.66 – 7.54 (m, 4H), 7.53 – 7.40 (m, 4H), 7.27 (d, J = 8.5 Hz, 2H), 4.36 – 4.13 (m, 6H), 3.99 (d, J = 10.4 Hz, 2H), 3.84 (d, J = 13.1 Hz, 2H), 3.12 (t, J = 12.0 Hz, 2H), 2.82 (t, J = 12.0 Hz, 2H), 2.17 (s, 6H), 1.84 (s, 4H), 1.55 – 1.36 (m, 4H), 1.31 (s, 18H). ^{13}C NMR (101 MHz, DMSO) δ 166.7, 162.8 (d, J = 2 Hz), 160.6, 159.4 (d, J = 244 Hz), 153.4, 153.2, 142.4 (d, J = 12 Hz) , 137.5, 135.8, 130.2 (d, J = 4 Hz), 129.4, 123.2, 122.6, 122.0, 117.3 (d, J = 15 Hz), 114.6, 108.0, 106.0 (d, J = 30 Hz), 69.1, 60.7, 46.3, 42.9, 31.7, 23.8, 13.4. MS: calcd for $C_{58}H_{67}Cl_2F_2N_{14}O_9S_2$ $[M-H]^-$, 1275.4; found 1275.6.



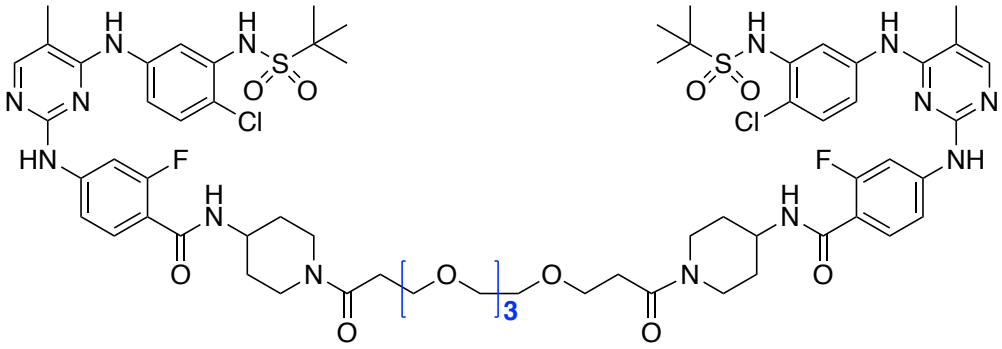
4.2

***N*,*N*'-((2,2'-(Ethane-1,2-diylbis(oxy))bis(acetyl))bis(piperidine-1,4-diyl))bis(4-((4-((4-chloro-3-((1,1-dimethylethyl)sulfonamido)phenyl)amino)-5-methylpyrimidin-2-yl)amino)-2-fluorobenzamide) (4.2).** Compound **4.2** was prepared in the same manner as compound **4.1** from compound **2.11** and 2,2'-(ethane-1,2-diylbis(oxy))diacetic acid**.** Yield (19 mg, 89%) as a white solid. Mp: 176.4 – 177.0 °C. Purity: 98% (HPLC). ^{1}H NMR (400 MHz, DMSO-d_6) δ 9.48 (s, 2H), 8.68 (s, 2H), 8.04 (s, 2H), 7.91 (dd, J = 7.9, 3.0 Hz, 2H), 7.82 – 7.62 (m, 6H),), 7.51 (t, J = 8.5 Hz, 2H), 7.48 – 7.39 (m, 4H), 4.37 – 4.14 (m, 6H), 4.11 – 3.98 (m, 2H), 3.84 (d, J = 13.3 Hz, 2H), 3.63 (s, 4H) 3.16 (t, J = 12.4 Hz, 2H), 2.83 (t, J = 12.1 Hz, 2H), 2.18 (s, 6H), 1.94 – 1.79 (m, 4H), 1.65 – 1.41 (m, 4H), 1.38 (s, 18H). ^{13}C NMR (101 MHz, DMSO) δ 167.0, 162.9 (d, J = 2Hz), 159.8 (d, J = 2Hz), 159.1, 157.3, 155.7, 144.8 (d, J = 12Hz), 138.9, 136.0, 130.2 (d, J = 2Hz), 129.0, 121.1, 120.5, 120.4, 114.8 (d, J = 14Hz), 113.2, 107.3, 104.4 (d, J = 28Hz), 69.5, 69.3, 60.4, 46.2, 43.1, 29.6, 23.9, 13.5. MS: calcd for $C_{60}H_{71}Cl_2F_2N_{14}O_{10}S_2$ [M-H]$^-$, 1319.4; found 1319.5.



4.3

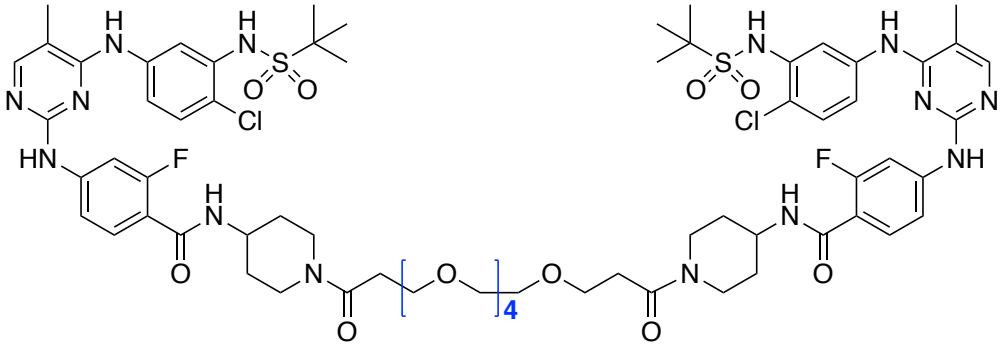
***N*,*N*'-((2,2'-((Oxybis(ethane-2,1-diyl))bis(oxy))bis(acetyl))bis(piperidine-1,4-diyl))bis(4-((4-((4-chloro-3-((1,1-dimethylethyl)sulfonamido)phenyl)amino)-5-methylpyrimidin-2-yl)amino)-2-fluorobenzamide) (4.3).** Compound **4.3** was prepared in the same manner as compound **4.1** from compound **2.11** and 2,2'-((oxybis(ethane-2,1-diyl))bis(oxy))diacetic acid**.** Yield (11 mg, 91%) as a transparent gel. Purity: >99% (HPLC). ^{1}H NMR (400 MHz, DMSO-d_6) δ 9.40 (s, 2H), 8.56 (s, 2H), 7.96 (s, 2H), 7.86 (dd, J = 8.0, 2.9 Hz, 2H), 7.77 (dd, J = 14.3, 1.8 Hz, 2H), 7.73 (d, J = 2.4 Hz, 2H), 7.58 (s, 2H), 7.49 – 7.31 (m, 6H), 4.25 – 4.10 (m, 6H), 3.99 (d, J = 9.1 Hz, 2H), 3.78 (d, J = 13.6 Hz, 2H), 3.57 (s, 8H), 3.10 (t, J = 12.4 Hz, 2H), 2.78 (t, J = 12.0 Hz, 2H), 2.12 (s, 6H), 1.89 -1.75 (m, 4H), 1.56 – 1.37 (m, 4H), 1.31 (s, 18H). ^{13}C NMR (101 MHz, DMSO) δ 166.99, 162.73 (d, J = 2 Hz), 159.50 (d, J = 211 Hz), 158.79, 158.09, 152.31, 141.80 (d, J = 11Hz), 137.06, 135.89, 130.25 (d, J = 5 Hz), 129.53, 123.66, 123.07, 122.35, 117.92 (d, J = 14 Hz), 114.88, 108.09, 106.45 (d, J = 28 Hz), 69.72, 69.50, 69.40, 60.68, 46.29, 43.02, 31.67, 23.76, 13.31. MS: calcd for $C_{62}H_{75}Cl_2F_2N_{14}O_{11}S_2$ [M-H]$^-$, 1363.5; found 1363.4.



4.4

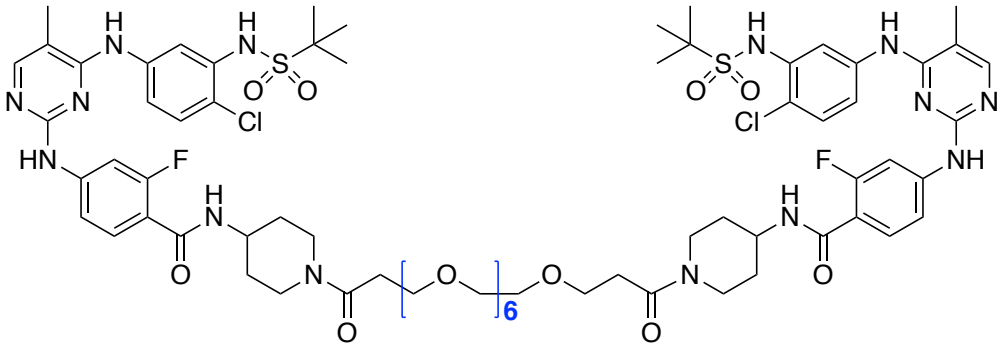
***N*,*N*'-((4,7,10,13-Tetraoxahexadecanedioyl)bis(piperidine-1,4-diyl))bis(4-((4-((4-chloro-3-((1,1-dimethylethyl)sulfonamido)phenyl)amino)-5-methylpyrimidin-2-yl)amino)-2-fluorobenzamide) (4.4).** Compound **4.4** was prepared in the same manner as compound **4.1** from compound **2.11** and 4,7,10,13-tetraoxahexadecanedioic acid**.** Yield (22 mg, 90%) as a transparent gel. Purity: >99% (HPLC). ^{1}H NMR (400 MHz, DMSO-d_6) δ 9.47 (s, 2H), 9.40 (brs, 2H), 8.68 (s, 2H), 8.00 (s, 2H), 7.92 – 7.71 (m, 8H), 7.52 – 7.45 (m, 2H), 7.45 – 7.37 (m, 4H), 4.28 (d, J = 12.6 Hz, 2H), 4.06 – 3.94 (m, 2H), 3.87 (d, J = 13.2 Hz, 2H), 3.63 (t, J = 6.7 Hz, 4H), 3.51(s, 12H), 3.12 (t, J = 12.2 Hz, 2H), 2.76 (t, J = 11.9

Hz, 2H), 2.58 (t, J = 6.8 Hz, 4H), 2.15 (s, 6H), 1.95 – 1.72 (m, 4H), 1.56 – 1.36 (m, 4H), 1.34 (s, 18H). ^{13}C NMR (DMSO, 101 MHz): δ 168.5, 163.0 (d, J = 2 Hz), 159.8 (d, J = 244 Hz), 159.0, 157.3, 155.8, 144.9 (d, J = 12 Hz), 139.0, 135.4, 130.2 (d, J = 5 Hz), 129.04, 121.2, 121.0, 120.7, 114.8 (d, J = 15 Hz), 113.2, 107.4, 104.2 (d, J = 28 Hz), 69.7 (PEG C start to overlap), 69.7, 69.6, 66.8, 60.5, 46.4, 43.8, 32.8, 23.8, 13.6. MS: calcd for $C_{66}H_{83}Cl_2F_2N_{14}O_{12}S_2$ [M-H]$^-$, 1435.5; found 1435.9.



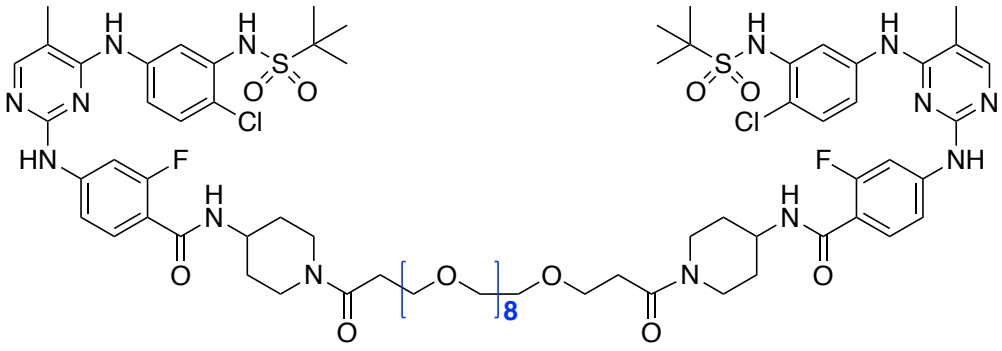
4.5

***N*,*N*'-((4,7,10,13,16-Pentaoxanonadecanedioyl)bis(piperidine-1,4-diyl))bis(4-((4-((4-chloro-3-((1,1-dimethylethyl)sulfonamido)phenyl)amino)-5-methylpyrimidin-2-yl)amino)-2-fluorobenzamide) (4.5).** Compound **4.5** was prepared in the same manner as compound **4.1** from compound **2.11** and 4,7,10,13,16-pentaoxanonadecanedioic acid**.** Yield (24 mg, 92%) as a transparent gel. Purity: 98% (HPLC). ^{1}H NMR (400 MHz, Methanol-d_4) δ 8.09 (d, J = 2.3 Hz, 2H), 7.79 (s, 2H), 7.64 (dd, J = 14.8, 1.9 Hz, 2H), 7.48 (t, J = 8.6 Hz, 2H), 7.37 (dd, J = 8.7, 2.4 Hz, 2H), 7.27 (d, J = 8.7 Hz, 2H), 7.15 (dd, J = 8.6, 1.9 Hz, 2H), 4.36 (d, J = 13.5 Hz, 2H), 4.07 – 3.98 (m, 2H), 3.92 (d, J = 13.9 Hz, 2H), 3.69 – 3.60 (m, 4H), 3.49 (s, 16H), 3.14 (t, J = 12.3 Hz, 2H), 2.76 (t, J = 12.0 Hz, 2H), 2.70 – 2.58 (m, 2H), 2.56 – 2.46 (m, 2H), 2.04 (s, 6H), 1.89 (dd, J = 22.9, 12.9 Hz, 4H), 1.53 – 1.35 (m, 4H), 1.28 (s, 18H). ^{13}C NMR (101 MHz, DMSO) δ 168.5, 163.0 (d, J = 3 Hz), 159.8 (d, J = 244 Hz), 159.1, 157.3, 155.7, 144.9 (d, J = 12 Hz), 138.9, 138.8, 130.2 (d, J = 4 Hz), 128.9, 121.1, 120.3, 120.2, 114.8 (d, J = 12 Hz), 113.2, 107.3, 104.2 (d, J = 29 Hz), 69.7(2 peaks, C from PEG linker overlap together), 69.6, 66.8, 60.1, 46.4, 43.8, 32.8, 24.0, 13.5. MS: calcd for $C_{68}H_{87}Cl_2F_2N_{14}O_{13}S_2$ [M-H]$^-$, 1479.5; found 1479.6.



4.6

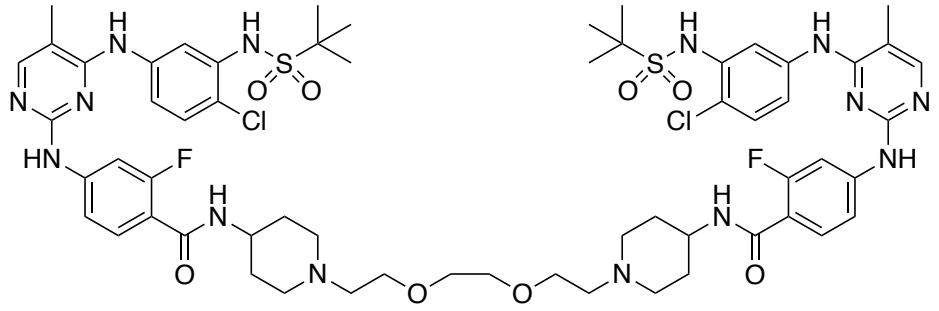
***N*,*N*'-((4,7,10,13,16,19,22-Heptaoxapentacosanedioyl)bis(piperidine-1,4-diyl))bis(4-((4-((4-chloro-3-((1,1-dimethylethyl)sulfonamido)phenyl)amino)-5-methylpyrimidin-2-yl)amino)-2-fluorobenzamide) (4.6).** Compound **4.6** was prepared in the same manner as compound **4.1** from compound **2.11** and 4,7,10,13,16,19,22-heptaoxapentacosanedioic acid**.** Yield (17 mg, 63%) as a transparent gel. Purity: >99% (HPLC). ^{1}H NMR (400 MHz, Chloroform-*d*) δ 8.58 (d, *J* = 2.5 Hz, 2H), 7.95 – 7.80 (m, 6H), 7.76 (dd, *J* = 2.0, 15.5 Hz, 2H), 7.25 (d, *J* = 8.7 Hz, 2H), 7.16 – 7.04 (m, 4H), 6.80 – 6.61 (m, 2H), 6.61 – 6.49 (m, 4H), 4.44 (d, *J* = 13.5 Hz, 2H), 4.14 (dt, *J* = 5.7, 12.4 Hz, 2H), 3.81 (d, *J* = 13.8 Hz, 2H), 3.71 (td, *J* = 2.6, 6.8 Hz, 4H), 3.68 – 3.45 (m, 28H), 3.12 (ddd, *J* = 2.8, 11.5, 14.1 Hz, 2H), 2.85 – 2.69 (m, 2H), 2.66 – 2.48 (m, 6H), 2.05 – 1.93 (m, 4H), 1.45 (dt, *J* = 5.7, 8.1 Hz, 4H), 1.36 (s, 18H). MS: calcd for $C_{72}H_{95}Cl_2F_2N_{14}O_{15}S_2$ $[M-H]^-$, 1567.6; found 1567.6.



4.7

***N*,*N*'-((4,7,10,13,16,19,22,25,28-Nonaoxahentriacontanedioyl)bis(piperidine-1,4-diyl))bis(4-((4-((4-chloro-3-((1,1-dimethylethyl)sulfonamido)phenyl)amino)-5-**

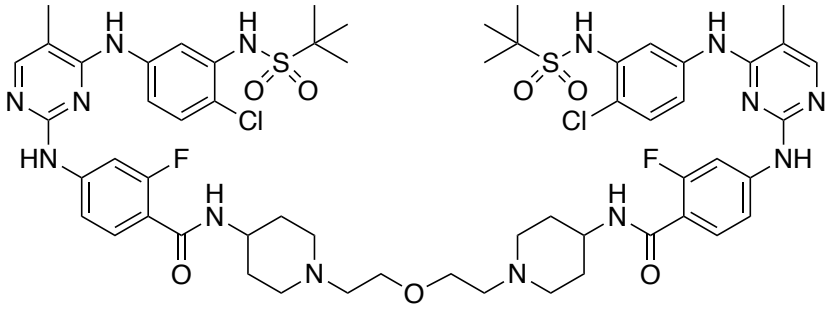
methylpyrimidin-2-yl)amino)-2-fluorobenzamide)(4.7). Compound **4.7** was prepared in the same manner as compound **4.1** from compound **2.11** and 4,7,10,13,16,19,22,25,28-nonaoxahentriacontanedioic acid**.** Yield (22 mg, 77%) as a white solid. Mp: 80.1 – 80.4°C. Purity: 98% (HPLC). ^{1}H NMR (400 MHz, DMSO-d_6) δ 10.30 (s, 2H), 9.45 (s, 4H), 8.02 (s, 2H), 7.96 (dd, J = 7.6, 2.4 Hz, 2H), 7.72 (d, J = 2.4 Hz, 2H), 7.67 – 7.55 (m, 4H), 7.54 – 7.42 (m, 4H), 7.27 (dd, J = 8.4, 2.0 Hz, 2H), 4.26 (d, J = 12.8 Hz, 2H), 4.08 – 3.92 (m, 2H), 3.87 (d, J = 13.3 Hz, 2H), 3.63 (t, J = 6.6 Hz, 4H), 3.50 (s, 32H), 3.14 (t, J = 13.1 Hz, 2H), 2.77 (t, J = 11.8 Hz, 2H), 2.58 (t, J = 6.7 Hz, 4H), 2.17 (s, 6H), 1.87 – 1.77 (m, 4H), 1.50 – 1.34 (m, 4H), 1.31 (s, 18H). ^{13}C NMR (101 MHz, DMSO) δ 168.5, 162.8 (d, J = 3 Hz), 160.7, 159.4 (d, J = 233 Hz), 153.8, 142.5 (d, J = 13 Hz), 137.5, 135.8, 130.2 (d, J = 4 Hz), 129.4, 124.14, 123.1, 122.6, 122.0, 117.2 (d, J = 14 Hz), 114.5, 107.9, 106.0 (d, J = 34 Hz) , 69.7 (C from PEG linker overlap together), 69.6, 66.8, 60.7, 46.4, 43.8, 32.8, 23.8, 13.4. MS: calcd for $C_{76}H_{103}Cl_2F_2N_{14}O_{17}S_2$ [M-H]$^-$, 1655.6; found 1655.9



4.8

***N*,*N*'-(((Ethane-1,2-diylbis(oxy))bis(ethane-2,1-diyl))bis(piperidine-1,4-diyl))bis(4-((4-((4-chloro-3-((1,1-dimethylethyl)sulfonamido)phenyl)amino)-5-methylpyrimidin-2-yl)amino)-2-fluorobenzamide) (4.8).** Compound **2.11** (10 mg, 17μmol), 1,2-bis(2-bromoethoxy)ethane (2.0 mg, 8.6 μmol), KI (2.9 mg, 17 μmol) and DIPEA (6.4 μL, 35 μmol) were added in N,N-dimethylformamide (0.5 mL). The reaction was stirred at room temperature for 12 h. DCM (20 mL) was added and the organic layer was washed with brine (3 × 10 mL) and dried over Na_2SO_4. The solvent was removed under reduced pressure and the residues was purified by silica gel column chromatography (DCM/MeOH) to give the title compound as a white solid (4.5 mg, 42%). Mp: 165.2 – 165.8 °C. Purity: 95% (HPLC). ^{1}H NMR (400 MHz, Methanol-d_4) δ 8.09 (s, 2H), 7.74 (s, 2H), 7.56 (dd, J = 14.8,

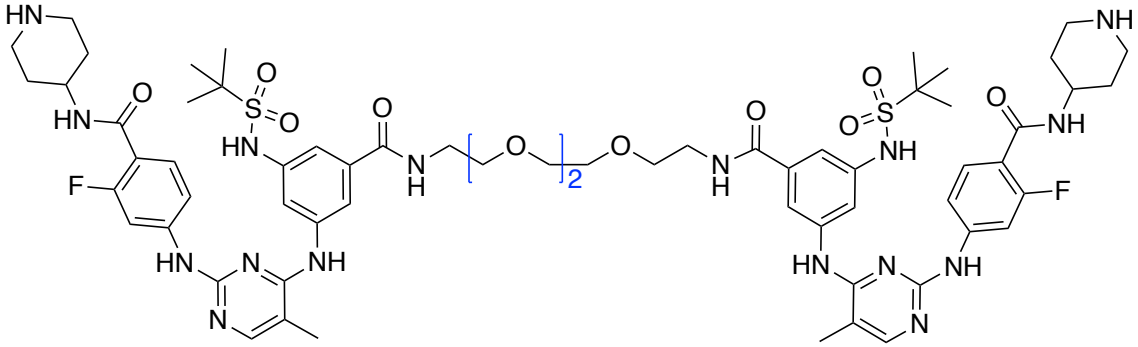
1.8 Hz, 2H), 7.42 (t, *J* = 8.7 Hz, 2H), 7.35 (dd, *J* = 8.7, 2.5 Hz, 2H), 7.23 (d, *J* = 8.7 Hz, 2H), 7.09 (dd, *J* = 8.6, 1.9 Hz, 2H), 3.99 – 3.91 (m, 2H), 3.69 (t, *J* = 5.0 Hz, 4H), 3.59 (s, 4H), 3.31 (d, *J* = 12.5 Hz, 4H), 3.00 (t, *J* = 4.9 Hz, 4H), 2.79 (t, *J* = 11.8 Hz, 4H), 2.08 - 2.05 (m, *J* = 6.1 Hz, 4H), 2.02 (s, 6H), 1.80 (q, *J* = 11.6 Hz, 4H), 1.28 (s, 18H). MS: calcd for $C_{60}H_{77}Cl_2F_2N_{14}O_8S_2$ $[M+H]^-$, 1293.5; found 1293.5



4.10

***N*,*N*'-((Oxybis(ethane-2,1-diyl))bis(piperidine-1,4-diyl))bis(4-((4-((4-chloro-3-((1,1-dimethylethyl)sulfonamido)phenyl)amino)-5-methylpyrimidin-2-yl)amino)-2-fluorobenzamide) (4.10).** 2,5-Dihydrofuran (40 mg, 0.57 mmol) was dissolved in DCM (4 mL) in a 10 mL round bottom flask and cooled to -78 °C. Ozone was bubbled through the solution until a faint blue color persisted (~20 min). Ozone was continued to be bubbled through the solution for an additional 5 min. Nitrogen was bubbled through the mixture to purge excess ozone until the blue color faded. Triphenylphosphine (299 mg, 1.1 mmol) was then added. The flask was transferred into a freezer (-20 °C) and let sit for 1 h.[128] The solution of 2,2'-oxydiacetaldehyde was used without further purification. 2,2'-Oxydiacetaldehyde solution (0.12 mL, 17 μmol) and AcOH (2.19 μL, 51 μmol) was added to compound **2.11** (20 mg, 34 μmol) in 1 mL of 1,2-dichloroethane. The mixture was stirred at ambient temperature for 1 h. Sodium triacetoxyborohydride (12 mg, 54 μmol) and $MgSO_4$ (17 mg, 136 μmol) were then added. The resulting mixture was stirred overnight. The solvents were removed under reduced pressure. The residue was portioned between ethyl acetate and 1M sodium bicarbonate solution. The organic phase was washed with 1M sodium bicarbonate solution and brine, dried over magnesium sulfate, filtered and concentrated. The residues were purified by silica gel column chromatography

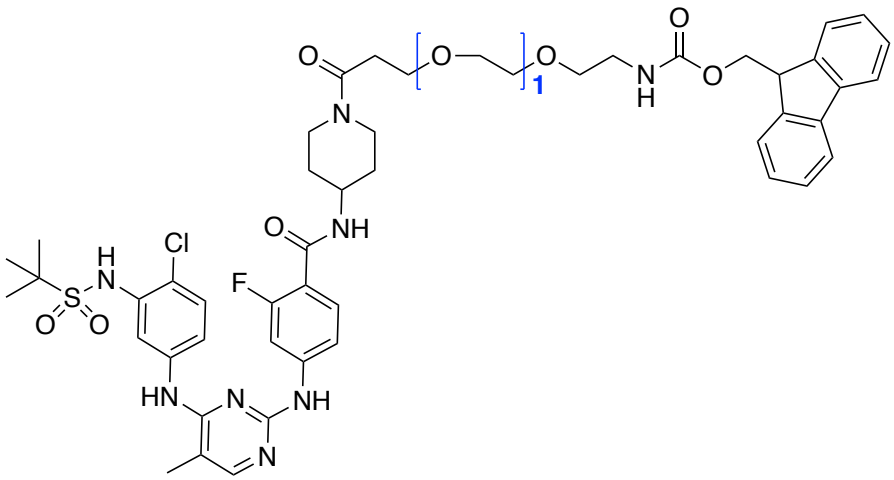
(MeOH/DCM/TEA) to give the title compound as a yellow solid (8.1 mg, 38%). Mp: 238.7 – 239.5 °C. Purity: >99% (HPLC). ^{1}H NMR (400 MHz, DMSO-d_6) δ 9.43 (s, 4H), 8.64 (s, 2H), 7.99 (s, 2H), 7.86 (d, J = 7.3 Hz, 2H), 7.77 (td, J = 7.1, 6.4, 2.1 Hz, 6H), 7.51 – 7.34 (m, 6H), 3.81 (s, 2H), 3.57 (s, 4H), 3.03 (d, J = 10.4 Hz, 4H), 2.72 (s, 4H), 2.30 (s, 4H), 2.13 (s, 6H), 1.88 (d, J = 28.1 Hz, 4H), 1.64 (d, J = 12.0 Hz, 4H), 1.33 (s, 18H). MS: calcd for $C_{58}H_{73}Cl_2F_2N_{14}O_7S_2$ $[M+H]^-$, 1249.5; found 1249.4



4.11

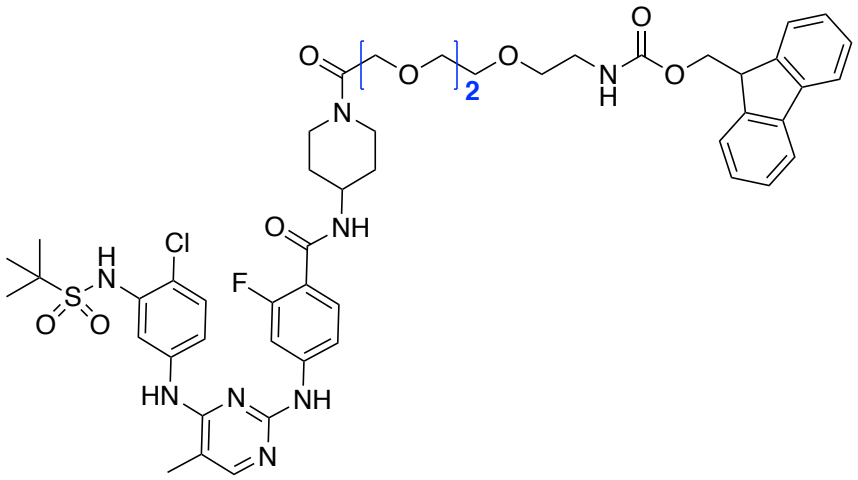
4,4'-(((((5,8,11-Trioxa-2,14-diazapentadecanedioyl)bis(5-((1,1-dimethylethyl)sulfonamido)-3,1-phenylene))bis(azanediyl))bis(5-methylpyrimidine-4,2-diyl))bis(azanediyl))bis(2-fluoro-*N*-(piperidin-4-yl)benzamide) (4.11). To a mixture of compound **3.39** (25 mg, 36 µmol), HATU (15 mg, 40 µmol) in anhydrous DMF (1 mL), DIPEA (19 µL, 109 µmol) was added. The solution was stirred at room temperature for 30 min followed by the addition of amine (3.5 mg, 18 µmol). The reaction solution was stirred at room temperature for 6 h. The mixture was diluted with EtOAc, and the organic layer was washed with brine (3 × 20 mL) and dried over Na_2SO_4. The solvent was removed under reduced pressure. The residues were added to a mixture of DCM (0.8 mL) and TFA (0.2 mL) and stirred at room temperature for 2 h. Solvent was removed in vacuo and the residues was purified by preparative HPLC to give the title compound as a white solid (13 mg, 45%). transparent gel. Purity: 95% (HPLC). ^{1}H NMR (400 MHz, Methanol-d_4) δ 7.86 (s, 1H), 7.83 (s, 1H), 7.79 (t, J = 1.8 Hz, 2H), 7.71 (dt, J = 8.8, 1.7 Hz, 2H), 7.67 – 7.52 (m, 4H), 7.40 (t, J = 13.0 Hz, 2H), 7.29 – 2.18 (m, 2H), 4.28 – 4.10 (m, 2H), 3.62 – 3.57 (m, 8H), 3.54 – 3.48 (m, 12H), 3.20 (t, J = 12.8, 4H), 2.33 – 2.15 (m, J = 11.7 Hz, 10H), 2.19

– 1.85 (m, 4H), 1.38 (s, 9H), 1.37 (s, 9H). MS: calcd for $C_{64}H_{85}F_2N_{16}O_{11}S_2$ $[M+H]^+$, 1355.6; found 1355.8



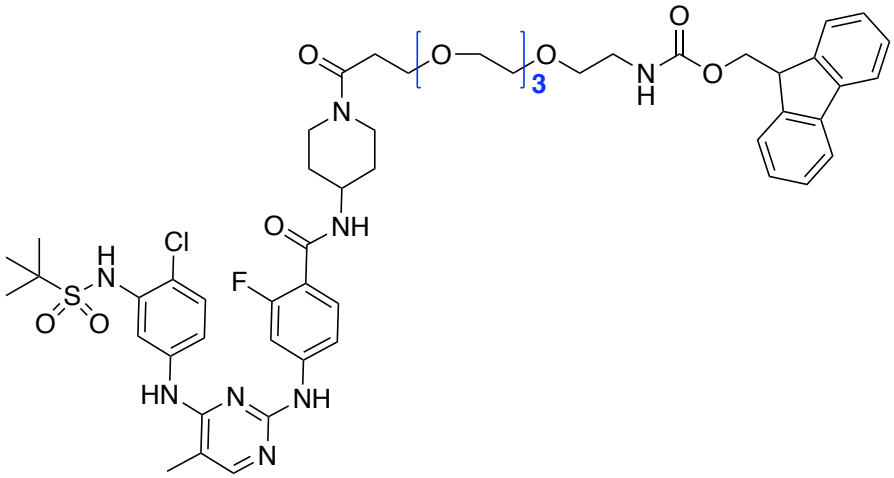
4.12

(9*H*-Fluoren-9-yl)methyl (2-(2-(3-(4-(4-((4-((4-Chloro-3-((1,1-dimethylethyl)sulfonamido)phenyl)amino)-5-methylpyrimidin-2-yl)amino)-2-fluorobenzamido)piperidin-1-yl)-3-oxopropoxy)ethoxy)ethyl)carbamate (4.12). Compound **4.12** was prepared in the same manner as compound **3.20** from compound **2.11** using 1-(9H-fluoren-9-yl)-3-oxo-2,7,10-trioxa-4-azatridecan-13-oic acid. Yield (44 mg, 89%) as a white solid. Mp: 169.6 – 170.3 °C. ^{1}H NMR (400 MHz, Methanol-d_4) δ 8.21 (s, 1H), 7.91 (s, 1H), 7.81 – 7.70 (m, J = 11.0 Hz, 3H), 7.67 – 7.53 (m, 3H), 7.46 (dd, J = 8.8, 2.5 Hz, 1H), 7.36 (dd, J = 8.2, 6.0 Hz, 3H), 7.33 – 7.20 (m, 3H), 4.46 (d, J = 13.8 Hz, 1H), 4.31 (d, J = 6.9 Hz, 1H), 4.23 – 4.05 (m, 2H), 3.97 (d, J = 13.8 Hz, 1H), 3.75 (q, J = 5.9 Hz, 2H), 3.70 – 3.39 (m, 6H), 3.36 (t, J = 6.0 Hz, 1H), 3.30 (t, J = 5.6 Hz, 2H), 3.20 (t, J = 12.1 Hz, 1H), 2.87 (t, J = 11.6 Hz, 1H), 2.65 (ddt, J = 40.4, 15.3, 7.8 Hz, 2H), 2.16 (s, 3H), 2.05 – 1.93 (m, 2H), 1.61 – 1.47 (m, 2H), 1.39 (s, 9H).



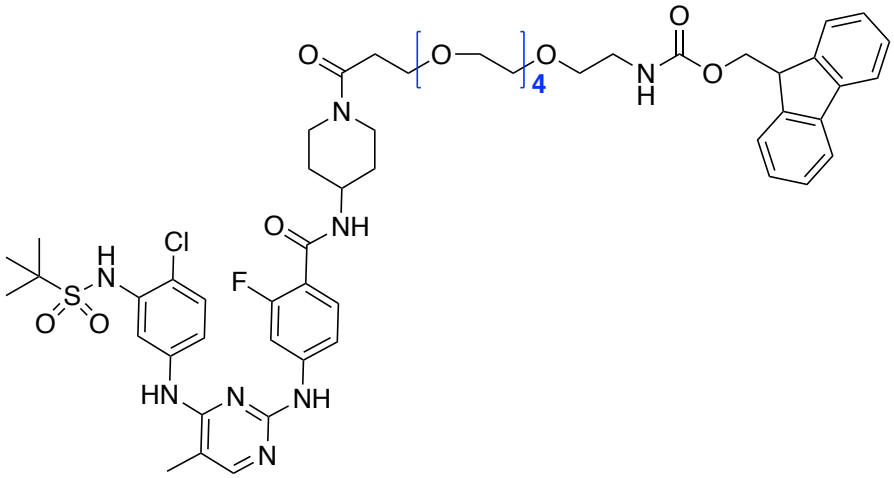
4.13

(9*H*-Fluoren-9-yl)methyl (2-(2-(2-(3-(4-(4-((4-((4-Chloro-3-((1,1-dimethylethyl)sulfonamido)phenyl)amino)-5-methylpyrimidin-2-yl)amino)-2-fluorobenzamido)piperidin-1-yl)-3-oxopropoxy)ethoxy)ethoxy)ethyl)carbamate (4.13). Compound **4.13** was prepared in the same manner as compound **3.20** from compound **2.11** using 1-(9*H*-fluoren-9-yl)-3-oxo-2,7,10,13-tetraoxa-4-azahexadecan-16-oic acid. Yield (78 mg, 91%) as a clear foam. ^{1}H NMR (400 MHz, Chloroform-*d*) δ 8.48 (s, 1H), 8.38 (s, 1H), 7.96 – 7.88 (m, 2H), 7.88 – 7.63 (m, 4H), 7.59 (d, *J* = 7.5 Hz, 2H), 7.38 (t, *J* = 7.5 Hz, 2H), 7.35 – 7.26 (m, *J* = 8.1, 7.7, 3.8 Hz, 4H), 7.26 – 7.16 (m, 2H), 6.89 (s, 1H), 6.65 (dd, *J* = 13.5, 7.6 Hz, 1H), 4.50 (d, *J* = 13.8 Hz, 1H), 4.38 (d, *J* = 7.0 Hz, 2H), 4.28 – 4.14 (m, 2H), 3.90 – 3.71 (m, 3H), 3.63 – 3.55 (m, 8H), 3.42 – 3.34 (m, *J* = 4.8, 4.2 Hz, 2H), 3.16 (t, *J* = 12.4 Hz, 1H), 2.82 (t, *J* = 12.2 Hz, 1H), 2.63 (d, *J* = 6.5 Hz, 2H), 2.13 (s, 3H), 2.11 – 1.96 (m, 2H), 1.55 – 1.30 (m, 11H).



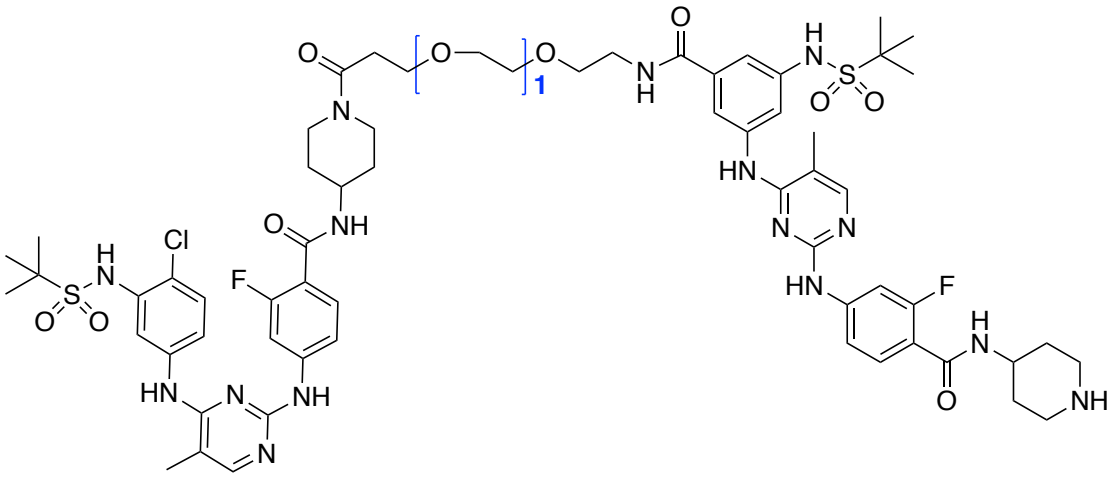
4.14

(9*H*-Fluoren-9-yl)methyl (15-(4-(4-((4-((4-Chloro-3-((1,1-dimethylethyl)sulfonamido)phenyl)amino)-5-methylpyrimidin-2-yl)amino)-2-fluorobenzamido)piperidin-1-yl)-15-oxo-3,6,9,12-tetraoxapentadecyl)carbamate (4.14). Compound **4.14** was prepared in the same manner as compound **3.20** from compound **2.11** using 1-(9*H*-fluoren-9-yl)-3-oxo-2,7,10,13,16-pentaoxa-4-azanonadecan-19-oic acid. Yield (46 mg, 85%) as a white solid. Mp: 132.2 – 132.6 °C. ^{1}H NMR (400 MHz, Methanol-d_4) δ 8.35 (d, J = 8.0, 1H), 8.14 (d, J = 5.2 Hz, 1H), 7.91 – 7.81 (m, J = 7.8 Hz, 1H), 7.80 – 7.73 (m, 2H), 7.66 – 7.58 (m, 3H), 7.46 (q, 3.4 Hz, 1H), 7.42 – 7.34 (m, 3H), 7.31 – 7.22 (m, 3H), 4.44 (d, J = 12.0 Hz, 1H), 4.32 (d, J = 6.9 Hz, 1H), 4.24 – 4.06 (m, 2H), 3.96 (d, J = 13.8 Hz, 1H), 3.71 (t, 4.3 Hz, 2H), 3.61 – 3.49 (m, 14H), 3.33 (t, J = 1.7 Hz, 2H), 3.29 (d, J = 5.7 Hz, 1H), 3.20 (t, J = 12.0 Hz, 1H), 2.84 (t, J = 12.0 Hz, 1H), 2.68 – 2.52 (m, 2H), 2.17 (s, 3H), 2.04 – 1.91 (m, 2H), 1.65 – 1.46 (m, 2H), 1.37 (s, 9H).



4.15

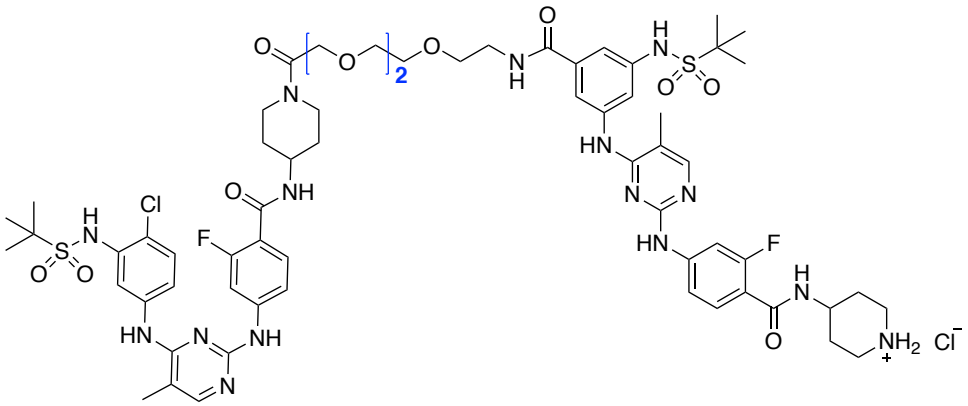
(9*H*-Fluoren-9-yl)methyl (18-(4-(4-((4-((4-Chloro-3-((1,1-dimethylethyl)sulfonamido)phenyl)amino)-5-methylpyrimidin-2-yl)amino)-2-fluorobenzamido)piperidin-1-yl)-18-oxo-3,6,9,12,15-pentaoxaoctadecyl)carbamate (4.15). Compound **4.15** was prepared in the same manner as compound **3.20** from compound **2.11** using 1-(9*H*-fluoren-9-yl)-3-oxo-2,7,10,13,16,19-hexaoxa-4-azadocosan-22-oic acid. Yield (51 mg, 91%) as a white solid. Mp: 81.7 – 82.5 °C. ^{1}H NMR (400 MHz, Methanol-d_4) δ 8.19 (d, J = 2.5 Hz, 1H), 7.90 (s, 1H), 7.76 – 7.69 (m, 3H), 7.66 – 7.58 (m, 3H), 7.45 (d, J = 2.4 Hz, 1H), 7.42 – 7.35 (m, 3H), 7.34 – 7.24 (m, 3H), 4.47 (d, J = 13.1 Hz, 1H), 4.35 (d, J = 6.8 Hz, 1H), 4.26 – 4.07 (m, J = 24.0, 8.6 Hz, 2H), 4.00 (d, J = 13.8 Hz, 1H), 3.73 (td, J = 6.2, 3.6 Hz, 2H), 3.64 – 3.49 (m, 18H), 3.36 (s, 1H), 3.28 (t, J = 4.8 Hz, 2H), 3.23(t, J = 12.6 Hz, 1H), 2.87 (t, J = 12.6 Hz, 1H), 2.70 (q, J = 6.5 Hz, 1H), 2.60 (q, 6.0 Hz, 1H), 2.16 (s, 3H), 2.07 – 1.94 (m, 2H), 1.64 – 1.46 (m, 2H), 1.39 (s, 9H).



4.16

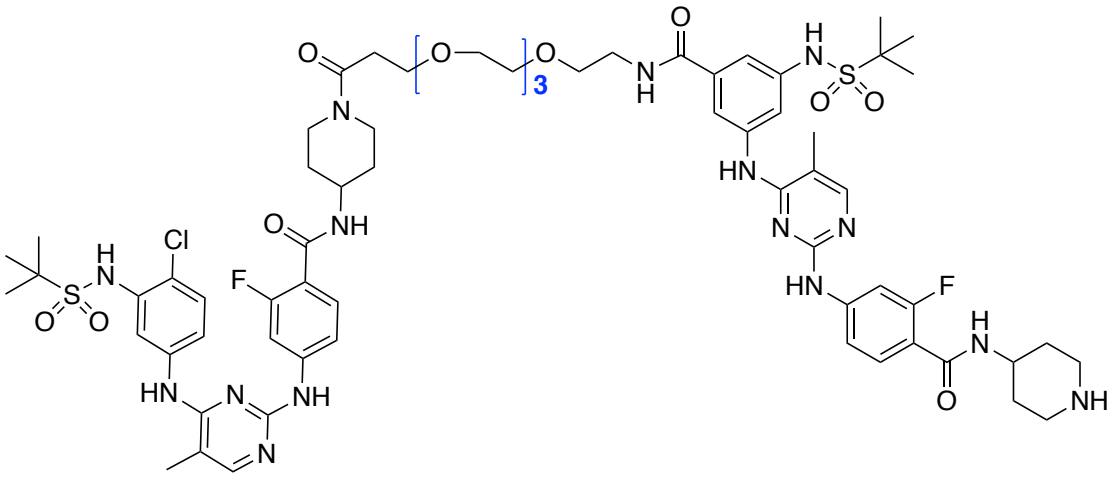
4-((4-((4-Chloro-3-((1,1-dimethylethyl)sulfonamido)phenyl)amino)-5-methylpyrimidin-2-yl)amino)-*N*-(1-(3-(2-(2-(3-((1,1-dimethylethyl)sulfonamido)-5-((5-methyl-2-((4-(piperidin-4-ylcarbamoyl)phenyl)amino)pyrimidin-4-yl)amino)benzamido)ethoxy)ethoxy)propanoyl)piperidin-4-yl)-2-fluorobenzamide (4.16). Compound **4.12** (19 mg, 19 µmol) was dissolved in a mixture of piperidine (0.1 mL) and DMF (0.4 mL) and stirred at room temperature for 4 h. The mixture was diluted with EtOAc, and the organic layer was washed with brine (3 × 20 mL) and dried over Mg_2SO_4. The solvent was removed under reduced pressure. The residue was dissolved in anhydrous DMF (1 mL). Compound **3.39** (16 mg, 23 µmol), HATU (8.8 mg, 23 µmol) and DIPEA (10 µL, 57 µmol) was added. The reaction solution was stirred at room temperature for 15 h. The mixture was diluted with EtOAc, and the organic layer was washed with brine (3 × 20 mL) and dried over Mg_2SO_4. The solvent was removed under reduced pressure. The residues were added to a mixture of DCM (0.8 mL) and TFA (0.2 mL) and stirred at room temperature for 2 h. Solvent was removed in vacuo and the residues was purified by silica gel column chromatography (MeOH/DCM/TEA) and preparative HPLC to give the title compound as a white solid (11 mg, 42%). Mp: 223.4 – 224.4 °C. Purity: >99% (HPLC). ^{1}H NMR (400 MHz, Methanol-d_4) δ 7.92 (d, J = 3.7 Hz, 1H), 7.83 (d, J = 5.5 Hz, 2H), 7.78 (s, 1H), 7.70 (s, 1H), 7.66 – 7.49 (m, 4H), 7.45 – 7.31 (m, 3H), 7.30 – 7.19 (m, 2H), 4.42 (d, J = 13.6 Hz, 1H), 4.15 – 4.05 (m, 1H), 4.15 – 4.05 (m, 1H), 4.05 – 3.94 (m, 1H), 3.81 – 3.71 (m, 2H), 3.68 – 3.46 (m, 10H), 3.27 – 3.12 (m, 3H), 2.93 – 2.81 (m, 1H), 2.65 (dd, J = 10.1, 6.2 Hz, 2H), 2.25 (d, J = 3.1 Hz, 6H), 2.22 – 2.17 (m, 2H), 2.02 – 1.89 (m, 4H),

1.61 – 1.47 (m, 2H), 1.37 (s, 9H), 1.35 (s, 9H). MS: calcd for $C_{62}H_{79}ClF_2N_{15}O_{10}S_2$ $[M+H]^+$, 1330.5; found 1330.7



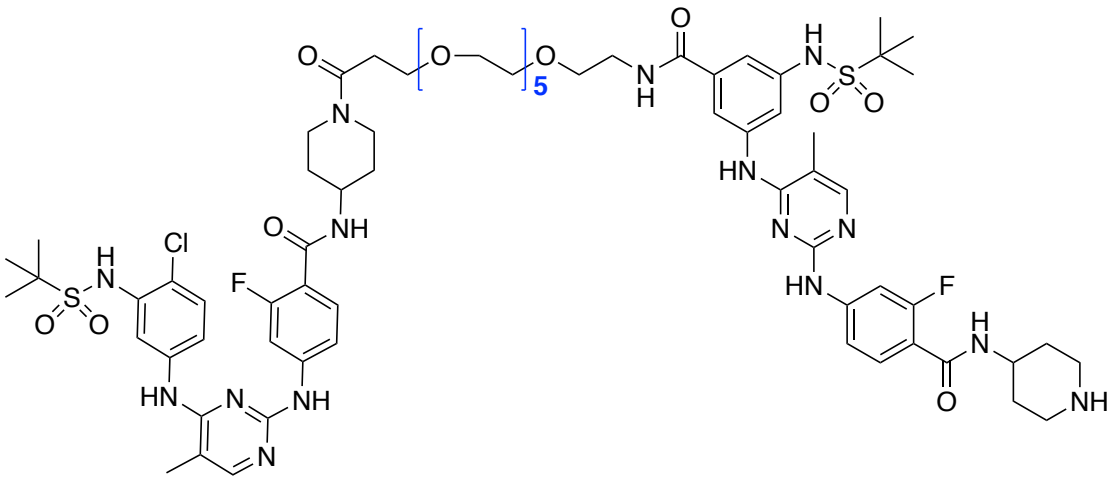
4.17

4-((4-((4-Chloro-3-((1,1-dimethylethyl)sulfonamido)phenyl)amino)-5-methylpyrimidin-2-yl)amino)-*N*-(1-(1-(3-((1,1-dimethylethyl)sulfonamido)-5-((5-methyl-2-((4-(piperidin-4-ylcarbamoyl)phenyl)amino)pyrimidin-4-yl)amino)phenyl)-1-oxo-5,8,11-trioxa-2-azatridecan-13-oyl)piperidin-4-yl)-2-fluorobenzamide(4.17). Compound **4.17** was prepared in the same manner as compound **4.16** from compound **4.13**. Yield (20 mg, 30%) as a white solid. Mp: 150.9 – 151.3 °C. Purity: >99% (HPLC). ^{1}H NMR (400 MHz, DMSO-d_6) δ 10.18 (s, 1H), 10.06 (s, 1H), 9.79 (s, 1H), 9.34 (s, 2H), 9.19 (s, 1H), 8.59 (d, J = 11.1 Hz, 1H), 8.46 – 8.24 (m, 2H), 8.15 – 7.82 (m, 4H), 7.74 (s, 2H), 7.63 – 7.50 (m, 3H), 7.51 – 7.35 (m, 4H), 7.31 (t, J = 8.3 Hz, 1H), 7.28 – 7.17 (m, 2H), 4.18 (d, J = 12.8 Hz, 1H), 4.05 – 3.85 (m, 2H), 3.77 (d, J = 13.2 Hz, 1H), 3.53 (t, J = 6.9 Hz, 2H), 3.42 – 3.32 (m, J = 10.7 Hz, 8H), 3.25 (dd, J = 14.0, 8.0 Hz, 3H), 3.13 – 2.89 (m, 3H), 2.86 – 2.58 (m, 2H), 2.57 – 2.46 (m, 2H), 2.09 (s, 6H), 1.91 (d, J = 15.7 Hz, 2H), 1.83 – 1.68 (m, 2H), 1.68 – 1.55 (m, 2H), 1.37 (dd, J = 14.5, 5.9 Hz, 2H), 1.24 (s, 9H), 1.21 (d, J = 2.8 Hz, 9H). MS: calcd for $C_{63}H_{81}ClF_2N_{15}O_{11}S_2$ $[M+H]^+$, 1360.5; found 1360.4



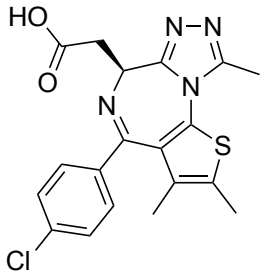
4.18

4-((4-((4-Chloro-3-((1,1-dimethylethyl)sulfonamido)phenyl)amino)-5-methylpyrimidin-2-yl)amino)-*N*-(1-(1-(3-((1,1-dimethylethyl)sulfonamido)-5-((5-methyl-2-((4-(piperidin-4-ylcarbamoyl)phenyl)amino)pyrimidin-4-yl)amino)phenyl)-1-oxo-5,8,11,14-tetraoxa-2-azaheptadecan-17-oyl)piperidin-4-yl)-2-fluorobenzamide (4.18). Compound **4.18** was prepared in the same manner as compound **4.16** from compound **4.14**. Yield (16 mg, 39%) as a transparent gel. Purity: >99% (HPLC). ^{1}H NMR (400 MHz, Methanol-d_4) δ 7.96 (d, J = 2.5 Hz, 1H), 7.86 (d, J = 12.9 Hz, 2H), 7.75 (d, J = 2.0 Hz, 2H), 7.64 (t, J = 2.0 Hz, 1H), 7.59 (td, J = 8.4, 4.9 Hz, 2H), 7.53 (d, J = 8.6 Hz, 1H), 7.46 (ddd, J = 13.3, 8.8, 2.0 Hz, 2H), 7.36 (dd, J = 8.7, 2.5 Hz, 1H), 7.24 (dt, J = 8.6, 2.3 Hz, 2H), 4.45 (d, J = 13.5 Hz, 1H), 4.16 (ddt, J = 21.7, 10.6, 5.3 Hz, 2H), 4.01 (d, J = 11.8 Hz, 1H), 3.74 (t, J = 6.2 Hz, 2H), 3.72 – 3.40 (m, 18H), 3.28 – 3.14 (m, 3H), 2.90 (t, J = 12.3 Hz, 1H), 2.68 (s, 2H), 2.35 – 2.19 (m, 8H), 2.06 – 1.88 (m, 4H), 1.59 (q, J = 11.7, 10.8 Hz, 2H), 1.38 (s, 9H), 1.36 (s, 9H). MS: calcd for $C_{66}H_{87}ClF_2N_{15}O_{12}S_2$ $[M+H]^+$, 1418.6; found 1418.5



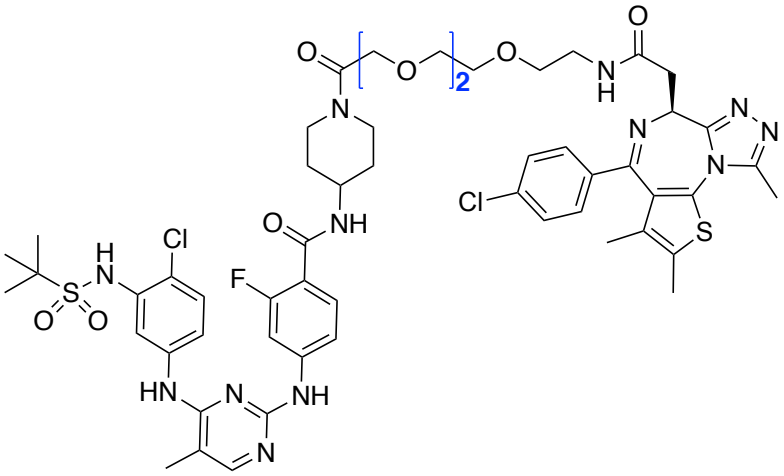
4.19

4-((4-((4-Chloro-3-((1,1-dimethylethyl)sulfonamido)phenyl)amino)-5-methylpyrimidin-2-yl)amino)-*N*-(1-(1-(3-((1,1-dimethylethyl)sulfonamido)-5-((5-methyl-2-((4-(piperidin-4-ylcarbamoyl)phenyl)amino)pyrimidin-4-yl)amino)phenyl)-1-oxo-5,8,11,14,17,20-hexaoxa-2-azatricosan-23-oyl)piperidin-4-yl)-2-fluorobenzamide (4.19). Compound **4.19** was prepared in the same manner as compound **4.16** from compound **4.15**. Yield (13 mg, 43%) as a transparent gel. Purity: >99% (HPLC). ^{1}H NMR (400 MHz, Methanol-d_4) δ 7.91 (d, J = 3.1 Hz, 1H), 7.88 – 7.76 (m, 3H), 7.72 (t, J = 1.7 Hz, 1H), 7.62 – 7.51 (m, 4H), 7.45 – 7.31 (m, 3H), 7.23 (dt, J = 8.6, 2.5 Hz, 2H), 4.44 (d, J = 13.1 Hz, 1H), 4.23 – 4.08 (m, 2H), 4.02 (d, J = 12.3 Hz, 1H), 3.75 (t, J = 6.1 Hz, 2H), 3.69 – 3.35 (m, 26H), 3.27 – 3.11 (m, 3H), 2.93 – 2.85 (m, 1H), 2.68 (td, J = 6.1, 3.7 Hz, 2H), 2.31 – 2.18 (m, 8H), 2.02 – 1.86 (m, 4H), 1.59 – 1.47 (m, 2H), 1.37 (s, 9H), 1.34 (d, J = 2.5 Hz, 9H). MS: calcd for $C_{70}H_{95}ClF_2N_{15}O_{14}S_2$ $[M+H]^+$, 1506.6; found 1506.9



4.20

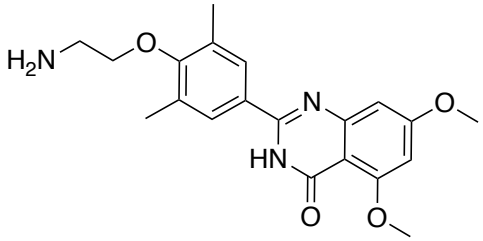
(*S*)-2-(4-(4-Chlorophenyl)-2,3,9-trimethyl-6*H*-thieno[3,2-*f*][1,2,4]triazolo[4,3-*a*][1,4]diazepin-6-yl)acetic acid (4.20). To a solution of *tert*-butyl (*S*)-2-(4-(4-chlorophenyl)-2,3,9-trimethyl-6*H*-thieno[3,2-*f*][1,2,4]triazolo[4,3-*a*][1,4]diazepin-6-yl)acetate (**JQ-1**, 20 mg, 44 mmol) in DCM (0.75 mL) was added TFA (0.25 mL) and the mixture was stirred at rt for 2 h. The solvent was removed under reduced pressure and the residue was treated with dichloromethane and concentrated to dryness three times to give the title compound as a colorless oil (16 mg, 91%). The ^{1}H NMR matches the reported data.



4.21

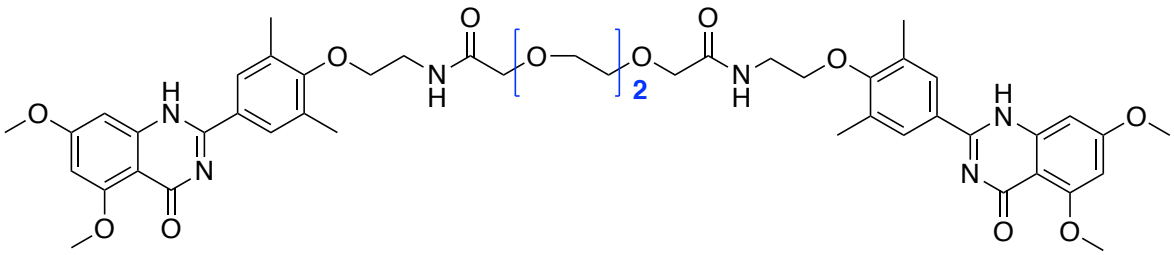
(*S*)-4-((4-((4-Chloro-3-((1,1-dimethylethyl)sulfonamido)phenyl)amino)-5-methylpyrimidin-2-yl)amino)-*N*-(1-(1-(4-(4-chlorophenyl)-2,3,9-trimethyl-6*H*-thieno[3,2-*f*][1,2,4]triazolo[4,3-*a*][1,4]diazepin-6-yl)-2-oxo-6,9,12-trioxa-3-azatetradecan-14-oyl)piperidin-4-yl)-2-fluorobenzamide (4.21). Compound **4.21** was prepared in the same manner as compound **4.16** from compound **4.13** and compound **4.20**. Yield (6.2 mg, 70%) as a white solid. Mp: 164.2 – 165.0 °C. Purity: 98% (HPLC). ^{1}H NMR (400 MHz, Chloroform-*d*) δ 8.55 (s, 1H), 7.97 – 7.82 (m, 2H), 7.82 – 7.67 (m, 2H), 7.33 (d, *J* = 8.2 Hz, 2H), 7.29 – 7.22 (m, 3H), 7.15 – 7.06 (m, 2H), 7.01 (d, *J* = 5.7 Hz, 1H), 6.60 (dd, *J* = 13.5, 6.9 Hz, 1H), 6.54 (s, 1H), 4.58 (t, *J* = 6.9 Hz, 1H), 4.43 (d, *J* = 13.6 Hz, 1H), 4.11 (s, 1H), 3.79 (s, 1H), 3.74 (t, *J* = 6.8 Hz, 2H), 3.64 3.55 (m, 8H), 3.53 (q, *J* = 5.0 Hz, 2H), 3.47 – 3.43 (m, 2H), 3.35 – 3.28 (m, 1H), 3.17 – 3.00 (m, 1H), 2.75 (q, *J* = 10.6 Hz, 1H), 2.66 -2.53 (m, 5H), 2.32 (s, 3H), 2.07 (s, 3H), 2.00 -1.90 (m, 2H), 1.59 (s, 3H), 1.35 (s, 11H). ^{13}C NMR (101 MHz, $CDCl_3$) δ 207.0, 169.3, 162.9 (d, *J* = 3 Hz), 161.5 (d,

J = 244 Hz), 160.3, 158.7, 157.3, 156.6, 155.9, 145.2 (d, *J* = 14 Hz) , 144.0, 141.3, 138.6, 135.7, 132.2 (d, *J* = 3 Hz), 129.2, 127.6 , 127.0 , 125.1, 119.9, 117.3, 117.0, 114.0, 113.9 (2 peaks), 112.8 (d, *J* = 12 Hz), 107.1, 104.5 (d, *J* = 30 Hz), 70.6, 70.5, 70.4, 70.3, 70.1, 67.5, 66.6, 62.7, 47.3, 46.8, 44.5, 41.0, 40.6, 33.5, 32.6, 31.7, 29.7, 29.3, 24.7, 13.2. MS: calcd for $C_{54}H_{62}Cl_2FN_{12}O_8S_2$ $[M-H]^-$, 1159.4; found 1159.1.



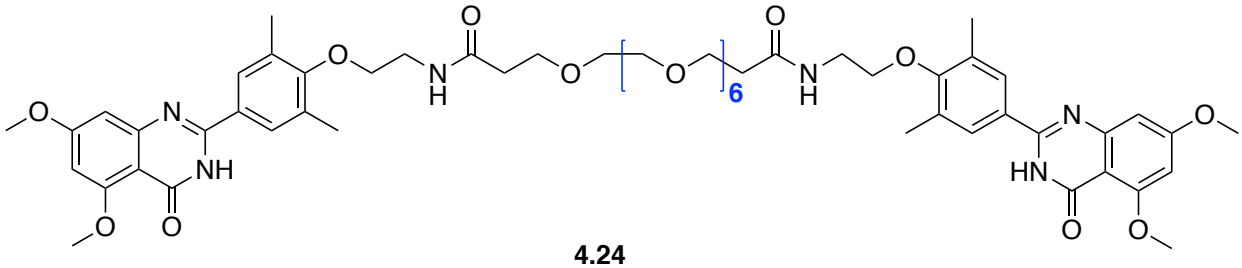
4.22

2-(4-(2-aminoethoxy)-3,5-dimethylphenyl)-5,7-dimethoxyquinazolin-4(1*H*)-one (4.22). To a schlenk flask was added RVX208 (200 mg, 0.54 mmol), PPh_3 (170 mg, 0.65 mmol), phthalimide (95 mg, 0.65 mmol) and anhydrous THF (2 mL) under N_2 atmosphere. The mixture was stirred for 10 min at 0 ºC. 10% DIAD THF solution (0.13 mL, 0.65 mmol) was added to this mixture through a syringe. The mixture was allowed to reach rt and stirred overnight. The reaction mixture was quenched with EtOH (1 mL) and concentrated. The residue was dissolved in EtOH (2 mL). Hydrazine monohydrate (0.4 mL) was added to this mixture and refluxed for another 2 h. The solution was concentrated under reduced pressure. The reaction mixture was diluted with 2 mL of EtOAc and 2 mL of KOH (1 M) and stirred for 30 min. The aqueous phase was extracted with EA. The mixture was diluted with EtOAc (3 × 10 mL), and the organic layer was washed with brine (3 × 20 mL) and dried over Mg_2SO_4. The solvent was removed under reduced pressure. The residues were purified by silica gel column chromatography (MeOH/DCM/TEA) to give the title compound as a yellow solid (129 mg, 65 %). Mp: 174.5 – 175.0 °C. Purity: 95% (HPLC). ^{1}H NMR (400 MHz, Methanol-*d*$_4$) δ 7.62 (d, *J* = 5.8 Hz, 2H), 6.71 (d, *J* = 2.2 Hz, 1H), 6.47 (d, *J* = 2.1 Hz, 1H), 3.98 (t, *J* = 5.7 Hz, 2H), 3.83 (d, *J* = 3.4 Hz, 6H), 3.63 (t, *J* = 5.6 Hz, 2H), 2.28 (d, *J* = 11.8 Hz, 6H).



4.23

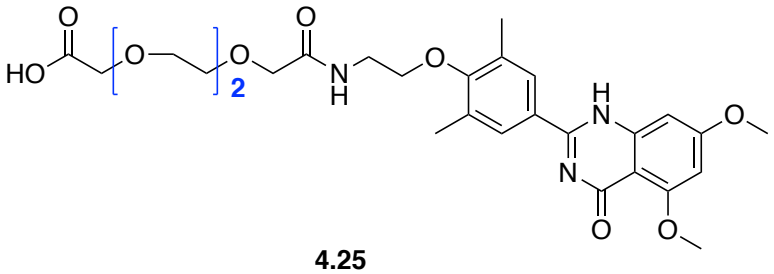
2,2'-((Oxybis(ethane-2,1-diyl))bis(oxy))bis(*N*-(2-(4-(5,7-dimethoxy-4-oxo-1,4-dihydroquinazolin-2-yl)-2,6-dimethylphenoxy)ethyl)acetamide) (4.23). Compound **4.23** was prepared in the same manner as compound **4.1** from compound **4.22** and 2,2'-((oxybis(ethane-2,1-diyl))bis(oxy))diacetic acid. Yield (14 mg, 56%) as a clear foam. Purity: 98% (HPLC). ^{1}H NMR (400 MHz, DMSO-d_6) δ 7.93 (s, 2H), 7.83 (s, 4H), 6.72 (s, 2H), 6.52 (s, 2H), 3.94 (s, 4H), 3.91 – 3.76 (m, 16H), 3.62 (s, 8H), 3.54 (d, J = 5.8 Hz, 4H), 2.27 (s, 12H). ^{13}C NMR (101 MHz, DMSO) δ 169.4, 164.4, 161.0, 159.2, 158.3, 153.1, 151.2, 130.7, 128.5, 126.3, 104.2, 100.0, 97.6, 70.3, 70.2, 70.0, 69.6, 56.0, 55.6, 38.5, 15.9. MS: calcd for $C_{48}H_{57}N_6O_{13}$ $[M+H]^+$, 925.4; found 925.1.



4.24

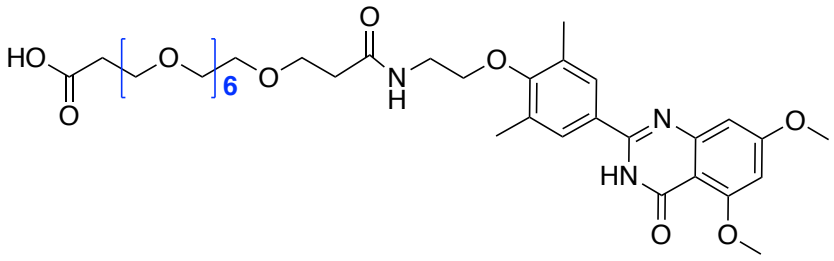
***N*^{1},*N*^{25}-Bis(2-(4-(5,7-dimethoxy-4-oxo-1,4-dihydroquinazolin-2-yl)-2,6-dimethylphenoxy)ethyl)-4,7,10,13,16,19,22-heptaoxapentacosanediamide (4.24).** Compound **4.24** was prepared in the same manner as compound **4.1** from compound **4.22** and 4,7,10,13,16,19,22-heptaoxapentacosanedioic acid**.** Yield (43 mg, 68%) as a transparent gel. Purity: >99% (HPLC). ^{1}H NMR (400 MHz, DMSO-d_6) δ 8.22 (s, 2H), 7.89 (s, 4H), 6.73 (d, J = 2.4 Hz, 2H), 6.51 (d, J = 2.4 Hz, 2H), 3.88 (s, 6H), 3.84 (s, 6H), 3.80 (t, J = 5.6 Hz, 4H), 3.62 (t, J = 6.4 Hz, 4H), 3.51 – 3.44 (m, 28H), 2.38 (t, J = 6.4 Hz, 4H), 2.28 (s, 12H). ^{13}C NMR (101 MHz, DMSO) δ 170.30, 164.17, 160.89, 159.78, 157.94, 153.02, 152.46, 130.66, 128.24, 127.41, 104.58, 101.02, 97.49, 70.49, 69.79, 69.71, 69.63,

69.50, 66.71, 55.90, 55.57, 45.58, 36.04, 15.95. MS: calcd for $C_{58}H_{77}N_6O_{17}$ $[M+H]^+$, 1129.5; found 1129.6.



4.25

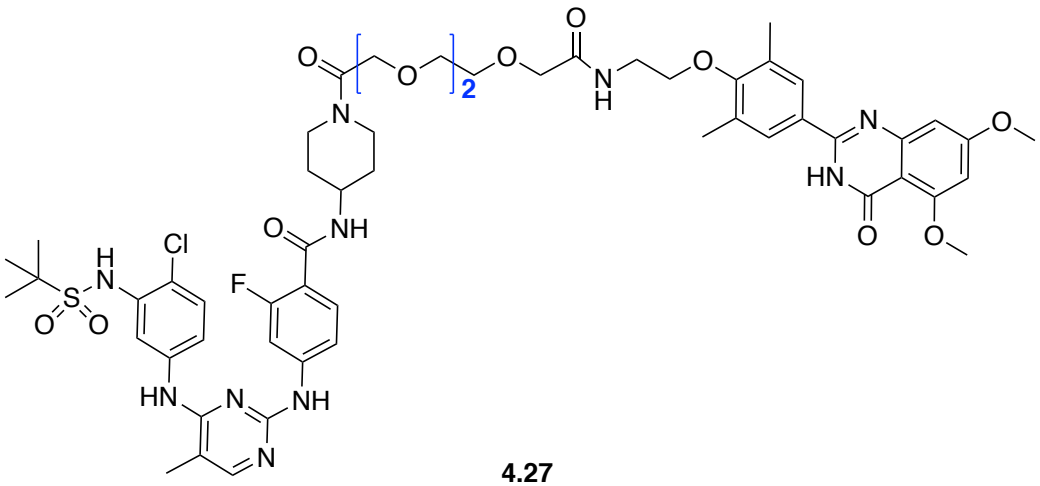
1-(4-(5,7-Dimethoxy-4-oxo-1,4-dihydroquinazolin-2-yl)-2,6-dimethylphenoxy)-4-oxo-6,9,12-trioxa-3-azatetradecan-14-oic acid (4.25). To a mixture of 2,2'-((oxybis(ethane-2,1-diyl))bis(oxy))diacetic acid (12 mg, 0.054 mmol) and HATU (45 mg, 0.12 mmol) in anhydrous DMF (1 mL), DIPEA (57 µL, 0.32 mmol) was added. The solution was stirred at room temperature for 30 min followed by the addition of compound **4.22** (20 mg, 0.054 mmol). The reaction solution was stirred at room temperature for 15 h. Water (1 mL) was added to this mixture and stirred at room temperature for another 1 h. The mixture was diluted with EtOAc, and the organic layer was washed with brine (3 × 20 mL) and dried over Mg_2SO_4. The solvents were removed under reduced pressure. The residues were purified by silica gel column chromatography (MeOH/DCM/AcOH) to give the title compound as a yellow gel (11 mg, 36%). ^{1}H NMR (400 MHz, Methanol-d_4) δ 7.71 (s, 2H), 6.80 (d, J = 2.3 Hz, 1H), 6.56 (d, J = 2.3 Hz, 1H), 4.11 (s, 2H), 4.07 (s, 2H), 3.99 – 3.91 (m, 8H), 3.82 – 3.64 (m, 10H), 2.37 (s, 6H).



4.26

1-(4-(5,7-Dimethoxy-4-oxo-1,4-dihydroquinazolin-2-yl)-2,6-dimethylphenoxy)-4-oxo-7,10,13,16,19,22,25-heptaoxa-3-azaoctacosan-28-oic Acid (4.26). Compound **4.26** was prepared in the same manner as compound **4.25** from compound **4.22** and 4,7,10,13,16,19,22-heptaoxapentacosanedioic acid. Yield (17 mg, 33%) as a transparent

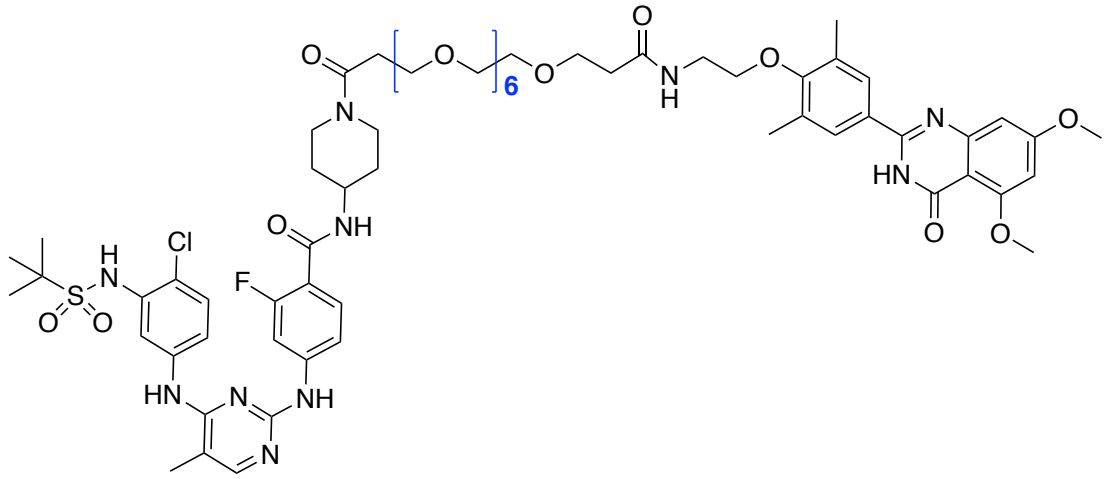
gel. ^{1}H NMR (400 MHz, Methanol-d_4) δ 7.61 (s, 2H), 6.68 (d, J = 2.2 Hz, 1H), 6.44 (d, J = 2.3 Hz, 1H), 3.82 (d, J = 3.2 Hz, 6H), 3.66 (t, J = 6.0 Hz, 2H), 3.60 (t, J = 6.2 Hz, 2H), 3.57 – 3.48 (m, 28H), 2.42 (t, J = 6.1 Hz, 4H), 2.26 (s, 6H).



4.27

4-((4-((4-Chloro-3-((1,1-dimethylethyl)sulfonamido)phenyl)amino)-5-methylpyrimidin-2-yl)amino)-*N*-(1-(1-(4-(5,7-dimethoxy-4-oxo-1,4-dihydroquinazolin-2-yl)-2,6-dimethylphenoxy)-4-oxo-6,9,12-trioxa-3-azatetradecan-14-oyl)piperidin-4-yl)-2-fluorobenzamide (4.27). To a solution of compound **4.25** (10 mg, 17 μmol) in 1 mL anhydrous DCM under N_2 was added 1-(3-dimethylaminopropyl)-3-ethylcarbodiimide hydrochloride (EDC, 4.0 mg, 21 μmol), HOBt (3.2 mg, 21 μmol). The resulting solution was stirred for 30 min, and compound **2.11** (10 mg, 17 mmol) and DIPEA (9.1 μL, 52 μmol) were added. The resulting mixture was stirred at rt for 15 h, then partitioned between EtOAc (3 × 10 mL) and 1M HCl (10 mL). The organic layer was washed with brine (1x10 mL), dried over Mg_2SO_4. The solvents were removed under reduced pressure. The residues were purified by silica gel column chromatography (MeOH/DCM) to give the title compound as a white solid (17 mg, 84%). 192.8 – 193.4 °C. Purity: 96% (HPLC). ^{1}H NMR (400 MHz, Methanol-d_4) δ 8.06 (d, J = 2.5 Hz, 1H), 7.75 (s, 1H), 7.56 (s, 2H), 7.56 – 7.49 (m, 1H), 7.44 (t, J = 8.7 Hz, 1H), 7.36 (dd, J = 2.6, 8.7 Hz, 1H), 7.26 (d, J = 8.8 Hz, 1H), 7.08 (dd, J = 2.1, 8.7 Hz, 1H), 6.60 (d, J = 2.2 Hz, 1H), 6.36 (d, J = 2.3 Hz, 1H), 4.27 (d, J = 13.1 Hz, 1H), 4.20 – 4.05 (m, 2H), 4.03 – 3.89 (m, 3H), 3.88 – 3.70 (m, 9H), 3.70 – 3.50 (m, 10H), 3.11 – 3.01 (m, 1H), 2.76 (t, J = 12.0 Hz,

1H), 2.23 (s, 6H), 2.03 (s, 3H), 1.84 (s, 2H), 1.46 – 1.34 (m, 2H), 1.27 (s, 9H). MS: calcd for $C_{55}H_{67}ClFN_{10}O_{12}S$ $[M+H]^+$, 1145.4; found 1145.4.



4.28

***N*^{1},*N*^{25}-Bis(2-(4-(5,7-dimethoxy-4-oxo-1,4-dihydroquinazolin-2-yl)-2,6-dimethylphenoxy)ethyl)-4,7,10,13,16,19,22-heptaoxapentacosanediamide (4.28).** Compound **4.28** was prepared in the same manner as compound **4.27** from compound **4.26** and compound **2.11.** Yield (15 mg, 88%) as a white solid. 91.0 – 91.5 °C. Purity: 98% (HPLC). ^{1}H NMR (400 MHz, Methanol-d_4) δ 8.20 (d, J = 2.6 Hz, 1H), 7.90 (s, 1H), 7.79 – 7.69 (m, 3H), 7.59 (t, J = 8.6 Hz, 1H), 7.49 (dd, J = 8.8, 2.5 Hz, 1H), 7.38 (d, J = 8.8 Hz, 1H), 7.26 (dd, J = 8.6, 2.1 Hz, 1H), 6.78 (d, J = 2.3 Hz, 1H), 6.54 (d, J = 2.3 Hz, 1H), 4.48 (d, J = 13.5 Hz, 1H), 4.20 – 4.07 (m, 1H), 4.03 (d, J = 13.9 Hz, 1H), 3.92 (s, 6H), 3.81 – 3.69 (m, J = 6.5 Hz, 6H), 3.66 – 3.55 (m, 26H), 3.25 (q, J = 8.0 Hz, 2 H), 2.88 (t, J = 12.7 Hz, 1H), 2.78 – 2.69 (m, 1H), 2.53 (t, J = 4.0 Hz, 2H), 2.20 (s, 6H), 2.16 (s, 3H), 2.07 – 1.98 (m, 2H), 1.65 – 1.50 (m, 2H), 1.27 (s, 9H). MS: calcd for $C_{65}H_{87}ClFN_{10}O_{16}S$ $[M+H]^+$, 1349.6; found 1349.5.

Bibliography

1. Patel, A. S.; Leong, J. Y.; Ramos, L.; Ramasamy, R. Testosterone is a contraceptive and should not be used in men who desire fertility. *World J. Men's Health* **2019**, *37*, 45-54.
2. Long, J. E.; Lee, M. S.; Blithe, D. L. Male contraceptive development: update on novel hormonal and nonhormonal methods. *Clin. Chem.* **2019**, *65*, 153-160.
3. Basaria, S. Male hypogonadism. *Lancet* **2014**, *383*, 1250-1263.
4. Kloner, R. A.; Carson, C.; Dobs, A.; Kopecky, S.; Mohler, E. R. Testosterone and Cardiovascular Disease. *J. Am. Coll. Cardiol.* **2016**, *67*, 545-557.
5. Gava, G.; Meriggiola, M. C. Update on male hormonal contraception. *Ther. Adv. Endocrinol. Metab.* **2019**, *10*, 9.
6. Xu, B. F.; Hao, Z. L.; Jha, K. N.; Zhang, Z.; Urekar, C.; Digilio, L.; Pulido, S.; Strauss, J. F.; Flickinger, C. J.; Herr, J. C. Targeted deletion of Tssk1 and 2 causes male infertility due to haploinsufficiency. *Dev. Biol.* **2008**, *319*, 211-222.
7. Shang, P.; Baarends, W. M.; Hoogerbrugge, J.; Ooms, M. P.; van Cappellen, W. A.; de Jong, A. A. W.; Dohle, G. R.; van Eenennaam, H.; Gossen, J. A.; Grootegoed, J. A. Functional transformation of the chromatoid body in mouse spermatids requires testis-specific serine/threonine kinases. *J. Cell Sci.* **2010**, *123*, 331-339.
8. Shetty, J.; Sinville, R.; Shumilin, I. A.; Minor, W.; Zhang, J. H.; Hawkinson, J. E.; Georg, G. I.; Flickinger, C. J.; Herr, J. C. Recombinant production of enzymatically active male contraceptive drug target hTSSK2-Localization of the TSKS domain phosphorylated by TSSK2. *Protein Expr. Purif.* **2016**, *121*, 88-96.
9. Hawkinson, J. E.; Sinville, R.; Mudaliar, D.; Shetty, J.; Ward, T.; Herr, J. C.; Georg, G. I. Potent pyrimidine and pyrrolopyrimidine inhibitors of testis-specific serine/threonine kinase2 (TSSK2). *Chemmedchem* **2017**, *12*, 1857-1865.
10. Sun, X. H.; Zhu, Y. Y.; Wang, L.; Liu, H. L.; Ling, Y.; Li, Z. L.; Sun, L. B. The Catsper channel and its roles in male fertility: a systematic review. *Reprod. Biol. Endocrinol.* **2017**, *15*, 65-77.
11. Schonbrunn, E.; Betzi, S.; Alam, R.; Martin, M. P.; Becker, A.; Han, H. J.; Francis, R.; Chakrasali, R.; Jakkaraj, S.; Kazi, A.; Sebti, S. M.; Cubitt, C. L.; Gebhard, A. W.; Hazlehurst, L. A.; Tash, J. S.; Georg, G. I. Development of highly potent and selective diaminothiazole inhibitors of cyclin-dependent kinases. *J. Med. Chem.* **2013**, *56*, 3768-3782.
12. Faber, B. E.; N., W.; Georg, G. I. Review of rationale and progress toward targeting cyclin-dependent kinase 2 (CDK2) for male contraception. *Biol. Reprod.* **2020**, *103*, 357-367.
13. Chung, S. S. W.; Cuellar, R. A. D.; Wang, X. Y.; Reczek, P. R.; Georg, G. I.; Wolgemuth, D. J. Pharmacological activity of retinoic acid receptor alpha-selective antagonists in vitro and in vivo. *ACS Med. Chem. Lett.* **2013**, *4*, 446-450.
14. Noman, M. A. A.; Kyzer, J. L.; Chung, S. S.; Wolgemuth, D. J.; Georg, G. I. Retinoic acid receptor antagonists for male contraception: current status. *Biol. Reprod.* **2020**, *103*, 390-399.
15. Matzuk, M. M.; McKeown, M. R.; Filippakopoulos, P.; Li, Q. L.; Ma, L.; Agno, J. E.; Lemieux, M. E.; Picaud, S.; Yu, R. N.; Qi, J.; Knapp, S.; Bradner, J. E. Small-molecule inhibition of BRDT for male contraception. *Cell* **2012**, *150*, 673-684.

16. Syeda, S. S.; Sanchez, G.; Hong, K. H.; Hawkinson, J. E.; Georg, G. I.; Blanco, G. Design, synthesis, and in vitro and in vivo evaluation of ouabain analogues as potent and selective Na,K-ATPase alpha 4 isoform inhibitors for male contraception. *J. Med. Chem.* **2018**, *61*, 1800-1820.
17. Syeda, S. S.; Sánchez, G.; McDermott, J. P.; Hong, K. H.; Blanco, G.; Georg, G. I. The Na+ and K+ transport system of sperm (ATP1A4) is essential for male fertility and an attractive target for male contraception. *Biol. Reprod.* **2020**, *103*, 343-356.
18. Murdoch, F. E.; Goldberg, E. Male contraception: Another holy grail. *Bioorg. Med. Chem. Lett.* **2014**, *24*, 419-424.
19. Johnston, D. S.; Goldberg, E. Preclinical contraceptive development for men and women. *Biol. Reprod.* **2020**, *103*, 147-156.
20. Miao, Z.; Guan, X.; Jiang, J.; Georg, G. I. BRDT inhibitors for male contraceptive drug discovery: current status. In *In Targeting Protein-Protein Interactions by Small Molecules*, Sheng, C.; Georg, G. I., Eds. Nature Singapore: Springer 2018; pp 287-315.
21. Tamkun, J. W.; Deuring, R.; Scott, M. P.; Kissinger, M.; Pattatucci, A. M.; Kaufman, T. C.; Kennison, J. A. Brahma - a regulator of drosophila homeotic genes structurally related to the yeast transcriptional activator SNF2 SW12. *Cell* **1992**, *68*, 561-572.
22. Smith, S. G.; Zhou, M. M. The bromodomain: a new target in emerging epigenetic medicine. *ACS Chem. Biol.* **2016**, *11*, 598-608.
23. Sanchez, R.; Zhou, M. M. The role of human bromodomains in chromatin biology and gene transcription. *Curr. Opin. Drug Discovery Dev.* **2009**, *12*, 659-665.
24. Sanchez, R.; Meslamani, J.; Zhou, M. M. The bromodomain: From epigenome reader to druggable target. *Biochim. Biophys. Acta, Gene Regul. Mech.* **2014**, *1839*, 676-685.
25. Sanchez, R.; Pieper, U.; Melo, F.; Eswar, N.; Marti-Renom, M. A.; Madhusudhan, M. S.; Mirkovic, N.; Sali, A. Protein structure modeling for structural genomics. *Nat. Struct. Biol.* **2000**, *7*, 986-990.
26. Muller, S.; Filippakopoulos, P.; Knapp, S. Bromodomains as therapeutic targets. *Expert Rev. Mol. Med.* **2011**, *13*, E29.
27. Verdin, E.; Ott, M. 50 years of protein acetylation: from gene regulation to epigenetics, metabolism and beyond. *Nat. Rev. Mol. Cell Biol.* **2015**, *16*, 258-264.
28. Falkenberg, K. J.; Johnstone, R. W. Histone deacetylases and their inhibitors in cancer, neurological diseases and immune disorders. *Nat. Rev. Drug Discov.* **2014**, *13*, 673-691.
29. Shi, J. W.; Vakoc, C. R. The mechanisms behind the therapeutic activity of bet bromodomain inhibition. *Mol. Cell* **2014**, *54*, 728-736.
30. Itzen, F.; Greifenberg, A. K.; Bosken, C. A.; Geyer, M. Brd4 activates P-TEFb for RNA polymerase II CTD phosphorylation. *Nucleic Acids Res.* **2014**, *42*, 7577-7587.
31. Bisgrovet, D. A.; Mahmoudi, T.; Henklein, P.; Verdin, E. Conserved P-TEFb-interacting domain of BRD4 inhibits HIV transcription. *Proc. Natl. Acad. Sci. U. S. A.* **2007**, *104*, 13690-13695.
32. Falkenberg, K. J.; Johnstone, R. W. Histone deacetylases and their inhibitors in cancer, neurological diseases and immune disorders. *Nat. Rev. Drug Discov.* **2014**, *13*, 673-691.

33. Guo, J. N.; Price, D. H. RNA polymerase II transcription elongation control. *Chem. Rev.* **2013**, *113*, 8583-8603.
34. Delmore, J. E.; Issa, G. C.; Lemieux, M. E.; Rahl, P. B.; Shi, J. W.; Jacobs, H. M.; Kastritis, E.; Gilpatrick, T.; Paranal, R. M.; Qi, J.; Chesi, M.; Schinzel, A. C.; McKeown, M. R.; Heffernan, T. P.; Vakoc, C. R.; Bergsagel, P. L.; Ghobrial, I. M.; Richardson, P. G.; Young, R. A.; Hahn, W. C.; Anderson, K. C.; Kung, A. L.; Bradner, J. E.; Mitsiades, C. S. BET bromodomain inhibition as a therapeutic strategy to target c-Myc. *Cell* **2011**, *146*, 903-916.
35. Dang, C. V.; Le, A.; Gao, P. Myc-induced cancer cell energy metabolism and therapeutic opportunities. *Clin. Cancer Res.* **2009**, *15*, 6479-6483.
36. Miller, D. M.; Thomas, S. D.; Islam, A.; Muench, D.; Sedoris, K. c-Myc and cancer metabolism. *Clin. Cancer Res.* **2012**, *18*, 5546-5553.
37. Denis, G. V.; McComb, M. E.; Faller, D. V.; Sinha, A.; Romesser, P. B.; Costello, C. E. Identification of transcription complexes that contain the double bromodomain protein Brd2 and chromatin remodeling machines. *J. Proteome Res.* **2006**, *5*, 502-511.
38. Wang, L.; Wolgemuth, D. J. BET protein BRDT complexes with HDAC1, PRTM5, and TRIM28 and functions in transcriptional repression during spermatogenesis. *J. Cell. Biochem.* **2016**, *117*, 1429-1438.
39. Shang, E. Y.; Salazar, G.; Crowley, T. E.; Wang, X.; Lopez, R. A.; Wang, X. Y.; Wolgemuth, D. J. Identification of unique, differentiation stage-specific patterns of expression of the bromodomain-containing genes Brd2, Br3, Brd4, and Brdt in the mouse testis. *Gene Expr. Patterns* **2004**, *4*, 513-519.
40. Jones, M. H.; Numata, M.; Shimane, M. Identification and characterization of BRDT: A testis-specific gene related to the bromodomain genes RING3 and Drosophila fsh. *Genomics* **1997**, *45*, 529-534.
41. Larose, H.; Shami, A. N.; Abbott, H.; Manske, G.; Lei, L.; Hammoud, S. S. Gametogenesis: A journey from inception to conception. In *Organ Development*, Wellik, D. M., Ed. 2019; Vol. 132, pp 257-310.
42. Govin, J.; Caron, C.; Lestrat, C.; Rousseaux, S.; Khochbin, S. The role of histones in chromatin remodelling during mammalian spermiogenesis. *Eur. J. Biochem.* **2004**, *271*, 3459-3469.
43. Shang, E. Y.; Nickerson, H. D.; Wen, D. C.; Wang, X. Y.; Wolgemuth, D. J. The first bromodomain of Brdt, a testis-specific member of the BET sub-family of double-bromodomain-containing proteins, is essential for male germ cell differentiation. *Development* **2007**, *134*, 3507-3515.
44. Gaucher, J.; Boussouar, F.; Montellier, E.; Curtet, S.; Buchou, T.; Bertrand, S.; Hery, P.; Jounier, S.; Depaux, A.; Vitte, A. L.; Guardiola, P.; Pernet, K.; Debernardi, A.; Lopez, F.; Holota, H.; Imbert, J.; Wolgemuth, D. J.; Gerard, M.; Rousseaux, S.; Khochbin, S. Bromodomain-dependent stage-specific male genome programming by Brdt. *EMBO J.* **2012**, *31*, 3809-3820.
45. Bourova-Flin, E.; Chuffart, F.; Rousseaux, S.; Khochbin, S. The role of bromodomain testis-specific factor, brdt, in cancer: a biomarker and a possible therapeutic target. *Cell J.* **2017**, *19*, 1-8.
46. Goudarzi, A.; Zhang, D.; Huang, H.; Barral, S.; Kwon, O. K.; Qi, S. K.; Tang, Z. Y.; Buchou, T.; Vitte, A. L.; He, T. M.; Cheng, Z. Y.; Montellier, E.; Gaucher, J.; Curtet, S.; Debernardi, A.; Charbonnier, G.; Puthier, D.; Petosa, C.; Panne, D.; Rousseaux, S.;

Roeder, R. G.; Zhao, Y. M.; Khochbin, S. Dynamic competing histone h4 k5k8 acetylation and butyrylation are hallmarks of highly active gene promoters. *Mol. Cell* **2016**, *62*, 169-180.
47. Pivot-Pajot, C.; Caron, C.; Govin, M.; Vion, A.; Rousseaux, S.; Khochbin, S. Acetylation-dependent chromatin reorganization by BRDT, a testis-specific bromodomain-containing protein. *Mol. Cell. Biol.* **2003**, *23*, 5354-5365.
48. Bryant, J. M.; Berger, S. L. Low-hanging fruit: targeting Brdt in the testes. *EMBO J.* **2012**, *31*, 3788-3789.
49. Garcia, B. A.; Hake, S. B.; Diaz, R. L.; Kauer, M.; Morris, S. A.; Recht, J.; Shabanowitz, J.; Mishra, N.; Strahl, B. D.; Allis, C. D.; Hunt, D. F. Organismal differences in post-translational modifications in histones H3 and H4. *J. Biol. Chem.* **2007**, *282*, 7641-7655.
50. Thorne, A. W.; Kmiciek, D.; Mitchelson, K.; Sautiere, P.; Cranerobinson, C. Patterns of histone acetylation. *Eur. J. Biochem.* **1990**, *193*, 701-713.
51. Zhang, K. L.; Williams, K. E.; Huang, L.; Yau, P.; Siino, J. S.; Bradbury, E. M.; Jones, P. R.; Minch, M. J.; Burlingame, A. L. Histone acetylation and deacetylation - Identification of acetylation and methylation sites of HeLa histone H4 by mass spectrometry. *Mol. Cell. Proteomics* **2002**, *1*, 500-508.
52. Christensen, M. E.; Rattner, J. B.; Dixon, G. H. Hyperacetylation of histone H-4 promotes chromatin decondensation prior to histone replacement by protamines during spermatogenesis in rainbow-trout. *Nucleic Acids Res.* **1984**, *12*, 4575-4592.
53. Rathke, C.; Baarends, W. M.; Awe, S.; Renkawitz-Pohl, R. Chromatin dynamics during spermiogenesis. *Biochim. Biophys. Acta, Gene Regul. Mech.* **2014**, *1839*, 155-168.
54. Bao, J. Q.; Bedford, M. T. Epigenetic regulation of the histone-to-protamine transition during spermiogenesis. *Reproduction* **2016**, *151*, R55-R70.
55. Wang, T.; Gao, H.; Li, W.; Liu, C. Essential role of histone replacement and modifications in male fertility. *Front. Genet.* **2019**, *10*.
56. Cho, C.; Willis, W. D.; Goulding, E. H.; Haesook, J. H.; Choi, Y. C.; Hecht, N. B.; Eddy, E. M. Haploinsufficiency of protamine-1 or-2 causes infertility in mice. *Nat. Genet.* **2001**, *28*, 82-86.
57. Sasaki, K.; Ito, T.; Nishino, N.; Khochbin, S.; Yoshida, M. Real-time imaging of histone H4 hyperacetylation in living cells. *Proc. Natl. Acad. Sci. U. S. A.* **2009**, *106*, 16257-16262.
58. Moriniere, J.; Rousseaux, S.; Steuerwald, U.; Soler-Lopez, M.; Curtet, S.; Vitte, A. L.; Govin, J.; Gaucher, J.; Sadoul, K.; Hart, D. J.; Krijgsveld, J.; Khochbin, S.; Muller, C. W.; Petosa, C. Cooperative binding of two acetylation marks on a histone tail by a single bromodomain. *Nature* **2009**, *461*, 664-668.
59. Miller, T. C. R.; Simon, B.; Rybin, V.; Grotsch, H.; Curtet, S.; Khochbin, S.; Carlomagno, T.; Muller, C. W. A bromodomain-DNA interaction facilitates acetylation-dependent bivalent nucleosome recognition by the BET protein BRDT. *Nat. Commun.* **2016**, *7*, 13855-13868.
60. Rousseaux, S.; Debernardi, A.; Jacquiau, B.; Vitte, A. L.; Vesin, A.; Nagy-Mignotte, H.; Moro-Sibilot, D.; Brichon, P. Y.; Lantuejoul, S.; Hainaut, P.; Laffaire, J.; de Reynies, A.; Beer, D. G.; Timsit, J. F.; Brambilla, C.; Brambilla, E.; Khochbin, S. Ectopic activation of germline and placental genes identifies aggressive metastasis-prone lung cancers. *Sci. Transl. Med.* **2013**, *5*, 186-210.

61. Fagerberg, L.; Hallstrom, B. M.; Oksvold, P.; Kampf, C.; Djureinovic, D.; Odeberg, J.; Habuka, M.; Tahmasebpoor, S.; Danielsson, A.; Edlund, K.; Asplund, A.; Sjostedt, E.; Lundberg, E.; Szigyarto, C. A.; Skogs, M.; Takanen, J. O.; Berling, H.; Tegel, H.; Mulder, J.; Nilsson, P.; Schwenk, J. M.; Lindskog, C.; Danielsson, F.; Mardinoglu, A.; Sivertsson, A.; von Feilitzen, K.; Forsberg, M.; Zwahlen, M.; Olsson, I.; Navani, S.; Huss, M.; Nielsen, J.; Ponten, F.; Uhlen, M. Analysis of the human tissue-specific expression by genome-wide integration of transcriptomics and antibody-based proteomics. *Mol. Cell. Proteomics* **2014**, *13*, 397-406.
62. Agarwala, R.; Barrett, T.; Beck, J.; Benson, D. A.; Bollin, C.; Bolton, E.; Bourexis, D.; Brister, J. R.; Bryant, S. H.; Canese, K.; Cavanaugh, M.; Charowhas, C.; Clark, K.; Dondoshansky, I.; Feolo, M.; Fitzpatrick, L.; Funk, K.; Geer, L. Y.; Gorelenkov, V.; Graeff, A.; Hlavina, W.; Holmes, B.; Johnson, M.; Kattman, B.; Khotomlianski, V.; Kimchi, A.; Kimelman, M.; Kimura, M.; Kitts, P.; Klimke, W.; Kotliarov, A.; Krasnov, S.; Kuznetsov, A.; Landrum, M. J.; Landsman, D.; Lathrop, S.; Lee, J. M.; Leubsdorf, C.; Lu, Z. Y.; Madden, T. L.; Marchler-Bauer, A.; Malheiro, A.; Meric, P.; Karsch-Mizrachi, I.; Mnev, A.; Murphy, T.; Orris, R.; Ostell, J.; O'Sullivan, C.; Palanigobu, V.; Panchenko, A. R.; Phan, L.; Pierov, B.; Pruitt, K. D.; Rodarmer, K.; Sayers, E. W.; Schneider, V.; Schoch, C. L.; Schuler, G. D.; Sherry, S. T.; Siyan, K.; Soboleva, A.; Soussov, V.; Starchenko, G.; Tatusova, T. A.; Thibaud-Nissen, F.; Todorov, K.; Trawick, B. W.; Vakatov, D.; Ward, M.; Yaschenko, E.; Zasypkin, A.; Zbicz, K.; Coordinators, N. R. Database resources of the national center for biotechnology information. *Nucleic Acids Res.* **2018**, *46*, D8-D13.
63. Filippakopoulos, P.; Knapp, S. Next-generation epigenetic inhibitors. *Science* **2020**, *368*, 367-368.
64. Korb, E.; Herre, M.; Zucker-Scharff, I.; Darnell, R. B.; Allis, C. D. BET protein Brd4 activates transcription in neurons and BET inhibitor JQ1 blocks memory in mice. *Nat. Neurosci.* **2015**, *18*, 1464-1473.
65. Lee, D. U.; Katavolos, P.; Palanisamy, G.; Katewa, A.; Sioson, C.; Corpuz, J.; Pang, J.; DeMent, K.; Choo, E.; Ghilardi, N.; Diaz, D.; Danilenko, D. M. Nonselective inhibition of the epigenetic transcriptional regulator BET induces marked lymphoid and hematopoietic toxicity in mice. *Toxicol. Appl. Pharmacol.* **2016**, *300*, 47-54.
66. Zhang, G. T.; Liu, R. J.; Zhong, Y. F.; Plotnikov, A. N.; Zhang, W. J.; Zeng, L.; Rusinova, E.; Gerona-Nevarro, G.; Moshkina, N.; Joshua, J.; Chuang, P. Y.; Ohlmeyer, M.; He, J. C.; Zhou, M. M. Down-regulation of NF-kappa B transcriptional activity in hiv-associated kidney disease by BRD4 inhibition. *J. Biol. Chem.* **2012**, *287*, 28840-28851.
67. Devaiah, B. N.; Lewis, B. A.; Cherman, N.; Hewitt, M. C.; Albrecht, B. K.; Robey, P. G.; Ozato, K.; Sims, R. J.; Singer, D. S. BRD4 is an atypical kinase that phosphorylates Serine2 of the RNA Polymerase II carboxy-terminal domain. *Proc. Natl. Acad. Sci. U. S. A.* **2012**, *109*, 6927-6932.
68. Moros, A.; Rodriguez, V.; Saborit-Villarroya, I.; Montraveta, A.; Balsas, P.; Sandy, P.; Martinez, A.; Wiestner, A.; Normant, E.; Campo, E.; Perez-Galan, P.; Colomer, D.; Roue, G. Synergistic antitumor activity of lenalidomide with the BET bromodomain inhibitor CPI203 in bortezomib-resistant mantle cell lymphoma. *Leukemia* **2014**, *28*, 2049-2059.

69. Wong, C.; Laddha, S. V.; Tang, L.; Vosburgh, E.; Levine, A. J.; Normant, E.; Sandy, P.; Harris, C. R.; Chan, C. S.; Xu, E. Y. The bromodomain and extra-terminal inhibitor CPI203 enhances the antiproliferative effects of rapamycin on human neuroendocrine tumors. *Cell Death Dis.* **2014**, *5*, 1450-1464.
70. Noel, J. K.; Iwata, K.; Ooike, S.; Sugahara, K.; Nakamura, H.; Daibata, M. Development of the BET bromodomain inhibitor OTX015. *Mol. Cancer Ther.* **2013**, *12*, 244-244.
71. Ozer, H. G.; El-Gamal, D.; Powell, B.; Hing, Z. A.; Blachly, J. S.; Harrington, B.; Mitchell, S.; Grieselhuber, N. R.; Williams, K.; Lai, T. H.; Alinari, L.; Baiocchi, R. A.; Brinton, L.; Baskin, E.; Cannon, M.; Beaver, L.; Goettl, V. M.; Lucas, D. M.; Woyach, J. A.; Sampath, D.; Lehmann, A. M.; Yu, L. B.; Zhang, J. Z.; Ma, Y.; Zhang, Y.; Spevak, W.; Shi, S. Y.; Severson, P.; Shellooe, R.; Carias, H.; Tsang, G.; Dong, K.; Ewing, T.; Marimuthu, A.; Tantoy, C.; Walters, J.; Sanftner, L.; Rezaei, H.; Nespi, M.; Matusow, B.; Habets, G.; Ibrahim, P.; Zhang, C.; Mathe, E. A.; Bollag, G.; Byrd, J. C.; Lapalombella, R. BRD4 profiling identifies critical chronic lymphocytic leukemia oncogenic circuits and reveals sensitivity to PLX51107, a novel structurally distinct bet inhibitor. *Cancer Discov.* **2018**, *8*, 458-477.
72. Nikolovska-Coleska, Z.; Wang, R. X.; Fang, X. L.; Pan, H. G.; Tomita, Y.; Li, P.; Roller, P. P.; Krajewski, K.; Saito, N. G.; Stuckey, J. A.; Wang, S. M. Development and optimization of a binding assay for the XIAP BIR3 domain using fluorescence polarization. *Anal. Biochem.* **2004**, *332*, 261-273.
73. Chan, K. H.; Zengerle, M.; Testa, A.; Ciulli, A. Impact of target chemotype and linkage vector on inducing protein degradation: comparison of bromodomain and extra-terminal (BET) degraders derived from triazolodiazepine (JQ1) and tetrahydroquinoline (I-BET726) BET inhibitor scaffolds. *J. Med. Chem.* **2018**, *61*, 504-513.
74. Gao, N.; Ren, J. X.; Hou, L.; Zhou, Y.; Xin, L.; Wang, J. D.; Yu, H. M.; Xie, Y.; Wang, H. P. Identification of novel potent human testis-specific and bromodomain-containing protein (BRDT) inhibitors using crystal structure-based virtual screening. *Int. J. Mol. Med.* **2016**, *38*, 39-44.
75. Ayoub, A. M.; Hawk, L. M. L.; Herzig, R. J.; Jiang, J. W.; Wisniewski, A. J.; Gee, C. T.; Zhao, P. L.; Zhu, J. Y.; Berndt, N.; Offei-Addo, N. K.; Scott, T. G.; Qi, J.; Bradner, J. E.; Ward, T. R.; Schonbrunn, E.; Georg, G. I.; Pomerantz, W. C. K. Bet bromodomain inhibitors with one-step synthesis discovered from virtual screen. *J. Med. Chem.* **2017**, *60*, 4805-4817.
76. Picaud, S.; Leonards, K.; Lambert, J. P.; Dovey, O.; Wells, C.; Fedorov, O.; Monteiro, O.; Fujisawa, T.; Wang, C. Y.; Lingard, H.; Tallant, C.; Nikbin, N.; Guetzoyan, L.; Ingham, R.; Ley, S. V.; Brennan, P.; Muller, S.; Samsonova, A.; Gingras, A. C.; Schwaller, J.; Vassiliou, G.; Knapp, S.; Filippakopoulos, P. Promiscuous targeting of bromodomains by bromosporine identifies BET proteins as master regulators of primary transcription response in leukemia. *Sci. Adv.* **2016**, *2*, e1600760.
77. Zhang, G. T.; Plotnikov, A. N.; Rusinova, E.; Shen, T.; Morohashi, K.; Joshua, J.; Zeng, L.; Mujtaba, S.; Ohlmeyer, M.; Zhou, M. M. Structure-guided design of potent diazobenzene inhibitors for the bet bromodomains. *J. Med. Chem.* **2013**, *56*, 9251-9264.
78. Paulson, C. N.; Guan, X. H.; Ayoub, A. M.; Chan, A.; Karim, R. M.; Pomerantz, W. C. K.; Schonbrunn, E.; Georg, G. I.; Hawkinson, J. E. Design, synthesis, and

characterization of a fluorescence polarization pan-bet bromodomain probe. *ACS Med. Chem. Lett.* **2018**, *9*, 1223-1229.
79. Picaud, S.; Wells, C.; Felletar, I.; Brotherton, D.; Martin, S.; Savitsky, P.; Diez-Dacal, B.; Philpott, M.; Bountra, C.; Lingard, H.; Fedorov, O.; Muller, S.; Brennan, P. E.; Knapp, S.; Filippakopoulos, P. RVX-208, an inhibitor of BET transcriptional regulators with selectivity for the second bromodomain. *Proc. Natl. Acad. Sci. U. S. A.* **2013**, *110*, 19754-19759.
80. Faivre, E. J.; McDaniel, K. F.; Albert, D. H.; Mantena, S. R.; Plotnik, J. P.; Wilcox, D.; Zhang, L.; Bui, M. H.; Sheppard, G. S.; Wang, L.; Sehgal, V.; Lin, X. Y.; Huang, X. L.; Lu, X.; Uziel, T.; Hessler, P.; Lam, L. T.; Bellin, R. J.; Mehta, G.; Fidanze, S.; Pratt, J. K.; Liu, D. C.; Hasvold, L. A.; Sun, C. H.; Panchal, S. C.; Nicolette, J. J.; Fossey, S. L.; Park, C. H.; Longenecker, K.; Bigelow, L.; Torrent, M.; Rosenberg, S. H.; Kati, W. M.; Shen, Y. Selective inhibition of the BD2 bromodomain of BET proteins in prostate cancer. *Nature* **2020**, *578*, 306-310.
81. Martin, M. P.; Olesen, S. H.; Georg, G. I.; Schonbrunn, E. Cyclin-dependent kinase inhibitor dinaciclib interacts with the acetyl-lysine recognition site of bromodomains. *ACS Chem. Biol.* **2013**, *8*, 2360-2365.
82. Ember, S. W. J.; Zhu, J. Y.; Olesen, S. H.; Martin, M. P.; Becker, A.; Berndt, N.; Georg, G. I.; Schonbrunn, E. Acetyl-lysine binding site of bromodomain-containing protein 4 (BRD4) interacts with diverse kinase inhibitors. *ACS Chem. Biol.* **2014**, *9*, 1160-1171.
83. Fiskus, W.; Sharma, S.; Qi, J.; Shah, B.; Devaraj, S. G. T.; Leveque, C.; Portier, B. P.; Iyer, S.; Bradner, J. E.; Bhalla, K. N. BET protein antagonist JQ1 is synergistically lethal with FLT3 tyrosine kinase inhibitor (TKI) and overcomes resistance to FLT3-TKI in AML cells expressing FLT-ITD. *Mol. Cancer Ther.* **2014**, *13*, 2315-2327.
84. Rousseau, T.; Cravino, A.; Bura, T.; Ulrich, G.; Ziessel, R.; Roncali, J. BODIPY derivatives as donor materials for bulk heterojunction solar cells. *Chem. Commun.* **2009**, 1673-1675.
85. Ember, S. W.; Lambert, Q. T.; Berndt, N.; Gunawan, S.; Ayaz, M.; Tauro, M.; Zhu, J. Y.; Cranfill, P. J.; Greninger, P.; Lynch, C. C.; Benes, C. H.; Lawrence, H. R.; Reuther, G. W.; Lawrence, N. J.; Schönbrunn, E. Potent dual BET bromodomain-kinase inhibitors as value-added multitargeted chemical probes and cancer therapeutics. *Mol. Cancer Ther.* **2017**, *16*, 1054-1067.
86. Siu, M.; Pastor, R.; Liu, W.; Barrett, K.; Berry, M.; Blair, W. S.; Chang, C.; Chen, J. Z.; Eigenbrot, C.; Ghilardi, N.; Gibbons, P.; He, H. Y.; Hurley, C. A.; Kenny, J. R.; Khojasteh, S. C.; Le, H.; Lee, L.; Lyssikatos, J. P.; Magnuson, S.; Pulk, R.; Tsui, V.; Ultsch, M.; Xiao, Y. S.; Zhu, B. Y.; Sampath, D. 2-Amino- 1,2,4 triazolo 1,5-a pyridines as JAK2 inhibitors. *Bioorg. Med. Chem. Lett.* **2013**, *23*, 5014-5021.
87. Chen, Z. H.; Wang, Z. Y.; Pang, J. C.; Yu, Y.; Bieerkehazhi, S.; Lu, J. X.; Hu, T.; Zhao, Y. L.; Xu, X.; Zhang, H.; Yi, J. S.; Liu, S. F.; Yang, J. H. Multiple CDK inhibitor dinaciclib suppresses neuroblastoma growth via inhibiting CDK2 and CDK9 activity. *Sci. Rep.* **2016**, *6*.
88. Nguyen, T. K.; Grant, S. Dinaciclib (sch727965) inhibits the unfolded protein response through a cdk1-and 5-dependent mechanism. *Mol. Cancer Ther.* **2014**, *13*, 662-674.

89. Gregory, G. P.; Hogg, S. J.; Kats, L. M.; Vidacs, E.; Baker, A. J.; Gilan, O.; Lefebure, M.; Martin, B. P.; Dawson, M. A.; Johnstone, R. W.; Shortt, J. CDK9 inhibition by dinaciclib potently suppresses Mcl-1 to induce durable apoptotic responses in aggressive MYC-driven B-cell lymphoma in vivo. *Leukemia* **2015**, *29*, 1437-1441.
90. Verstovsek, S.; Passamonti, F.; Rambaldi, A.; Barosi, G.; Rosen, P. J.; Rumi, E.; Gattoni, E.; Pieri, L.; Guglielmelli, P.; Elena, C.; He, S.; Contel, N.; Mookerjee, B.; Sandor, V.; Cazzola, M.; Kantarjian, H. M.; Barbui, T.; Vannucchi, A. M. A phase 2 study of ruxolitinib, an oral JAK1 and JAK2 inhibitor, in patients with advanced polycythemia vera who are refractory or intolerant to hydroxyurea. *Cancer* **2014**, *120*, 513-520.
91. Tanaka, M.; Roberts, J. M.; Seo, H. S.; Souza, A.; Paulk, J.; Scott, T. G.; DeAngelo, S. L.; Dhe-Paganon, S.; Bradner, J. E. Design and characterization of bivalent BET inhibitors. *Nat. Chem. Biol.* **2016**, *12*, 1089-1096.
92. Waring, M. J.; Chen, H. W.; Rabow, A. A.; Walker, G.; Bobby, R.; Boiko, S.; Bradbury, R. H.; Callis, R.; Clark, E.; Dale, I.; Daniels, D. L.; Dulak, A.; Flavell, L.; Holdgate, G.; Jowitt, T. A.; Kikhney, A.; McAlister, M.; Mendez, J.; Ogg, D.; Patel, J.; Petteruti, P.; Robb, G. R.; Robers, M. B.; Saif, S.; Stratton, N.; Svergun, D. I.; Wang, W. X.; Whittaker, D.; Wilson, D. M.; Yao, Y. Potent and selective bivalent inhibitors of BET bromodomains. *Nat. Chem. Biol.* **2016**, *12*, 1097-1104.
93. Armstrong, C. T.; Mason, P. E.; Anderson, J. L. R.; Dempsey, C. E. Arginine side chain interactions and the role of arginine as a gating charge carrier in voltage sensitive ion channels. *Sci. Rep.* **2016**, *6*, 21759-21769.
94. Rice, P.; Longden, I.; Bleasby, A. EMBOSS: The European molecular biology open software suite. *Trends Genet.* **2000**, *16*, 276-277.
95. Madeira, F.; Park, Y. M.; Lee, J.; Buso, N.; Gur, T.; Madhusoodanan, N.; Basutkar, P.; Tivey, A. R. N.; Potter, S. C.; Finn, R. D.; Lopez, R. The EMBL-EBI search and sequence analysis tools APIs in 2019. *Nucleic Acids Res.* **2019**, *47*, 636-641.
96. Jameson, D. M.; Croney, J. C. Fluorescence polarization: Past, present and future. *Comb. Chem. High Throughput Screen.* **2003**, *6*, 167-176.
97. Lea, W. A.; Simeonov, A. Fluorescence polarization assays in small molecule screening. *Expert Opin. Drug Discov.* **2011**, *6*, 17-32.
98. Jameson, D. M.; Ross, J. A. Fluorescence polarization/anisotropy in diagnostics and imaging. *Chem. Rev.* **2010**, *110*, 2685-2708.
99. Cheng, Y.; Prusoff, W. H. Relationship between inhibition constant (K1) and concentration of inhibitor which causes 50 percent inhibition (I50) of an enzymatic-reaction. *Biochem. Pharmacol.* **1973**, *22*, 3099-3108.
100. Munson, P. J.; Rodbard, D. An exact correction to the cheng-prusoff correction. *J. Recept. Res.* **1988**, *8*, 533-546.
101. Urick, A. K.; Hawk, L. M. L.; Cassel, M. K.; Mishra, N. K.; Liu, S.; Adhikari, N.; Zhang, W.; dos Santos, C. O.; Hall, J. L.; Pomerantz, W. C. K. Dual screening of BRTF and BRD4 using protein-observed fluorine nmr uncovers new bromodomain probe molecules. *ACS Chem. Biol.* **2015**, *10*, 2246-2256.
102. Yu, J. L.; Chen, T. T.; Zhou, C.; Lian, F. L.; Tang, X. L.; Wen, Y.; Shen, J. K.; Xu, Y. C.; Xiong, B.; Zhang, N. X. NMR-based platform for fragment-based lead discovery used in screening BRD4-targeted compounds. *Acta Pharmacol. Sin.* **2016**, *37*, 984-993.

103. de Rezende, L. C. D.; Vaidergorn, M. M.; Moraes, J. C. B.; Emery, F. D. Synthesis, photophysical properties and solvatochromism of meso-substituted tetramethyl bodipy dyes. *J. Fluoresc.* **2014**, *24*, 257-266.
104. Wu, W. H.; Cui, X. N.; Zhao, J. Z. Hetero Bodipy-dimers as heavy atom-free triplet photosensitizers showing a long-lived triplet excited state for triplet-triplet annihilation upconversion. *Chem. Commun.* **2013**, *49*, 9009-9011.
105. Thivierge, C.; Bandichhor, R.; Burgess, K. Spectral dispersion and water solubilization of BODIPY dyes via palladium-catalyzed C-H functionalization. *Org. Lett.* **2007**, *9*, 2135-2138.
106. Zhu, S. L.; Bi, J. H.; Vegesna, G.; Zhang, J. T.; Luo, F. T.; Valenzano, L.; Liu, H. Y. Functionalization of BODIPY dyes at 2,6-positions through formyl groups. *RSC Adv.* **2013**, *3*, 4793-4800.
107. Bui, M. H.; Lin, X. Y.; Albert, D. H.; Li, L. M.; Lam, L. T.; Faivre, E. J.; Warder, S. E.; Huang, X. L.; Wilcox, D.; Donawho, C. K.; Sheppard, G. S.; Wang, L.; Fidanze, S.; Pratt, J. K.; Liu, D.; Hasvold, L.; Uziel, T.; Lu, X.; Kohlhapp, F.; Fang, G. W.; Elmore, S. W.; Rosenberg, S. H.; McDaniel, K. F.; Kati, W. M.; Shen, Y. Preclinical characterization of BET family bromodomain inhibitor ABBV-075 suggests combination therapeutic strategies. *Cancer Res.* **2017**, *77*, 2976-2989.
108. Ali, I.; Choi, G.; Lee, K. BET inhibitors as anticancer agents: a patent review. *Recent Pat. Anticancer Drug Discov.* **2017**, *12*, 340-364.
109. Li, J.; Wang, P. Q.; Zhou, B. H.; Shi, J. Y.; Liu, J.; Li, X. R.; Fan, L. M.; Zheng, Y. X.; Ouyang, L. Development of 4,5-dihydro-benzodiazepinone derivatives as a new chemical series of BRD4 inhibitors. *Eur. J. Med. Chem.* **2016**, *121*, 294-299.
110. Filippakopoulos, P.; Qi, J.; Picaud, S.; Shen, Y.; Smith, W. B.; Fedorov, O.; Morse, E. M.; Keates, T.; Hickman, T. T.; Felletar, I.; Philpott, M.; Munro, S.; McKeown, M. R.; Wang, Y. C.; Christie, A. L.; West, N.; Cameron, M. J.; Schwartz, B.; Heightman, T. D.; La Thangue, N.; French, C. A.; Wiest, O.; Kung, A. L.; Knapp, S.; Bradner, J. E. Selective inhibition of BET bromodomains. *Nature* **2010**, *468*, 1067-1073.
111. Philpott, M.; Yang, J.; Tumber, T.; Fedorov, O.; Uttarkar, S.; Filippakopoulos, P.; Picaud, S.; Keates, T.; Felletar, I.; Ciulli, A.; Knapp, S.; Heightman, T. D. Bromodomain-peptide displacement assays for interactome mapping and inhibitor discovery. *Mol. Biosyst.* **2011**, *7*, 2899-2908.
112. Pardanani, A.; Hood, J.; Lasho, T.; Levine, R. L.; Martin, M. B.; Noronha, G.; Finke, C.; Mak, C. C.; Mesa, R.; Zhu, H.; Soll, R.; Gilliland, D. G.; Tefferi, A. TG101209, a small molecule JAK2-selective kinase inhibitor potently inhibits myeloproliferative disorder-associated JAK2V617F and MPLW515L/K mutations. *Leukemia* **2007**, *21*, 1658-1668.
113. Friesner, R. A.; Murphy, R. B.; Repasky, M. P.; Frye, L. L.; Greenwood, J. R.; Halgren, T. A.; Sanschagrin, P. C.; Mainz, D. T. Extra precision glide: Docking and scoring incorporating a model of hydrophobic enclosure for protein-ligand complexes. *J. Med. Chem.* **2006**, *49*, 6177-6196.
114. Halgren, T. A.; Murphy, R. B.; Friesner, R. A.; Beard, H. S.; Frye, L. L.; Pollard, W. T.; Banks, J. L. Glide: A new approach for rapid, accurate docking and scoring. 2. Enrichment factors in database screening. *J. Med. Chem.* **2004**, *47*, 1750-1759.
115. Friesner, R. A.; Banks, J. L.; Murphy, R. B.; Halgren, T. A.; Klicic, J. J.; Mainz, D. T.; Repasky, M. P.; Knoll, E. H.; Shelley, M.; Perry, J. K.; Shaw, D. E.; Francis, P.;

Shenkin, P. S. Glide: A new approach for rapid, accurate docking and scoring. 1. Method and assessment of docking accuracy. *J. Med. Chem.* **2004**, *47*, 1739-1749.
116. Adcock, S. A.; McCammon, J. A. Molecular dynamics: Survey of methods for simulating the activity of proteins. *Chem. Rev.* **2006**, *106*, 1589-1615.
117. Zhang, X. H.; Wong, S. E.; Lightstone, F. C. Toward fully automated high performance computing drug discovery: A massively parallel virtual screening pipeline for docking and molecular mechanics/generalized born surface area rescoring to improve enrichment. *J. Chem. Inf. Model.* **2014**, *54*, 324-337.
118. Tubert-Brohman, I.; Sherman, W.; Repasky, M.; Beuming, T. Improved Docking of Polypeptides with Glide. *J. Chem. Inf. Model.* **2013**, *53*, 1689-1699.
119. Hou, T. J.; Wang, J. M.; Li, Y. Y.; Wang, W. Assessing the Performance of the MM/PBSA and MM/GBSA Methods. 1. The Accuracy of Binding Free Energy Calculations Based on Molecular Dynamics Simulations. *J. Chem. Inf. Model.* **2011**, *51*, 69-82.
120. Jung, M. E.; Ouk, S.; Yoo, D.; Sawyers, C. L.; Chen, C.; Tran, C.; Wongvipat, J. Structure-activity relationship for thiohydantoin androgen receptor antagonists for castration-resistant prostate cancer (CRPC). *J. Med. Chem.* **2010**, *53*, 2779-2796.
121. Farrants, A. K. O. Chromatin remodelling and actin organisation. *FEBS Lett.* **2008**, *582*, 2041-2050.
122. Wu, Q.; Heidenreich, D.; Zhou, S.; Ackloo, S.; Kramer, A.; Nakka, K.; Lima-Fernandes, E.; Deblois, G.; Duan, S. L.; Vellanki, R. N.; Li, F. L.; Vedadi, M.; Dilworth, J.; Lupien, M.; Brennan, P. E.; Arrowsmith, C. H.; Muller, S.; Fedorov, O.; Filippakopoulos, P.; Knapp, S. A chemical toolbox for the study of bromodomains and epigenetic signaling. *Nat. Commun.* **2019**, *10*.
123. Gilan, O.; Rioja, I.; Knezevic, K.; Bell, M. J.; Yeung, M. M.; Harker, N. R.; Lam, E. Y. N.; Chung, C. W.; Bamborough, P.; Petretich, M.; Urh, M.; Atkinson, S. J.; Bassil, A. K.; Roberts, E. J.; Vassiliadis, D.; Burr, M. L.; Preston, A. G. S.; Wellaway, C.; Werner, T.; Gray, J. R.; Michon, A. M.; Gobbetti, T.; Kumar, V.; Soden, P. E.; Haynes, A.; Vappiani, J.; Tough, D. F.; Taylor, S.; Dawson, S. J.; Bantscheff, M.; Lindon, M.; Drewes, G.; Demont, E. H.; Daniels, D. L.; Grandi, P.; Prinjha, R. K.; Dawson, M. A. Selective targeting of BD1 and BD2 of the BET proteins in cancer and immunoinflammation. *Science* **2020**, *368*, 387-398.
124. Krissinel, E. Crystal contacts as nature's docking solutions. *J. Comput. Chem.* **2010**, *31*, 133-143.
125. Krissinel, E.; Henrick, K. Inference of macromolecular assemblies from crystalline state. *J. Mol. Biol.* **2007**, *372*, 774-797.
126. Vagedes, P.; Saenger, W.; Knapp, E. W. Driving forces of protein association: The dimer-octamer equilibrium in arylsulfatase A. *Biophys. J.* **2002**, *83*, 3066-3078.
127. Schwartz, M. P.; Cunin, F.; Cheung, R. W.; Sailor, M. J. Chemical modification of silicon surfaces for biological applications. *Physica Status Solidi a-Applications and Materials Science* **2005**, *202*, 1380-1384.
128. Zimmermann, K.; Sang, X. P.; Mastalerz, H. A.; Johnson, W. L.; Zhang, G. F.; Liu, Q. J.; Batt, D.; Lombardo, L. J.; Vyas, D.; Trainor, G. L.; Tokarski, J. S.; Lorenzi, M. V.; You, D.; Gottardis, M. M.; Lippy, J.; Khan, J.; Sack, J. S.; Purandare, A. V. 9H-Carbazole-1-carboxamides as potent and selective JAK2 inhibitors. *Bioorg. Med. Chem. Lett.* **2015**, *25*, 2809-2812.

129. Gibson, M. S.; Bradshaw, R. W. Gabriel synthesis of primary amines. *Angewandte Chemie-International Edition* **1968**, *7*, 919-930.
130. Smeets, A.; Willot, P.; De Winter, J.; Gerbaux, P.; Verbiest, T.; Koeckelberghs, G. End group-functionalization and synthesis of block-copolythiophenes by modified nickel initiators. *Macromolecules* **2011**, *44*, 6017-6025.
131. Schönbrunn, E.; Lawrence, N. J.; Lawrence, H. R. Potent dual BRD4-kinase inhibitors as cancer therapeutics. WO/2016/022460, Nov, 2016.